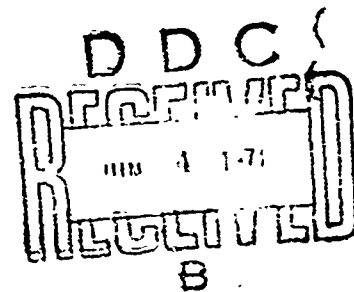AD724336

JANAIR

JOINT ARMY NAVY AIRCRAFT INSTRUMENTATION RESEARCH

IFR Steep-Angle Approach:
Effects of System Noise and
Aircraft Control-Augmentation Variables

J. D. Wolf

M. F. Barrett

D D C

B

NOTICE

Change of Address

Organizations receiving JANAIR reports on the initial distribution list should
confirm correct address. This list is located at the end of the report just
prior to the DD Form 1473. Any change in address or distribution list
should be conveyed to the Office of Naval Research, Code 461, Arlington,
Virginia 22217, ATTN: JANAIR Chairman.

Disposition

When this report is no longer needed, it may be transmitted to other organi-
zations. Do not return it to the originator or the monitoring office.

Disclaimer

The findings in this report are not to be construed as an official Department
of Defense or Military Department position unless so designated by other
official documents.

DOCUMENT CONTROL DATA - R & D

(Security classification of title, body of abstract and indexing annotation must be entered when the overall report is classified)

1. ORIGINATING ACTIVITY (Corporate author)	2a. REPORT SECURITY CLASSIFICATION
Honeywell Inc., Systems and Research Center 2345 Walnut Street, St. Paul, Minnesota 55113	UNCLASSIFIED
	2b. GROUP

3. REPORT TITLE

IFR STEEP-ANGLE APPROACH: EFFECTS OF SYSTEM NOISE AND AIRCRAFT CONTROL-AUGMENTATION VARIABLES

4. DESCRIPTIVE NOTES (Type of report and inclusive dates)

Final Report, January 1969 through June 1970

5. AUTHOR(S) (First name, middle initial, last name)

James D. Wolf and Mike F. Barrett

6. REPORT DATE	7a. TOTAL NO. OF PAGES	7b. NO. OF REFS
July 1970	314	40

8a. CONTRACT OR GRANT NO.	9a. ORIGINATOR'S REPORT NUMBER(S)
N00014-68-C-0191	
b. PROJECT NO. NR 213-061	12571-FR2
c.	9b. OTHER REPORT NO(S) (Any other numbers that may be assigned this report)
d.	JANAIR Report 700810

10. DISTRIBUTION STATEMENT

This document has been approved for public release and sale; its distribution is unlimited.

11. SUPPLEMENTARY NOTES	12. SPONSORING MILITARY ACTIVITY
Joint Army - Navy Aircraft Instrumentation Research Program (JANAIR)	U.S. Navy, Office of Naval Research Aeronautics, Code 461 Arlington, Virginia 22217

13. ABSTRACT

The objective of this study was to investigate, by means of real-time man-in-the-loop simulation techniques, piloting performance as influenced by approach-signal degradation and aircraft control-augmentation variables during IFR steep-angle approaches and landings with vertical-lift aircraft. Simulation evaluations also included aircraft-type, display-format, approach-angle, and display-quickening variables to increase the generality of study results. Variable-velocity simulations of Bell UH-1 and Ryan XV-5 aircraft were utilized as test vehicles. Interpreted within the constraints imposed by the simulations, study results indicated that increased filtering of measurement noise is beneficial during approach but may have a degrading effect during hovering flight. Generally, both flight-path error and pilot control activity increased with increased measurement noise. With one exception data trends also indicated improved performance with aircraft outer-loop control augmentation.

DD FORM 1473 REPLACES DD FORM 1473, 1 JAN 64, WHICH IS OBSOLETE FOR ARMY USE.

14 KEY WORDS	LINK A		LINK B		LINK C	
	ROLE	WT	ROLE	WT	ROLE	WT
IFR						
Simulation						
Landing						
VTOL						
Helicopter						
Displays						
Quickening						
UH-1						
XV-5						

JANAIR

Joint Army-Navy Aircraft Instrumentation Research

JANAIR Report 700810

IFR STEEP-ANGLE APPROACH: EFFECTS OF SYSTEM
NOISE AND AIRCRAFT CONTROL-AUGMENTATION
VARIABLES

J. D. Wolf and M. F. Barrett
Honeywell Inc.

April 1971

(Honeywell Document No. 12571-FR2)

FOREWORD

This report presents work which was performed under the Joint Army-Navy Aircraft Instrumentation Research (JANAIR) Program, a research and exploratory development program directed by the United States Navy, Office of Naval Research. Special guidance is provided to the program for the Army Electronics Command, the Naval Air Systems Command, and the Office of Naval Research through an organization known as the JANAIR Working Group. The Working Group is currently composed of representatives from the following offices:

- U.S. Navy, Office of Naval Research, Aeronautics, Code 461, Arlington, Virginia 22217

    - Aircraft Instrumentation and Control Program Area

- U.S. Navy, Naval Air Systems Command, Washington, D.C.

    - Avionics Division; Navigation Instrumentation and Display Branch (NAVAIR 5337)

    - Crew Systems Division: Cockpit/Cabin Requirements and Standards Branch (NAVAIR 5313)

- U.S. Army, Army Electronics Command, Avionics Laboratory, Fort Monmouth, New Jersey

    - Instrument Technical Area (AMSEL-VL-I)

The Joint Army-Navy Aircraft Instrumentation Research Program objective is: To conduct applied research using analytical and experimental investigations for identifying, defining and validating advanced concepts which may be applied to future, improved Naval and Army aircraft instrumentation systems. This includes sensing elements, data processors, displays and man/machine interfaces for fixed- and rotary-wing aircraft for all flight regimes.

ACKNOWLEDGEMENTS

ABSTRACT

The objective of this study was to investigate, by means of real-time man-in-the-loop simulation techniques, piloting performance as influenced by approach-signal degradation and aircraft control-augmentation variables during IFR steep-angle approaches and landings with vertical-lift aircraft. Simulation evaluations also included aircraft-type, display-format, approach-angle, and display-quickening variables to increase the generality of study results. Variable-velocity simulations of Bell UH-1 and Ryan XV-5 aircraft were utilized as test vehicles. Interpreted within the constraints imposed by the simulations, study results indicated that increased filtering of measurement noise is beneficial during approach but may have a degrading effect during hovering flight. Generally, both flight-path error and pilot control activity increased with increased measurement noise. With one exception, data trends also indicated improved performance with aircraft outer-loop control augmentation.

CONTENTS

ILLUSTRATIONS

xi

TABLES

ABBREVIATIONS AND SYMBOLS

ABBREVIATIONS

A/D	analog to digital
BDHI	bearing distance heading indicator
cg	center of gravity
CRT	cathode ray tube
CTOL	conventional takeoff and landing
D/A	digital to analog
FAA	Federal Aviation Administration
FD	flight director
GCA	ground-controlled approach
GW	gross weight
HSD	horizontal situation display
IAS	indicated airspeed
IEVD	integrated electronic vertical display
IFR	instrument flight rules
ILS	instrument landing system
JANAIR	Joint Army-Navy Aircraft Instrumentation Research
OLCS	outer-loop control system
PPI	plan position indicator
PPI-AR	plan position indicator - aircraft referenced
PPI-IR	plan position indicator - inertially referenced
RMS	root mean square

RTCA	Radio Technical Commission for Aeronautics
SAA	steep-angle approach
SAS	stability-augmentation system
STOL	short takeoff and landing
VFR	visual flight rules
VSD	vertical situation display
VTOL	vertical takeoff and landing
V/STOL	vertical/short takeoff and landing
wrt	with respect to

SYMBOLS

A	approach angle (independent variable)
AI_θ, AI_ϕ, AI_{col}	pitch, roll, and collective activity indices
A_{1S}	cosine component of main-rotor cyclic-pitch angle
A_{1S_S}	A_{1S} is due to cyclic-stick input
B	bearing of aircraft with respect to ground station
B_n	noise-corrupted bearing measurement
B_{1S}	sine component of cyclic-pitch angle
B_{1S_S}	B_{1S} due to cyclic-stick input
C	control-augmentation mode (independent variable)
D	display format (independent variable)
E	angle of elevation of aircraft with respect to ground station
E_n	noise-corrupted elevation measurement
E_X, E_Y, E_Z	aircraft longitudinal, lateral, and vertical position error from command position

$E[\;]$	denotes expected value of quantity enclosed
F	filter level (independent variable)
g	gravity (32.2 ft/sec^2)
ID	identification code number used to select various levels of independent variables
K_X, K_Y, K_Z	longitudinal, lateral, and vertical position-error quickening-symbol gains
$K_{\dot{X}}$, $K_{\dot{Y}}$, $K_{\dot{Z}}$	longitudinal, lateral, and vertical velocity-error quickening-symbol gains
K_θ, K_ϕ	pitch and roll attitude-error quickening-symbol gains
KNF	unit of nose-fan-door efficiency
LAG_X, $LAG_{\dot{X}}$	response times of position output and rate output of α-β filter (i.e., time required for response to reach 90 percent of steady-state value)
N	noise level (independent variable)
n_R, n_B, n_E	noise components of range, bearing and elevation
p	roll rate
P	mission phase (also used to indicate level of confidence for significance tests)
q	pitch rate
Q	quickening-gain level (independent variable)
r	yaw rate
R	range of aircraft with respect to ground station (slant range)
R_n	noise-corrupted range measurement
R_X, R_Y, R_Z	ratios of α-β filter position-input- to position-output-noise standard deviations for longitudinal, lateral and vertical axes

$R_{\dot{X}}$, $R_{\dot{Y}}$, $R_{\dot{Z}}$ — ratios of α-β filter position-input- to rate-output-noise standard deviations for longitudinal, lateral and vertical axes

R_X, $R_{\hat{X}}$, $R_{\dot{\hat{X}}}$, $R_{\dot{\hat{X}}_{lim}}$ — autocorrelation functions of noise input, position- and rate-output estimates of α-β filter, and rate-output estimate from rate limiter

RMS_X, RMS_Y, RMS_Z — root-mean-square longitudinal, lateral, and vertical position errors

S — subject (independent variable)

S_X, $S_{\hat{X}}$, $S_{\dot{\hat{X}}}$, $S_{\dot{\hat{X}}_{lim}}$ — power spectral densities of noise input, position- and rate-output estimates of α-β filter, and rate-output estimate from rate limiter

T — sampling period of α-β filter (i.e., compute-cycle time)

u — X body-axis perturbation velocity

v — Y body-axis perturbation velocity

V — vehicle (independent variable)

w — Z body-axis perturbation velocity

X, $\dot{X}$, $\ddot{X}$ — longitudinal inertial-axis position, rate, and acceleration

$\hat{X}$, $\dot{\hat{X}}$ — longitudinal position and rate estimates of α-β filter

X_B, $\dot{X}_B$, $\ddot{X}_B$ — longitudinal body-axis position, rate, and acceleration

X_C, $\dot{X}_C$ — longitudinal commanded position and rate

X_G — longitudinal distance from ground station to landing site

X_I, $\dot{X}_I$, $\ddot{X}_I$ — longitudinal inertial-axis position, rate, and acceleration

X_n — noise-corrupted inertial longitudinal-position measurement

X_Q, $\ddot{X}_Q$ — pitch-axis quickening-symbol displacement and rate of displacement on display

X_T — longitudinal distance from ground station to aircraft

Y, $\dot{Y}$, $\ddot{Y}$	lateral inertial-axis position, rate, and acceleration
$\hat{Y}$, $\dot{\hat{Y}}$	lateral position and rate estimates of α-β filter
Y_B, $\dot{Y}_B$, $\ddot{Y}_B$	lateral body-axis position, rate, and acceleration
Y_C	lateral command position
Y_I, $\dot{Y}_I$, $\ddot{Y}_I$	lateral inertial-axis position, rate, and acceleration
Y_n	noise-corrupted inertial lateral-position measurement
Y_Q	roll-axis component of quickening-symbol displacement on display
z	standard deviation of unit normal distribution
Z, $\dot{Z}$, $\ddot{Z}$	vertical inertial-axis position, rate, and acceleration
$\hat{Z}$, $\dot{\hat{Z}}$	vertical position and rate estimates of α-β filter
Z_B, $\dot{Z}_B$, $\ddot{Z}_B$	vertical body-axis position, rate, and acceleration
Z_I, $\dot{Z}_I$, $\ddot{Z}_I$	vertical inertial-axis position, rate, and acceleration
Z_n	noise-corrupted inertial vertical-position measurement
α, β	filter parameters
β_S	differential wing-fan louver angle $(\beta_{SR} - \beta_{SL})$
β_V	differential wing-fan louver angle $(\beta_{VR} - \beta_{VL})$
γ	glideslope angle
δ_θ, δ_ϕ, δ_{col}	pitch, roll, and collective stick displacements (recorded as dependent variables)
δ_{θ_c}, δ_{ϕ_c}, δ_{R_c}	pitch, roll and rudder control inputs
ΔR_n, ΔB_n, ΔE_n	deviations in range, bearing and elevation measurements due to random noise.
ΔX_n, ΔY_n, ΔE_n	deviations in inertial longitudinal, lateral and vertical position measurements due to random noise on range, bearing and elevation measurements

$\Delta\psi$	difference between approach path and aircraft heading
$\theta, \dot{\theta}$	pitch attitude and attitude rate
ϑ_{TR}	blade pitch of tail rotor
σ	standard deviation
σ^2	variance
$\phi, \dot{\phi}$	roll attitude and attitude rate
$\psi, \dot{\psi}$	yaw and yaw rate

NOMENCLATURE

Activity Indices

Root mean square of the rate of pilot's control inputs into the simulated vehicle. These values are used as performance measures and provide an indication of the pilot's activity as he controls the simulated vehicle.

Alpha-Beta Filter

Name of the digital filter used in this study to provide smoothed estimates of position and rate from the simulated measurements.

Autocorrelation Function

A measure of interaction (or correlation) of a process with itself as a function of time. Normalized autocorrelation is an autocorrelation function normalized such that it is bounded by unity.

A/D

Analog to Digital - An interface between an analog and a digital computer which converts the continuous data of the analog computer to the discrete representation of the digital computer.

Constant-Slope Approach

An approach in which the ratio of the vertical-to-horizontal velocity remains constant.

Cumulative Probability Density Function

The probability that the value of a random variable X is less than some real number x.

Dependent Variables

Variables of an experiment which describe system performance. These performance measures are assumed to reflect changes in the levels of the independent variables of the experiment and are thus considered to be "dependent".

D/A

Digital to Analog - An interface between a digital and an analog computer which converts the discrete data of the digital computer to the continuous representation of the analog computer.

HSD

Horizontal Situation Display - A class of display formats which presents a horizontal or downward-looking view.

Independent Variables	Parameters of a system which are varied to investigate their effect on system performance.
Parabolic Approach	An approach in which the flight-path profile is concave downward such that the commanded altitude increases as the square root of the distance from the landing site.
PSD	Power Spectral Density - A measure of the amount, of energy contained in each frequency component of a signal.
RMS	Root-mean-square-- $\sqrt{\sum_{i=1}^{N} X_i^2 / N}$, where X_i denotes a measured parameter, and N is the total number of measurements recorded.
Standard Deviation	$\sqrt{\left[\sum_{i=1}^{N} (X_i - \bar{X})^2 / N\right]}$ where $\bar{X}$ is the mean value of the observations (X_i) and N is the total number of observations.
Statistical Significance	A probability statement that an observed difference deviates from zero by an amount greater than can be attributed to random sampling fluctuations.
VSD	Vertical Situation Display - A class of display formats which presents a vertical or forward-looking view.

SECTION I

INTRODUCTION

The unique performance capabilities of vertical takeoff and landing (VTOL) aircraft are significant contributors to the effectiveness and scope of tactical air operations. These capabilities allow terminal-area penetration and landing in terrain with a variety of topographical characteristics, with minimal or no landing site preparation required. Clearance of terrain obstructions adjacent to restricted landing areas can be accomplished by flying approach profiles consisting of relatively high vertical and low forward velocities and relatively high angles of attack. These nominal approach profile characteristics constitute what is commonly considered as a "steep-angle approach" (SAA). Steep approaches with rotary-wing aircraft, for example, include flight-path angles of 12 to 15 degrees or greater.

Operational steep-angle approaches are, however, currently limited to visual-flight-rule (VFR) conditions. If rotary-wing and other future generation vertical-lift aircraft are to accomplish their mission objectives independent of visibility conditions, operations into remote and restricted landing zones must be supported by an instrument-flight-rule (IFR) steep-approach capability. This capability should ultimately include landings under near zero-zero conditions to take full advantage of the potential of vertical-lift performance.

In the absence of VFR approach and landing cues, all flight-control information must be electronically sensed or computed for display to the pilot, with the pilot serving as a primary element in the control loop or, alternatively, as a monitor of automatic system performance. In either case, a comprehensive display of status and command information is necessary to facilitate the precise and reliable control of the vertical-lift aircraft during transition through the low-airspeed flight regime associated with a steep-approach gradient.

One of the objectives of the Joint Army-Navy Aircraft Instrumentation Research (JANAIR) Program has been to define, develop and evaluate display concepts for this purpose. As an initial step toward the definition of an IFR steep-angle approach and landing capability for vertical takeoff and landing (VTOL) aircraft, Honeywell was tasked to perform investigations which had the following primary objectives:

- Task I - The definition of displayed information parameters
  required for all-visibility, steep-angle approaches
  and landings with tactical vertical-lift aircraft of the
  1975 to 1980 era; and the development, simulation,
  and evaluation of alternative display formats incorporating the required information.

These investigations (Ref. 1) were oriented toward developing display system concepts by initially evaluating the display/operator/task interface. Consistent with this philosophy, the initial phase (Task I) of the SAA program emphasized the man-in-the-loop evaluation of alternative display formats for use in performance of the SAA task. Alternative display formats representative of both horizontal- and vertical-situation concepts were empirically evaluated by means of real-time man-in-the-loop simulation techniques. Approach-angle and profile characteristics were also evaluated to determine their differential effects upon piloting performance and to increase the generality of display-comparison results.

During the course of this investigation, several additional specific problem or task areas requiring further evaluation were identified. Each of these task areas is subsumed within, or related directly to, the problem of display requirements for IFR steep-angle approach with vertical-lift aircraft because each implies a category of conditions or constraints within which the selected display configuration may be operated. Relevant task areas identified for further study include:

- **Task II**   - The effect of approach-system noise and filter variables on pilot performance of the SAA task

- **Task III** - An evaluation of alternative vehicle control-augmentation modes

- **Task IV**   - Determination of the effects of varying wind conditions during SAA

- **Task V**   - Determination of the effects of selected situational contingencies during SAA

- **Task VI**   - Definition of preliminary recommendations for a manual SAA system based on the results of the above tasks.

Results of studies performed to evaluate effects of Task II and Task III variables above are the subject of this report. An outline of display and display-related variables investigated in the SAA program is shown in Table 1-1. It will be noted that evaluation of selected display formats and approach angles as variables has been continued in the Task II and III study phases reported here, supporting the overall objectives of this program ---the investigation of display requirements for manually controlled IFR steep-angle approaches.

Following is a brief description of the content of major sections of this report:

Table 1-1. SAA Variables Investigated

Variables or Conditions Evaluated	Study Phases		
	(Complete) I	(Current) II	III
Display Formats	IEVD PPI-AR PPI-IR F.D.	IEVD PPI-AR	IEVD PPI-AR
Approach Angles	6° 15° 24°	6° 15°	6° 15°
Aircraft	UH-1 XV-5	UH-1 XV-5	UH-1 XV-5
Approach Modes	Const. Slope Parabolic	Const. Slope	Const. Slope
Signal Filter Lags	None	Low Medium High	Low High
Signal Noise Levels	None	None Medium High	None High
Quickening Gains	High	High Low	High
Control Augmentation Modes	SAS	SAS	SAS SAS + OLCS SAS + ψHold SAS + OLCS + ψHold

(Shaded cells represent variables in each study phase)

1-3

- Background: Generic configurations of vertical-life aircraft and approach-aid systems are briefly reviewed for general reader orientation and background to the present study program.

- Study Definition - Task II: Descriptions of all variables and task characteristics simulated in the Task II study phase are presented.

- Preliminary Simulation - Task II: The training of pilot subjects, refinement of simulation methodology and selection of specific variable levels for investigation in the Task II study are described.

- Formal Simulation - Task II: The Task II experimental design for conducting formal investigations, dependent and independent variables evaluated, and data reduction procedures are presented.

- Study Results - Task II: Results yielded by the statistical and subjective analysis of performance data generated during Task II formal simulations are discussed.

- Study Definition - Task III: Descriptions of all variables and task characteristics simulated in the Task III study phase are presented.

- Preliminaty Simulation - Task III: The training of pilot subjects, refinement of simulation methodology and selection of specific variable levels for investigation in the Task III study are described.

- Formal Simulation - Task III: The Task III experimental design for conducting formal investigations, dependent and independent variables evaluated, and data reduction procedures are presented.

- Study Results - Task III: Results yielded by the statistical and subjective analysis of performance data generated during Task III formal simulations are discussed.

- Summary and Conclusions: Results of both Task II and Task III study phases are summarized, and conclusions are drawn as to the effects upon piloting performance of all experimental variables investigated.

SECTION II

BACKGROUND

Two primary requisites associated with the performance of IFR steep approaches and vertical landings are the vehicle itself and the approach-aid subsystems necessary to accomplish IFR penetration. Each of these systems is discussed briefly in the following paragraphs for reader orientation and to serve as a basis for the definition of the scope of the present study program.

VEHICLE REQUIREMENTS

A variety of aircraft configurations have the inherent design characteristics necessary for the performance of low-speed approaches and vertical landings. Generic features of all aircraft in this class are a lift-to-weight ratio greater than unity below aerodynamic stall speeds and controllable vehicle rotational and translational axes in the same speed range.

The majority of VTOL aircraft now operational or under prototype development are of one of the following types (representative examples of each type are also shown):

- Rotary-Wing: (Bell UH-1)
- Jet-Lift: (Hawker Siddeley Harrier)
- Tilt-Wing: (Ling-Temco-Vought XC-142)
- Compound Rotary-Wing: (Lockheed AH-56)
- Ducted-Fan: (Ryan XV-5)

Aircraft representing the first two vertical-life concepts are now operational, while the latter three are in the prototype-development and flight-test stages. Further discussion of these VTOL aircraft and other similar vertical-lift variations may be found in Reference 2 through 9. Control problems and design considerations associated with flight of these aircraft in the low-speed range are also discussed in these sources. Additional background information relating vertical-life aircraft applications and the steep-angle-approach problem is given in References 10 through 15.

In general, it can be stated that some degree of control and stability difficulty is experienced with all configurations, especially at the low airspeeds and high descent rates associated with a steep-angle approach. In addition to the common problems of excessive power requirement and low longitudinal aerodynamic stability resulting from flight at low substall airspeeds, each configuration has its relatively unique difficulties. Examples are blade-tip vortex

2-1

impingement, nose-up pitching moment, and wing-stall problems for rotary-winged, ducted-fan and tilt-winged configurations, respectively.

APPROACH AND LANDING-AID REQUIREMENTS

Three basic functions are served by the approach-aid system being proposed or now under development for tactical use with vertical-life aircraft (Ref. 16). Functions required are:

- The generation of a landing reference: The frame of reference with respect to the desired landing site must be defined

- The measurement of position relative to this reference: The approaching vehicle's position relative to this frame of reference must be determined.

- The choice of approach path: The desired approach path must be defined to allow computation of error and command information.

These functions are allocated in various combinations to ground-based and airborne components. Four configurations represent a majority of systems currently under study. These are:

- Airborne ground mapper, e.g., airborne radar

- Ground-based sky mapper with data link to aircraft

- Ground-based pattern generator and airborne pattern sensor (beam-guided system)

- Airborne radar tracker and ground-based omnidirectional beacon (beacon-guided system)

Ground-mapper systems represent the only non-cooperative configuration consisting of all airborne system components (unless used in conjunction with corner reflectors around a landing zone). Systems representative of the latter three configurations above are considered cooperative, having both ground and airborne components. Of these configurations, beam- and beacon-buided concepts are currently receiving the most developmental emphasis. In cooperative systems, measurement of aircraft position with respect to a desired landing zone is typically defined in spherical coordinates (range, bearing and elevation) which may in turn be transformed to position coordinates (X, Y and Z) referenced to the desired approach path.

A more detailed discussion of these various configurations, their operating characteristics and their required operating environment may be found in References 13 through 23.

SECTION III

STUDY DEFINITION - TASK II

OBJECTIVES

The primary objective of the Task II study phase was to investigate effects of approach-system noise and filter characteristics on pilot performance of the SAA task. Interactive effects of these variables were evaluated in conjunction with other relevant system variables to obtain increased generality of the study results.

Descriptions of all variables and task characteristics simulated in this study phase are given in the following paragraphs and in Appendix A. A more extensive treatment of the basis for development of display formats, quickening gains, and the approach and landing task simulated for this study is given in Reference 1.

AIRCRAFT SELECTION AND DESCRIPTION

Two aircraft simulated for use in this study were the Bell UH-1 helicopter and the Ryan XV-5 ducted-fan VTOL. These vehicles are representative of two general configurations of tactical vertical-life aircraft potentially operational in the 1975 and 1980 time period. Other factors in the choice of these aircraft were the availability of data and the status of contemporary simulations.

- Ryan XV-5: This vehicle is a mid-wing, ducted-fan research aircraft. It is capable of conventional takeoff and landing (CTOL) and flight to high subsonic speeds in addition to its VTOL performance in the fan-supported mode. The three-view drawing in Figure 3-1 (from Ref. 24) indicates the dimensions and configuration of the vehicle. For aerodynamic flight, manual control is through control stick and rudder pedals to conventional aerodynamic surfaces. In the fan mode of operation, attitude, thrust direction, and lift are controlled primarily through the collective and differential vectoring of louvers mounted directly under the wing fans, and doors under the nose fan. Louver and door operations and the resulting control functions for this vehicle are shown in Figure 3-2.

- Bell UH-1: The UH-1 is a turbine-powered single-rotor helicopter. It has a gross weight of between 8500 and 9500 pounds and a cruise speed of 120 to 140 mph, depending on model suffix designation. Rate of climb is approximately 2350 ft/min. A three-view drawing of the UH-1 is shown in Figure 3-3 (from Ref. 25). The main rotor is a two
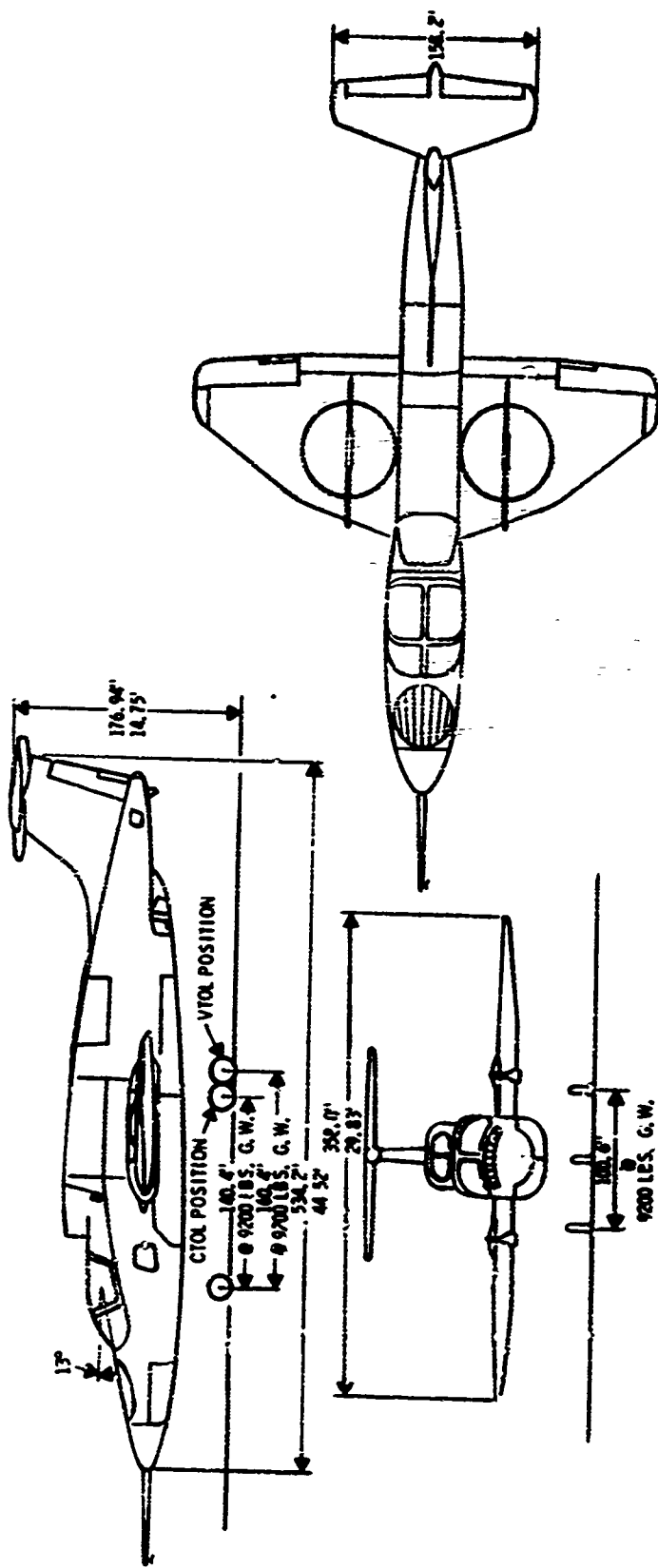
Figure 3-1. Ryan XV-5: Three-View Drawing
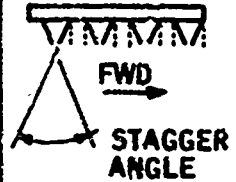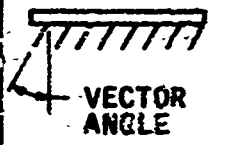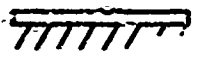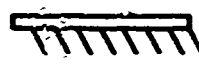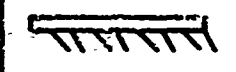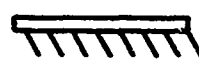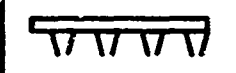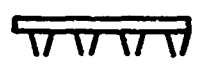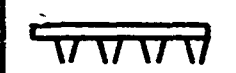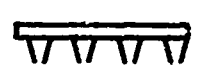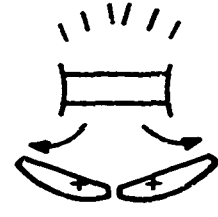
RIGHT FAN	LEFT FAN	NOSE FAN	FUNCTION
FWD → STAGGER ANGLE	FWD →		LIFT-COLLECTIVE STAGGER
VECTOR ANGLE			ACCELERATION CONTROL-COLLECTIVE VECTOR
			DIRECTIONAL TRIM AND CONTROL-DIFFERENTIAL VECTORING
			LATERAL TRIM AND CONTROL-DIFFERENTIAL STAGGER
			PITCH TRIM AND CONTROL (NOSE UP)
			PITCH TRIM AND CONTROL (NOSE DOWN)

Figure 3-2.   VTOL Flight-Control System Operation

3-3
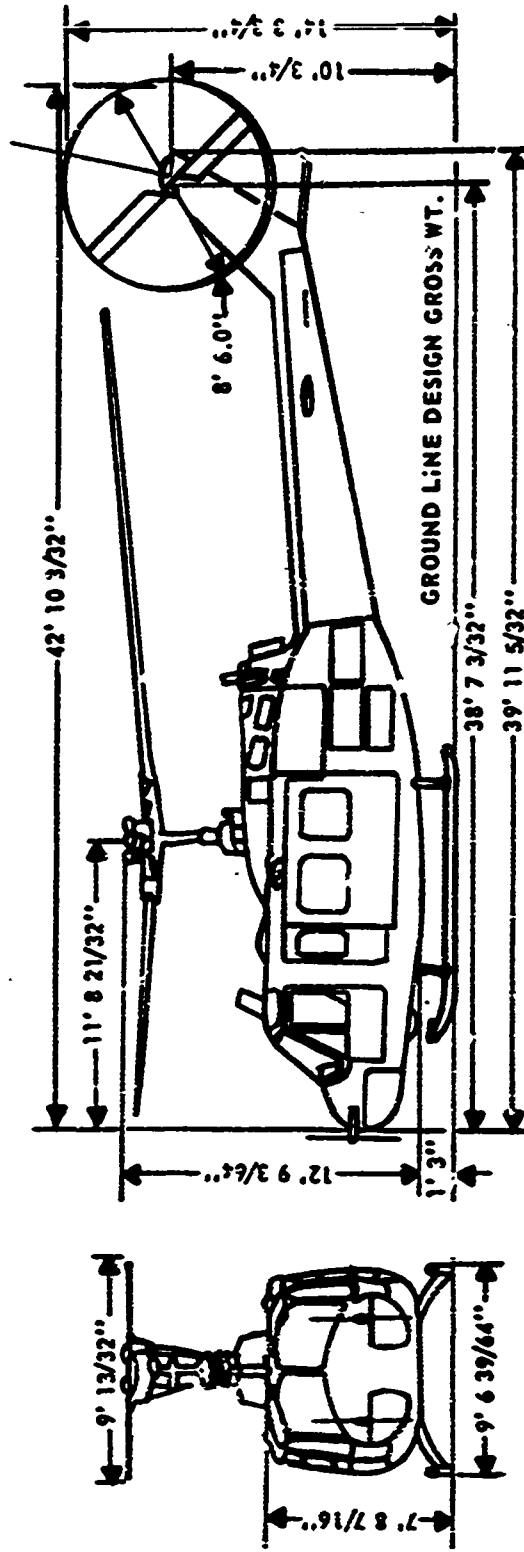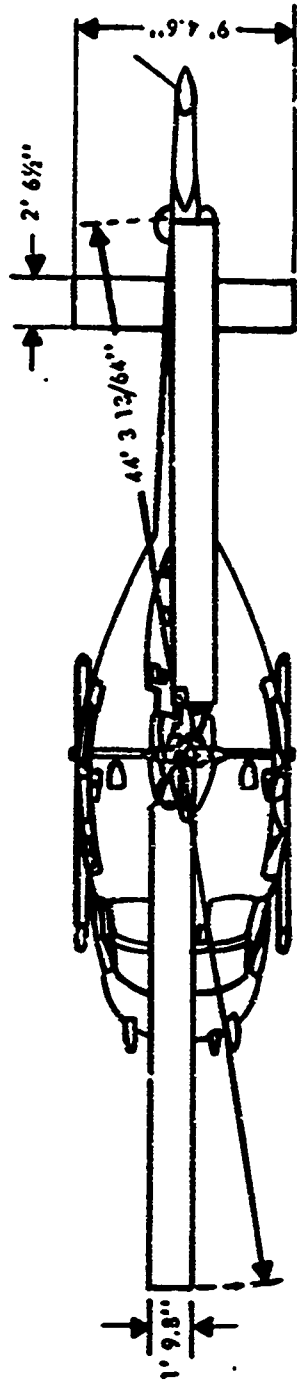
Figure 3-3. Bell UH-1: Three-View Drawing

bladed see-saw type and is speed governed over its operating range. A degree of stability augmentation is provided by a damped stabilizer bar 90 degrees out of phase with the rotor blades. The flight control system is a conventional helicopter mechanical-boost type which controls collective and cyclic pitch and tail rotor. Fore-and-aft cyclic pitch is augmented by an aerodynamic elevator for increased controllability and extended center-of-gravity (cg) range.

Variable-velocity simulations of both aircraft were programmed on Honeywell's hybrid-computer facility (see Appendix A). Nonlinear force and moment equations and aerodynamic lags were computed digitally, while inertial dynamics were synthesized on the analog portion of the hybrid simulator. Examples of the flight characteristics gained by this variable-velocity simulation technique include: (1) complete aerodynamic cross coupling in all control axes in the presence of gusts, control inputs and vehicle drift rates and (2) continuous change in vehicle trim conditions as a function of airspeed, mass loading and aerodynamic loading.

APPROACH-TASK DEFINITION

The approach and landing task simulated was considered to represent the terminal segment of a nominal tactical mission, beginning at the point of acquisition of a ground-based approach and landing aid, and terminating at touch down.

Based on information gained in previous studies (Ref. 1) from questionnaire and literature sources, the following assumptions were made in defining the approach and landing task simulated:

- Localizer (lateral-position) error at the point of acquisition resulting from enroute navigation errors would be nulled prior to glide-slope capture.

- Except for initial heading changes necessary for localizer null, the approach would be directly toward the landing site to minimize low-altitude and low-speed exposure in the terminal area.

- Approaches would be commanded to a hover point of 50 feet above the landing site rather than directly to the ground.

- An approach profile would be commanded such that a minimum of 90 seconds would be spent on the glide slope.

Simplified plan and profile views of this approach- and landing-mission segment are shown in Figures 3-4 and 3-5. This segment is divided into four phases:

- Initial approach: Localizer acquisition is initiated from a course parallel to the commanded approach course but with some degree of lateral error resulting from enroute navigation inaccuracy. This error is nulled, and ground-speed is reduced to that required for glide-slope intercept.

- Final approach: The glide slope is acquired, and the commanded flight path is maintained to the point of hover.

- Hover: The hover point is maintained until descent is commanded.

- Descent: Longitudinal and lateral position are maintained while power is reduced for a descent to touch down.

The primary piloting tasks associated with each phase are summarized below:

- Initial-Approach Phase

    - Maintain stable vehicle attitudes

    - Null lateral flight-path error

    - Maintain commanded altitude

    - Establish commanded ground speed

- Final-Approach Phase

    - Maintain stable vehicle attitudes

    - Maintain lateral flight-path null

    - Establish and maintain vertical flight-path null

    - Maintain commanded ground speed

    - Decelerate forward and vertical velocities as commanded

3-6

LATERAL DEVIATION
W.R.T. GLIDE PATH

RIGHT

0

LEFT

FINAL
APPROACH

INITIAL
APPROACH

②

③

←RANGE→

①

① LOCALIZER ACQUISITION

② GLIDE-SLOPE ACQUISITION

③ HOVER PRIOR TO DESCENT TO T.D.
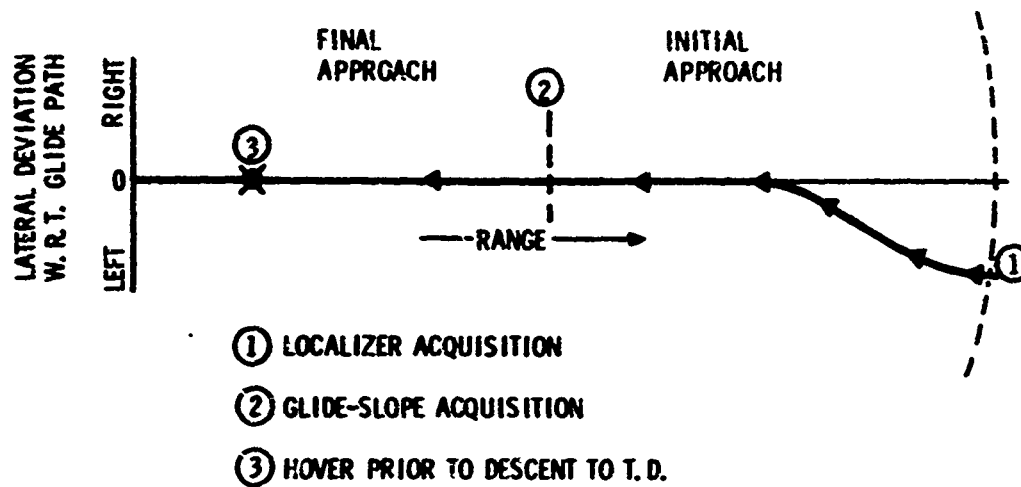
Figure 3-4.   Simplified Plan View of Approach-Mission
Segment

ALTITUDE →

②

INITIAL
APPROACH

①

FINAL
APPROACH

③

T.D.

←RANGE→

①
• LOCALIZER ACQUISITION
• TERMINATION OF ENROUTE-NAVIGATION TASK
• BEGINNING OF APPROACH AND LANDING TASK

② • GLIDE-SLOPE ACQUISITION

③ • HOVER PRIOR TO DESCENT TO T.D.
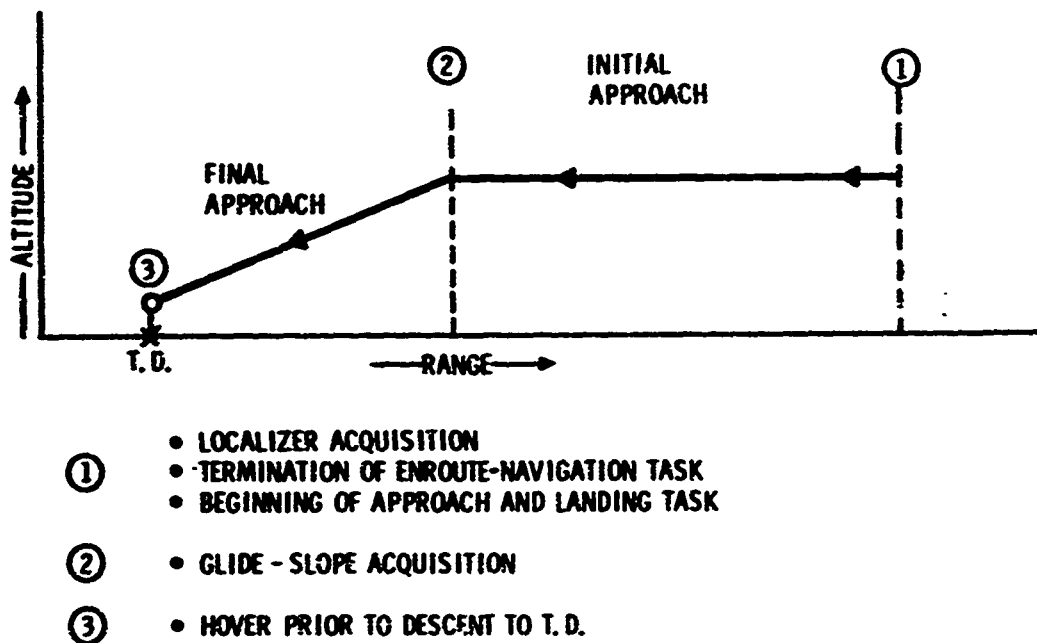
Figure 3-5.   Simplified Profile View of Approach-Mission
Segment

3-7

- **Hover Phase**

  - Maintain stable vehicle attitudes

  - Establish and maintain commanded lateral position
    (with respect to landing site)

  - Establish and maintain commanded longitudinal
    position

  - Maintain commanded altitude

- **Descent Phase**

  - Maintain stable vehicle attitudes

  - Maintain commanded lateral position

  - Maintain commanded longitudinal position

  - Establish safe vertical descent rate

  - Minimize horizontal translation rates

APPROACH-ANGLE SELECTION AND DESCRIPTION

Two alternative "final-approach" angles were simulated in the Task II study. Constant-gradient glide-slope angles of 6 and 15 degrees were selected to cover the range of steep angles generally considered to be feasible for operational vertical-lift aircraft. In Figure 3-6 corresponding terrain or obstacle clearance altitudes for the 6- and 15-degree slopes terminating at a 50-foot hover altitude are compared with a more shallow slope of 3 degrees. At a ground range of 1000 feet from a landing site, for example, terrain-clearance altitude for the 15-degree slope is approximately three times that of the 3-degree slope. If these slopes were terminated at the landing site (zero altitude) rather than at hover, clearance altitudes for the 6-degree slope would be approximately double those resulting with the more shallow 3-degree slope.

Three constraints applied in defining these glide slopes were: (1) that the duration of the final approach be 90 seconds, (2) that the total commanded deceleration not exceed 2.4 ft/sec^2, and (3) that the commanded descent rates for the 6- and 15-degree approaches be 684 and 1290 ft/min, respectively. These constraints established a unique initial altitude and range for each approach angle. Descent rates were based on data given in Reference 14. Although numerous sources referenced discussed approach angles feasible, only the above-referenced study yielded sufficient actual flight data from
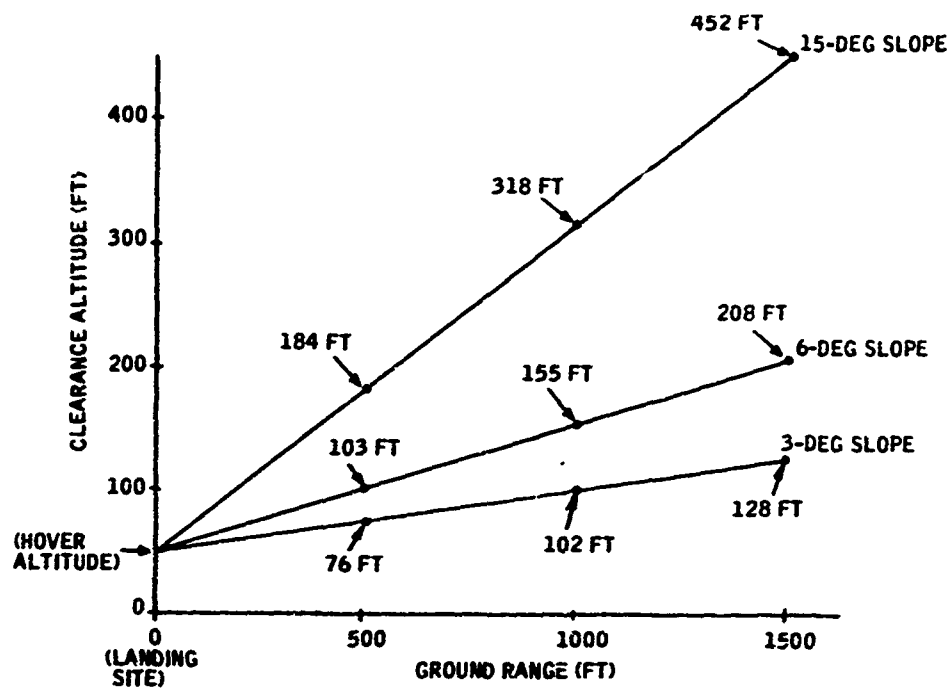
Figure 3-6. Obstacle Clearance Altitudes for Various Approach
Angles versus Range-to-Hover Point

which the forward- and vertical-velocity components typically experienced
during steep approaches could be estimated. In this study (Ref. 14), an S-61N
helicopter was flown on approach glide-path angles of from 3 to 55 degrees
during flight tests of a portable approach-aid system. Descent rates experi-
enced were recorded at intervals of altitude and presented in the above-
referenced report. Data from this report for angles of 3, 6, 9, 15, and 24
degrees were averaged for each angle and are shown in Figure 3-7. A
regression line was fitted to data for angles up to 15 degrees, as shown in
this figure, with a zero-slope straight-line fit representing angles beyond
15 degrees. This function showing the relationship between approach angle
and vertical velocity served as a basis for selecting the vertical- and forward-
velocity components to be commanded for the approach angles used in the
present study.

During the approaches programmed for the Task II SAA study (Figure 3-8)
the pilot was commanded a constant ground speed and descent rate to a point
from which a deceleration of both ground speed and descent rate was com-
manded. Deceleration was commanded such that total deceleration was
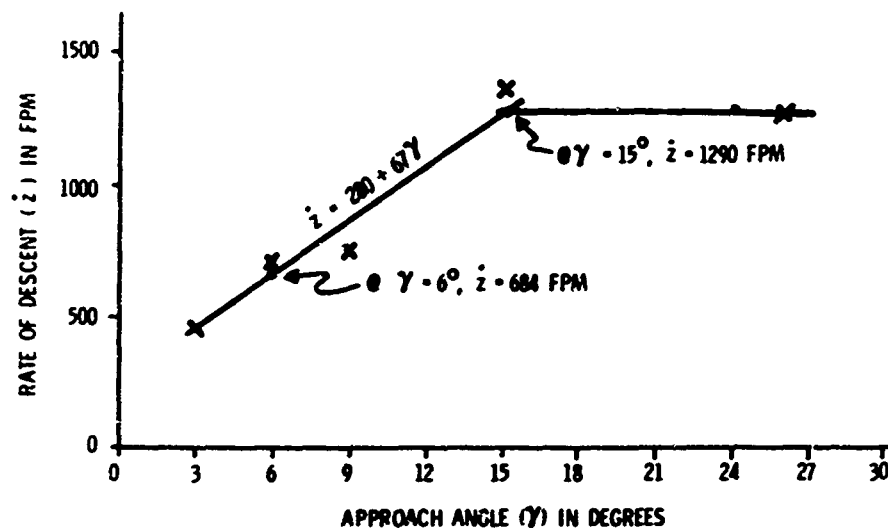
Figure 3-7. FAA Report Data: S-61N Helicopter

0.075g, with ground speed and descent rate being reduced to zero at the hover position. The entire final approach, assuming exact following of displayed commands, required 90 seconds.

DISPLAY-FORMAT SELECTION AND DESCRIPTION

Two of four display-format alternatives previously investigated (Ref. 1) were selected for continued simulation and evaluation in the Task II study. Each format consisted of an aircraft-referenced primary display and associated peripheral instrumentation, with the latter being selected as necessary for the presentation of information parameters not included on the primary display. Variations between formats were limited, to the greatest possible extent, to the primary-display configurations.

The two primary displays selected are representative of two general modes or categories of display-information presentation: (1) vertical-situation displays and (2) horizontal-situation displays. In the first category are those displays which are oriented normal to the ground plane and typically present a forward-looking view to the pilot. The second category includes those displays depicting the ground plane itself, presenting a downward-looking view. The configurations selected were:

ALTITUDE (FEET)

GROUNDSPEED : 36 kt
DESCENT   390 ft/min

GROUNDSPEED 52 kt
DESCENT   550 ft/min

RANGE (FEET)

SEGMENT 2

Groundspeed and descent rate are
decelerated to zero at constant,
but unequal, rates.

Hover is defined at the end of
segment 2, at an altitude of 50 ft
with descent rate and groundspeed
= 0.

SEGMENT 1

Groundspeed (64 kt) and descent rate (584 ft/min) are constant.
The groundspeed is a continuation from the area outside segment 1,
while the 684-ft/min descent is commanded upon entrance to
segment 1.

Prior to segment 1,
flight has been at
constant altitude for
60 seconds.

(a) 6-degree Approach

ALTITUDE (FEET)

GROUNDSPEED -   kt
DESCENT = 930 ft/min

RANGE (FEET)

SEGMENT 2

Groundspeed and
descent rate are de-
creased to zero at
constant, but unequal,
rates.

Hover is defined at the
end of segment 2, at
an altitude of 50 ft
with descent rate and
groundspeed = 0.

SEGMENT 1

Groundspeed (47 kt) and descent rate (1290 ft/min) are constant.

The groundspeed is a continuation from the area outside segment 1,
while the 1290-ft/min descent rate is commanded upon entrance to
segment 1.

Prior to segment 1,
flight has been at
constant altitude for
60 seconds.

(b) 15-degree Approach

Figure 3-8.   Constant-Slope Approaches

3-11

- Vertical-Situation Display
  - IEVD (Integrated Electronic Vertical Display)

- Horizontal-Situation Display
  - Aircraft-Referenced PPI (Plan Position Indicator)

A detailed description of these formats is given in the following paragraphs.

IEVD Format

The vertical-situation format evaluated was a simulation of the Norden IEVD (Refs. 26 and 27). Format characteristics simulated for the present study were selected to represent the most significant features of the IEVD concept, but with some variation and simplification to facilitate computer-programming requirements and to most efficiently adapt the general display concept for use with the IFR steep-approach and landing task simulated. The IEVD display format, as simulated (Figure 3-9), consisted of the primary IEVD display, a sideslip indicator directly above the IEVD, and rate-of-climb, vector-angle, and BDHI (bearing, distance, heading) indicators to the left of and below the IEVD.
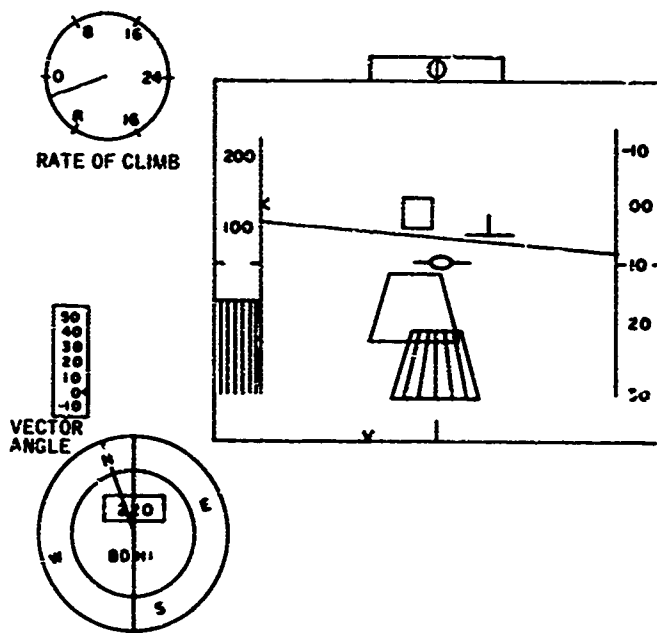
Figure 3-9. IEVD Format

Display elements, and their functions, are summarized in Table 3-1. Altitude and airspeed (ground speed as simulated) tapes are located at the left and right sides, respectively, of the IEVD, with an artificial horizon shown between the two tapes. Command-altitude information was displayed on a cursor adjacent to the altitude tape. Fiducial marks at tape center indicated actual altitude and also served as a null reference for the altitude cursor. Tracking the moving cursor to scale center was required to maintain commanded altitude. This symbol was driven by combined altitude-error and altitude-rate-error terms with gains of $K_Z = 0.01$ in/ft and $K_{\dot{Z}} = 0.05$ in/ft/sec, respectively.

Position errors during hover and descent phases were displayed as deviations of a trapezoid (command position) from a stationary longitudinally-lined trapezoid (own-ship position) with a scaling of 0.01 in/ft. Similarly, scaling of the square "ILS symbol," used for the display of vertical and lateral glide-path error, was 0.01 in/ft on both axes. Null for this symbol was a static boresight reference located at display center.

The inverted T-shaped "lead-vehicle" symbol served as the longitudinal- and lateral-quickened element on the IEVD. This symbol was also referenced to the center boresight, and translated vertically and laterally to command pitch and roll inputs (see Figure 3-10). The fixed boresight was tracked to the moving quickened element in a "fly-to" manner to be consistent with the reference axes and orientation of this display format.
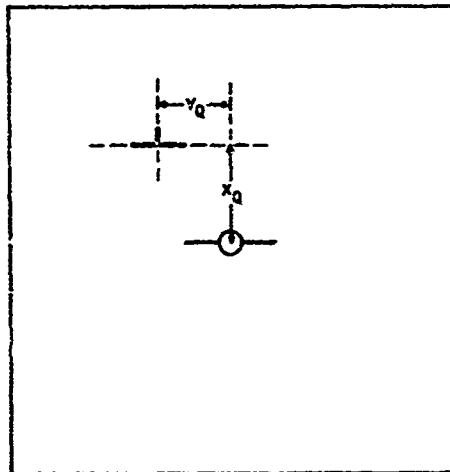
Figure 3-10. IEVD Format: Quickened-Symbol Movement Axes

Heading information was integrated into the IEVD in the form of a simplified heading-command cursor (approach-path course) referenced to a fiducial mark along the bottom edge of the display, and was scaled at ±45 degrees full-scale deflection. Artificial-horizon pitch-axis scaling was ±25 degrees for full deflection.

Table 3-1. IEVD Format Instrumentation: Moving
Display Elements and Functions

Indicator	Display Element	Display Function	Driving Functions
IEVD	Lead Vehicle Symbol	Longitudinal- and lateral-quickened command	Longitudinal: Pitch-axis quickening (X_Q) Lateral: Roll-axis quickening (Y_Q)
	Artificial Horizon	Pitch and roll attitude	Pitch and roll attitudes
	Altitude Tape	Altitude	Altitude relative to landing site
	Altitude Cursor	Altitude command	Altitude error and altitude-rate error
	Forward Speed Tape	Ground speed	Ground speed
	Heading Cursor	Heading	Approach heading (relative to aircraft heading)
	ILS Symbol	Glide path	Vertical and lateral glide-path deviation
	Command Position Symbol	Hover indicator	Command longitudinal and lateral position during hover and descent
Sideslip Indicator	Lateral Scale	Sideslip	Aircraft sideslip
BDHI	Heading Dial	Heading	Aircraft heading
	Radius Line	Relative bearing	Relative bearing to landing site
	Digital Readout	Range	Ground range to landing site
Vector-Angle Indicator	Vertical Scale	Vector angle	Collective vector angle (XV-5 aircraft)
Rate-of-Climb Indicator	Dial	Rate of climb	Vertical velocity

3-14

Not shown in Figure 3-9 is a warning indicator (flashing "X" symbol) placed directly below the primary IEVD display. This symbol appeared during the 500-foot intervals prior to glide-slope intercept and prior to the deceleration command at termination on the final-approach phase, thus serving to warn the pilot of these two significant pending changes in commanded vertical and forward velocity.

The static representation in Figure 3-9 shows a situation near the end of the approach as it would appear on the IEVD format. Depicted in this example are the following status and command information cues:

- Range to the desired hover point is 220 feet (numeric readout on BDHI).

- Aircraft heading is approximately 015 degrees (heading dial on BDHI).

- Relative bearing to hover point is approximately 340 degrees (radius line on BDHI).

- Aircraft is descending at approximately 250 ft/min (rate of climb dial).

- Aircraft altitude is 50 feet (tape on left side of IEVD).

- Ground speed is 10 knots (tape on right side of IEVD).

- Aircraft is pitched down and rolled left approximately 4 degrees and 5 degrees, respectively, (horizon line on IEVD).

- Aircraft is below and to right of desired glide path ("ILS symbol" on IEVD is above and to left of boresight symbol).

- Aircraft is approaching hover point with small lateral error to the right of desired path ("command position" trapezoid on IEVD is above and to left of "own-ship position" trapezoid).

- Pilot is being commanded to pitch up and roll left to obtain additional deceleration and lateral-position correction, respectively, ("lead vehicle" symbol on IEVD is above and to right of boresight symbol).

- Pilot is being commanded to increase collective lift input to obtain additional altitude (altitude-command cursor on IEVD is above altitude tape fiducial marks).

3-15

- Pilot is being commanded a left rudder or antitorque pedal input to return aircraft to desired approach heading (heading-command cursor on IEVD is to left of its fiducial mark reference).

The total IEVD format, including peripheral instrumentation, was computed digitally and displayed on a 19-inch-diagonal CRT. Dimensions of the primary IEVD display, as simulated, were 7 by 7 inches.

PPI Format

The aircraft-referenced PPI format evaluated is shown in Figure 3-11. This format included a centrally located PPI primary display and peripheral instruments. A downward-looking view is presented on this primary display, with the vertical display axis referenced to the longitudinal axis of the aircraft.
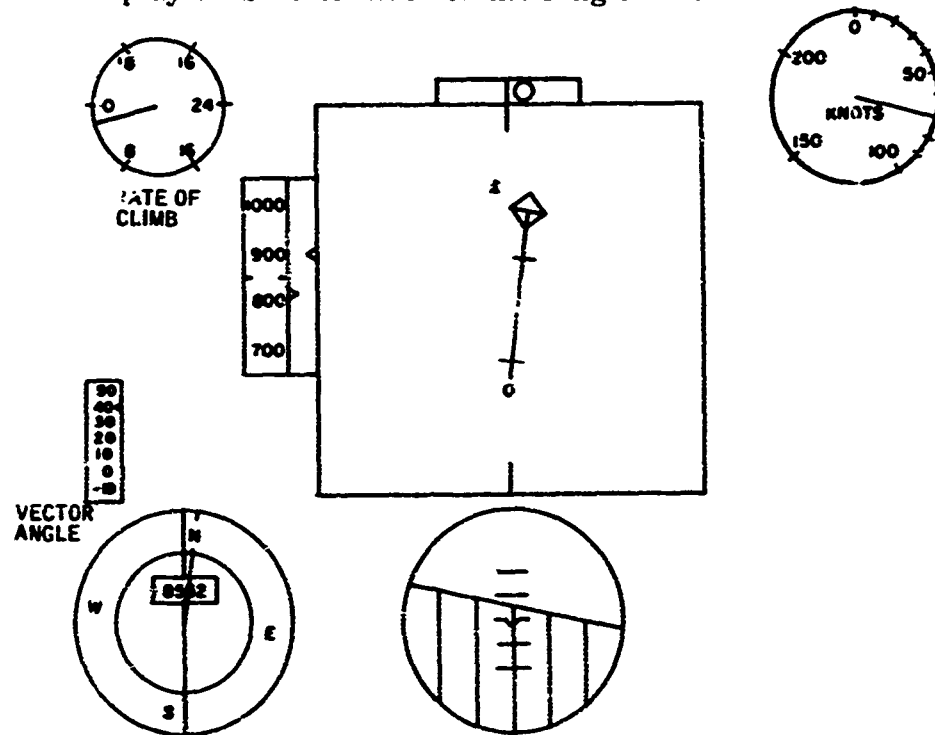
Figure 3-11. Aircraft-Referenced PPI Format

Own-ship position within the PPI display space was indicated by a circle located 1.5 inches from bottom display center. Although aircraft-referenced, the PPI was earth-stabilized with respect to aircraft pitch and roll attitude to avoid translations of the moving approach-path and landing-site symbology with attitude changes on these axes. Translational movements of this symbology depicted a change in aircraft position, while rotational movements about the

earth-stabilized vertical aircraft axis (own-ship symbol) indicated aircraft
heading relative to commanded approach heading. Computed landing-site
position was shown as the center of a scaled 1000-foot-diameter box, with a
line representing the command-approach path projecting outward from the
landing-site point. Two markers located on the approach-path line (shown
in Figure 3-11) represented the points of glide-slope intercept and decelera-
tion command. Scale sensitivity of the display ground-plane and approach-
path and landing-site symbology was increased with decreasing range at two
points during the approach. The initial PPI scaling was 4000 ft/in. (4000 feet
per inch of display) on both axes, with changes to 2000 ft/in. and 750 ft/in.
at ranges of 500 feet prior to glide-slope intercept and deceleration-command
points, respectively. These scale changes resulted in increased PPI status
display sensitivity as the aircraft approached the landing site and were accom-
plished at intervals during the approach profile selected to minimize inter-
ference with the piloting task. Also, because of the scale-change points
selected, the changes in display scaling themselves served as a warning of
impending glide-slope intercept and deceleration-command maneuvers.

A summary of the central and peripheral display elements and functions associ-
ated with the Aircraft-Referenced PPI Format is given in Table 3-2. Rate-of-
climb, sideslip, vector-angle, and BDHI indicators were identical to those
programmed for use with the IEVD. Additional peripheral instrumentation
required for the PPI format included groundspeed, attitude, and altitude indi-
cators located to the right, below, and left, respectively, of the central PPI.
The altitude indicator consisted of an altitude tape similar to that programmed
for the IEVD, and two vertically moving cursors. The cursor located imme-
diately to the right of the altitude tape displayed command altitude, or altitude
error, while the second cursor was driven by altitude-rate error scaled at
$K_{\dot{Z}} = 0.05$ in/ft/sec. Assuming an initial altitude error, tracking the rate-
error cursor against the altitude-error cursor resulted in a return of the air-
craft to its commanded altitude. Maintenance of commanded altitude then
resulted in both cursors positioned directly across from the fiducial marks
(actual altitude) at tape center.

An asterisk served as the longitudinal- and lateral-quickened element on the
PPI display. The PPI landing-site point represented the command-tracking
reference for the quickened element, with vertical and lateral quickened-symbol
deviations from the landing site corresponding to aircraft pitch and roll com-
mands, respectively, (see Figure 3-12).

3-17

Table 3-2. Aircraft-Referenced PPI Format Instrumentation: Moving Display Elements and Functions

Indicator	Display Element	Display Function	Driving Functions
PPI	Asterisk	Longitudinal- and lateral-quickened command	Longitudinal: Pitch-axis quickening (X_Q); Lateral: Roll-axis quickening (Y_Q)
	Approach-Path/Landing-Site Symbol	Position, heading, and quickened tracking reference	• Landing-site position relative to aircraft; • Approach heading relative to aircraft heading
Sideslip Indicator	Lateral Scale	Sideslip	Aircraft sideslip
Ground-Speed Indicator	Dial	Ground speed	Ground speed
Attitude Indicator	Artificial Horizon	Pitch and roll attitudes	Pitch and roll attitudes
BDHI	Heading Dial	Heading	Aircraft heading
	Radius Line	Relative bearing	Relative bearing to landing site
	Digital Readout	Range	Ground range to landing site
Vector-Angle Indicator	Vertical Scale	Vector angle	Collective vector angle (XV-5 aircraft)
Altitude Indicator	Altitude Tape	Altitude	Altitude relative to landing site
	Altitude Cursor	Altitude command	Commanded altitude
	Altitude-Rate Cursor	Command-altitude tracking symbol	Altitude-rate error
Rate-of-Climb Indicator	Dial	Rate of climb	Vertical velocity
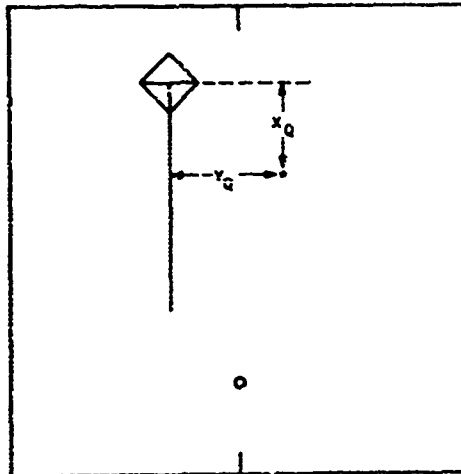
Figure 3-12. Aircraft-Referenced PPI Format: Quickened
Symbol Movement Axes

The static representation in Figure 3-11 depicts a situation near the point of glideslope intercept as it would appear on the aircraft-referenced PPI format. The following status and command information cues are indicated:

- Range to the desired hover point is 8552 feet (numeric readout on BDHI)

- Aircraft heading is approximately 350 degrees (heading dial on BDHI)

- Relative bearing to hover point is approximately 5 degrees (radius line on BDHI)

- Aircraft is descending at approximately 200 ft/min (rate-of-climb dial)

- Aircraft altitude is 850 feet (altitude tape to left of PPI)

- Ground speed is 70 knots (dial to right of PPI)

- Aircraft is pitched down and rolled left approximately 4 degrees and 10 degrees, respectively (artificial horizon below PPI)

- Aircraft is near lateral alignment with desired flight path ("Own-ship position" symbol on PPI is approximately aligned with the command approach path)

- Aircraft is above desired flight path (cursor immediately to right of altitude tape indicates command altitude of 810 feet)

- Pilot is being commanded to pitch up and roll right to decelerate to command ground speed and maintain lateral flight path alignment, respectively (quickened tracking symbol on PPI is above and to left of its landing-site reference point)

- Pilot is being commanded to decrease collective lift input to descend to command altitude (altitude-rate cursor to left of PPI is above command-altitude cursor)

- Pilot is being commanded a right rudder or antitorque pedal input to null aircraft slip angle (sideslip indicator ball is to right of its center reference)

As with the IEVD format, the PPI display format was computed digitally and displayed on a 19-inch-diagonal CRT. Dimensions of the primary PPI display were 7 by 7 inches.

DISPLAY-QUICKENING SELECTION AND DESCRIPTION

In addition to the basic information parameters displayed on each format, a requirement for the display of quickened or derivative information to the pilot was determined (Ref. 1). This requirement was based on results of vehicle stability analyses performed, and the definition of approach profiles to be flown.

Complexity of the lateral and longitudinal control task was reduced by the display of quickened information consisting of the sum of position-derivative terms with appropriate weighting coefficients. Quickening terms were combined to drive a single tracking symbol on each of the primary displays. The displaced position of the quickened symbol from its command tracking reference was calculated by the following equations:

At a range greater than 50 feet from hover point

$$X_Q = K_{\dot{X}} (\dot{X}_I - \dot{X}_C) + K_\theta \theta$$

$$Y_Q = K_Y (Y_I - Y_C) + K_{\dot{Y}} \dot{Y}_I + K_\phi \phi$$

and at a range of less than 50 feet from hover point

$$X_Q = K_X (X_B - X_C) + K_{\dot{X}} \dot{X}_B + K_\theta \theta$$

$$Y_Q = K_Y (Y_B - Y_C) + K_{\dot{Y}} \dot{Y}_B + K_\phi \phi$$

where

X_Q, Y_Q = pitch- and roll-axis components of distance, on display, of quickened symbol from it   commanded position

K_X, K_Y = longitudinal and lateral position-error coefficients

$K_{\dot{X}}, K_{\dot{Y}}$ = longitudinal and lateral velocity coefficients

K_θ, K_ϕ = pitch- and roll-attitude coefficients

X_B, Y_B = body-axis longitudinal and lateral positions

X_C, Y_C = commanded longitudinal and lateral positions

X_I, Y_I = inertial-axis longitudinal and lateral positions

$\dot{X}_B, \dot{Y}_B$ = body-axis longitudinal and lateral velocities

$\dot{X}_C$ = commanded forward velocity

$\dot{X}_I, \dot{Y}_I$ = inertial-axis longitudinal and lateral velocities

θ = pitch attitude (high passed with 5-second time constant to allow for change of pitch trim with velocity

ϕ = roll attitude

During the initial- and final-approach phases, and to a range of 50 feet from the hover point, a rate of closure toward the landing site was commanded ($\dot{X}_C$). As can be noted above, the form of the pitch-axis quickening equation was then changed, as the aircraft approached to within 50 feet of the hover point, to command a position (X_C) rather than a closure rate.

Also at a range of 50 feet, the reference axes for the equations were changed from an inertial-axis (landing-site) reference frame to a body-axis (aircraft) reference frame. This distinction is shown in Figures 3-13 and 3-14. During the approach phases (Figure 3-13) null of a specific approach path was commanded. After the aircraft had penetrated to within 50 feet of the hover point (Figure 3-14), aircraft velocity was assumed to be at or near zero, and a minimum-distance translation directly toward the hover point was commanded, independent of aircraft heading or direction of position error.

3-21
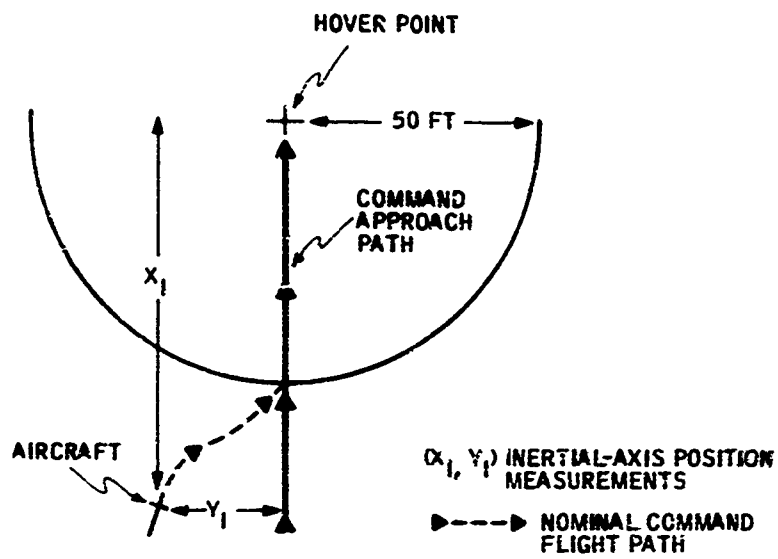
Figure 3-13. Inertial Reference Axes
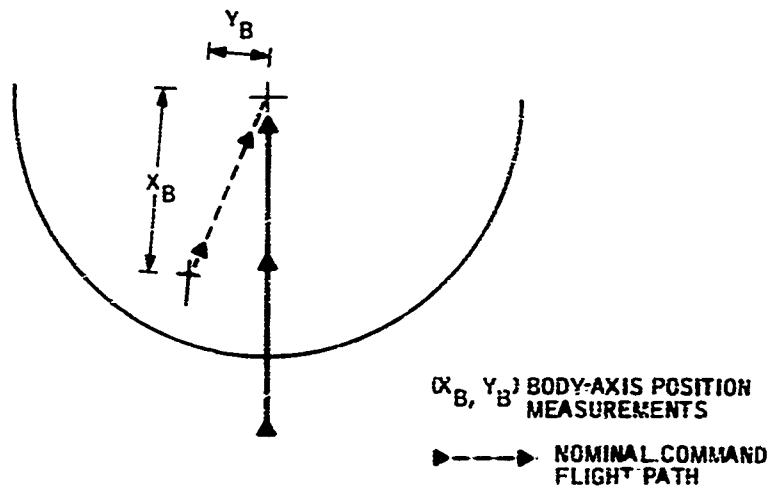
Figure 3-14. Body Reference Axes

Two sets of lateral and longitudinal quickening-term coefficients were tested in the Task II study. Quickening gains were introduced as an experimental variable in this study to evaluate the interactive effects of quickening gain with varying levels of noise introduced into the nominal approach-aid system assumed. As indicated in the discussion of simulated system-noise characteristics which follows this subsection, position and translational-velocity quickening terms were computed from sensed bearing, elevation and range information, and were therefore sensitive to noise characteristics of these signals.

One set of coefficients evaluated was identical to those used in the initial study phase of the SAA program (Ref. 1). These "high-gain" coefficients, listed below, were previously found to yield stable and precise pilot-control performance under conditions of no system noise.

- High-gain coefficients

$$\underline{\text{XV-5}}$$

Pitch axis	Roll axis
$K_X = 0.0044$	$K_Y = 0.0022$ in. /ft
$K_{\dot{X}} = 0.044$	$K_{\dot{Y}} = 0.044$ in. /ft/sec
$K_\theta = 0.132$	$K_\varphi = 0.059$ in. /deg

$$\underline{\text{UH-1}}$$

Pitch axis	Roll axis
$K_X = 0.0044$	$K_Y = 0.0022$ in. /ft
$K_{\dot{X}} = 0.044$	$K_{\dot{Y}} = 0.044$ in. /ft/sec
$K_\theta = 0.092$	$K_\varphi = 0.039$ in. /deg

Coefficients listed are interpreted as, for example, $K_X = 0.0044$ inch of quickened-symbol displacement on the display per foot of longitudinal position error.

The set of "low-gain" coefficients listed below constituted a second level of the quickening-gain variable evaluated. Based on preliminary simulations, these coefficients were selected as approximate minimum values for the reduction of effects of system noise without significantly degrading overall piloting performance on the approach and landing task simulated.

3-23

- Low-gain coefficients

<div align="center">XV-5</div>

Pitch axis	Roll axis
K_X = 0.0022	K_Y = 0.0011 in./ft
$K_{\dot{X}}$ = 0.022	$K_{\dot{Y}}$ = 0.022 in./ft/sec
K_θ = 0.066	K_ϕ = 0.030 in./deg

<div align="center">UH-1</div>

Pitch axis	Roll axis
K_X = 0.0022	K_Y = 0.0011 in./ft
$K_{\dot{X}}$ = 0.022	$K_{\dot{Y}}$ = 0.022 ft./ft/sec
K_θ = 0.092	K_ϕ = 0.039 in./deg

It may be noted that, with two exceptions (K_θ and K_ϕ for the UH-1 vehicle), these coefficients are one-half the values of high-gain coefficients. However, all position and translational-velocity terms, or all terms sensitive to approach-system noise, were reduced to one-half the high-gain values.

APPROACH-GUIDANCE-SYSTEM NOISE CHARACTERISTICS SIMULATED

Calculation Model

As previously indicated, one of the primary objectives of the Task II study was to evaluate the effects of approach-guidance-system noise on performance of the IFR steep-angle approach task. However, since the objective was not to investigate characteristics of any one specific guidance system, a generalized model was defined for simulation which was conceptually similar to a number of guidance systems currently under development. The concept assumed, shown in simplified form in Figure 3-15, was a cooperative system consisting of both ground and airborne components combined to serve three basic functions listed in Section II of this report: (1) generation of a landing reference; (2) measurement of position relative to this reference; and (3) choice of approach path. This concept as developed for simulation purposes did not consider the actual technique of measurement, but did assume the availability of sensed signals representing aircraft slant range, bearing and elevation with respect to a desired ground station.

<div align="center">3-24</div>
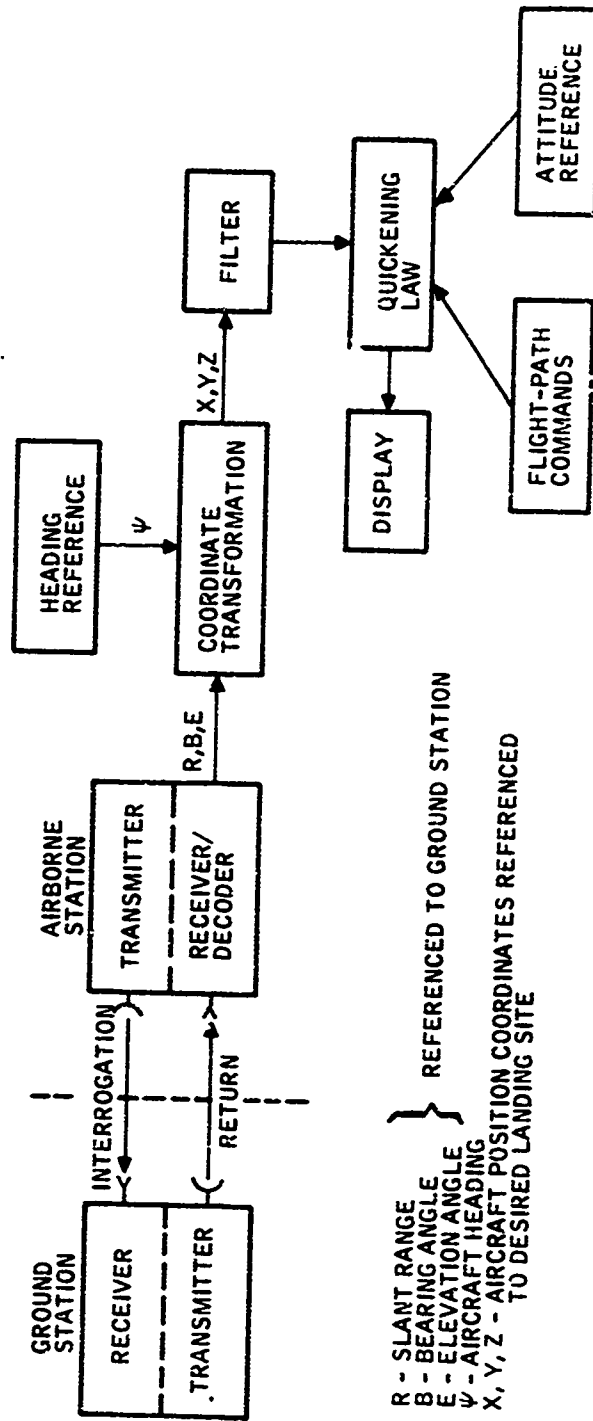
Figure 3-15. Assumed Approach-Guidance System

R — SLANT RANGE
B — BEARING ANGLE
E — ELEVATION ANGLE
ψ — AIRCRAFT HEADING
X, Y, Z — AIRCRAFT POSITION COORDINATES REFERENCED TO DESIRED LANDING SITE

} REFERENCED TO GROUND STATION

ATTITUDE REFERENCE

FILTER

QUICKENING LAW

FLIGHT-PATH COMMANDS

HEADING REFERENCE

COORDINATE TRANSFORMATION

DISPLAY

X,Y,Z

ψ

R,B,E

AIRBORNE STATION

TRANSMITTER

RECEIVER/DECODER

INTERROGATION

RETURN

GROUND STATION

RECEIVER

TRANSMITTER

The calculation model for generating these signals in the Task II study was based on an existing digital-computer model from Reference 1 in which aircraft position in space was defined in inertial- or landing-site-referenced coordinates. "Perfect" range (R), bearing (B), and elevation (E) signals describing own-ship position were calculated from

$$X_G = \frac{50 \text{ ft}}{\tan \gamma}$$

$$X_T = X_I + X_G$$

$$R = \left(X_T^2 + Y_I^2 + Z_I^2 \right)^{1/2}$$

$$B = \tan^{-1} \left(\frac{YI}{XT} \right)$$

$$E = \sin^{-1} \frac{Z_I}{\sqrt{X_T^2 + Y_I^2 + Z_I^2}}$$

where X_I, Y_I and Z_I are "perfect" inertial-position components referenced to the desired landing site (see Figure 3-16).

Measurement-noise characteristics of the assumed system were simulated by adding independent random-noise components of Gaussian distribution and zero mean* to each of these signals to yield:

$$R_n = R + n_R$$

$$B_n = B + n_B$$

$$E_n = E + n_E$$

with n_R, n_B and n_E indicating noise components of range, bearing and elevation, respectively.

---

*Bias or static-accuracy characteristics were not simulated since these components of signal inaccuracy may be accounted for by adding them to position errors resulting from pilot-in-the-loop system performance.

PLAN VIEW

PROFILE VIEW

γ = GLIDE-SLOPE ANGLE

X_G = LONGITUDINAL DISTANCE FROM GROUND STATION TO LANDING SITE

X_I, Y_I, Z_I = LONGITUDINAL, LATERAL, AND VERTICAL DISTANCES FROM LANDING SITE TO AIRCRAFT

X_T = LONGITUDINAL DISTANCE FROM GROUND STATION TO AIRCRAFT

R,B, E = RANGE, BEARING, AND ELEVATION OF AIRCRAFT WRT GROUND STATION
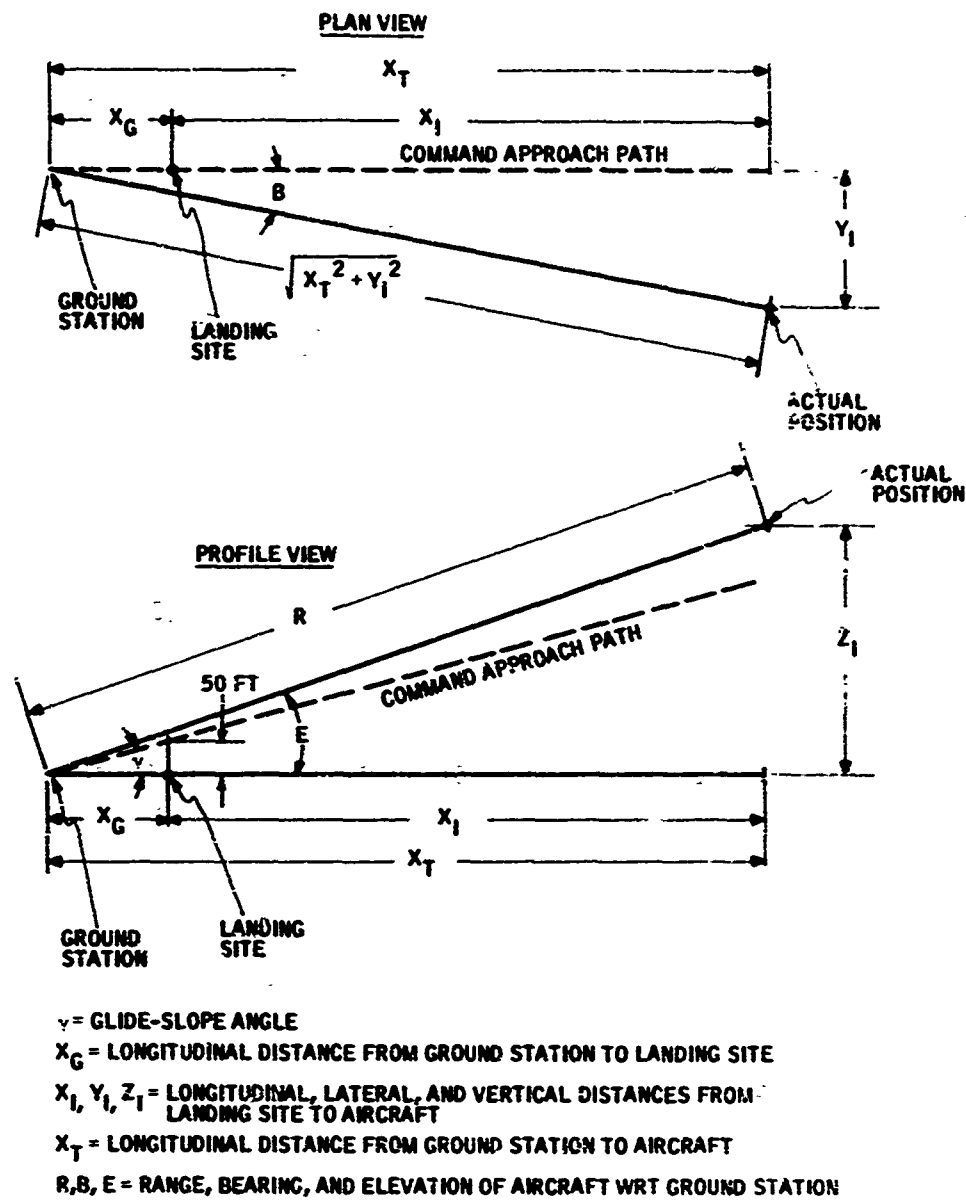
Figure 3-16. Measurement-System Geometry

3-27

Noise-corrupted range and angular measurements were then transformed back to inertial-position coordinates, as follows, to be filtered for use in driving the required display-quickening elements:

$$X_n = R_n \cos E_n \cos B_n - X_G$$

$$Y_n = R_n \cos E_n \sin B_n$$

$$Z_n = R_n \sin E_n$$

where X_n, Y_n and Z_n are the resulting noise-corrupted inertial components of longitudinal, lateral and vertical position. A block diagram of the calculation model for this measurement system, coordinate transformation and filter simulation is shown in Figure 3-17.

For the measurement-noise amplitudes considered, the above equations for X_n, Y_n and Z_n may be written as follows:

$$\Delta X_n = -R \cos E \sin B \, \Delta B_n - R \sin E \cos B \, \Delta E_n + \cos E \cos B \, \Delta R_n$$

$$\Delta Y_n = R \cos E \cos B \, \Delta B_n - R \sin E \sin B \, \Delta E_n + \cos E \sin B \, \Delta R_n$$

$$\Delta Z_n = R \cos E \, \Delta E_n + \sin E \, \Delta R_n$$

since ΔX_n is distributed around a zero mean, the variance (σ^2) of X_n may be expressed as

$$E[\Delta X_n^2] = \sigma_{X_n}^2$$

where $E[\ ]$ denotes an expected value. The variance in longitudinal-position measurement due to noise is then

$$\sigma_{X_n}^2 = E[(-R \cos E \sin B \, \Delta B_n - R \sin E \cos B \, \Delta E_n + \cos E \cos B \, \Delta R_n)^2]$$

Since the noise components n_R, n_B, and n_E are uncorrelated in this simulation model, the expected values of cross products in the above equation are zero, and the equation reduces to

$$\sigma_{X_n}^2 = E[R^2 \cos^2 E \sin^2 B \, \Delta B_n^2 + R^2 \sin^2 E \cos^2 B \, \Delta E_n^2 + \cos^2 E \cos^2 B \, \Delta R_n^2]$$

$$= R^2 \cos^2 E \sin^2 B \, \sigma_{B_n}^2 + R^2 \sin^2 E \cos^2 B \, \sigma_{E_n}^2 + \cos^2 E \cos^2 B \, \sigma_{R_n}^2$$

3-28
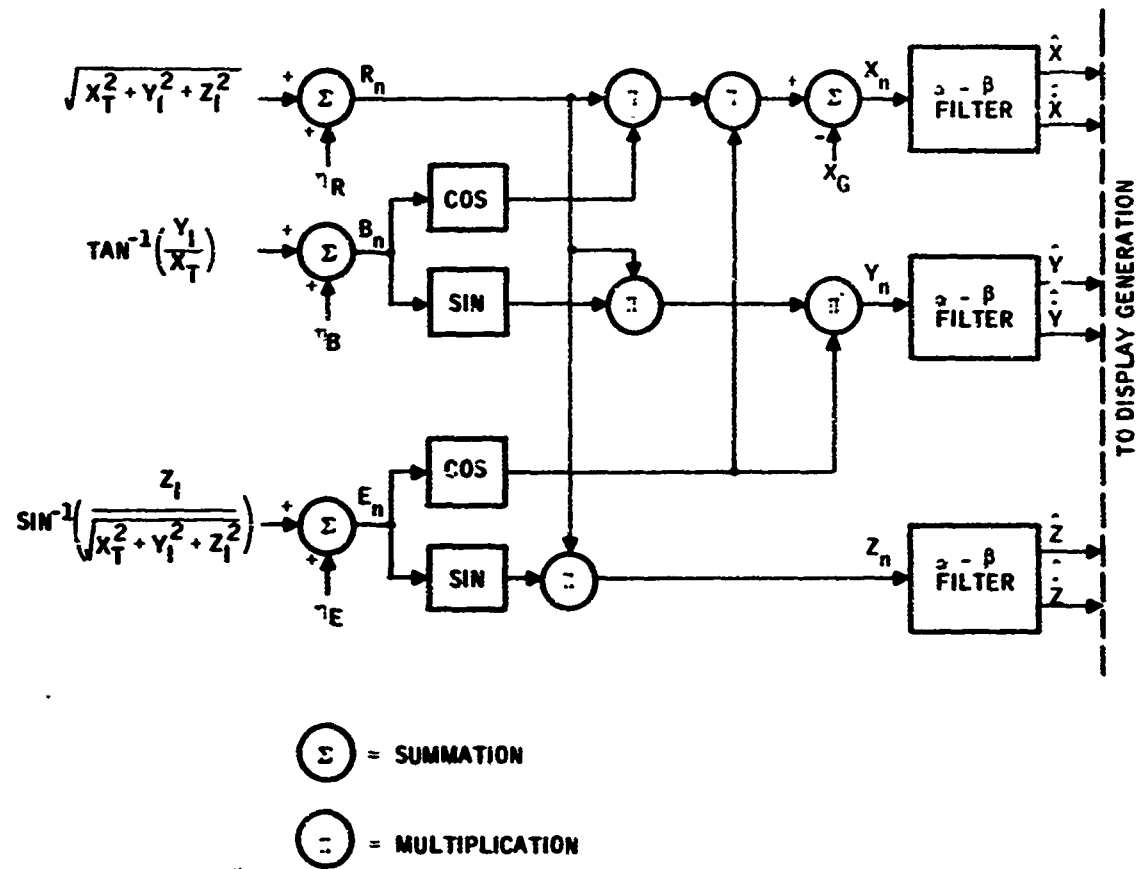
Figure 3-17.   Measurement-Noise Calculations

3-29

Similarly, variance components in lateral and vertical position measurement due to noise may be expressed as

$$\sigma_{Y_n}^2 = R^2 \cos^2 E \cos^2 B \, \sigma_{B_n}^2 + R^2 \sin^2 E \sin^2 B \, \sigma_{E_n}^2 + \cos^2 E \sin^2 B \, \sigma_{R_n}^2$$

$$\sigma_{Z_n}^2 = R^2 \cos^2 E \, \sigma_{E_n}^2 + \sin^2 E \, \sigma_{R_n}^2$$

From the above equations it may be noted that the variances in position measurements are combinations of variance components due to noise in range, bearing and elevation measurements. However, because of the measurement-system geometry previously described, variances in X_n, Y_n and Z_n are influenced predominantly by variances in R_n, B_n and E_n signals, respectively.

Noise Levels Simulated

Minimum performance values tentatively recommended by the Radio Technical Commission for Aeronautics (RTCA) Special Committee 117* for noise levels on approach-system bearing and elevation signals were used as a basis for selecting noise levels to be simulated in the Task II study. Maximum noise specified by the RTCA for these signals (Ref. 29) is approximately 0.035 degree (one standard deviation), with noise being defined to include spatial, temporal and resolution perturbations. Less specific information was available which could serve as a basis for selecting noise amplitudes associated with sensed range signals. Minimum performance values for ranging accuracy recommended by the RTCA suggest noise levels "compatible with a tolerable range-rate error; e. g., 10 ft/sec" (Ref. 29).

The selection of specific noise levels on bearing, range and elevation signals to be evaluated in the present study was based on preliminary simulations where noise amplitudes were varied in conjunction with the variation of signal-filter response characteristics. Discussion of the signal-filtering variable appears in the following subsection. Results of these preliminary simulations indicated that one-standard-deviation noise level of up to 0.070 degree on bearing and elevation signals and 2.0 feet on range would yield sufficient performance degradation with minimum signal filtering to allow evaluation of the effects of system noise on piloting performance. Specific noise levels for formal evaluation were selected to represent equal intervals within these ranges

---

*"This committee is composed of expert operational and technical representatives from both government and industry. Its objective is to develop a precision guidance-system concept for approach and landing and an associated signal structure." (Ref. 28).

(see Table 3-3), with a "no-measurement-noise" condition being included to allow evaluation of the filter-response variable independent of the noise variable.

Table 3-3. Measurement-Noise Levels Evaluated

Noise Level	Standard Deviation of Noise		
	σ_{B_n} (deg)	σ_{E_n} (deg)	σ_{R_n} (ft)
No Measurement Noise	0.0	0.0	0.0
Intermediate Measurement Noise	0.035	0.035	1.0
High Measurement Noise	0.070	0.070	2.0

APPROACH-GUIDANCE-SYSTEM FILTER CHARACTERISTICS SIMULATED

Filter Model

In addition to the investigation of effects of system measurement noise, a second primary objective of the Task II SAA study was to evaluate the effects on piloting performance of degraded transient-response characteristics of filters used for the reduction of measurement-system noise. In the design of signal filters, some compromise is always necessary between the extent of noise filtering allowable and response lags resulting due to the filtering process. The combined evaluation of noise and filter-response variables in this study allowed investigation of the interactive effects of these variables as they relate to the steep-approach task.

The guidance system defined for simulation purposes assumed availability of sensed slant-range, bearing and evaluation signals to be transformed and filtered for the generation of aircraft position and velocity relative to a desired landing site. These information parameters were required to drive quickened and other command symbols on the two display formats being evaluated.

Of the numberous digital filter (e.g., Kalman, α-β, least-squares) and analog-filter techniques available, the digital α-β filter was selected for simulation. The mathematical representation for this filter (Ref. 30) is

3-31

$$\hat{X}_{k+1} = (1-\alpha)\,\hat{X}_k + (1-\alpha)\,T\,\hat{\dot{X}}_k + \alpha\,X_n$$

$$\hat{\dot{X}}_{k+1} = \frac{-\beta}{T}\,X_k + (1-\beta)\,\hat{\dot{X}}_k + \frac{\beta}{T}\,X_n$$

where

T = sampling period (sec)

X_n = measured raw position at time = $(k+1)T$

$\hat{X}_k$ = estimated position at time = kT

$\hat{\dot{X}}_k$ = estimated velocity at time = kT

α, β = filter weighting coefficients

It may be noted that the $\alpha - \beta$ filter outputs include both estimated (filtered) position and velocity terms. Based on analytical results obtained in Reference 30, the coefficient β was defined as

$$\beta = \alpha^2/(2-\alpha)$$

to yield the best compromise in simultaneous estimation of position and velocity with filter outputs being slightly under-damped for all values of α. The above referenced analysis did not specify an optimum value for α since the selection of a value for this coefficient would be a function of the relative importance of good noise smoothing (low α) and good transient response (high α).

A filter model as described above was simulated for each of the three position-coordinate signals as shown in Figure 3-17. Outputs of these filters served as inputs to the previously described display-quickened-symbol and altitude-command-symbol driving equations.

Filter Characteristics

Noise-smoothing characteristics of the filter simulated are described in subsequent paragraphs in terms of two ratios:

$$R_X = \frac{\sigma_{\hat{X}}}{\sigma_{X_n}} = \frac{\text{steady-state standard deviation of position output}}{\text{standard deviation of position input}}$$

3-32

and

$$R_{\dot{X}} = \frac{\sigma_{\dot{\hat{X}}}}{\sigma_{X_n}} = \frac{\text{steady-state standard deviation of velocity output}}{\text{standard deviation of position input}}$$

In terms of the filter coefficients α and β, and the filter update rate $(1/T)$, these equations are expressed as

$$R_X = \sqrt{\frac{2\alpha^2 + \beta(2 - 3\alpha)}{\alpha(4 - \beta - 2\alpha)}}$$

and

$$R_{\dot{X}} = \sqrt{\frac{1}{T^2}\left[\frac{2\beta^2}{\alpha(4 - \beta - 2\alpha)}\right]}$$

Effects of signal lag due to filtering were evaluated in the present study by varying the coefficient α (and consequently β) while holding T constant. The coefficient β was defined as above, while T, the filter sampling period, was set at the hybrid-simulator compute-cycle time of 0.075 second $(1/T = 13.3\text{Hz})$.

The functional relationships between α and filter-output characteristics R_X, $R_{\dot{X}}$, LAG_X and $LAG_{\dot{X}}$ (response times to 90 percent of steady-state value) are shown in Figures 3-18 and 3-19 for T = 0.075 second. Interpretation of these figures is aided by noting that for $\alpha = 0.0$, $R_X = R_{\dot{X}} = 0.0$ (no signal output from filter). For $\alpha = 1.0$, $LAG_X = LAG_{\dot{X}} = 0.0$, $R_X = 1.0$ and $R_{\dot{X}}$ is a pure differentiation of the raw-position measurements.

The effect of varying T in these filter equations is shown by example in Figures 3-20 and 3-21. Although T was held constant in the Task II study, it may be observed in Figure 3-20 that it would be beneficial for purposes of noise reduction to have a higher system data rate. As an example, for a given lag on $\dot{X}$ (e. g., $LAG_{\dot{X}} = 1.0\,\text{sec}$) a data rate of $1/T = 13.3\text{Hz}$ yields a ratio $(R_{\dot{X}})$ of approximately $\sigma_{\dot{\hat{X}}}/\sigma_{X_n} = 0.75$. For the same $LAG_{\dot{X}}$ (obtainable by selection of a different α), an increase in data rate to 100Hz would yield a reduction in $R_{\dot{X}}$ to approximately $\sigma_{\dot{\hat{X}}}/\sigma_{X_n} = 0.27$. Thus if a given system were capable of furnishing a higher (or lower) data rate than that simulated here, comparably higher (or lower) noise levels than those shown in Table 3-3 could be accepted with the same filter model. The effect of holding the coefficient α constant over differing data rates is shown in Figure 3-21 for $\alpha = 0.25$. For this α, $LAG_{\dot{X}}$ increases abruptly below data rates of approximately 10Hz.

Selection of specific levels of α to be evaluated was based on preliminary simulations in which the approach-and-landing-mission segment was flown using a range of α coefficients under conditions of no measurement noise.

3-33
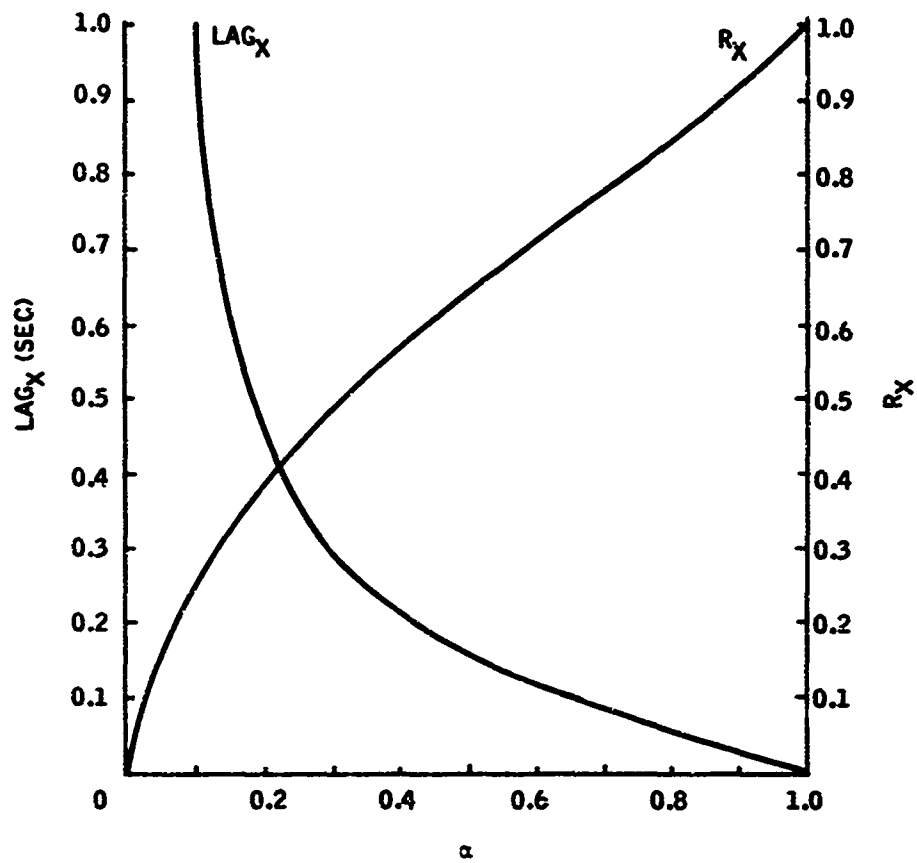
Figure 3-18. Effect of α on Response Time (Lag$_X$) and Noise
Reduction (R$_X$) on Position Output of α-β Filter
for T = 0.075 sec
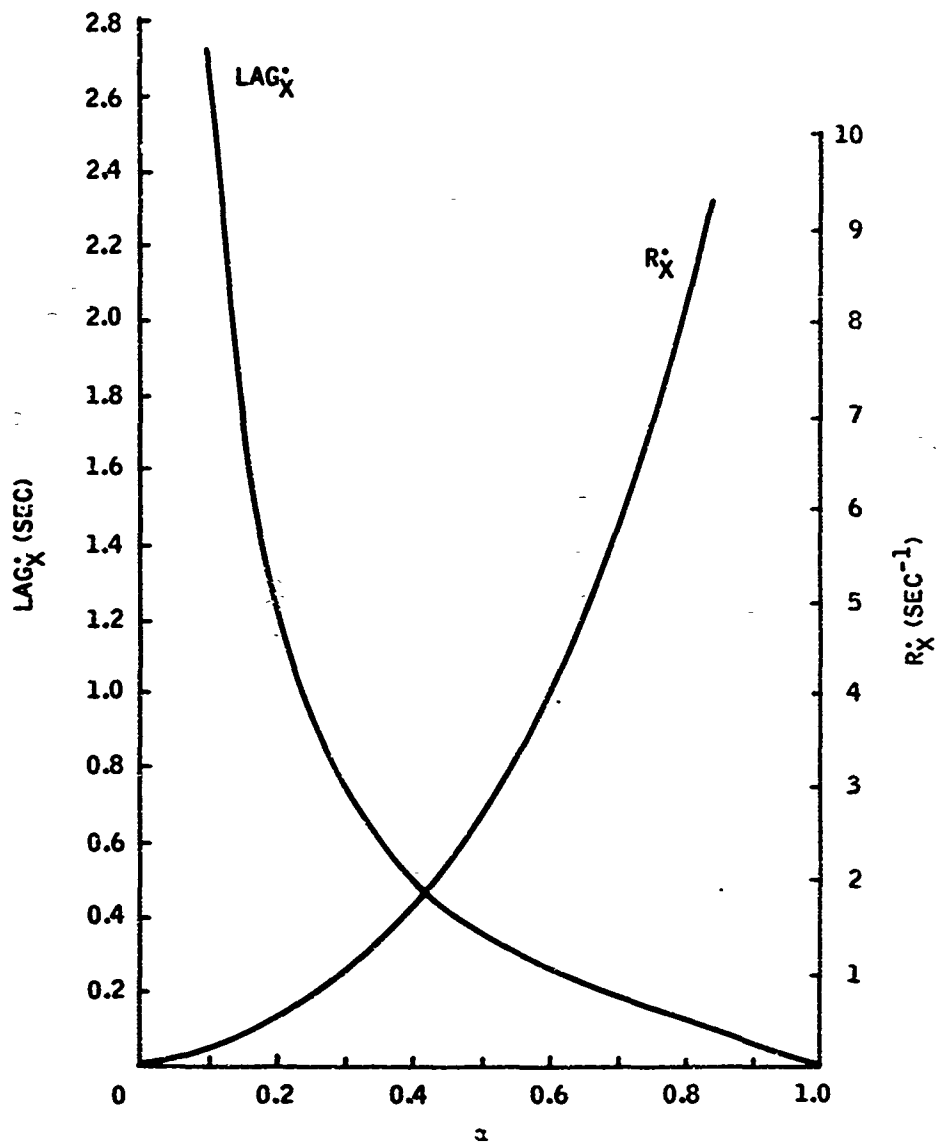
Figure 3-19. Effect of α on Response Time (Lag$_{\dot{x}}$) and Noise Reduction (R$_{\dot{x}}$) on Rate Output of α-β Filter for T = 0.075 sec

3-35
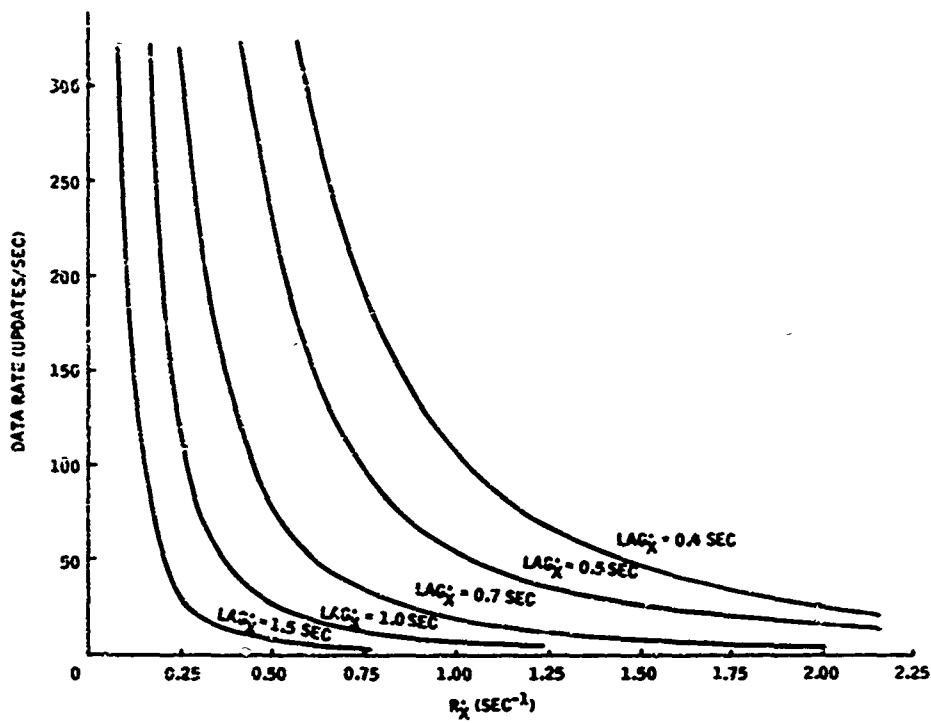
Figure 3-20. Relationship Between Filter Update Rate and $R_{\dot{X}}$ for Constant $Lag_{\dot{X}}$
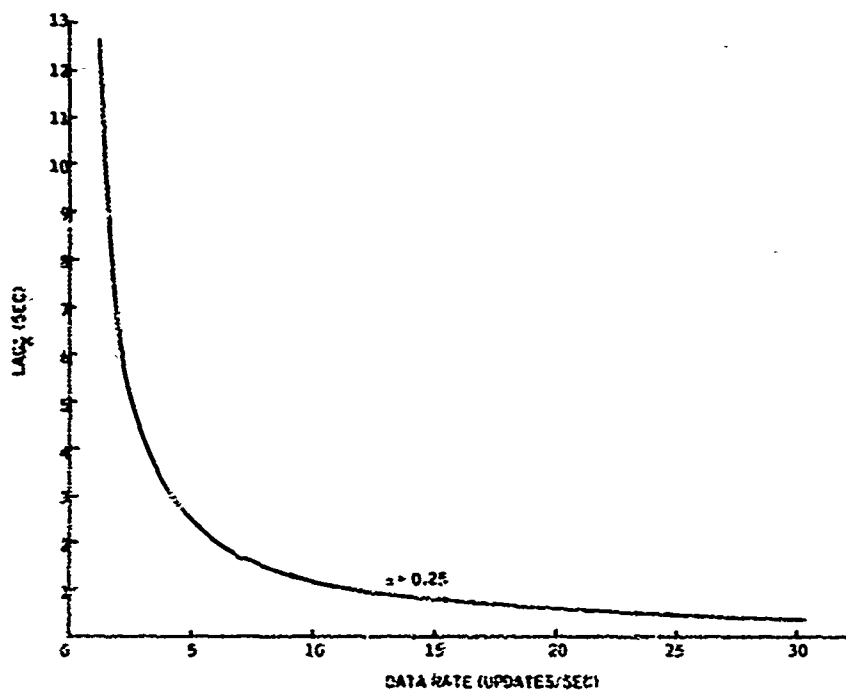
Figure 3-21. Relationship Between Filter Update Rate and $Lag_{\dot{X}}$ for $\alpha = 0.25$

Results of varying α simultaneously in the three simulated filters (with inputs X_n, Y_n and Z_n as shown in Figure 3-17) yielded an indicated working range of $0.15 < \alpha < 0.50$ for both vehicles tested. Increased signal lags associated with $\alpha = 0.15$ resulted in clearly degraded piloting performance while task difficulty associated with $\alpha = 0.50$ was not perceptibly different from that resulting in a baseline condition with no signal lags simulated.

Specific values of the filter coefficient α selected for formal evaluation are shown in Table 3-4. Also indicated are the corresponding values of R_X, $\dot{R}_X$, LAG_X and $LAG_{\dot{X}}$ resulting for each α with $T = 0.075$ second.

Table 3-4. Filtering Characteristics* for Values of α Selected

α	R_X	$\dot{R}_X$ (sec^{-1})	LAG_X (sec)	$LAG_{\dot{X}}$ (sec)
0.15	0.34	0.31	0.63	1.75
0.25	0.44	0.72	0.34	0.83
0.50	0.64	2.64	0.16	0.37

*$(R_X = R_Y = R_Z, \dot{R}_X = \dot{R}_Y = \dot{R}_Z$, etc.)

In terms of the range, bearing and elevation measurement-noise levels selected (Table 3-3), these values of α resulted in filtered position- and rate-output-noise standard deviations shown in Table 3-5. Filter-output noise levels are shown in angular units where necessary since noise as transformed to X, Y, Z coordinates would increase linearly as a function of range from the ground station.

At increased ranges the velocity estimates $\hat{\dot{X}}$, $\hat{\dot{Y}}$ and $\hat{\dot{Z}}$ were found to generate intolerably high noise amplitudes when scaled through the display gains required for quickened- and altitude-command-symbol driving equations. For example, at a point on the command flight path 2 nautical miles from the assumed guidance-signal source, a noise component $\sigma_{B_n} = 0.07$ degree is approximately equal to

$$\sigma_{Y_n} \simeq \frac{12,160 \text{ ft}}{\cot 0.07 \text{ deg}} \simeq 15 \text{ feet}$$

Table 3-5. Simulated Noise Levels at Output of $\alpha - \beta$ Filter

Filter Parameter α	Position Input to Filter			Position Output of Filter			Rate Output of Filter		
	σ_{R_n}(ft)	σ_{B_n}(deg)	σ_{E_n}(deg)	σ_R(ft)	σ_B(deg)	σ_E(deg)	$\sigma_{\dot{R}}$(fps)	$\sigma_{\dot{B}}$(deg/sec)	$\sigma_{\dot{E}}$(deg/sec)
0.50	0.0	0.000	0.000	0.000	0.000	0.000	0.000	0.000	·.00
	1.0	0.035	0.035	·.640	0.022	0.022	2.640	0.092	0.092
	2.0	0.070	0.070	1.280	0.045	0.045	5.280	0.185	0.185
0.25	0.0	0.000	0.000	0.000	0.000	0.000	0.000	0.000	0.000
	1.0	0.035	0.035	0.440	0.015	0.015	0.720	0.025	0.025
	2.0	0.070	0.070	0.880	0.031	0.031	1.440	0.050	0.050
0.15	0.0	0.000	0.000	0.000	0.000	0.000	0.000	0.000	0.000
	1.0	0.035	0.035	0.340	0.012	0.012	0.310	0.011	0.011
	2.0	0.070	0.070	0.680	0.024	0.024	0.620	0.022	0.022

With $\alpha = 0.50$ and $R_{\dot{Y}} = 2.64$, the resulting lateral-velocity noise component

$$\sigma_{\hat{\dot{Y}}} = 2.64\,\sigma_{Y_n} = 39.6 \text{ ft/sec}$$

appears as a noise level on the lateral quickening axis (Y_Q) with an amplitude of

$$\sigma_{Y_Q} \simeq K_{\dot{Y}}\,(\sigma_{\hat{\dot{Y}}}) = 0.044\,\frac{\text{in.}}{\text{ft/sec}}\,(39.6 \text{ ft/sec}) = 1.74 \text{ inch}$$

where σ_{Y_Q} is the standard deviation in inches of lateral-axis display-quickening noise*. This problem was resolved by displacement rate limiting the quickened-symbol and altitude-command-symbol driving equations as shown, by example, in Figure 3-22. Results of preliminary simulation flights indicated that limiting rates of displacement of these symbols on the display to 1.0 in./sec would yield a sufficient reduction in high display-noise levels to allow initiation of the simulated approach task at ranges of approximately 2 nautical miles. Under conditions of no measurement noise this limiter model did not effect symbol-motion dynamics.

Actual noise levels on the quickened-symbol lateral axis resulting from use of this limiter are shown in Figures 3-23 through 3-25 for the various combinations of α, σ_{β_n} and $K_{\dot{Y}}$ studied. Since the altitude-command-symbol gain $(K_{\dot{Z}})$ was approximately the same as the "high-gain" alternative on $K_{\dot{Y}}$ (i.e., $K_{\dot{Z}} = 0.05$ in./ft/sec and $K_{\dot{Y}} = 0.044$ in./ft/sec) and noise on $K_{\dot{Z}}$ was predominantly due to E_n, display-noise levels resulting on the altitude-command symbol were similar to those shown in Figures 3-24 and 3-25. Noise amplitudes resulting on the longitudinal display-quickening axis (σ_{X_Q}) were approximately constant as a function of range for a given α and σ_{R_n} because of the predominant contribution of R_n in feet to σ_{X_Q} (see Table 3-6).

It may be observed in Figures 3-23 through 3-25 that the extent of nonlinearity in σ_{Y_Q} as a function of range varies with α and the limiter input-noise amplitude approximated by $K_{\dot{Y}}\,(\sigma_{\hat{\dot{Y}}})$. For $\alpha = 0.15$, the sample-to-sample autocorrelation of $\hat{\dot{Y}}$

$$R_{\hat{\dot{Y}}}\,(\tau) = \langle \hat{\dot{Y}}(t)\,\hat{\dot{Y}}\,(t+\tau) \rangle = \lim_{T \to \infty} \frac{1}{2T} \int_{-T}^{T} \hat{\dot{Y}}(t)\,\hat{\dot{Y}}\,(t+\tau)\,dt$$

is sufficiently high to preclude any significant effect of symbol rate limiting. Conversely, with $\alpha = 0.50$, filter-output autocorrelation in $\hat{\dot{Y}}$ is appreciably reduced, allowing the limiter to have a more significant effect on σ_{Y_Q} as range increases.

---

*The contribution of $\sigma_{\hat{Y}}$ to σ_{Y_Q} is not significant. For $\sigma_{Y_n} = 15$ ft and $\alpha = 0.50$, $\sigma_{\hat{Y}} = 9.6$ ft and $K_Y\,(\sigma_{\hat{Y}}) = 0.0022$ in./ft (9.6 ft) = 0.021 in.
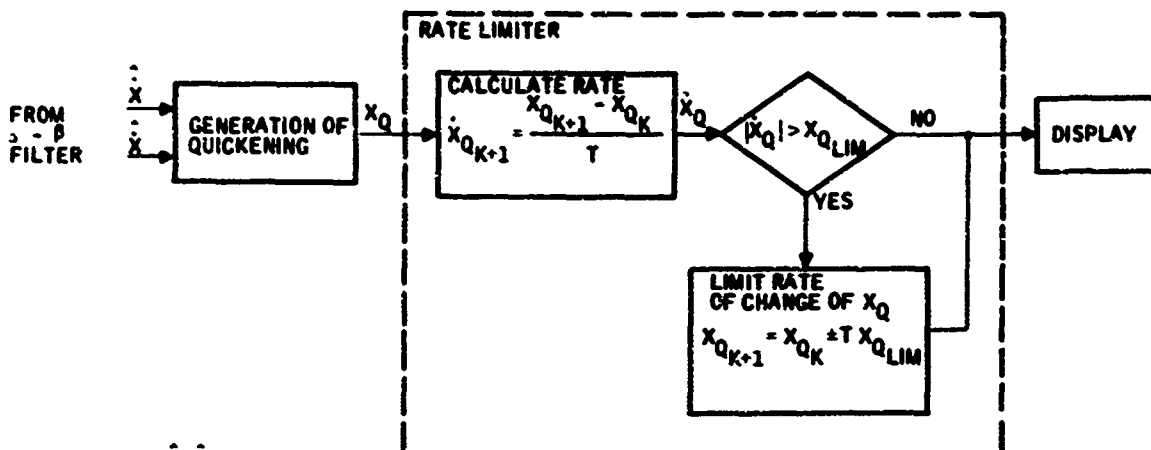
$\dot{X}, \ddot{X} =$ ESTIMATED LONGITUDINAL POSITION AND RATE FROM $\alpha - \beta$ FILTER

$X_Q, \dot{X}_Q =$ PITCH-AXIS QUICKENING-SYMBOL DISPLACEMENT AND RATE

$T =$ SAMPLE PERIOD OF DIGITAL COMPUTER

$\dot{X}_{Q_{LIM}} =$ MAXIMUM RATE OF CHANGE OF X_Q SPECIFIED

$X_{Q_K}, X_{Q_{K+1}} =$ VALUE OF X_Q AT TIME KT AND (K+1) T RESPECTIVELY

Figure 3-22. Rate-Limiter Model
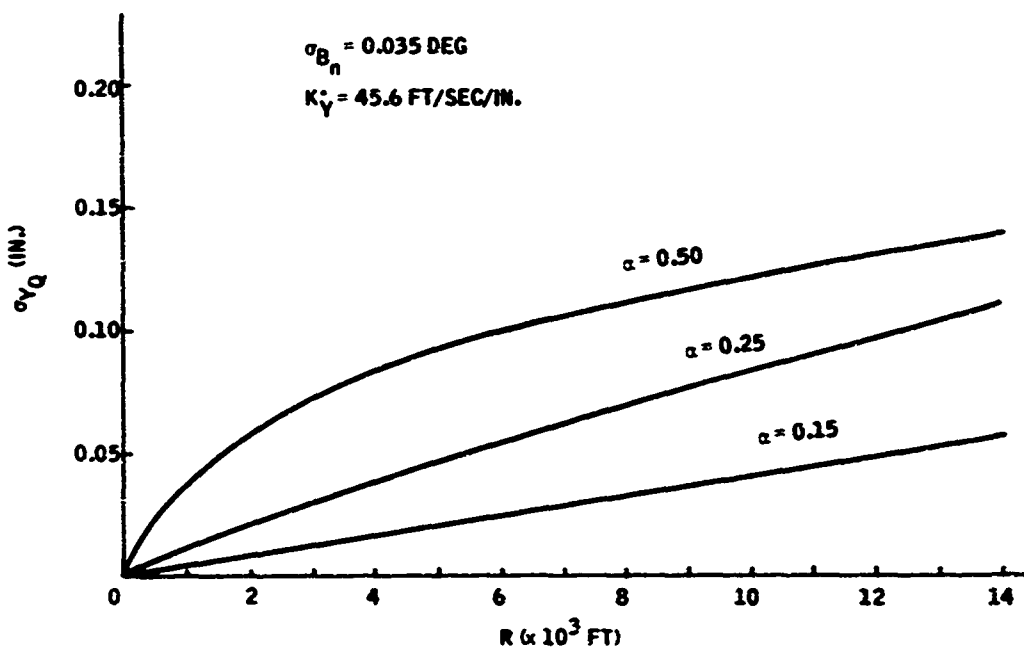
Figure 3-23. Noise on Lateral-Axis Quickening as a Function of Range

3-40
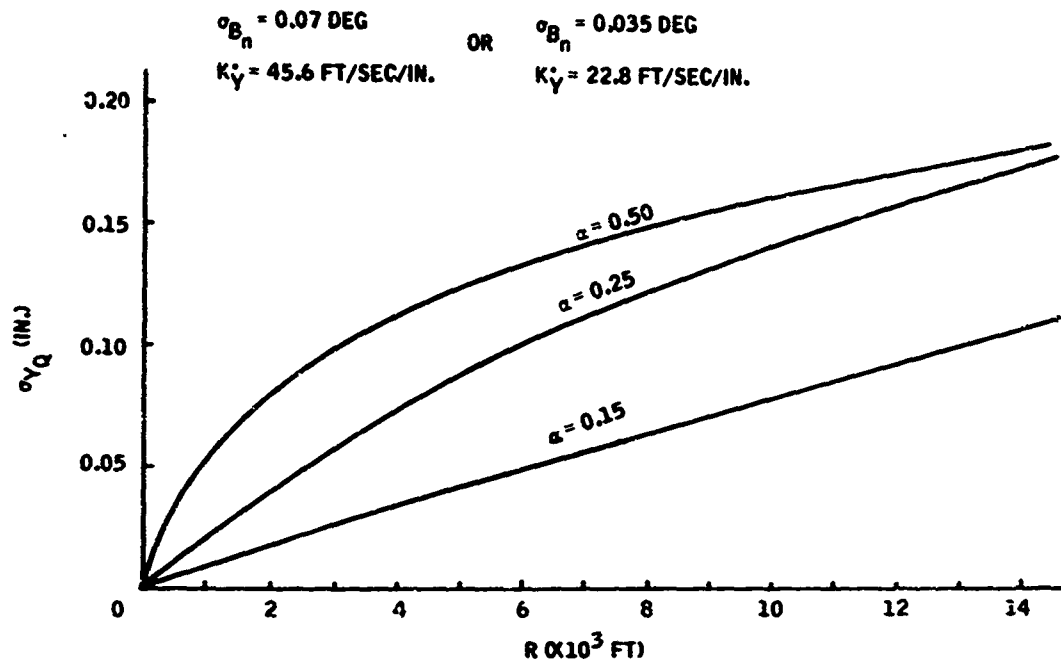
Figure 3-24. Noise on Lateral-Axis Quickening as a Function
of Range
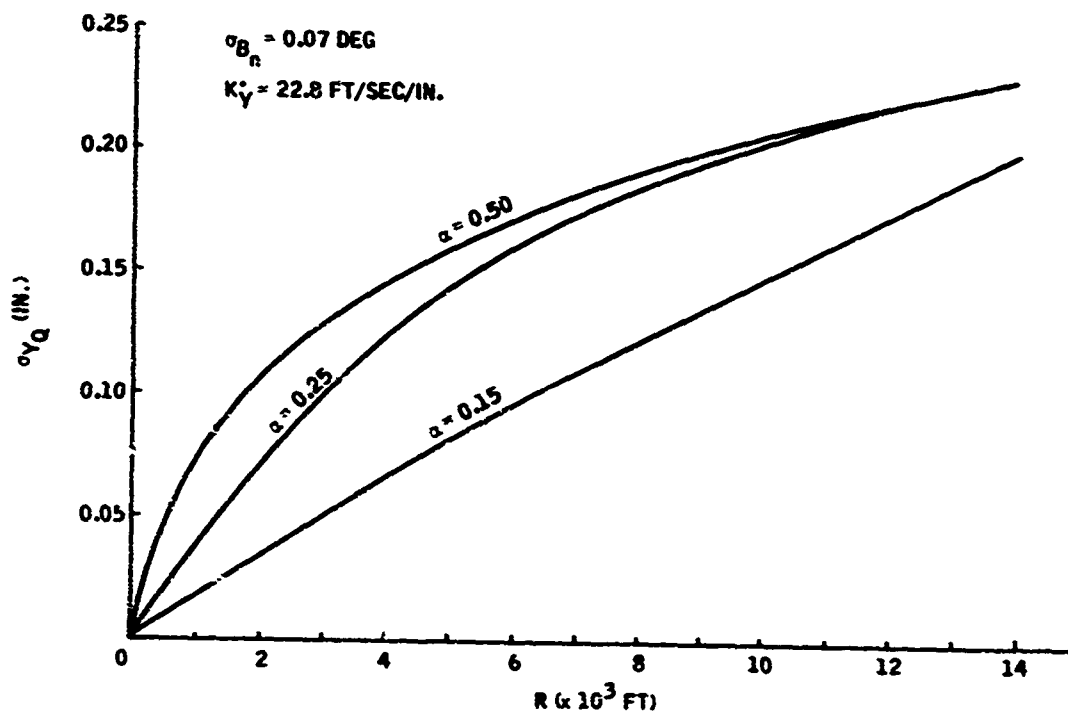
Figure 3-25. Noise on Lateral-Axis Quickening as a Function
of Range

3-41

Table 3-6. Approximate Longitudinal Display-Quickening-Axis Noise Levels for σR_n = 1.0 and 2.0 Feet

α	$\sigma_{X_n} \approx \sigma_{R_n}$ (ft)	$\sigma_{\dot{X}}$ (fps)	$K_{\dot{X}}$ (in./fps)	σ_{X_Q} (in.)
0.15	1.0	2.64	0.022	0.051
	1.0	2.64	0.044	0.079
	2.0	5.28	0.022	0.079
	2.0	5.28	0.044	0.107
0.25	1.0	0.72	0.022	0.016
	1.0	0.72	0.044	0.032
	2.0	1.44	0.022	0.032
	2.0	1.44	0.044	0.063
0.50	1.0	0.31	0.022	0.007
	1.0	0.31	0.044	0.014
	2.0	0.62	0.022	0.014
	2.0	0.62	0.044	0.027

Spectral and distribution characteristics of measurement noise simulated for the Task II study are shown in Appendix B. The following general statements summarize these characteristics:

- The autocorrelation of filtered position and rate signals increases with decreasing α (see Figures B1 and B2)

- If, hypothetically, the limiter model were used with a filter coefficient of α = 1.0, for high noise levels (e.g., σ_{Y_n} = 15 ft), high-frequency noise components would be attenuated while those below approximately 0.2 Hz would be amplified (see Figure B3).

- For α = 0.50 and σ_{Y_n} = 15 feet, the rate-limiter model yields a relatively high attenuation of high-frequency measurement-noise components, and some amplification of noise components below 0.2 Hz (see Figure B4)

- For σ_{Y_n} = 15 feet and as α decreases, the limiter has relatively less effect on the spectral content of noise on the display (see Figures B5 and B6).

- As σ_{Y_n} decreases and fewer measurement noise samples are limited, the effects of α becomes more predominant in determining displayed-noise characteristics (see Figures B7 through B10).

- The Gaussian-amplitude-distribution characteristics of simulated measurement noise (Figure B11) are not appreciably affected by the α - β filter model (Figures B12 and B13) or the display-symbol rate-limiter model (Figure B14).

SECTION IV

PRELIMINARY SIMULATION - TASK II

OBJECTIVES

The primary objectives of the preliminary-simulation phase of the study were:

- The refinement of simulation procedures and techniques to be used in the formal-simulation phase of the study

- The empirical evaluation, selection and verification of specific levels of noise, filter and quickening-gain variables to be included in the formal-simulation study phase

- The familiarization and training of subjects on selected experimental-variable combinations to be evaluated in the formal-simulation phase

PROCEDURAL REFINEMENT

A number of standardized procedures were established to minimize both time and potential experimenter error normally associated with conducting a complex simulation study.

Analog-computer potentiometer settings for each vehicle simulation were recorded on paper punch tape to be used for automatically setting coefficients required in the analog portions of the simulations. Digital programs were transferred from cards to magnetic tape to avoid program input errors during set up.

Frequently changing parameters associated with replication, subject, quickening, approach-angle, filter and noise variables were coded in the form of a seven-digit identification (ID) number. A desired combination of experimental treatment levels could be introduced by the experimenter by input of an appropriate ID number on the simulator console typewriter. This number was automatically recorded on all digitally computed performance-summary listings for later verification of test conditions.

PRELIMINARY SYSTEM EVALUATION

During preliminary simulations, three Honeywell engineering personnel served as pilot/subjects for the final determination of system parameters which would remain constant in the formal-simulation phase. Test conditions selected were then verified during initial practice sessions with the military pilots who would be serving as subjects for the duration of the preliminary and formal experimentation. Levels of quickening-gain, filter and noise variables previously described in Section III were selected at this time.

PILOT FAMILIARIZATION AND TRAINING

Military pilots who would be serving as subjects during the formal simulation phase were trained under the various experimental conditions prior to initiation of formal-data collection. Each pilot received a minimum of two "completed" practice flights on selected treatment combinations to be evaluated (a flight was considered "completed" if control of the aircraft was maintained through all phases of the approach and landing mission). Formal-data-collection flights immediately followed the completion of practice sessions with the respective vehicles.

Pilot training sessions were begun using the UH-1 vehicle simulation, with task familiarization being conducted in two phases. Initially each of four pilots received a series of 16 practice flights consisting of two replications on treatment conditions resulting from the factorial combination of the following variable levels:

- Quickening gains (two levels, as defined in Section III)

- Approach angles (two levels)

- Display formats (two levels)

- Measurement noise (one level - no measurement noise)

- Filter lag (one level - minimum lag, i.e., $\alpha = 0.5$)

A second and more extensive training phase was then conducted in which two replications were given on each of the 24 treatment conditions resulting from a factorial combination of the following variable levels:

- Quickening gains (two levels)

- Approach angles (two levels)

- Display formats (two levels)

- Measurement noise (one level - maximum noise level)

- Filter lag (three levels)

The resulting two-phase training series of 64 practice flights per pilot consisted of practice on all conditions to be treated during formal experimentation with the exception of the intermediate level of simulated measurement noise.

Measures selected as summary indicators of pilot skill acquisition during training were:

- Total time to complete the simulated approach and landing

- Root-mean-square (RMS) lateral and vertical flight-path errors during the "final-approach" phase

- RMS longitudinal and lateral positions errors during the "descent-from-hover" phase

Practice data resulting for each of these summary measures are shown in Figures 4-1 through 4-5. Data shown are averaged in consecutive blocks of trials, with each block containing data from two flights per pilot to yield eight flights per block. Nominal or average performance indicated for each block is represented by the median value of data for each set of eight flights while performance variabilities around each median are indicated by 19th and 81st percentile points. These specific percentile points were selected as indicators of training performance variability to facilitate data reduction while training was in progress (i.e., the 19th- and 81st-percentile points from each set of eight flights defines a range of performance not including the highest or the lowest scores).

It may be observed in these figures that, in terms of the performance measures indicated, piloting performance with practice during the initial training phase (first eight trial blocks) did not improve appreciably. This is attributable to two predominant factors: (1) three of the four pilots being trained had served as test subjects in a previous study phase (Ref. 1), and (2) the summary performance data presented do not reflect the relatively high frequency of vehicle control losses resulting during initial stages of practice. In the latter portion of this practiced sequence, sufficient piloting skill had been acquired to allow nearly consistent completion of the simulated approach and landing task.

A general decrease in position-error and total-time scores is apparent in the second and more difficult practice phase. In a majority of instances, errors appear to be approaching an asymptotic performance level in that final block-to-block variabilities do not reflect large or consistent downward trends.

4-3

Figure 4-1. Median Total Time (and 19th and 81st Percentiles) for Each Practice Block; UH-1 Aircraft

Figure 4-2. Median RMS_Y Error (and 19th and 81st Percentiles) for Each Practice Block; UH-1 Aircraft; Final Approach Phase

4-4

Figure 4-3. Median RMS$_Z$ Error (and 19th and 81st Percentiles) for Each Practice Block; UH-1 Aircraft; Final Approach Phase

Figure 4-4. Median RMS$_X$ Error (and 19th and 81st Percentiles) for Each Practice Block; UH-1 Aircraft; Descent Phase

4-5

Figure 4-5. Median RMS_y Error (and 19th and 81st Percentiles) for Each Practice Block; UH-1 Aircraft; Descent Phase

A similar familiarization and training sequence was given to the four pilots who would be serving as test subjects using the XV-5 vehicle simulation. Based on results of the above-described UH-1 training sequence and the initial XV-5 training phase, the second XV-5 training phase was reduced in scope by omitting the intermediate level of filter lag ($\alpha = 0.25$) from the scheduled training sequence to yield a total of 48 practice flights per pilot on this vehicle.

Training performance data for the XV-5 vehicle are shown in Figures 4-6 through 4-10. Resulting performance levels during training indicate no consistent trend toward improved performance with continued practice. Although three of the four pilots serving as test subjects with this vehicle had previously completed the formal-data-collection phase on the UH-1 vehicle, the fourth pilot having no previous experience with either aircraft simulation was able to consistently complete the approach and landing task using the XV-5 after approximately five attempts.

In summary, of primary importance is the fact that all pilots who served in the formal-simulation study phase were familiarized during training with all relevant task characteristics to be evaluated experimentally.
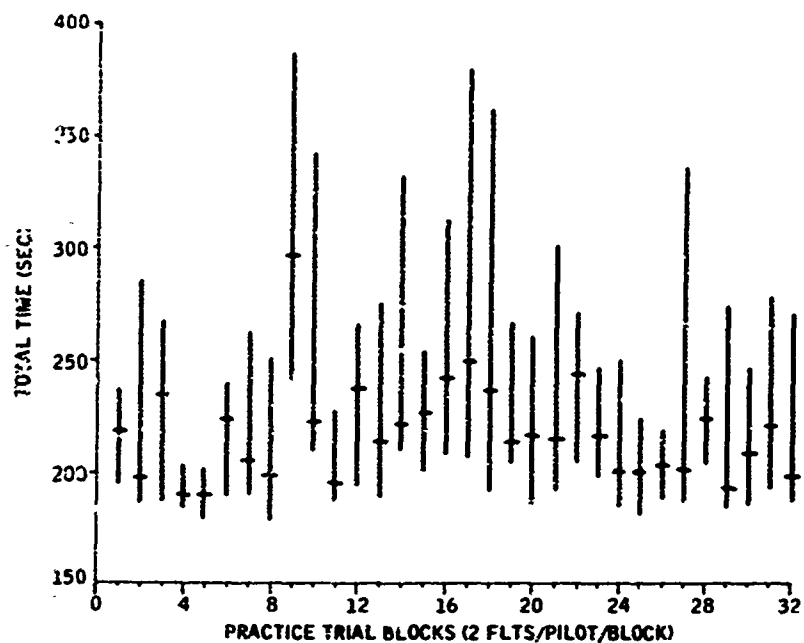
4-6
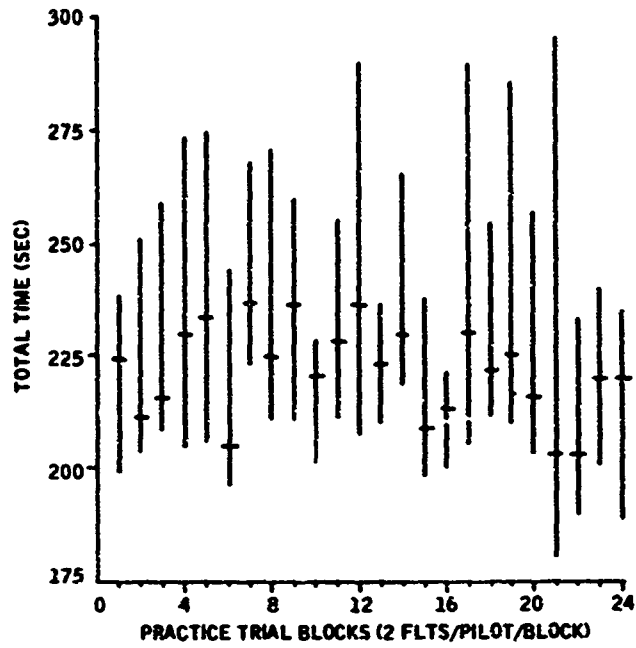
Figure 4-6. Median Total Time (and 19th and 81st Percentiles)
for Each Practice Block; XV-5 Aircraft

Figure 4-7. Median RMS_y Error (and 19th and 81st Percentiles)
for Each Practice Block; XV-5 Aircraft; Final-
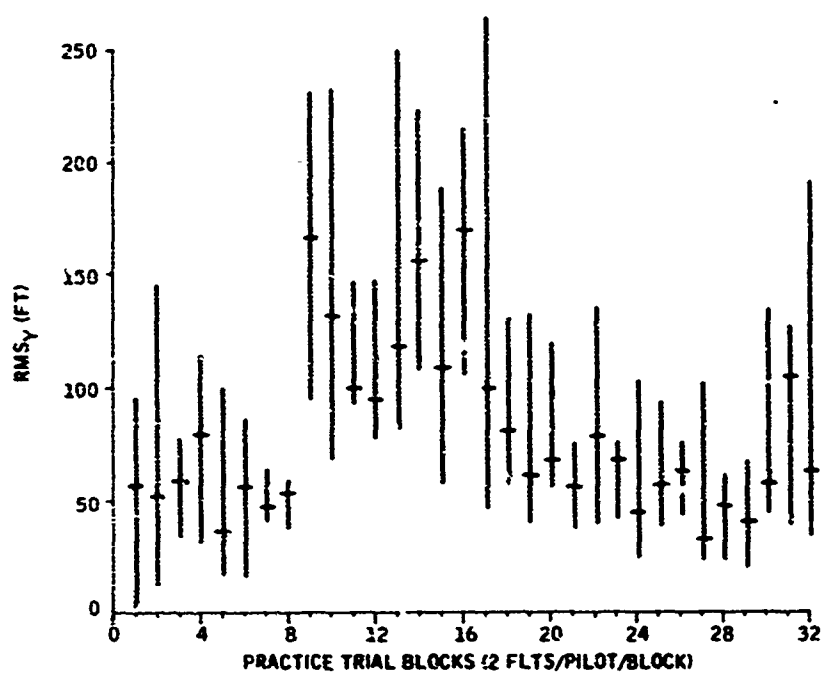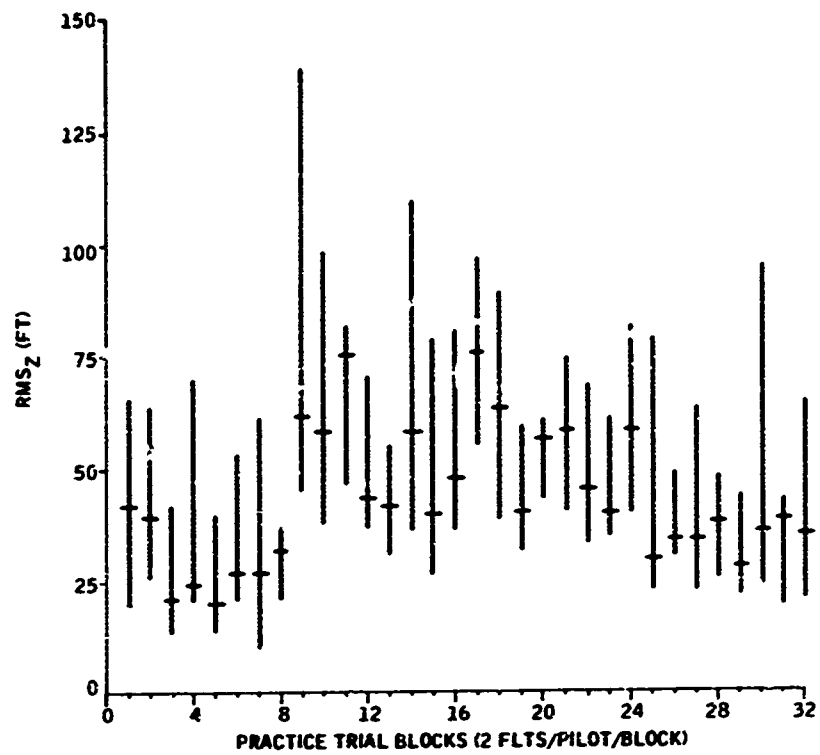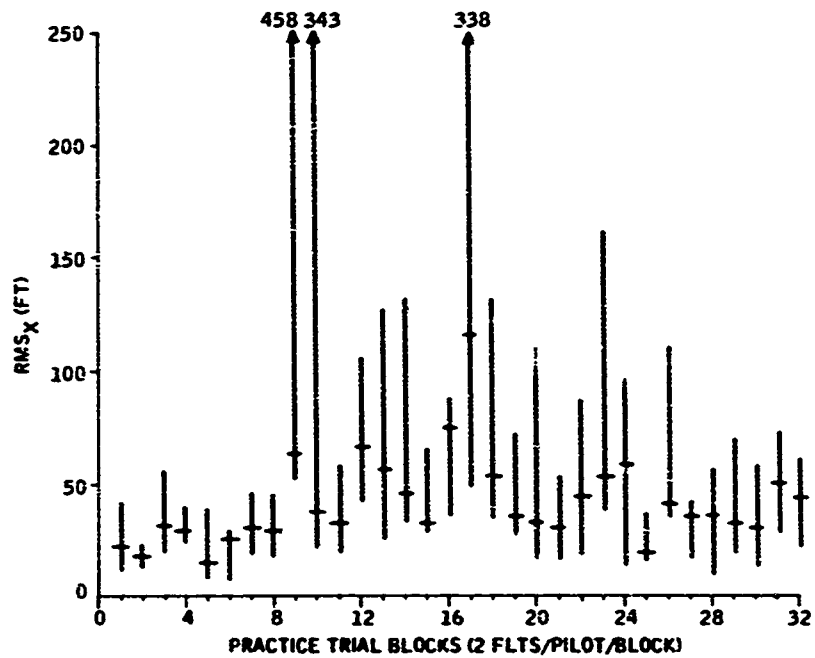Approach Phase

4-7

Figure 4-8. Median RMS_Z Error (and 19th and 81st Percentiles)
for Each Practice Block; XV-5 Aircraft; Final-
Approach Phase

Figure 4-9. Median RMS_X Error (and 19th and 81st Percentiles)
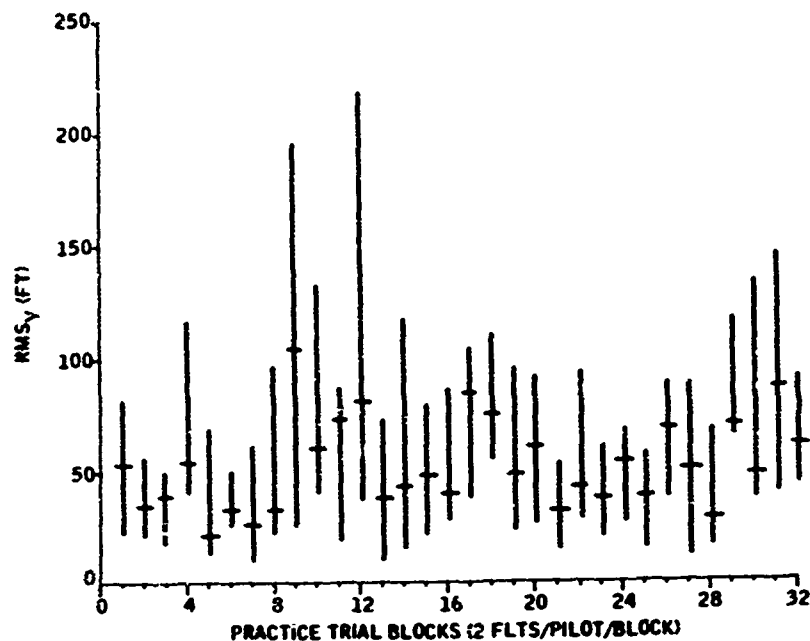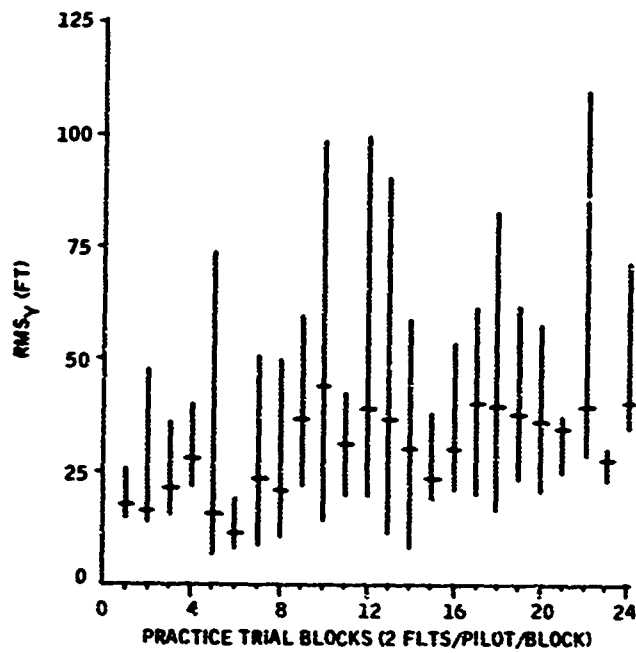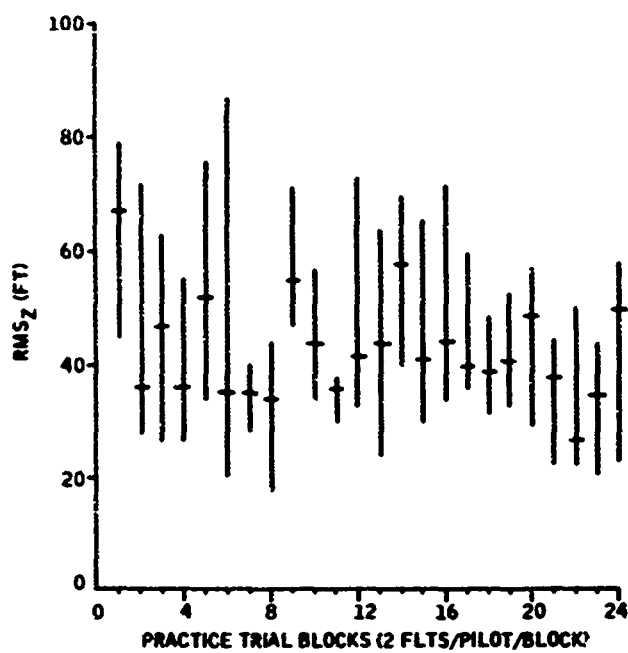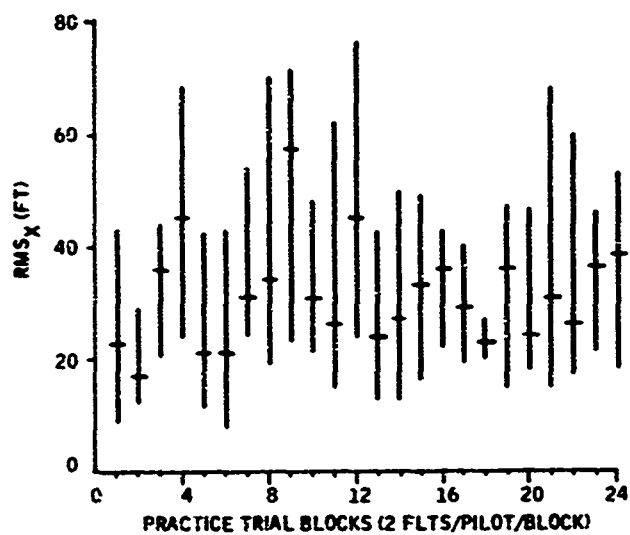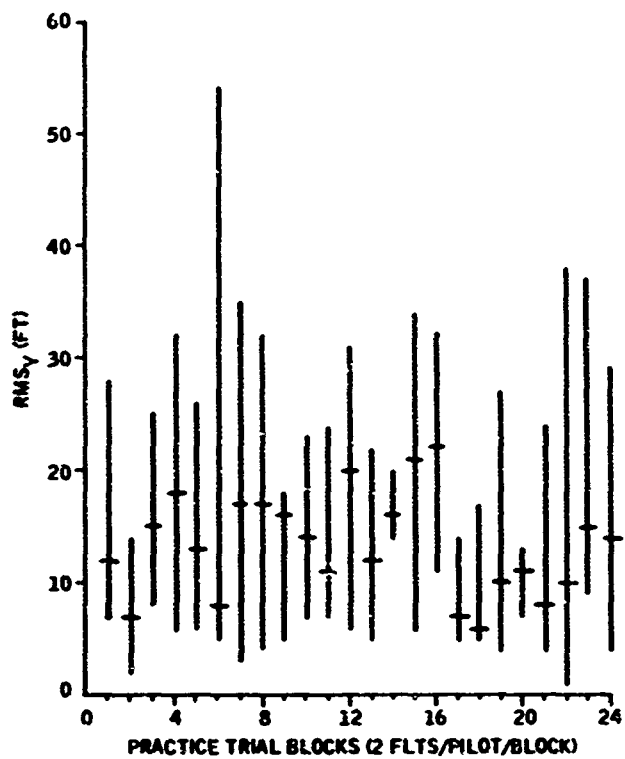for Each Practice Block; XV-5 Aircraft; Descent
Phase

4-8

Figure 4-10. Median RMS_y Error (and 19th and 81st Percentiles)
for Each Practice Block; XV-5 Aircraft; Descent
Phase

4-9

SECTION V

FORMAL SIMULATION - TASK II

The objectives of the formal simulation phase of the Task II study were to conduct a systematic simulation and evaluation of measurement-system noise and filtering characteristics, and the interactive effects of these variables on selected levels of other relevant system and task variables including approach angle, display format and display-quickening gain. Descriptions of the task characteristics simulated, the independent and dependent variables evaluated, and the experimental plan followed in conducting the formal evaluation are given below. Results obtained from these simulations are presented in Section VI.

SIMULATED APPROACH AND LANDING MISSION

The simulated approach and landing mission segment consisted of four "active" or time-consuming phases:

- **Initial-Approach Phase:** The initial condition for each flight was a point in space, the position of which was defined (for a given approach angle) to be to the left of the command approach path, and (3) at a range which would require approximately 60 seconds of flight time prior to glideslope intercept. At this initial point, the aircraft was programmed to be flying at 71 knots ground speed, and on a course parallel to the command approach path. Nulling of the initial lateral error and a reduction in ground speed from 71 knots to the commanded velocity for the final-approach phase (see Section III) was required.

- **Final-Approach Phase:** The final-approach phase was begun at a range computed such that time spent on the final approach would be 90 seconds if the final approach was flown exactly as commanded. This phase was terminated when the criteria defining initiation of the hover phase were met.

- **Hover Phase:** The hover phase was programmed to last for 20 seconds once begun. Criteria which were required to be simultaneously met before this timing interval was begun were a horizontal position error of less than 50 feet, an altitude error of less than 20 feet, and translational rates of less than 10 ft/sec. During the hover interval, a position was commanded at an altitude of 50 feet directly above the landing site.

● <u>Descent Phase</u>: At the end of the 20-sec hover interval, a descent to the landing site was commanded, independent of the vehicle's position errors at that time. Pilots were instructed to minimize position, horizontal-rate, and attitude errors prior to ground contact, but to avoid using excessive time in doing so.

INDEPENDENT VARIABLES

The following independent variables were incorporated into the formal-simulation phase of the study:

● <u>Subjects</u>: Five helicopter-rated pilots served as subjects for formal-data collection. One of the four pilots utilized in data collection with the UH-1 was transferred, necessitating the substitution and training of a fifth pilot for data collection with the XV-5 vehicle. All pilots were currently serving, or had previously served, on active-duty status, and each had between 2000 and 5000 hours flying time in various rotary-wing aircraft including the UH-1. All pilots held instrument ratings.

● <u>Vehicles</u>: Two simulated vehicles, the UH-1 and XV-5, were used. Practice and formal-data collection sessions were completed with the UH-1 simulation prior to the beginning of simulation flights with the XV-5 vehicle.

● <u>Display Formats</u>: Two display formats were evaluated. Each of these formats, described previously, included either a primary horizontal-situtation (PPI-AR) or vertical-situation (IEVD) display supplemented with peripherally located conventional instrumentation.

● <u>Approach Angles</u>: Two alternative approach angles (6 and 15 deg) were simulated for evaluation.

● <u>Quickening Gains</u>: Two sets of quickening coefficients, nominally defined as "high gain" and "low gain" were evaluated (see Section III).

● <u>Measurement-System Noise</u>: Three levels of simulated measurement system noise, nominally defined as "no noise", "intermediate noise" and "high noise" were evaluated (see Section III).

● <u>Filter Lags</u>: Three levels of signal filtering, previously defined in terms of the filter coefficient α , were evaluated.

5-2

DEPENDENT VARIABLES

The following performance measures were recorded during appropriate phases of the simulated task and served as a basis for interpreting pilot performance as a function of the treatment conditions described above:

- **Vertical and Lateral Flight·Path Deviations:** Root-mean-square (RMS) errors were recorded for vertical (RMS_Z) and lateral (RMS_Y) deviations from the command flight path during the final-approach phase, with only RMS_Z being recorded during the initial approach. Also, instantaneous vertical and lateral errors (E_Z and E_Y) were recorded along the flight path at 250-foot intervals.

- **Position Errors During Hover and Descent:** Position-error measures recorded for the hover phase were RMS_X (longitudinal position), RMS_Y and RMS_Z errors, with RMS_X and RMS_Y also being recorded during descent from hover.

- **Terminal Position Errors, Rates and Attitudes:** Aircraft position with respect to the command touchdown point (E_X and E_Y), translational rates ($\dot{X}_B$, $\dot{Y}$ and $\dot{Z}$), and attitudes (θ and ϕ) were measured at $Z = 0.0$ et. Also, since it was of interest to determine the accuracy with which the command approach path could be terminated at ground contact rather than hover at $Z = 50$ feet, these terminal data were also recorded at the instant that the aircraft reached $Z = 50$ feet during either the final-approach or hover phase, and again at the end of the hover phase itself prior to vertical descent to touchdown.

- **Time:** Times required to complete the initial-approach, final-approach and descent phases were recorded. The hover phase was programmed to be a constant 20 seconds.

- **Activity Indices:** Measures of pilot control-input activity for the pitch and roll center stick and collective (lift) stick were computed as RMS rates of the respective control movements. These activity indices (AI_θ, AI_ϕ, and AI_{col}) were scaled in arbitrary units for each vehicle simulation, and served as a basis for making inferences concerning the relative effects of experimental treatments upon pilot "workload" or task difficulty.

- **Control Losses:** Flights during which loss of vehicle control resulted were terminated by the experimenter or terminated automatically by ground contact. When a control loss resulted, the existing experimental conditions were recorded by the experimenter, and the flight was repeated.

5-3

A summary of dependent variables measured or computed, and the mission phases during which they were recorded, is given in Table 5-1. Specific measures were relevant for only certain mission phases. For example, RMS_x was computed only during hover and descent phases since a longitudinal position was not commanded until the hover phase was reached. Similarly, RMS_y was not meaningful during the initial-approach phase because of the initial lateral position error of 500 feet from which the simulated mission was begun.

EXPERIMENTAL PLAN

A plan of independent-variable combinations for the Task II study formal-simulation phase is summarized in Figure 5-1. This plan included a full-factorial combination of two display formats (D), two approach angles (A), two quickening-gain levels (Q), three measurement-noise levels (N) and three levels of filter lag (F) for each aircraft. Combined across aircraft, the total matrix set consisted of 144 experimental cells. Each pilot was required to complete four replications (flights) per cell resulting in a total of 2304 simulated flights to be scheduled for formal data collection.

Characteristics of the simulation held constant for the duration of the formal experiment included:

- Aircraft stability-augmentation systems (see Appendix A)

- System information update rate (13.3 Hz)

- Display gains and scale factors (with the exception of display-quickening gains and PPI-format scale changes noted in Section III).

- Turbulence level (see Appendix A)

SIMULATION SCHEDULE

A simulation schedule was developed which would counterbalance order effects of the various experimental variables to the maximum extent possible, but would minimize problems associated with transfer between test conditions. In developing this schedule variables were first ranked in order of anticipated sensitivity to transfer due to alternative of variable levels. This ranking, given below, was used as a basis for determining the frequency with which levels of each variable would be alternated in the schedule defined for data collection with each vehicle.

Table 5-1. Summary of Dependent-Variable Measurement or Computation

Variable	Initial Approach	Final Approach	Hover	Descent From Hover	Terminal Data Recorded At:		
					Comm. Hover Altitude (Z = 50 ft)	End Of Hover Phase	Gnd. Contact (Z = 0 ft)
Time	o————	———o—	—o—	—o			
RMS_X			o—	—o			
RMS_y		o———	—o—	—o			
RMS_Z	o———	———o—	—o—	—o			
EX					Δ	Δ	Δ
E_Y		o– – –o			Δ	Δ	Δ
E_Z		o– – –o					
$\dot{X}_B$					Δ	Δ	Δ
$\dot{Y}_B$					Δ	Δ	Δ
$\dot{Z}$					Δ	Δ	Δ
θ					Δ	Δ	Δ
ϕ					Δ	Δ	Δ
AI_θ	o———	———o—	—o—	—o			
AI_ϕ	o———	———o—	—o—	—o			
AI_{col}	o———	———o—	—o—	—o			

Key: o————o Continuous recording or computation
  o– – –o Periodic sampling
  Δ   Instantaneous sampling (terminal data)

VEHICLES (2)

UH-1   XV-5

QUICKENING GAINS (2)

FILTER RESPONSE LAGS (3)

NOISE LEVELS (3)

- THE ABOVE MATRICES ARE DUPLICATED FOR EACH LEVEL OF THE APPROACH-ANGLE (2) AND DISPLAY (2) VARIABLES
- THE TOTAL NUMBER OF CELLS IN THE RESULTING MATRIX SET IS 144
- THE USE OF 4 PILOTS WITH 4 FLTS/CELL/PILOT YIELDS A TOTAL OF 2304 FLTS IN THIS MATRIX SET
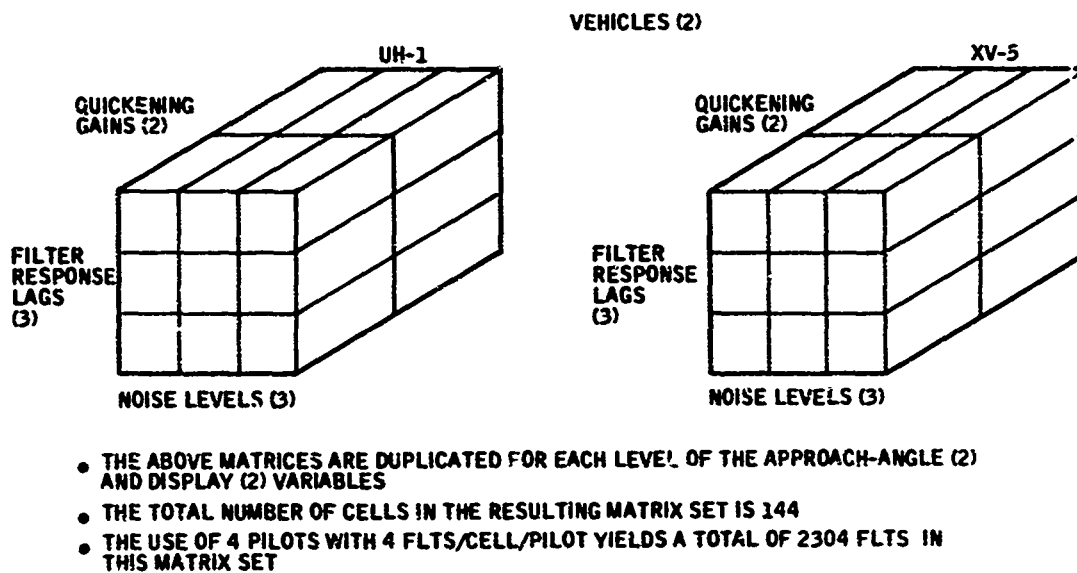
Figure 5-1. Experimental Plan for Task II Study

- Display formats - least frequently alternated
- Quickening gains
- Approach angles
- Filter lags
- Noise levels - most frequently alternated

For each subject, display format was altered once (for each vehicle) with presentation order of levels of this variable being counterbalanced between subjects. Similarly, for each display format, quickening gains were altered once, with presentation order of levels of this variable being counterbalanced between displays and between subjects. This process was repeated in a comparable manner for each of the independent variables listed above. In all cases the required four replications per cell were completed before proceeding to the next scheduled cell.

The data-collection schedule as developed by this process was repeated for each vehicle.

DATA ANALYSIS

Performance data resulting from the formal-simulation phase were analyzed, and are summarized in Section VI. Analyses, including the calculation of means, medians, standard deviations and analyses of variance were performed directly from data-output cards with a digital computer.

In the analyses of variance, the subject factor was considered as random, with with all other factors considered to be fixed effects.

SECTION VI
STUDY RESULTS - TASK II

Selected results of the analysis of pilot-performance data obtained during the Task II study formal-simulation phase are discussed in this section. Graphs of these data are presented in Appendix C. Since a summary presentation of all results obtained in graphical form would be prohibitive because of their volume, only selected samples judged to be of primary relevance in interpreting effects of the experimental variables under study are presented.

Performance results from each simulated vehicle are discussed separately below, with a further classification of study results into the following general categories:

- Results of analyses of variance performed on dependent variables having values not distributed around zero (e.g., time and RMS errors)

- Lateral and vertical glide-path errors recorded at 250-foot intervals during the final-approach phase

- Summary results of terminal-data dependent variables having values distributed around zero (e.g., $\dot{Y}_B$ and ϕ at ground contact)

Reference to independent variables and their associated levels in this report section and in figures appearing in Appendix C is simplified by use of the following code:

- Display formats (D)

    D_1: PPI-AR format

    D_2: IEVD format

- Approach angles (A)

    A_1: 6-degree glideslope

    A_2: 15-degree glideslope

- Quickening gains (Q)

    Q_1: "high-gain" quickening

    Q_2: "low-gain" quickening

6-1

- Filtering coefficients (F)

    F_1: minimum lag and noise reduction

    F_2: intermediate lag and noise reduction

    F_3: high lag and noise reduction

- Measurement noise (N)

    N_1: no measurement noise

    N_2: intermediate measurement noise

    N_3: high measurement noise

Also since data are referenced or illustrated as a function of mission phase (or data sampling point), the following additional coding is used:

- Phase (P)

    P_1: initial-approach phase

    P_2: final-approach phase

    P_3: hover phase

    P_4: descent (from hover) phase

    P_5: terminal data recorded at first contact
    with command hover attitude (Z = 50. 0 ft)

    P_6: terminal data recorded at end of hover phase

    P_7: terminal data recorded at ground contact
    (Z = 0. 0 ft)

ANALYSIS-OF-VARIANCE RESULTS FOR UH-1 VEHICLE

Condensations of analysis-of-variance summary tables indicating confidence levels for main effects and interactions are shown in Tables 6-1 through 6-5. Those effects found to be statistically significant at confidence levels between $p < 0.10$ and $p < 0.005$ are indicated.

Table 6-1. Condensation of Analysis-of-Variance Summary Tables; Phase 1; UH-1 Aircraft

Source	Dependent Variable				
	Time	RMS_Z	AI_θ	AI_ϕ	AI_{col}
D		0.100*	0.100	0.100	0.025
A		0.100	0.025		0.100
Q		0.100	0.005	0.100	
F		0.100			
N		0.005		0.005	
DA					
DQ			0.100		0.100
AQ					
DF					
AF		0.100			
QF					
DN			0.100	0.005	0.100
AN					
QN					
FN					
DAQ		0.025	0.100		
DAF		0.100			
DQF					
AQF					
DAN					
DQN					
AQN					
DFN					
AFN		0.005			
QFN					0.025
DAQF		0.100	0.025		
DAQN					
DAFN					
DQFN					
AQFN					
DAQFN					

*$P < 0.100$

Table 6-2. Condensation of Analysis-of-Variance Summary Tables; Phase 2; UH-1 Aircraft

Source	Dependent Variable					
	Time	RMS_Y	RMS_Z	AI_ϑ	AI_ϕ	AI_{col}
D					0.100*	
A		0.100	0.100			0.100
Q			0.100	0.025	0.100	
F		0.100				
N		0.005	0.005	0.005	0.005	
DA			0.100			
DQ				0.100		
AQ						
DF		0.100	0.100			
AF						
QF				0.100		
DN						
AN					0.025	
QN		0.100	0.025	0.025	0.005	
FN	0.025	0.005	0.025		0.100	
DAQ						
DAF						
DQF						
AQF						0.100
DAN						
DQN						
AQN						
DFN						
AFN						
QFN						
DAQF			0.100		0.100	0.025
DAQN						0.025
DAFN						
DQFN						
AQFN						
DAQFN						

*$P < 0.100$

Table 6-3. Condensation of Analysis-of-Variance Summary Tables; Phase 3; UH-1 Aircraft

Source	Dependent Variable					
	RMS_X	RMS_Y	RMS_Z	AI_θ	AI_ϕ	AI_{col}
D A Q F N	 0.025* 0.100	 0.100 		 0.025 0.025	 0.100 	 0.100
DA DQ AQ DF AF QF DN AN QN FN	 0.025 	 0.025	 0.005 0.100	 0.025 		
DAQ DAF DQF AQF DAN DQN AQN DFN AFN QFN	 0.100 0.100	 0.100 		 0.100 0.100 0.025 		0.100
DAQF DAQN DAFN DQFN AQFN	 0.100 			0.100 	 0.100 	
DAQFN						

*$P < 0.025$

Table 6-4. Condensation of Analysis-of-Variance Summary Tables; Phase 4; UH-1 Aircraft

Source	Dependent Variable					
	Time	RMS_X	RMS_Y	AI_θ	AI_ϕ	AI_{col}
D						
A						
Q				0.100^*	0.100	
F						
N		0.100				
DA						
DQ						
AQ						
DF						
AF						
QF						
DN						
AN				0.100		
QN		0.100		0.005	0.100	
FN		0.100				
DAQ						
DAF						
DQF	0.100					
AQF			0.100			
DAN						
DQN						
AQN						
DFN			0.100			
AFN			0.100			
QFN			0.025		0.100	
DAQF						
DAQN	0.100					
DAFN				0.025	0.100	
DQFN						
AQFN						
DAQFN	0.100					

$^*P < 0.100$

6-6

Table 6-5. Condensation of Analysis-of-Variance Summary Tables;
Phases 5 and 7; UH-1 Aircraft

Source	Dependent Variable	
	$\dot{Z}$ (Phase 5)	$\dot{Z}$ (Phase 7)
D		0.100[*]
A	0.025	
Q	0.100	
F		
N	0.100	0.100
DA		
DQ		
AQ		
DF		
AF	0.100	
QF		
DN		
AN		
QN	0.100	
FN		
DAQ		
DAF		
DQF		
AQF		
DAN		
DQN		
AQN		
DFN		
AFN		
QFN		
DAQF		
DAQN		
DAFN		0.100
DQFN		
AQFN		
DAQFN		0.100

[*]$P < 0.100$

6-7

Differences Due to Display Format

Differences between the two display formats simulated averaged across effects of all other independent variables (i.e., the main effect for display formats) are shown in Figures C1 through C4, Appendix C. Average performance data are plotted in those figures for mission phases for which the respective dependent-variable measures were computed. Although not consistently supported by statistical significance ("N.S." in figures indicates "not significant at $p < 0.10$"), consistent trends in these data suggest a difference between display formats in the form of a tradeoff between position-control accuracy and pilot control activity. The IEVD format (D_2) yielded up to 8-foot RMS-error reductions compared to the PPI-AR format (Figures C1 and C2), but at the cost of increased pilot control activity (Figures C3 and C4).

Differences Due to Approach Angle

Examples of the effect on piloting performance of differences in approach angle are shown in Figures C5 through C8. Lateral and vertical flight-path errors (RMS_y and RMS_z) during the final-approach phase (P_2) were approximately 9 feet greater for the steeper 15-degree approach angle (A_2). Higher pitch-cyclic and collective control activities which were statistically significant for the initial- and final-approach phases (Figures C7 and C8) are attributable to the greater speed reduction required prior to intercept of the 15-degree glideslope, and increased difficulty in altitude control while on this slope.

Differences Due to Quickening Gain

An interactive effect in the pitch and roll axes between position-control accuracy and pilot control activity similar to that described above for display formats also resulted due to differences in display quickening gain simulated (Figures C9 through C12). RMS position errors averaged between four and eight feet less for the "high-gain" quickening alternative (Q_1) with a compensating increase resulting in pitch- and roll-cyclic control activity for Q_1 in all mission phases.

Differences Due to Signal Filtering

Overall effects of the signal-filtering variable on piloting performance are shown in Figures C13 through C15. Statistically significant main effects resulted for RMS_y and RMS_z errors in phases P_2 and P_1 respectively. Although not significant statistically, other data presented in these figures do suggest interpretable trends. For example, in Figure C14, the beneficial effect of increased filtering during the final-approach phase (P_2) is apparent

6-8

in its effect on reduced RMSy errors. During hover and descent from hover (P_3 and P_4), effects of increased filtering are the opposite. Because of the proximity of the aircraft to the signal source during P_3 and P_4, noise levels are relatively lower than during the approach, and less filtering is required. Trends reflecting larger RMSy errors in P_3 and P_4 with increased filtering are attributed to greater sensitivity of aircraft control to signal lags in hovering flight.

Differences Due to Measurement Noise

Tests of the main effect for measurement noise yielded the anticipated results in that measurement noise had a more appreciable effect during phases associated with increased range from the signal source. Figures C16 and C17 exemplify these findings. Lateral errors (RMSy) during the final-approach phase increased from 30 feet for the "no-noise" condition to 54 feet for the "high-noise" condition, while error levels during hover were approximately 30 feet for all levels of noise simulated (Figure C16). Effects on altitude-control accuracy with increased noise levels followed a similar pattern as shown in Figure C17. The contributions of measurement-noise effects to pitch- and roll-axis control activity are illustrated in Figures C18 and C19. Effects of measurement noise on pitch-cyclic control activity (Figure C18) are similar for all mission phases because of the predominant contribution of R_N in feet, rather than degrees, to the noise amplitude appearing on pitch-axis quickening (X_Q). Increased roll-axis control activity (Figure C19) due to noise reflects the fact that noise appearing on the lateral-axis quickening (Y_Q) was influenced primarily by B_N, in degrees, resulting in higher display-noise levels on Y_Q at increased ranges.

Display-by-Angle (DA) Interaction Results

The dependent variable RMSz yielded the only significant DA interaction from analyses of variance performed on UH-1 flight-performance data. As shown in Figure C20, differences in RMS altitude error as a function of approach angle were greatest for the IEVD format (D_2), ranging from 34 feet for the 6-degree angle (A_1) to 47 feet for the 15-degree approach angle during the final-approach phase.

Display-by-Filter (DF) Interaction Results

The significant DF interaction for RMSy during the final-approach phase (Figure C21) is useful as an aid in interpreting the trend toward differences in the main effect for displays previsouly discussed (Figure C2). Differences between displays in terms of RMSy error during final approach, depicted in Figure C21, were greatest for the lowest level of signal filtering (F_1), and became negligible as the level of filtering was increased (F_3). This interaction

6-9

is attributed to a basic difference between the two display formats evaluated.
As quickened-symbol noise levels associated with reduced filtering increased,
pilots placed greater reliance on the use of aircraft-attitude information pre-
sented on the artificial horizon as a cross reference to subjectively "filter"
noise-degraded quickened-symbol commands. Cross referencing in this
manner, more easily accomplished on the IEVD format because of the super-
position of attitude and quickened-command information on the primary IEVD
display, is considered to be the reason for relatively lower RMS errors
yielded with this format under conditions of minimum signal filtering (F_1).
Conversely, larger error levels resulting with the PPI-AR display (D_1) with
minimum filtering are attributed to more "conservative" pilot control-input
responses to noise-degraded quickening commands because of the lack of
close spatial proximity of displayed-attitude and quickening-command infor-
mation.

Display-by-Noise (DN) Interaction Results

Significant DN interactions were limited to those based on control-activity
data recorded during the initial-approach phase. As exemplified by data for
the roll axis shown in Figure C22, roll-cyclic control activity was highest
for the IEVD format (D_2) under "no-measurement-noise" conditions. As
measurement noise was increased, relatively greater increases in control
activity also resulted with this format compared to those associated with
the PPI-AR format.

Quickening-by-Filter (QF) Interaction Results

Trends in the QF interaction for pitch-axis control activity measuring during
the final-approach phase (Figure C23) suggest different effects of signal
filtering for each quickening level simulated. For "high-gain" quickening
(Q_1), a reduction in control activity corresponds to a reduction in noise due
to increased filtering. Conversely, the effect on control activity with the
"low-gain" quickening level appears to be more directly related to signal
lag caused by increased filtering. However, these interactive effects are
small relative to the main effect due to quickening levels.

Quickening-by-Noise (QN) Interaction Results

Significant QN interactions found in the analysis-of-variance results (Figures
C24 through C28), contribute to interpretation of main-effects data for the
quickening-gain variable previously shown in Figures C9 through C12. Gen-
erally, effects of increased noise on piloting-performance accuracy were
less for the "low-gain" quickening level (Q_2). For example, during the
descent from hover phase (P_4), RMS_X errors averaged 12 feet greater for
Q_2 than for Q_1. As noise levels were increased this difference was reduced

6-10

to approximately 5 feet (Figure C24). Similarly, RMS_Y errors during the final-approach phase averaged 13 feet greater for Q_2 under conditions of no noise while essentially no difference between Q_1 and Q_2 resulted under high-noise condition N_3 (Figure C25). Although altitude-command-symbol gains were not changed with levels of quickened symbol gain, an indirect effect on altitude control during final approach was observed due to the quickening-gain variable (Figure C26). Altitude errors defined as RMS_Z were higher with Q_1 for all noise levels, with Q_1 gains also being relatively more sensitive to increasing noise levels. These relationships suggest that the longitudinal/lateral control task was more demanding with Q_1 at higher noise levels, resulting in some sacrifice of attention to the altitude control task. This interpretation is consistent with data from pitch and roll control-activity measures shown in Figures C27 and C28.

Filtering-by-Noise (FN) Interaction Effects

Data resulting from this interaction effect are of particular interest since they represent the effects on piloting performance of the tradeoff between display-noise reduction and signal-lag increase due to filtering. Average time required to complete the final-approach phase for each filter-and-noise-level combination is shown in Figure C29. Nominal time for completion of this phase was 90 seconds if flown exactly as commanded. It may be noted as an aid in interpreting these data that differences in time to complete this phase were due predominantly to additional time required to meet hover criteria at the end of the final approach (i.e., time differences reflect the accuracy with which the final approach was terminated). As indicated in Figure C29, no interpretable differences in final-approach time resulted across filter levels under the no-noise condition N_1. Noise levels N_2 and N_3 did, however, yield an anticipated increment in time required under minimum-filtering condition F_1 (approximately 15 seconds), but resulted in only small increases in time required (up to 3 seconds) for intermediate and high filter levels F_2 and F_3. Figures C30 through C33, depicting significant FN interactions for various RMS position-error measures and approach phases, indicate similar trends. Under condition N_1 the effects of signal lag due to increased filtering are apparent. As measurement noise is increased, effects of additional signal filtering are beneficial in terms of reduced RMS position errors. It should again be noted that these interaction data are useful for more detailed interpretation of main-effects data previously presented. In Figure C14, for example, the filter main effect for P_2 indicates reduced RMS_Y errors with increased signal filtering. However, the extent of this error reduction is, as would be expected, a function of the level of measurement noise (see Figure C31). For display-noise levels below those associated with N_2 during the final approach, a level of signal filtering comparable to F_1 may be most appropriate.

FLIGHT-PATH-ERROR INTERVAL DATA FOR UH-1 VEHICLE

Representative examples of instantaneous vertical and lateral flight-path errors (E_Z and E_Y) recorded at 250-foot intervals during the final-approach phase (P_2) are shown in Figures C34 through C39 of Appendix C. As plotted, these data depict error time histories which show intervals during approach where flight-path errors tend to be largest and/or most variable from flight to flight. Each point plotted is the median (50th percentile) of 16 samples from four simulated flights per pilot per experimental cell, while variabilities around each point define the ±34th-percentile range associated with each median. This specific range was selected to illustrate flight-to-flight data variability since it approximates plus and minus one standard deviation of a normal distribution.

In interpreting these figures it should be noted that vertical (E_Z) and lateral (E_Y) error scales are considerably expanded beyond the scaling of range from the hover point to facilitate reading of error levels. Error sequences begin with the first sample at 250 feet after slope intercept (right side of figures), and continue to the last sample recorded near final-approach termination.

Levels of independent variables defining the test conditions associated with each figure shown are indicated by alphanumeric codes similar to those previously described. Additional coding of vehicle ($V = 1$ and $V = 2$ denote UH-1 and XV-5 respectively) and aircraft control-augmentation mode (C) are also given. Because control-augmentation mode was a variable in the Task III study to be discussed later in this report, the identifier "C" was introduced here to allow use of a consistent coding scheme for both study tasks. The code $C = 1$ shown in Figures C34 through C39 simply refers to the use of a three-axis SAS for both vehicles in the Task II study.

Interval data for the following test conditions are shown in these figures

Variables

	Q	N	F	A	C	D	V
	1	1	1	1	1	1	1
	1	1	1	2	1	1	1
Variable	1	3	1	1	1	1	1
Levels	1	3	1	2	1	1	1
	1	3	3	1	1	1	1
	1	3	3	2	1	1	1

where, for example, the treatment combination listed in the last row includes $Q = 1$ (high-gain quickening), $N = 3$ (high noise level), etc. Examples shown are all for the PPI-AR display format.

6-12

Generally, altitude-error ... indicate some altitude-command overshoot at slope inter ..., with increased altitude errors again during the pitch-up maneuver as ...iated with deceleration to hover. Under conditions of no measurement r ⋅ (Figures C34 and C35), increased altitude-error variabilities for the ...eeper 15-degree approach angle may be observed. The degrading effects of measurement noise are apparent in the comparison of data in these figures to that shown in Figures C36 and C37. Average (median) errors and between-flight error variabilities increase appreciably for both approach angles under the noise condition depicted. Effects of additional filtering (Figures C38 and C39) for the same level of measurement noise appear to have the greatest influence on reduction of flight-to-flight error variability. Although not shown in Appendix C, equivalent data for the IEVD display format yielded comparable results.

TERMINAL DATA FOR UH-1 VEHICLE

Terminal position errors, translational rates, and attitudes for the same test conditions as those described above are shown in Figures C40 through C45. Data presented are in a similar form, depicting medians and ±34th-percentile ranges around each median for terminal measures recorded at three points near or at termination of the approach and landing mission simulated. The points, previously defined in this report section as P_5, P_6, and P_7, are indicated for data associated with each test condition.

Fore-aft translational-velocity data in Figure C40 indicate that a forward-velocity ($+\dot{X}_B$) component was predominant at first contact with the command hover altitude of 50 feet (P_5). A primary contributor to this result was a tendency for negative altitude errors (below glide path) near termination of the approach to hover, resulting in first contact with hover altitude on the approach side of the commanded hover point (see Figure C42). Longitudinal velocities (Figure C40) were reduced to median values near zero by the end of the hover phase (indicated by sampling point P_6), and were maintained at approximately the same level to ground contact (P_7). For P_6 and P_7, increased noise had the effect of increasing variability in $\dot{X}_B$ samples while increased filtering with the high noise levels yielded a reduction of flight-to-flight sample variability to nominally the same level as that shown for the "no-noise" condition (N_1). Lateral-velocity data sampled at these three points also yielded increased variability due to noise, but, as shown in Figure C41, do not reflect appreciable decreases in sample variability due to a further increase in signal filtering. Vertical velocities at ground contact, not illustrated in these figures, averaged between 4 and 6 ft/sec. Longitudinal and lateral position-error components sampled at P_6 and P_7 (Figures C42 and C43) indicate noise and filter effects similar to those described above for translational-velocity data. Increased variabilities in aircraft-attitude samples (Figures C44 and C45) associated with high noise and filtering levels suggest degraded aircraft-control stability under these conditions.

CONTROL-LOSS DATA FOR UH-1 VEHICLE

Of the 1152 simulated approaches and landings flown with the UH-1 vehicle during formal-data collection in the Task II study, a total of 10, or 0.87 percent resulted in loss of aircraft control. These are distributed across variable levels for each independent variable as shown in Table 6-6. Because of the small number of control losses and the fact that six of the ten resulted with only one of the four pilots, generalization of these data is not advisable.

In all cases of control loss, the simulation was stopped, reset to initial conditions and restarted. Data from missions in which control losses occurred were not included in the analyses reported in this section.

Table 6-6. Control-Loss Data for UH-1

Variable	Variable Level		
	1	2	3
Q	8*	2	
N	4**	3	3
F	4	3	3
A	6	4	
D	8	2	

*i.e., eight of ten control losses resulted under conditions with "high-gain" quickening (Q_1)

**i.e., four of ten control losses resulted under conditions with no measurement noise (N_1)

ANALYSIS-OF-VARIANCE RESULTS FOR XV-5 VEHICLE

Condensations of analysis-of-variance summary tables indicating confidence levels for main effects and interactions are shown in Tables 6-7 through 6-11. As with UH-1 vehicle data previously presented, tests found to be statistically significant at confidence levels between $p < 0.10$ and $p < 0.005$ are indicated.

6-14

Table 6-7. Condensation of Analysis-of-Variance Summary Tables; Phase 1; XV-5 Aircraft

Source	Dependent Variable				
	Time	RMS_Z	AI_θ	AI_ϕ	AI_{col}
D		0.100*		0.100	0.100
A		0.100		0.100	0.100
Q					
F	0.100	0.100			0.025
N		0.005	0.100	0.005	
DA	0.100				0.100
DQ					
AQ					
DF					
AF		0.025			
QF					
DN					
AN					
QN					
FN			0.025	0.025	
DAQ		0.100			
DAF		0.100			
DQF					
AQF					
DAN					
DQN					
AQN					
DFN					
AFN				0.100	
QFN			0.100		
DAQF					
DAQN					
DAFN				0.100	
DQFN					
AQFN					
DAQFN					

*P < 0.100

6-15

Table 6-8.   Condensation of Analysis-of-Variance Summary Tables; Phase 2; XV-5 Aircraft

Source	Dependent Variable					
	Time	RMS_Y	RMS_Z	AI_θ	AI_ϕ	AI_{col}
D				0.100*		
A				0.025	0.100	
Q						
F	0.005	0.005	0.005		0.100	
N	0.100	0.005	0.005	0.100	0.025	
DA						
DQ						
AQ						
DF						
AF						
QF	0.025					
DN		0.025	0.100			
AN						
QN				0.100	0.100	
FN	0.100	0.005		0.025	0.100	
DAQ						
DAF						0.100
DQF						
AQF	0.005	0.100				
DAN						0.100
DQN						
AQN					0.100	
DFN						
AFN			0.100		0.100	
DQN					0.100	
DAQF						
DAQN						
DAFN						
DQFN	0.100					
AQFN						
DAQFN						

*$P < 0.100$

6-16

Table 6-9. Condensation of Analysis-of-Variance Summary Tables; Phase 3; XV-5 Aircraft

Source	Dependent Variables					
	RMS_X	RMS_Y	RMS_Z	AI_θ	AI_ϕ	AI_{col}
D						
A						
Q	0.100*	0.100				
F	0.100		0.005		0.100	
N		0.025		0.025		
DA						
DQ	0.100					
AQ						
DF						
AF	0.100					
QF						
DN				0.100		
AN					0.100	
QN						
FN		0.025				
DAQ						
DAF						
DQF						
AQF						
DAN				0.100		
DQN						
AQN						
DFN				0.005		
AFN						
QFN					0.100	
DAQF						
DAQN						0.100
DAFN		0.100				
DQFN						
AQFN	0.005					
DAQFN						

*P < 0.100

6-17

Table 6-10. Condensation of Analysis-of-Variance Summary Tables; Phase 4; XV-5 Aircraft

Source	Time	RMS_X	RMS_Y	AI_θ	AI_ϕ	AI_{col}
D A Q F N	 0.005	 0.100* 0.025 0.035	 0.100 0.005	 0.100 0.025	 0.100 	
DA DQ AQ DF AF QF DN AN QN FN	 0.100 	 0.025 0.025 0.100 0.100	 0.100	 0.025 0.025	 0.100 	
DAQ DAF DQF AQF DAN DQN AQN DFN AFN QFN	 0.100 	 0.100 		 0.025 		 0.100
DAQF DAQN DAFN DQFN AQFN						
DAQFN						

*P < 0.100

6-18

Table 6-11. Condensation of Analysis-of-Variance Summary Tables; Phases 5 and 7; XV-5 Aircraft

Source	Dependent Variable	
	$\dot{Z}$ (Phase 5)	$\dot{Z}$ (Phase 7)
D		
A	0.025*	
Q		
F	0.025	
N		
DA		
DQ	0.100	
AQ	0.025	
DF		
AF		
QF	0.005	
DN		0.100
AN		
QN		
FN		
DAQ		
DAF		0.100
DQF		
AQF		
DAN	0.100	
DQN		
AQN		
DFN		
AFN		
QFN	0.100	
DAQF	0.100	
DAQN		
DAFN		
DQFN		
AQFN	0.100	
DAQFN		

*P < 0.025

6-19

Differences Due to Display Format

Data selected to depict the effect of display-format differences on piloting performance with the XV-5 vehicle are shown in Figures C46 through C50 of Appendix C. General trends in these data are similar to those resulting with the UH-1 vehicle in that RMS position errors tend to be greater for the PPI-AR format (D_1) while control-activity indexes are higher for the IEVD format (D_2). Longitudinal RMS position errors during the hover phase (P_3) averaged from 10 to 15 feet greater than for the descent phase (P_4) because of a tendency to overshoot the hover point with the XV-5 vehicle. As indicated in Figure C46, this characteristic was common to both display formats simulated.

Differences Due to Approach Angle

The approach-angle variable did not yield significant differences in flight-path-control accuracy (RMS_Y and RMS_Z) during final approach with this vehicle. RMS errors during P_2 ranged from $RMS_Y \simeq 22$ feet to $RMS_Z \simeq 32$ feet. Differences in pitch control activity due to approach angle varied as a function of mission phase (Figure C51), while significant differences for roll control activity yielded lower hover-control-activity indexes for the steeper 15-degree approach angle (Figure C52).

Differences Due to Quickening Gain

As with the UH-1 vehicle, RMS_X and RMS_Y position errors (Figures C53 and C54) were lower for the "high-gain" quickening level. However, absolute differences between Q_1 and Q_2 in terms of position errors were small, ranging from 2 feet for RMS_Y during P_3 to approximately 9 feet for RMS_X during P_4. Measures of pitch and roll control activity did not yield statistically significant differences due to quickening-gain levels.

Differences Due to Signal Filtering

Effects of the signal filtering on piloting performance are shown in Figures C55 through C58 of Appendix C. The statistically significant difference in RMS_X for the filter main effect (Figure C55) is attributable to increases in signal lag since performance is degraded as level of filtering increases. The net effect of increased filtering on RMS_Y during final approach (P_2) is just the opposite as lateral errors are reduced with increased filtering (Figure C56). This finding, consistent with data previously described for the UH-1 vehicle, suggests the beneficial effect of signal filtering (due to noise reduction) during final approach where signal lags apparently have relatively less effect on position-control performance. The same interpretation may be applied to trends in RMS_Z data for P_2 shown in Figure C57 and roll-axis control-activity data in Figure C58.

6-20

Differences Due to Measurement Noise

The main effect for measurement noise yielded small but statistically significant differences for RMS_X recorded during descent from hover (Figure C59). Average RMS_X ranged from 18.5 feet for N_1 to 22.5 feet for N_3 during this phase. Larger increments of RMS_Y and RMS_Z errors due to measurement noise were found for the initial- and final-approach phases (P_1 and P_2), while hover and descent phases (P_3 and P_4) again yielded relatively small but statistically significant effects for RMS_Y (Figures C60 and C61). Relationships between noise levels and RMS errors are consistent with those previously discussed for the UH-1 vehicle. Control-activity-index data, shown in Figures C62 and C63, also reflected significant increasing trends with noise as did comparable data recorded with the UH-1.

Display-by-Quickening (DQ) Interaction Results

Measures of RMS_X error during hover yielded a significant DQ interaction (Figure C64) indicating relatively larger longitudinal position errors for the "low-gain" quickening level (Q_2) used in conjunction with the PPI-AR display format (D_1). Although this additional error is most likely attributable to an increase degree of overshoot of the command-hover point, reasons for additional error of this type with the display/quickening combination D_1Q_2 are not clear.

Display-by-Noise (DN) Interaction Results

Significant DN interactions for RMS_Y (Figures C65) and RMS_Z (Figure C66) flight-path errors during final approach yielded similar relationships. Under conditions of no noise, error levels for both display formats were nominally the same. Under conditions of measurement noise, error levels increased for both formats, but increased relatively more for the PPI-AR format. For example, the total increment in RMS_Y across noise levels was 17.9 feet for the PPI-AR format and 6.0 feet for the IEVD format. Sensitivities of pitch control activity to increased noise also varied as a function of display format during hover and descent phases (Figures C67 and C68). Increments in control activity from levels resulting with no noise were smallest for the PPI-AR format in both phases.

Quickening-by-Noise (QN) Interaction Results

Although the quickening main effect was significant for hover and descent phases in terms of RMS_X (Figure C53), a QN interaction for RMS_X resulted only in the descent phase (Figure C69). In this phase the "low-gain" quickening

level (Q_2) was somewhat more sensitive to increased noise levels. However, this interactive effect was small (1 to 2 feet) compared to the main-effect difference due to quickening levels (approximately 9 feet RMS_X). Significant QN interactions for pitch and roll control-activity indexes are shown in Figures C70 through C72. All indicate trends toward lower control activity with high noise levels for Q_2, while differences are not consistent across phases for lower measurement-noise levels associated with N_1 and N_2.

Filter-by-Noise (FN) Interaction Results

Average times to complete the final-approach phase for each filter-and-noise-level combination are shown in Figure C73. As with the UH-1 vehicle, deviations from the nominal 90-second time required to complete this phase were due predominantly to additional time required to meet hover criteria at termination of the approach. Consistent with data obtained from flights with the UH-1, time required for completion of final approach during XV-5 flights increased with high-noise/low-filtering combinations. Increased filtering had the effect of reducing time differentials with increased noise to nearly zero. Statistically significant FN interactions for RMS-position-error measures recorded during the various mission phases are shown in Figures C74 through C77. All examples reflect small degrading effects of signal lag with filtering under "no-noise" condition N_1. The beneficial effects of signal filtering upon performance are apparent for higher noise levels, especially during final approach (Figure C75) where the filtering levels studied yielded a 15-foot reduction in RMS_y for N_3. Examples of significant FN interactions for pitch and roll control-activity indexes during P_2 also reflected the same increasing and decreasing trends as a function of the interaction between noise and filter variables (Figures C78 and C79).

FLIGHT-PATH-ERROR INTERVAL DATA FOR XV-5 VEHICLE

Examples of instantaneous vertical and lateral flight-path errors (E_z and E_y) for test conditions identical to those previously presented for the UH-1 are shown for the XV-5 vehicle in Figures C80 through C85 of Appendix C. Error averages and variabilities plotted for each sampling point are defined as previously described. Altitude errors for the steeper 15-degree approach flown under "no-noise" conditions (Figure C81) indicate less flight-to-flight variability for the XV-5 than for the UH-1 vehicle (see Figure C35). Where differences between vehicles do occur as a function of test conditions shown, lower average errors and error variabilities most typically characterize piloting performance with the XV-5.

TERMINAL DATA FOR XV-5 VEHICLE

Terminal position-error, translational-rate, and attitude data resulting from flights with the XV-5 vehicle are shown in Figures C86 through C91 of Appendix C. Examples given are for the same test conditions as those used above in describing 250-foot interval data. Data presented are in a similar form, depicting medians and ±34th-percentile ranges around each median for terminal data recorded at three sampling points previously defined as P_5, P_6 and P_7.

Longitudinal-velocity measures $(\dot{X}_B)$ yielded generally decreasing trends in averages and variabilities across these sampling points, with minimum deviations from $\dot{X}_B = 0.0$ ft/sec typifying samples taken at ground contact (P_7). These trends, shown in Figure C86, also indicate only minor changes in performance due to measurement-noise and filter effects. At ground contact average (median) $\dot{X}_B$ was near zero in all cases, with variabilities (±34th-percentile deviations from the median) being greatest under conditions including high noise and filtering levels (N_3F_3). Median lateral velocities $(\dot{Y}_B)$ were at or near zero in all cases shown, with variability ranges exceeding 1.0 ft/sec only under conditions of high noise and minimum signal filtering (Figure C87). Vertical velocities at ground contact, not shown in these figures, averaged between 4.0 and 5.0 ft/sec. Lateral position-error and roll-attitude variabilities at ground contact (P_7) were also relatively higher for the N_3F_1 condition as depicted in Figures C89 and C91. Comparable terminal data for the longitudinal axis (Figures C88 and C90) did not, however, yield similar trends. Increased variabilities in E_X and X_B appeared primarily at P_5 under conditions of both high-noise and high-filtering levels (N_3F_3), suggesting relatively greater effects of signal lag on longitudinal-axis control during the flare maneuver.

CONTROL-LOSS DATA FOR XV-5 VEHICLE

Of the 1152 approaches and landings flown with the XV-5 vehicle simulation during formal-data collection in the Task II study, a total of eight, or 0.69 percent resulted in loss of aircraft control. Table 6-12 summarizes the distribution of control losses across variable levels for each independent variable evaluated. These occurrences were distributed approximately evenly across pilots, with two pilots each having two control losses, and the remaining two pilots having one and three losses respectively. Although the number of control losses was small, these events are distributed across measurement-noise levels in such a manner as to suggest an increased tendency for loss of aircraft control under the high-noise condition N_3. Additional interpretation of contributions of the variables to these data are not advisable because of the small control-loss sample resulting.

6-23

Table 6-12. Control-Loss Data for XV-5

Variable	Variable Level		
	1	2	3
Q	4*	4	
N	1	0	7
F	4	1	3
A	5	3	
D	5	3	

*i.e., four of eight control losses resulted under conditions of "high-gain" quickening (Q_1)

SECTION VII
STUDY DEFINITION - TASK III

OBJECTIVES

The primary objective of the Task III study phase was to investigate the effects of selected alternative aircraft control-augmentation modes on pilot performance of the steep-angle approach and landing task. Interactive effects of this variable with other relevant system variables were also evaluated in a manner similar to that previously described for the Task II study to obtain increased generality of study results and to preserve a maximum level of continuity toward the overall program objective of investigating display requirements for performance of IFR steep approaches.

Variables and task characteristics simulated in the Task III study are discussed in the following paragraphs and in Appendix A.

APPROACH TASK SIMULATED

The approach and landing task simulated, identical to that described in Section III for the Task II study, consisted of four mission phases:

- Initial Approach
- Final Approach
- Hover
- Descent from Hover

AIRCRAFT SIMULATED

Continued use was made of both the UH-1 and XV-5 aircraft simulations. However, the simulations were modified as necessary to allow selection by the experimenter from among four alternative aircraft control-augmentation modes. These alternative modes are described in detail below.

APPROACH ANGLES SIMULATED

The 6- and 15-degree constant-gradient approach angles included in the previous study also constituted the two approach-angle variable levels for the Task III study phase.

7-1

DISPLAY FORMATS SIMULATED

The IEVD and aircraft-referenced PPI formats were simulated for continued evaluation in conjunction with the aircraft control-augmentation variable in this study phase. Display-quickening gains were held constant during the Task III study, with gains used being those defined in Section III of this report as "high-gain" coefficients.

SYSTEM NOISE AND FILTER CHARACTERISTICS SIMULATED

Combinations of no measurement noise/"minimum" signal filtering (N_1 F_1) and "high" measurement noise/"high" signal filtering (N_3 F_3), as previously defined in Sections III and VI of this report, were simulated for the present study. Inclusion of the resulting two-level measurement-noise/filtering variable in the Task III study allowed evaluation of the selected aircraft control-augmentation modes under conditions of both near-perfect signal accuracy, and degraded signal accuracy due to noise and filtering lags.

AIRCRAFT CONTROL-AUGMENTATION MODES SIMULATED

The primary objective of the Task III study was to evaluate the effects of alternative aircraft control-augmentation modes on pilot performance of the IFR steep-angle approach task.

Experience with the IFR approach and landing problem as simulated in the Task I SAA study (Ref. 1) suggested that specific modes of aircraft control augmentation, added to supplement the three-axis stability-augmentation system (SAS) used with the simulated UH-1 and XV-5 vehicles, would aid in unburdening the pilot during critical phases of the approach and landing maneuver. Observations of pilot responses in this study indicated that the level of pilot workload is greatest during terminal phases of the approach when effects of aerodynamic damping upon the vehicle are at a minimum. This interval includes the period of deceleration from approach speed to hover, the period of hover itself, and descent from hover.

Beginning at initiation of deceleration from command-approach speed, the pilot's control task becomes increasingly difficult. Groundspeed and descent rate must be dissipated at a commanded rate if the desired flight path is to be followed. Piloting the XV-5 VTOL vehicle through this approach segment requires, for example, frequent changes in "vector angle" and aircraft trim which adds additional burden to the control task. Both vehicles require more frequent rudder inputs for yaw control as aerodynamic-damping effects are lost with decreasing velocity. Yaw control during deceleration and hover is a relatively more difficult task to perform with the simulated UH-1 helicopter because of yaw moments caused by cross coupling from other required control inputs (primarily collective and cyclic pitch).

7-2

Based on these observations, four alternative aircraft control-augmentation modes were selected and simulated for systemstic comparison as levels of an experimental variable in the Task III study. These four models are described in the following paragraphs.

Three-Axis Stability-Augmentation System (SAS)

The three-axis SAS mode used in previous Task I and II studies with both simulated aircraft was also included in Task III as a baseline test condition to which pilot performance and other control-augmentation modes could be compared. It is generally agreed that stability augmentation is a minimum level of control augmentation for V/STOL aircraft under low-speed and hovering flight conditions (e.g., Refs. 10, 36, 37, and 38).

Control laws simulated for the UH-1 rate-stabilization system were the following:

- Pitch axis: B_{1S_S} (deg) $= \delta_{\theta_c} - 0.312 \left[\frac{3S}{3S+1}\right] \dot{\theta}$

- Roll axis: A_{1S_S} (deg) $= \delta_{\phi_c} - 0.125\ \dot{\phi}$

- Yaw axis: $\theta_{TR} = \delta_{R_c} - 0.755 \left[\frac{S}{S+1}\right] \dot{\psi}$

where

$\delta_{\theta_c},\ \delta_{\phi_c},\ \text{and}\ \delta_{R_c}$ = pitch, roll and rudder control inputs

$\dot{\theta},\ \dot{\phi},\ \text{and}\ \dot{\psi}$ = pitch, roll and yaw rates in deg/sec

B_{1S_S} = B_{1S} due to cyclic-stick input (see Ref. 33)

B_{1S} = sine component of main-rotor cyclic-pitch angle

A_{1S_S} = A_{1S} due to cyclic-stick input

A_{1S} = cosine component of main-rotor cyclic-pitch angle

θ_{TR} = blade pitch of tail rotor

7-3

These SAS configurations use a conventional shaped rate-feedback command to control actuators, with pitch- and yaw-rate feedbacks high passed (Ref. 39).

Rate stabilization system control laws simulated for the XV-5 vehicle were the following:

- Pitch axis: KNF (percent) = $\delta_{\theta_c} - 0.12 \, \dot{\theta}$

- Roll axis: β_S (deg) = $\delta_{\phi_c} - 1.0 \, \dot{\phi}$

- Yaw axis: β_V (deg) = $\delta_{R_c} - 1.56 \, \dot{\psi}$

where

$\delta_{\theta_c}, \; \delta_{\phi_c}, \; \delta_{R_c}$ = pitch, roll and rudder control inputs

$\dot{\theta}, \; \dot{\phi}, \; \dot{\psi}$ = pitch, roll and yaw rates in deg/sec

KNF = percent nose-fan-door efficiency (see Ref. 32)

β_S = wing-fan-louver stagger angle

β_V = wing-fan-louver vector angle

Stability-augmentation loops formed a basic three-axis rate damper in this mode in a manner similar to that previously simulated as a "maneuvering mode" for the XV-5 vehicle (Ref. 40).

Block diagrams of the SAS modes simulated for the UH-1 and XV-5 vehicles are shown in Figures 7-1 and 7-2, respectively. Additional control modes simulated, as described below, are also shown in these figures.

The SAS gains given above for both vehicles were established empirically during preliminary simulations in the Task I SAA study (Ref. 1), and were selected to yield a satisfactory compromise in aircraft handling qualities for the speed range and control tasks required in this program. Although the fixed-gain systems described above represent a performance compromise because of the wide variation in aircraft dynamics associated with the speed range simulated, development of scheduled-gain or adaptive-gain mechanizations for these aircraft was not within the scope of the present study program. However, for purposes of comparative evaluation, fixed-gain mechanizations (characteristic of all alternative control-augmentation modes simulated for this study) offer the advantage of conceptual simplicity to aid in the interpretation of piloting performance with alternative modes being tested.
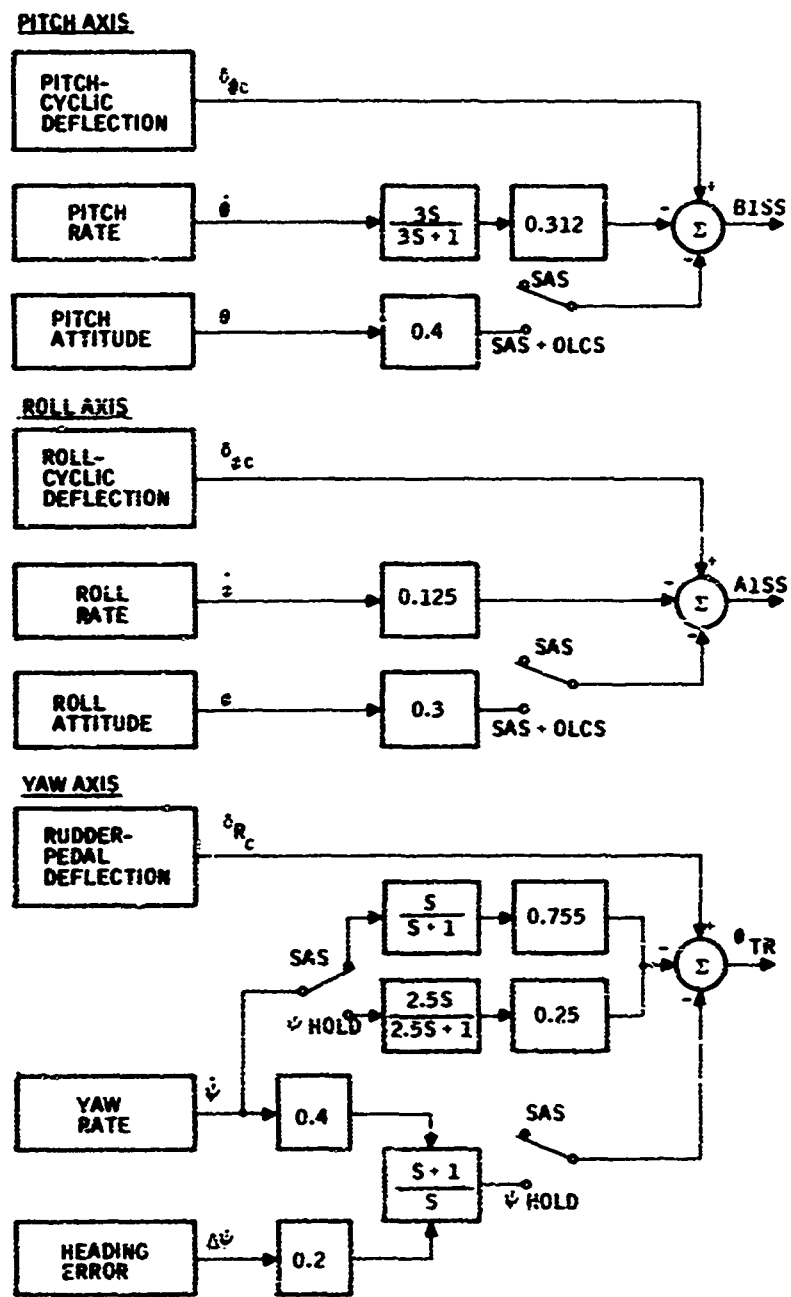
Figure 7-1. UH-1 Control-Augmentation Modes Simulated

7-5
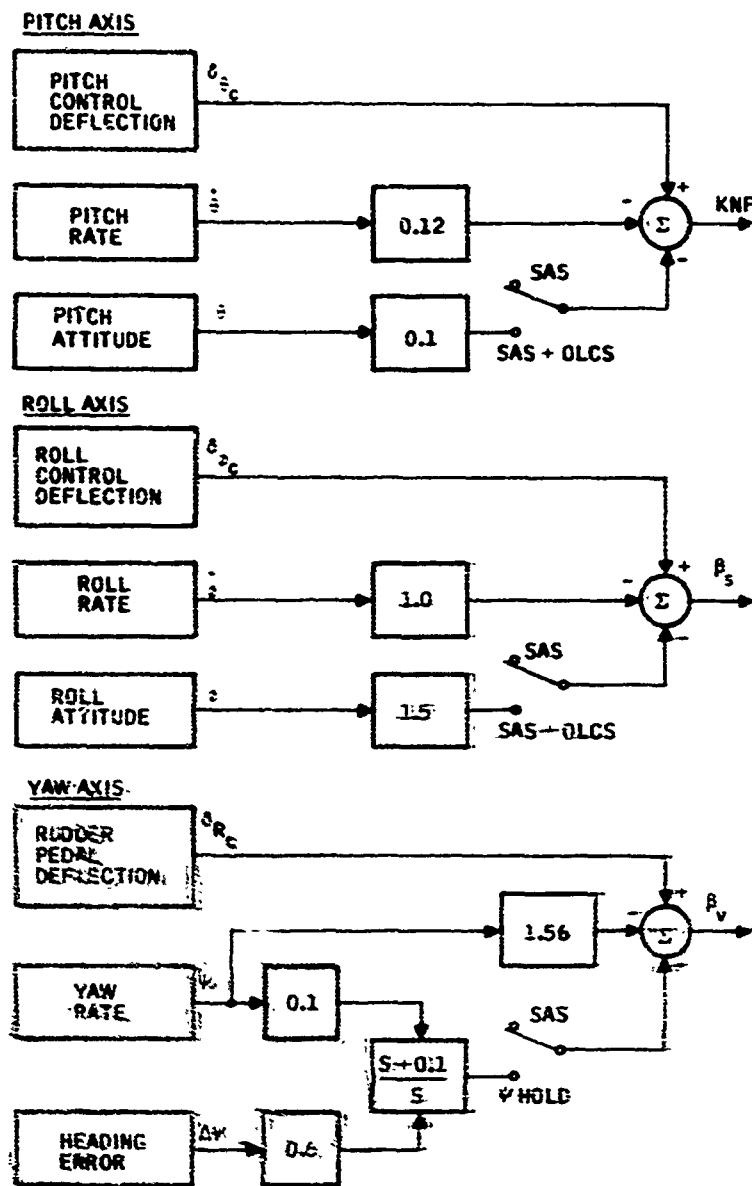
Figure 7-2. XV-5 Control-Augmentation Modes Simulated

Time histories depicting response characteristics of the stability-augmented UH-1 at hover and 120 ft/sec are shown in Figures 7-3 and 7-4. These responses were recorded for 0.25-inch-step control displacements in the pitch, roll and yaw axes. Comparable vehicle-response data for the stability-augmented XV-5 with 0.5-inch control displacements are shown in Figures 7-5 and 7-6.

Three-Axis SAS with Outer-Loop Control System in Pitch and Roll Axes (SAS + OLCS)

A second level of the aircraft control-augmentation variable evaluated in the Task III study included the SAS described above plus pitch- and roll-attitude feedback to form an outer-loop control system (OLCS) in these two control axes. In addition to the basic stability-augmentation (inner) loops, additional automatic control modes (outer loops), which bring the pilot one integration closer to the parameter he is attempting to control, are highly desirable in a vertical-lift aircraft. With rate feedback, attitude changes are accomplished by an initial control displacement followed by a return of the control to neutral position as the desired aircraft attitude is established. This control/response relationship is normally satisfactory for forward flight where aircraft flight path is being controlled and some degree of aerodynamic damping exists. However, for the hover task where the pilot must maintain position relative to a point on the ground, the use of both attitude and attitude-rate feedback loops is known to have a facilitating effect upon piloting performance (Refs. 36, 37 and 38).

Control laws simulated for the SAS + OLCS mode with the UH-1 vehicle are given below and are illustrated in Figure 7-1.

- Pitch axis: B_{IS} (deg) = δ_{θ_c} - 0.312 $\left(\frac{3S}{3S + 1}\right)\dot{\theta}$ - 0.4 θ

- Roll axis: A_{IS} (deg) = δ_{ϕ_c} - 0.125 $\dot{\phi}$ - 0.3 ϕ

- Yaw axis: θ_{TR} (deg) = δ_{R_c} - 0.755 $\left(\frac{S}{S + 1}\right)\dot{\psi}$

As indicated the basic rate-stabilized vehicle was further augmented by incorporating pitch- and roll-attitude feedbacks to provide fast, well-damped inner loops. These attitude-augmented inner loops modified the vehicle's rate response to control-stick displacement to a vehicle attitude response proportional to control displacement (Figures 7-7 and 7-8).

Control laws for the SAS + OLCS mode simulated with the XV-5 aircraft, illustrated in Figure 7-2, were:
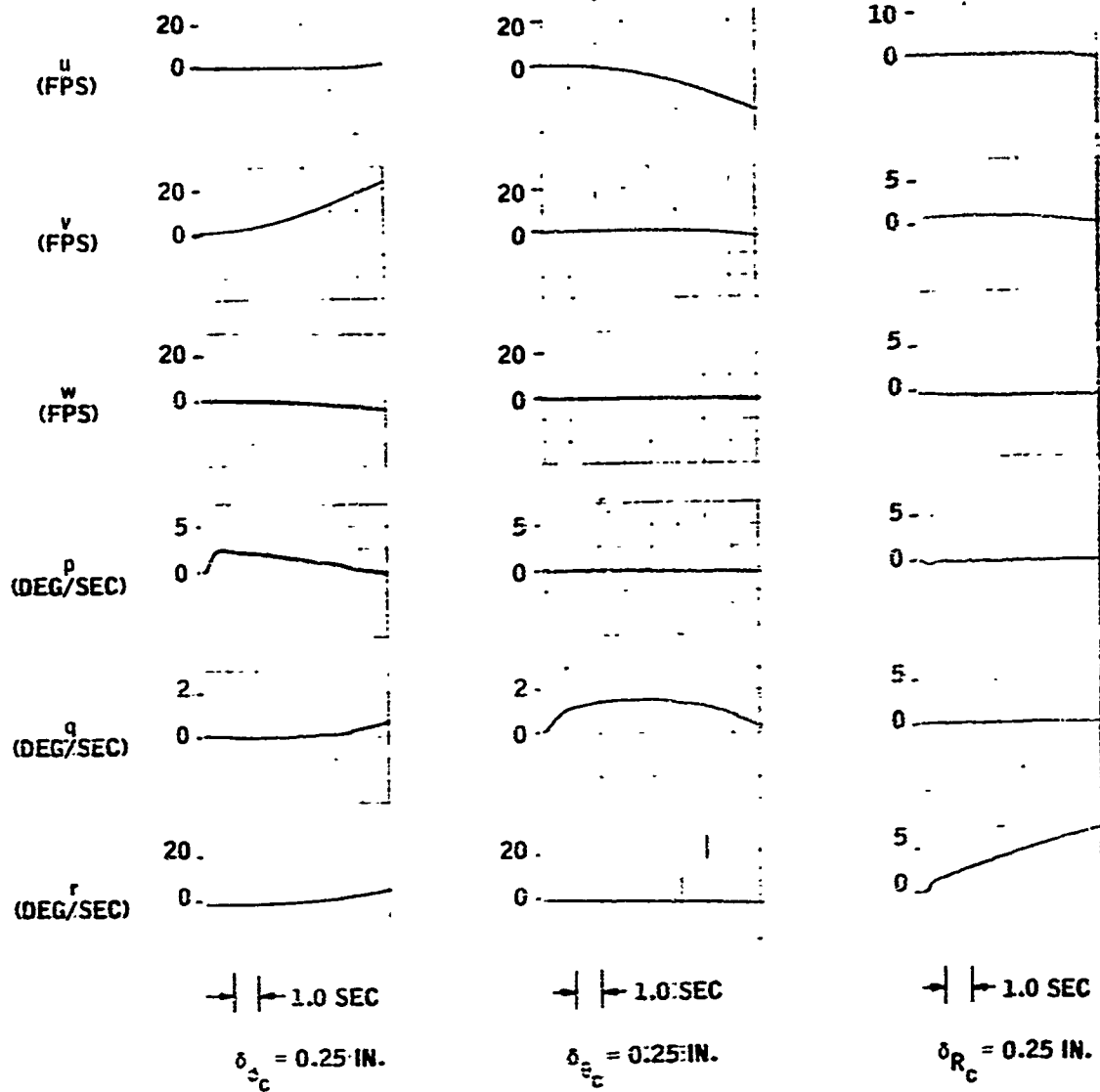
Figure 7-3. Rate-Augmented UH-1 Response Characteristics: Hover
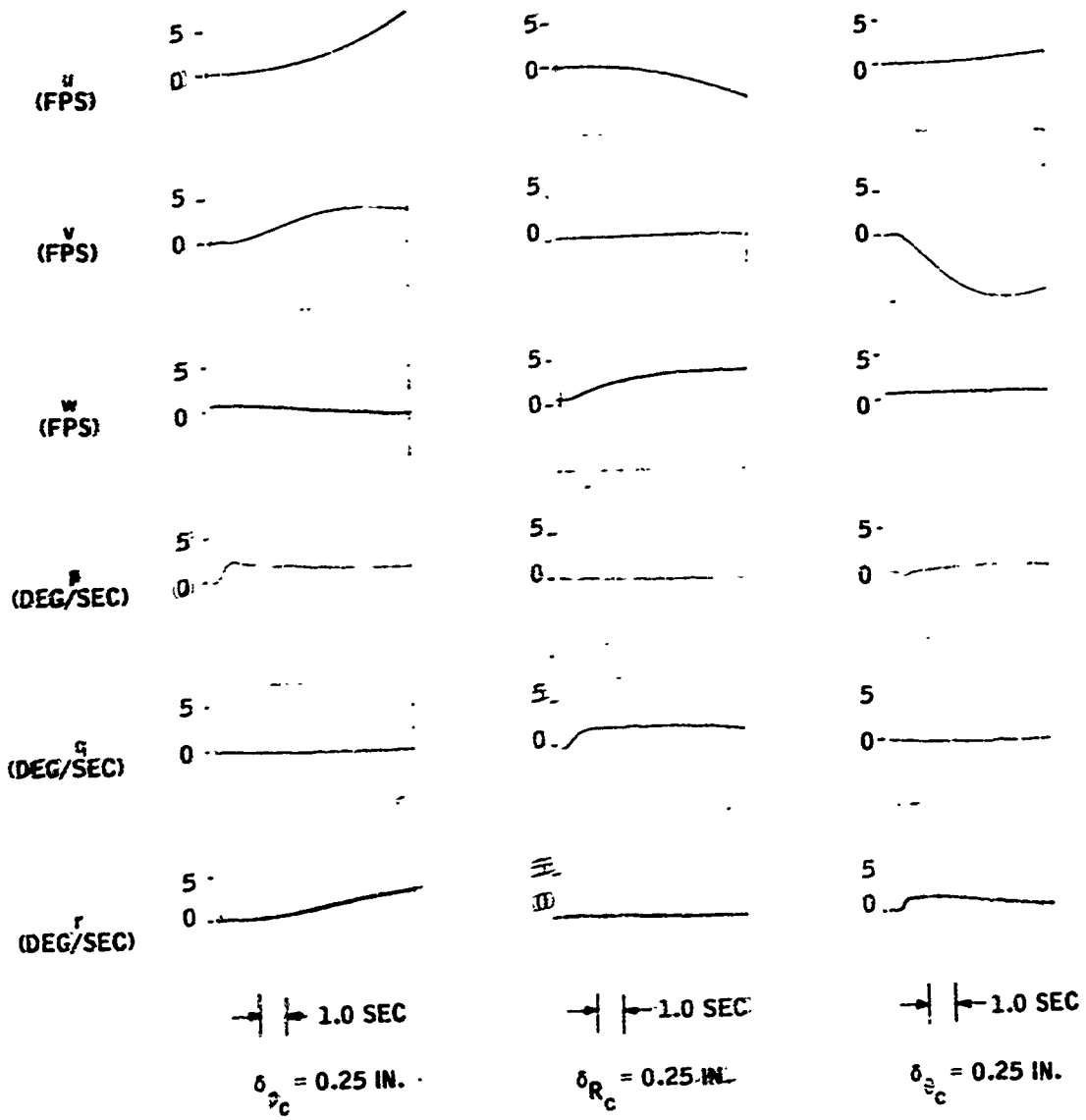
Figure 7-4. Rate-Augmented UH-1 Response Characteristics: 120 ft/sec
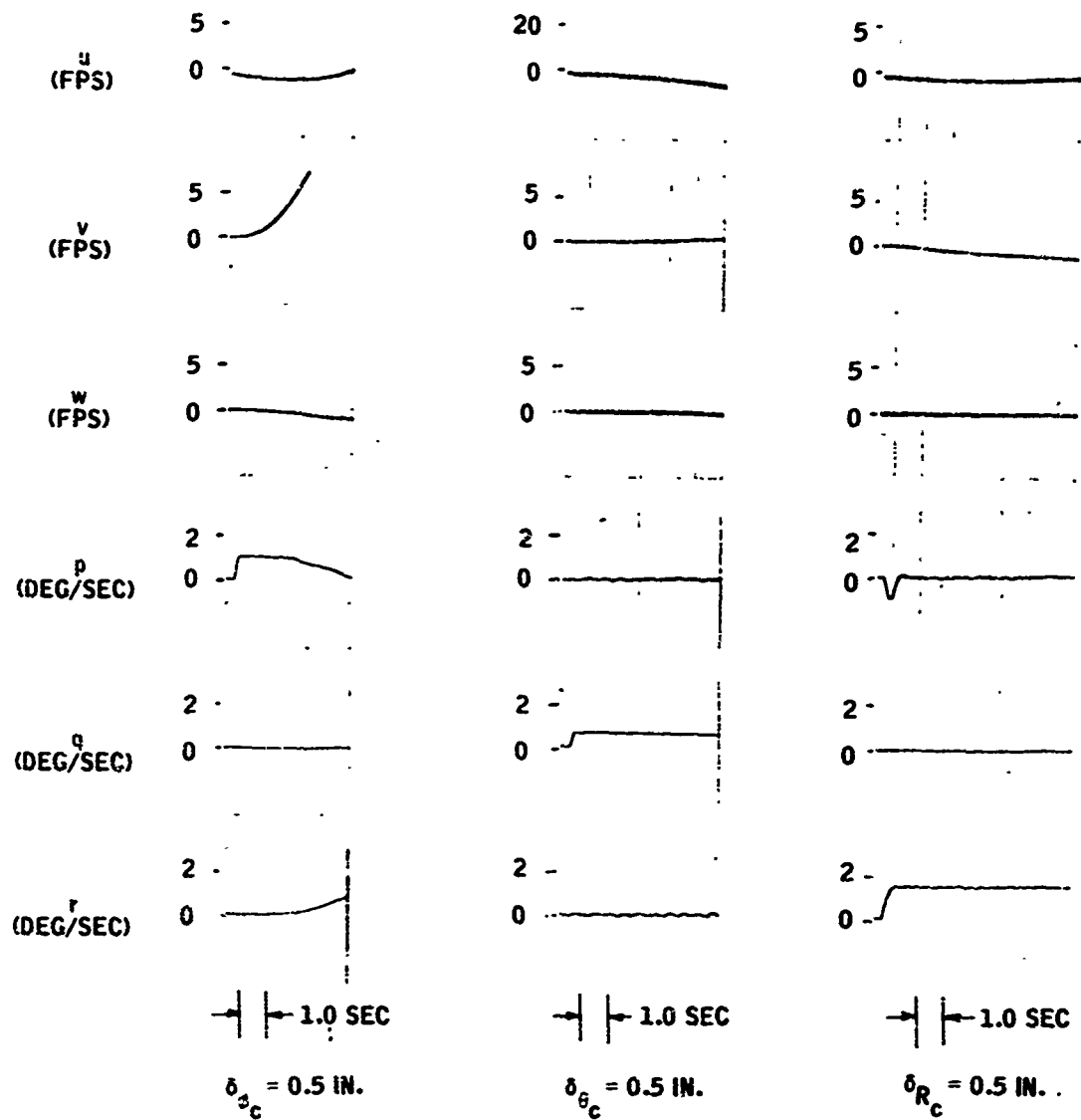
Figure 7-5. Rate-Augmented XV-5 Response Characteristics:
            Hover
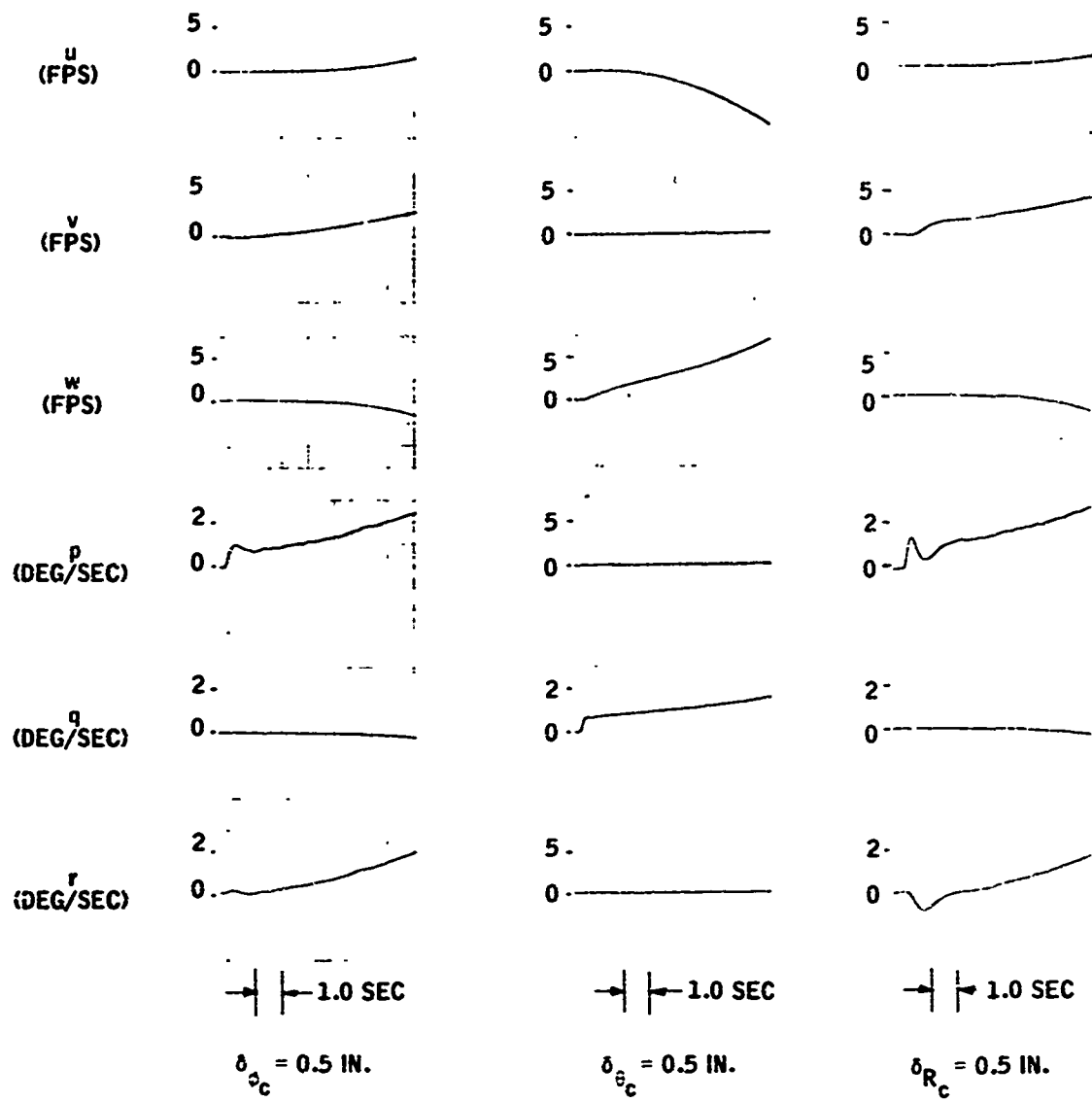
Figure 7-6. Rate-Augmented XV-5 Response Characteristics:
120 ft/sec

7-11
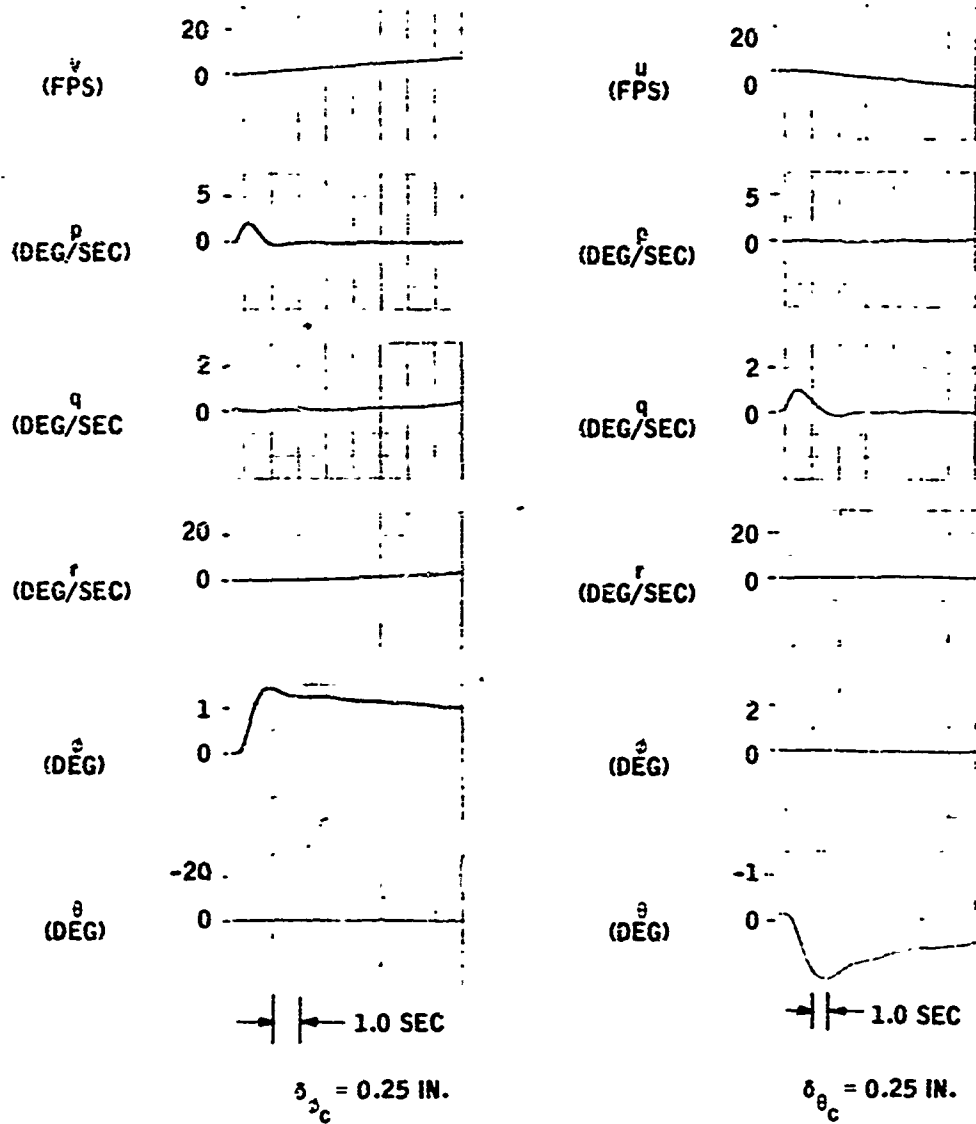
Figure 7-7.   Rate- and Attitude-Augmented UH-1
Response Characteristics: Hover
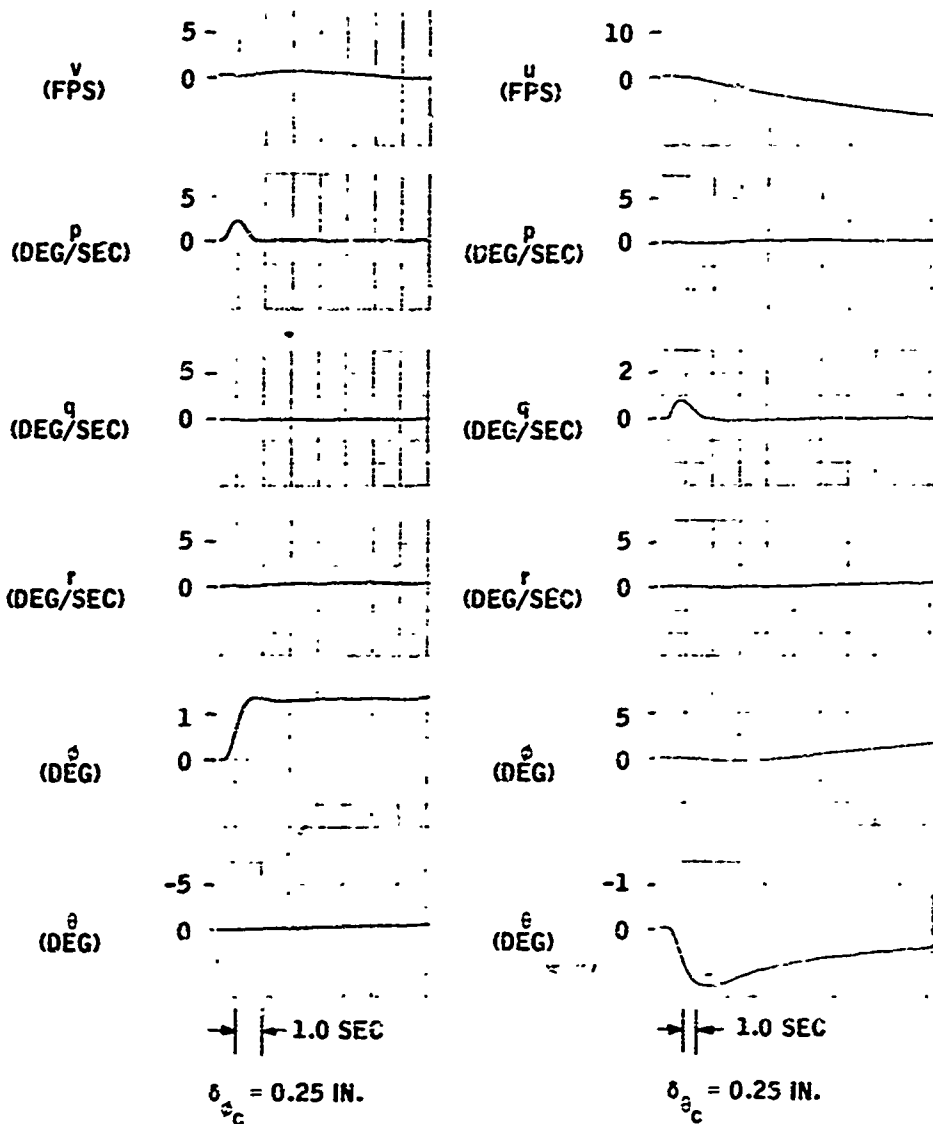
Figure 7-8.   Rate- and Attitude-Augmented UH-1 Response
Characteristics: 120 ft/sec

- Pitch axis: KNF (percent) = $\delta_{\theta_c} - 0.12\ \dot{\theta} - 0.1\ \theta$

- Roll axis: β_S (deg) = $\delta_{\phi_c} - 1.0\ \dot{\phi} - 1.5\ \phi$

- Yaw axis: β_V (deg) = $\delta_{R_c} - 1.56\ \dot{\psi}$

Control-stick-position feedback gains in the pitch and roll axes were chosen to provide an attitude-control effectiveness of approximately 3.0 degrees attitude change per inch of control-stick displacement. Time histories demonstrating attitude-control effectiveness in the pitch and roll axes are presented in Figures 7-9 and 7-10.

Three-Axis SAS with Heading Hold (SAS + ψ Hold)

The third control-augmentation mode simulated was identical to the SAS mode described above for the aircraft pitch and roll axes but was upgraded to also include an automatic heading hold (ψ hold). Heading hold was selected to evaluate effects of simplifying the pilot's control task by reducing the number of axes or functions to be controlled. The yaw axis was a logical choice for this purpose since rudder inputs at speeds simulated were required primarily in response to only gust perturbations and cross-coupling effects from other control inputs (e.g., collective inputs on the UH-1), and were not required for glide-path and hovering control. This hold mode was manually engaged by the pilot prior to glide-slope intercept during the "initial-approach" phase after lateral errors had been nulled and the aircraft flight path had been aligned nominally along the required approach heading. Once engaged, further attention to yaw-axis control was not required of the pilot as aircraft heading was automatically maintained at approximately the command-approach heading through the remaining approach phases (final approach, hover, and descent from hover).

The UH-1 heading-hold control mode simulated was

$$\theta_{TR} = -0.25\left(\frac{2.5S}{2.5\ S + 1}\right)\dot{\psi} - (0.4\ \dot{\psi} + 0.2\ \Delta\psi)\left(\frac{S}{S + 1}\right)$$

where $\Delta\psi$ represents heading error relative to command-approach heading. For this mode, yaw SAS gain was decreased from 0.755 to 0.25 deg/sec/deg and the high-pass time constant was increased from 1.0 to 2.5 seconds (see Figure 7-1) to provide a responsive control of heading. Yaw rate and attitude feedbacks were summed through a proportional-plus-integral shaping network to increase heading-hold accuracy and increase its operational range while maintaining a relatively simple mechanization. Time histories demonstrating heading-hold performance for the UH-1 are presented in Figure 7-11. Loop

7-14
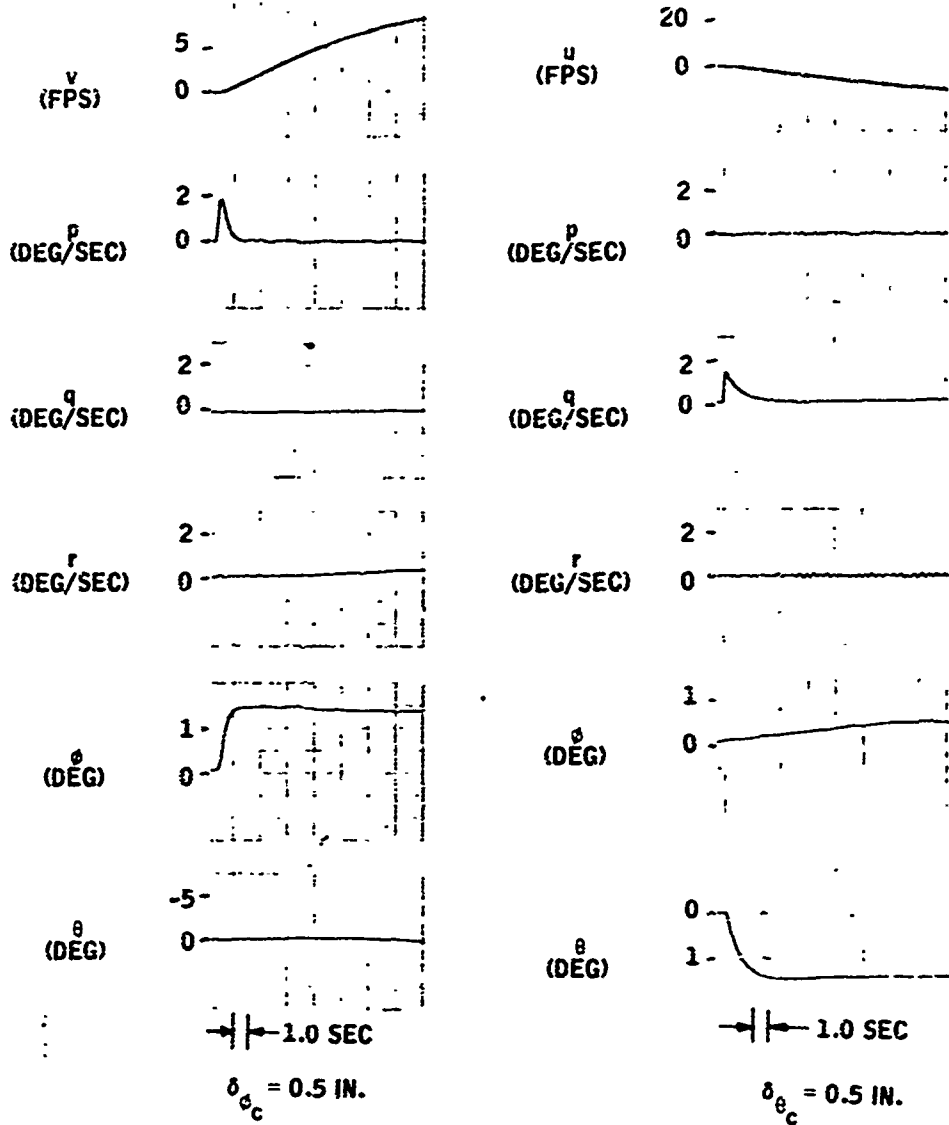
Figure 7-9.   Rate- and Attitude-Augmented XV-5
Response Characteristics: Hover

7-15
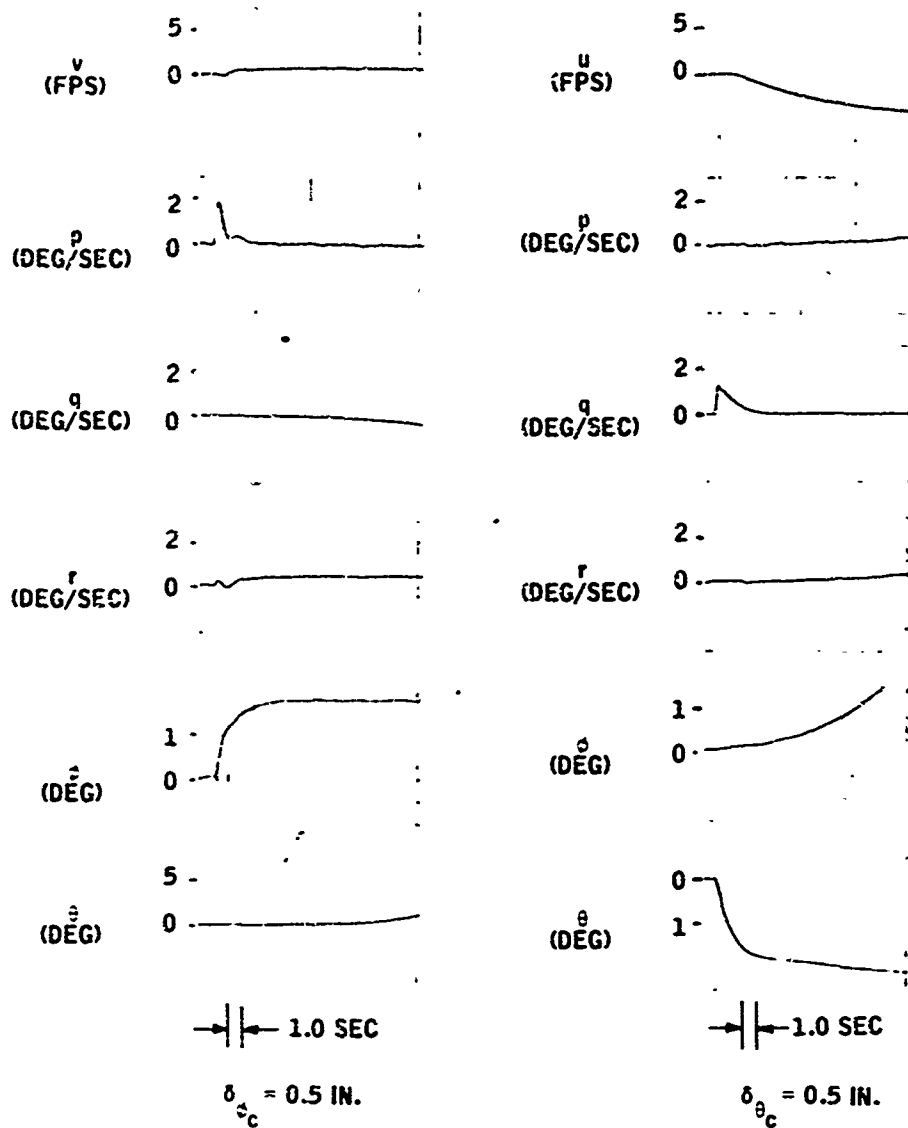
Figure 7-10.   Rate- and Attitude-Augmented XV-5 Response
Characteristics: 120 ft/sec

7-16
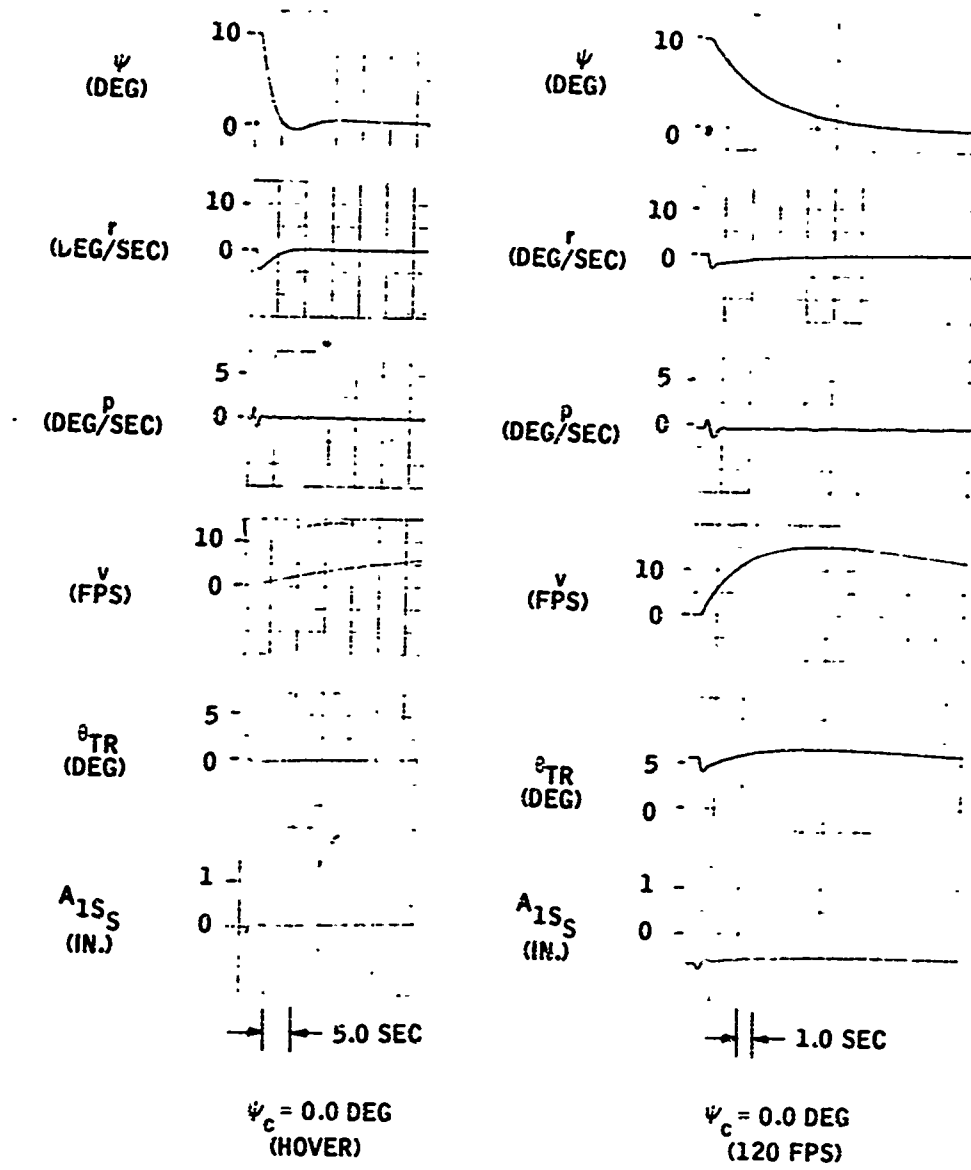
Figure 7-11. UH-1 Heading-Hold Response Characteristics

gains were adjusted to damp heading errors with a 90-percent response time of between 3 to 10 seconds with less than 10-percent overshoot.

The heading hold configured for the XV-5 aircraft, shown in Figure 7-2, was

$$\beta_V = 1.56 \, \dot{\psi} - (0.1 \, \dot{\psi} + 0.6 \, \Delta\psi) \left[\frac{S + 0.1}{S} \right]$$

Time histories demonstrating performance of this configuration are depicted in Figure 7-12, and indicate a 90-percent response time in hover of approximately 7 seconds.

SAS + OLCS with Heading Hold (SAS + OLCS + ψ Hold)

The fourth level of the control-augmentation-mode variable simulated for evaluation was identical to the SAS + OLCS mode described above, upgraded to also include the automatic heading-hold function (ψ hold). Heading-hold mechanizations for both aircraft were the same as for the SAS + ψ-hold mode. In terms of degree of control augmentation, the SAS + OLCS + ψ-hold mode represented the highest level of augmentation simulated for evaluation in the Task III study. Inclusion of this mode for testing facilitated the comparison of piloting performance on the steep approach and landing task with SAS and SAS + OLCS modes, as well as each of these modes with and without automatic heading hold.

7-18
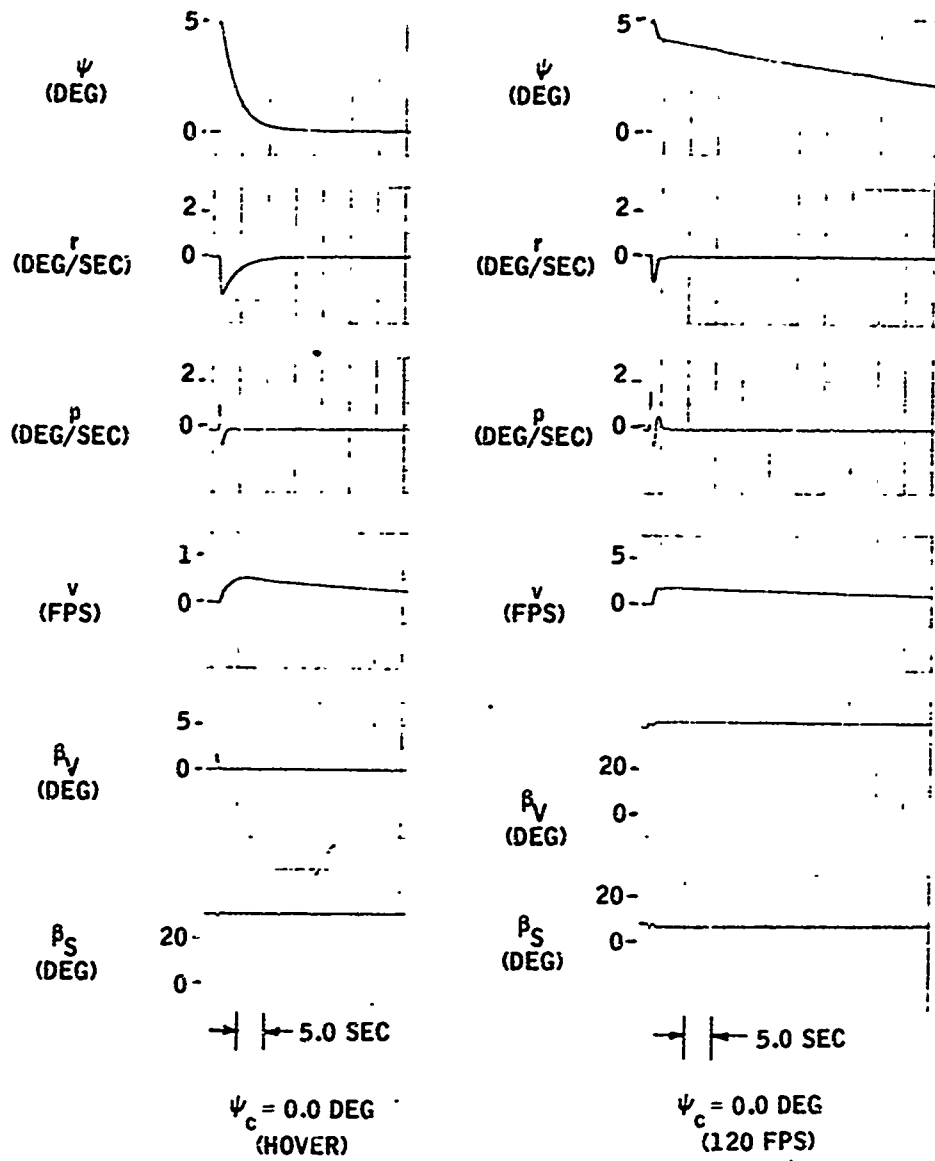
Figure 7-12. XV-5 Heading-Hold Response Characteristics

7-19

SECTION VIII
PRELIMINARY SIMULATION - TASK III

OBJECTIVES

The objectives of the preliminary-simulation phase of the study were:

- The refinement of simulation procedures to be used in the formal-simulation phase

- The empirical selection and verification of feedback coefficients for the control-augmentation modes to be evaluated

- The familiarization and training of subjects of experimental-variable combinations to be evaluated in the formal-simulation phase

PROCEDURAL REFINEMENT

Use of the standardized experimentation procedures established for the Task II SAA study (see Section IV) was continued in the present study.

However, since control-augmentation modes were mechanized on the analog portion of the hybrid simulator, selection of levels of this variable by the experimenter was not through use of the previously described seven-digit ID number code. Although the ID number did include a code for levels of the control-augmentation variable (C_1 through C_4) for purposes of data documentation and identification, the setting of feedback coefficients and mode switching was performed directly by the experimenter at the analog-computer console.

The thumb-actuated "autopilot-cutout" switch mounted on the left side of the "cyclic" control grip was mechanized for use as a heading-hold-engage switch. A single actuation of this switch by the pilot prior to glideslope intercept engaged the heading-hold mode for the duration of the approach to landing.

PRELIMINARY SYSTEM EVALUATION

Preliminary system evaluation emphasized the selection and testing of alternative feedback coefficients required for levels of the control-augmentation variable. Coefficients established with two Honeywell engineering employees serving as pilot/subjects were verified during initial practice sessions with the military pilots who would be serving as subjects for the duration of the Task III preliminary- and formal-experimentation sessions.

8-1

PILOT FAMILIARIZATION AND TRAINING

Military pilots who would be serving as subjects during the formal-simulation phase were trained under the various experimental conditions prior to initiation of formal-data collection. Each pilot received a minimum of two "completed" practice flights on each of the treatment combinations to be evaluated (a flight was considered "completed" if control of the aircraft was maintained through all phases of the approach and landing mission). Formal-data-collection flights immediately followed the completion of practice sessions with the respective vehicles.

Pilot training sessions were begun using the UH-1 vehicle. Each of four pilots received a series of 64 practice flights consisting of two replications on treatment conditions resulting from the factorial combinations of the following variable levels (as defined in Section VII):

- Approach angles (two levels)

- Display formats (two levels)

- Measurement-noise/filter-lag (two levels)

- Control-augmentation modes (four levels)

It may be noted that pilots were trained with all levels of all variables to be evaluated during the Task III formal-simulation phase.

Measures selected as summary indicators of pilot skill acquisition during training were:

- Total time to complete the simulated approach and landing

- Root-mean-square (RMS) lateral and vertical flight-path errors during the "final-approach" phase

- RMS longitudinal and lateral position errors during the "descent-from-hover" phase

Practice data resulting for each of these measures with the UH-1 vehicle are shown in Figures 8-1 through 8-5. Data shown are averaged in consecutive blocks of trials to depict performance averages and variabilities for each block as described in Section IV of this report.

Two general observations summarize these data: (1) lack of appreciable improvement in performance over the training series is attributable to all pilots having previously served as test subjects in the SAA program during either Task I or Task II study phases, and (2) data do reflect trends related to the ordering of test conditions during practice. Each pilot completed all
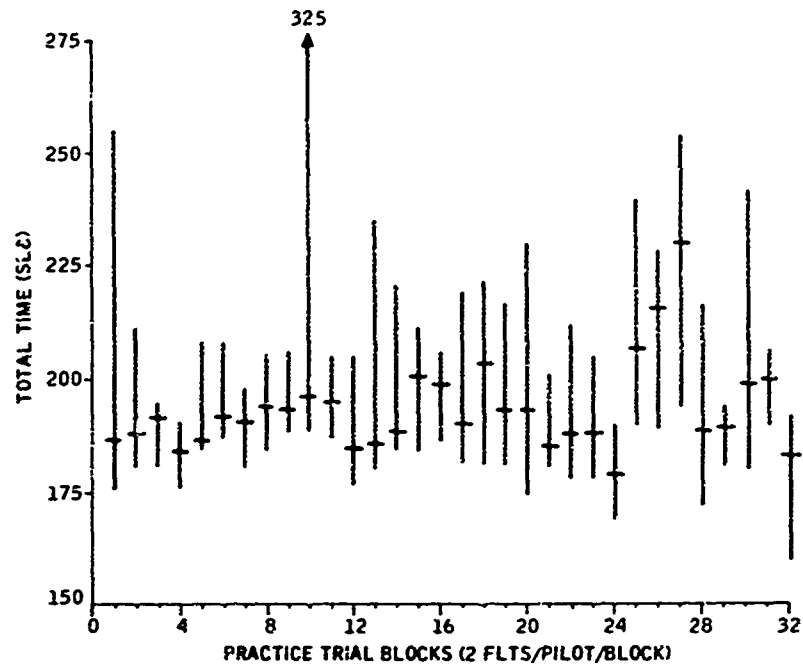
Figure 8-1.   Median Total Time (and 19th and 81st Percentiles)
for Each Practice Block; UH-1 Aircraft
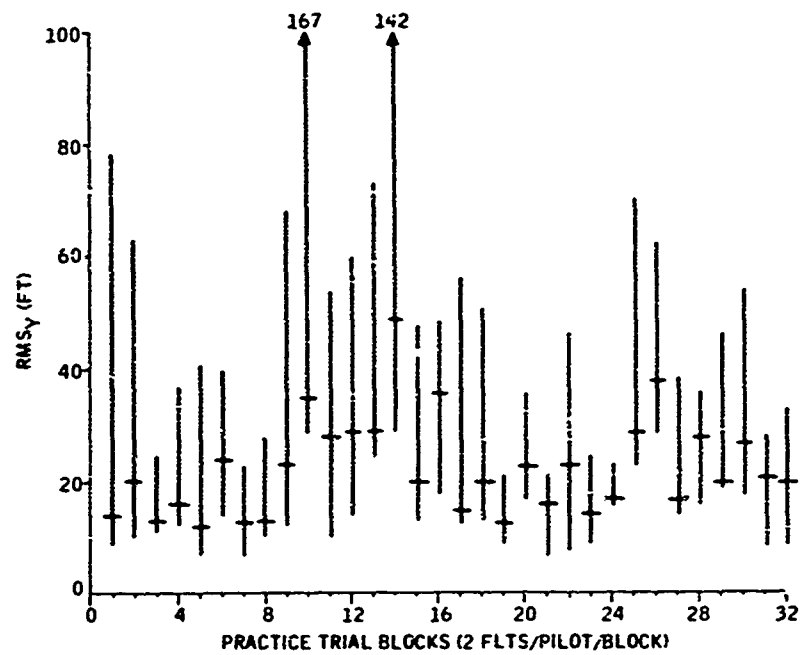
Figure 8-2.   Median RMS$_Y$ Error (and 19th and 81st Percentiles)
for Each Practice Block; UH-1 Aircraft; Final-
Approach Phase

8-3
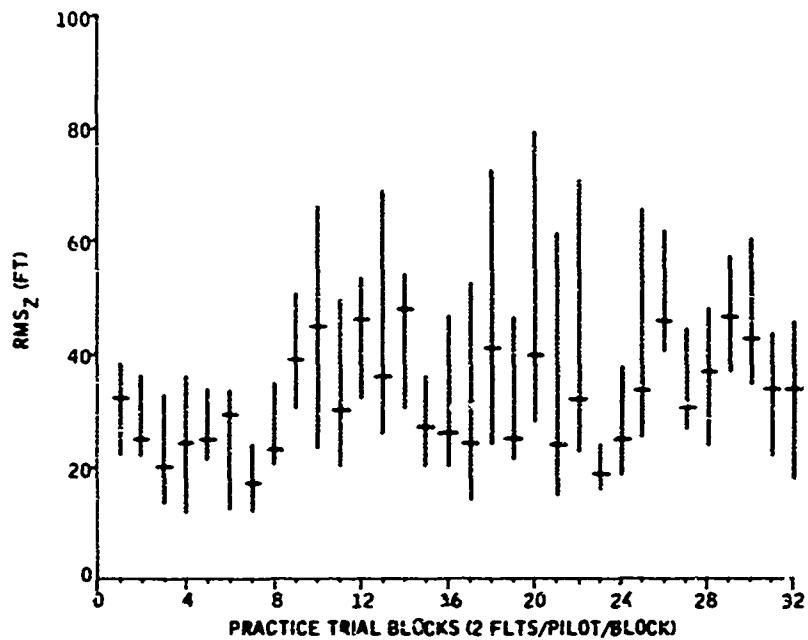
Figure 8-3. Median RMS_Z Error (and 19th and 81st Percentiles) for Each Practice Block; UH-1 Aircraft; Final-Approach Phase
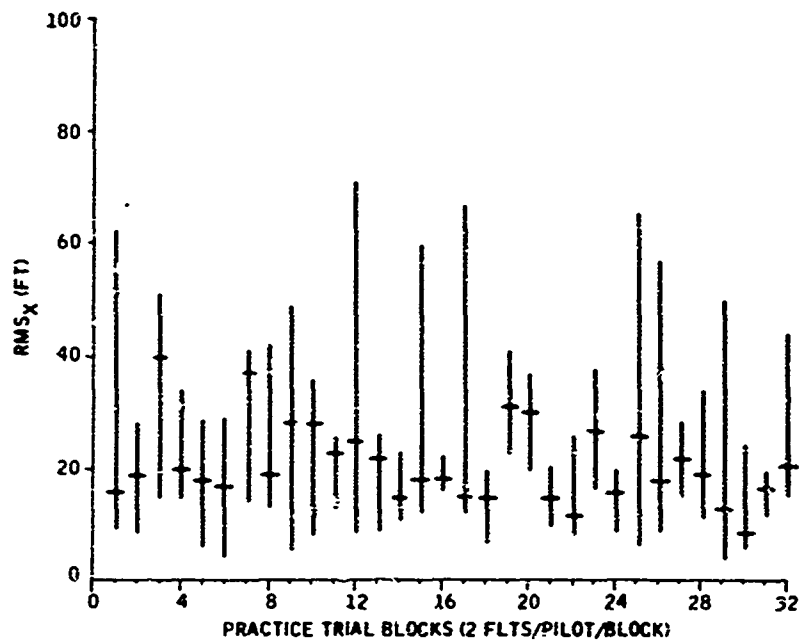
Figure 8-4. Median RMS_X Error (and 19th and 81st Percentiles) for Each Practice Block; UH-1 Aircraft; Descent Phase

3-4
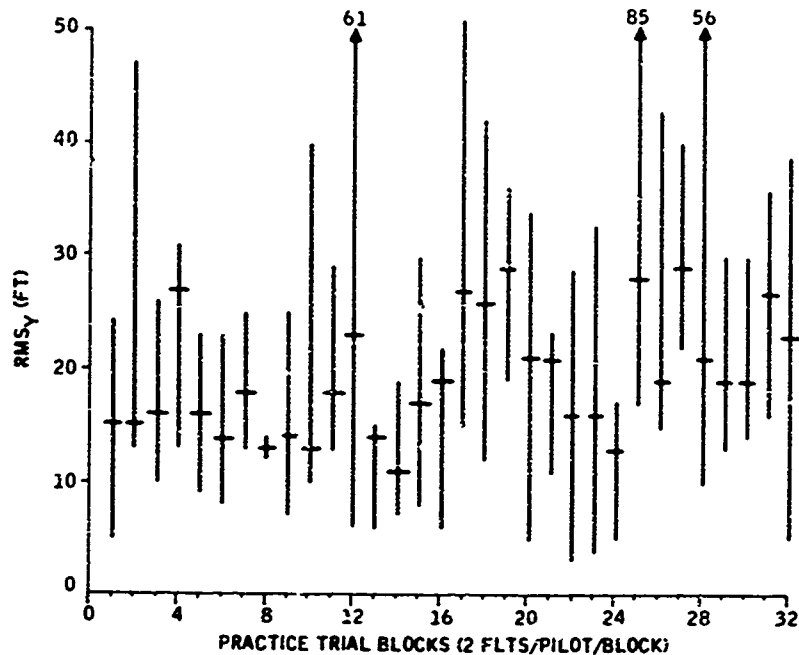
Figure 8-5. Median RMS$_Y$ Error (and 19th and 81st Percentiles) for Each Practice Block; UH-1 Aircraft; Descent Phase

required practice flights on one display format prior to initiation of practice with the second format (ordering of formats was counterbalanced between pilots). For each format, practice was first given for all approach-angle and control-mode combinations with the least difficult level of the measurement-noise/filter-lag variable (N_1 F_1). This sequence was then repeated, with the same display format, for the most difficult noise/filter variable level (N_3 F_3). Thus, for example, the downward trend in "total-time" data for practice blocks 25 through 32 (Figure 8-1) reflects improvement in performance under the N_3 F_3 condition following prior experience with the same angle, display and control-mode combinations under the N_1 F_1 condition.

An identical practice sequence was given for the XV-5 preceding formal-data collection with this aircraft. Summary performance data from these practice sessions are presented in Figures 8-6 through 8-10. Trends are similar to those shown for the UH-1, with no appreciable improvement in performance with continued practice. This effect is again attributable to the transfer of experience gained in previous SAA study phases.

Of primary importance is the fact that all pilots who served in the formal-simulation study phase were familiarized during training with all task characteristics to be evaluated experimentally.

8-5
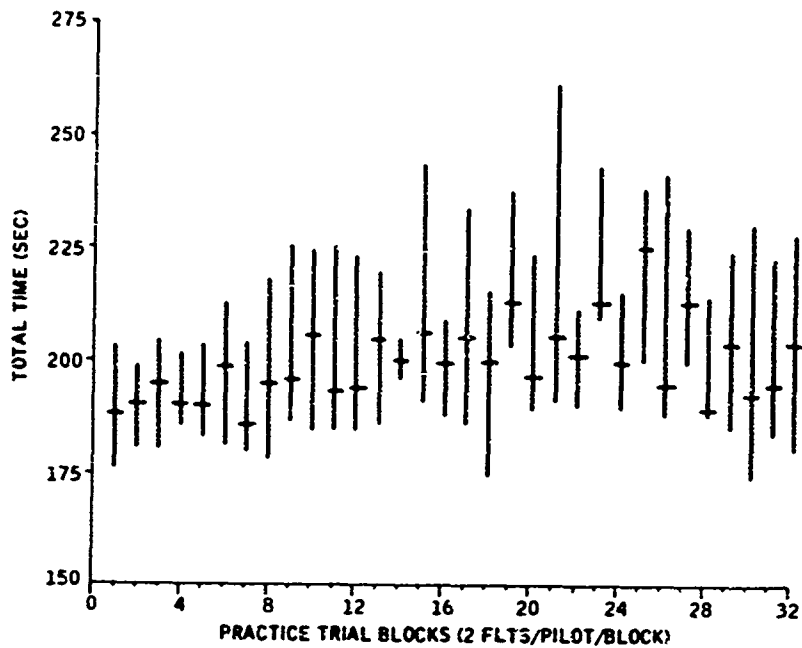
Figure 8-6. Median Total Time (and 19th and 81st Percentiles)
for Each Practice Block; XV-5 Aircraft
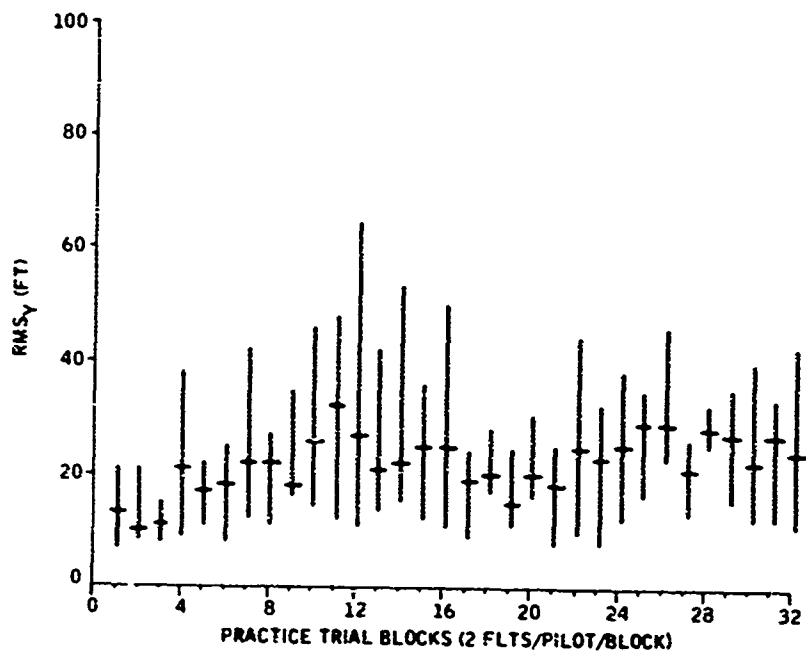
Figure 8-7. Median RMS_Y Error (and 19th and 81st Percentiles)
for Each Practice Block; XV-5 Aircraft; Final-
Approach Phase
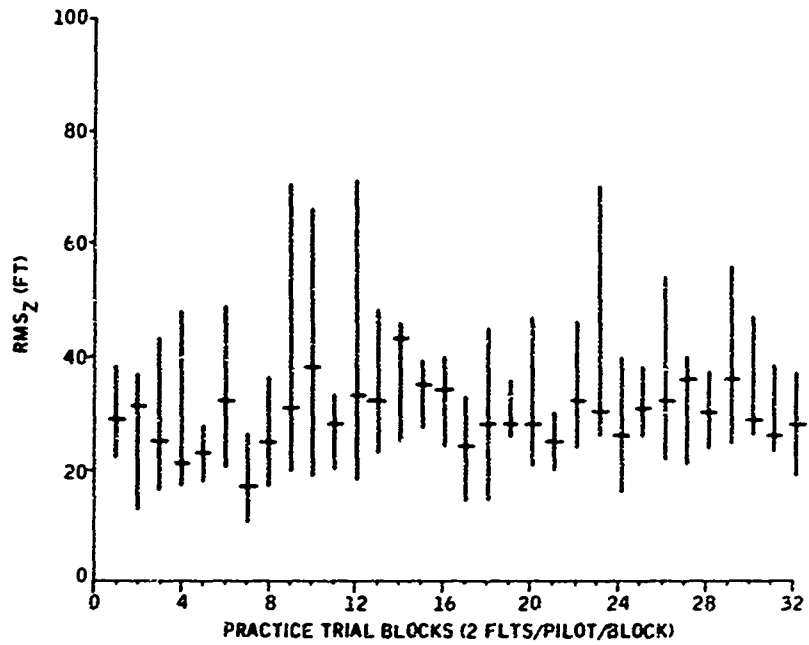
Figure 8-8. Median RMS$_Z$ Error (and 19th and 81st Percentiles) for Each Practice Block; XV-5 Aircraft; Final-Approach Phase
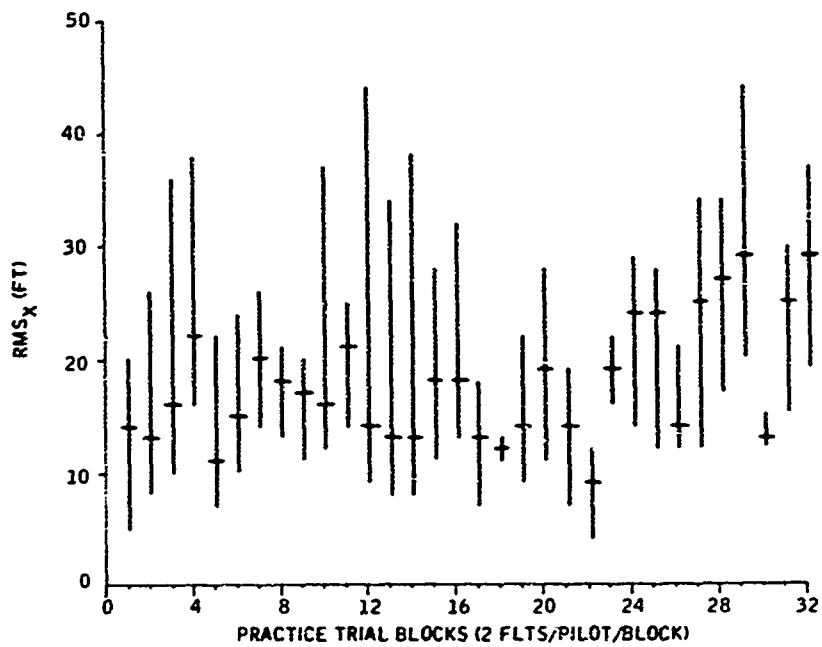
Figure 8-9. Median RMS$_X$ Error (and 19th and 81st Percentiles) for Each Practice Block; XV-5 Aircraft; Descent Phase

8-7
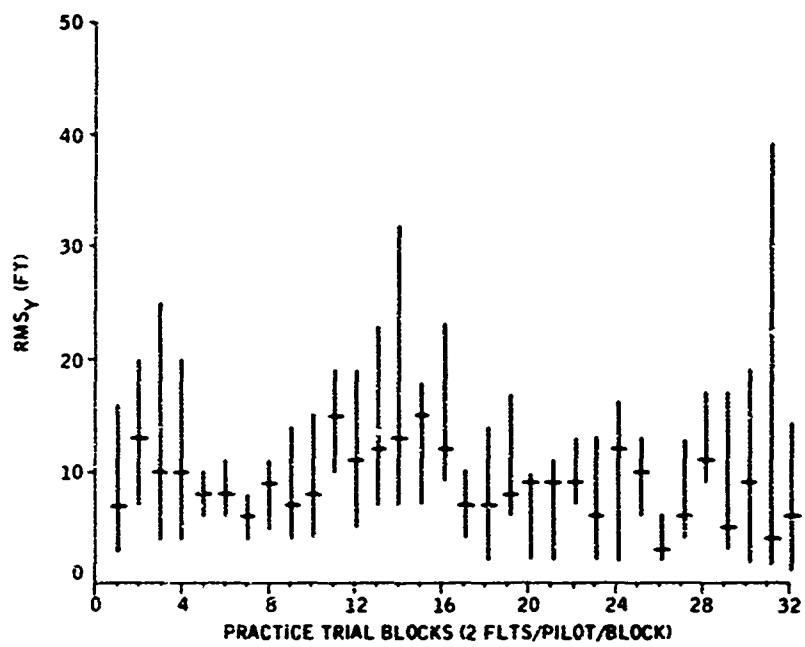
Figure 8-10. Median RMS_Y Error (and 19th and 81st Percentiles) for Each Practice Block; XV-5 Aircraft; Descent Phase

SECTION IX

FORMAL SIMULATION - TASK III

The objectives of the formal-simulation phase of the Task III study were to conduct a systematic simulator evaluation of the four aircraft control-augmentation modes previously defined, as well as the interactive effects of this variable with other relevant system and task variables including approach angle, display format, and measurement-system noise/filter characteristics. Descriptions of the task characteristics simulated, the independent and dependent variables evaluated, and the experimental plan followed in conducting the formal evaluation are summarized below. Results obtained from these simulations are presented in Section X.

SIMULATED APPROACH AND LANDING MISSION

The simulated approach and landing mission segment consisted of the four "active" or time-consuming phases defined in Section V, including "initial-approach", "final-approach", "hover", and "descent" phases.

INDEPENDENT VARIABLES

The following independent variables were incorporated into the study formal-simulation phase:

- Subjects: Four helicopter-rated pilots served as test subjects during formal-data collection with each vehicle. All pilots were currently serving, or had previously served, on active-duty status, and each had between 2000 and 5000 hours experience in various rotary-wing aircraft including the UH-1. All pilots were instrument rated.

- Vehicles: Two simulated vehicles, the UH-1 and XV-5, were used. Practice- and formal-data collection were completed with the UH-1 simulation prior to initiation of simulation flights with the XV-5 vehicle.

- Display Formats: Two display formats were evaluated. Each of these formats, described previously, included a primary horizontal-situation (PPI-AR) or vertical-situation (IEVD) display supplemented with peripherally located conventional instrumentation.

9-1

- Approach Angles: Two alternative approach angles (6 and 15 degrees) were simulated for evaluation.

- Noise/Filter Characteristics: Two levels of a combined measurement-system-noise/filter-lag variable were evaluated (no-measurement-noise/"minimum"-signal-filtering and "high"-measurement-noise/"high"-signal-filtering).

- Aircraft Control-Augmentation Modes: Four levels of the control-augmentation-mode variable, defined in Section VII, were evaluated.

DEPENDENT VARIABLES

The following performance measures were recorded during appropriate phases of the simulated task, and served as a basis for interpreting pilot performance as a function of the treatment conditions described above:

- Vertical and Lateral Flight-Path Deviations: Root-mean-square (RMS) errors were recorded for vertical (RMS_Z) and lateral (RMS_Y) deviations from the command flight path during the final-approach phase, with only RMS_Z being recorded during the initial approach. Also, instantaneous vertical and lateral errors (E_Z and E_Y) were recorded along the flight path at 250-foot intervals.

- Position Errors During Hover and Descent: Position-error measures recorded for hover phase were RMS_X (longitudinal position), RMS_Y and RMS_Z errors, with RMS_X and RMS_Y also being recorded during descent from hover.

- Terminal Position Errors, Rates and Attitudes: Aircraft position with respect to the command touch-down point (E_X and E_Y), translational rates ($\dot{X}_B$, $\dot{Y}_B$ and $\dot{Z}$) and attitudes (θ and ϕ) were measured at $Z = 0.0$ feet. Also, since it was of interest to determine the accuracy with which the command approach path could be terminated at ground contact rather than hover at $Z = 50$ ft, these terminal data were also recorded at the instant that the aircraft reached $Z = 50$ feet during either the final-approach or hover phase, and again at the end of the hover phase, itself, prior to vertical descent to touch down.

- **Time**: Times required to complete the initial-approach, final-approach and descent phases were recorded. The hover phase was programmed to be a constant 20 seconds.

- **Activity Indices**: Measures of pilot control-input activity for the pitch and roll center stick and collective (lift) stick were computed as RMS rates of the respective control movements. These activity indices (AI_θ, AI_ϕ, and AI_{col}) were scaled in arbitrary units for each vehicle simulation, and served as a basis for making inferences concerning the relative effects of experimental treatments upon pilot "workload" or task difficulty.

- **Continuous Time-History Data**: Strip-chart recordings of aircraft pitch and roll attitudes (θ, ϕ), heading (ψ), altitude (Z) and pitch; roll- and lift-stick displacements (δ_θ, δ_ϕ, ϕ_{col}) were obtained from all flights in the formal-simulation study phase. Representative samples were selected to show typical time histories of these parameters.

- **Control Losses**: Flights during which loss of vehicle control resulted were terminated by the experimenter or terminated automatically by ground contact. When a control loss resulted, the existing experimental conditions were recorded by the experimenter, and the flight was repeated.

A summary of dependent variables measured or computed, and the mission phases during which they were recorded, is given in Table 9-1. Specific measures were relevant for only certain mission phases. For example, RMS_X was computed only during hover and descent phases since a longitudinal position was not commanded until the hover phase was reached. Similarly, RMS_Y was not meaningful during the initial-approach phase because of the initial lateral position error of 500 feet from which the simulated mission was begun.

EXPERIMENTAL PLAN

A plan of independent-variable combinations for the Task III study formal-simulation phase is summarized in Figure 9-1. This plan included a full-factorial combination of two display formats (D), two approach angles (A), two levels of the combined noise/filter variable (N), and four levels of air-craft control augmentation (C). The total matrix set consisted of 64 test cells when combined across aircraft. Each pilot was required to complete four replications (flights) per cell, resulting in a total of 1024 simulated flights to be scheduled for formal-data collection.

Table 9-1. Summary of Dependent-Variable Measurement or Computation

Variable	Initial Approach	Final Approach	Hover	Descent from Hover	Terminal Data Recorded at.		
					Comm. Hover Alt. (Z = 50 ft)	End of Hover Phase	Gnd. Contact (Z = 0 ft)
Time							
RMS_X							
RMS_Y							
RMS_Z							
E_X					Δ	Δ	Δ
E_Y					Δ	Δ	Δ
E_Z							
$\dot{X}_B$					Δ	Δ	Δ
$\dot{Y}_B$					Δ	Δ	Δ
$\dot{Z}$					Δ	Δ	Δ
θ					Δ	Δ	Δ
ϕ					Δ	Δ	Δ
AI_θ							
AI_ϕ							
AI_{col}							
θ							
ϕ							
ψ							
z							
δ_θ							
δ_ϕ							
δ_{col}							
(Phase)							

○———○ Continuous Recording or Computation

○ – – –○ Periodic Sampling

VEHICLES (2)

UH-1

DISPLAY FORMATS (2)

APP. ANGLES (2)

CONTROL-AUG. MODES (2)

XV-5

DISPLAY FORMATS (2)

APP. ANGLES (2)

CONTROL-AUG. MODES (2)
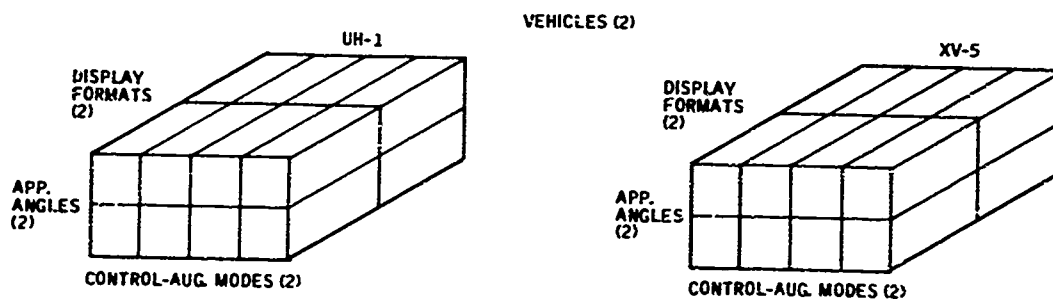
- THE ABOVE MATRICES ARE DUPLICATED FOR EACH LEVEL (2) OF THE COMBINED SYSTEM NOISE AND FILTERING VARIABLE
- THE TOTAL NUMBER OF CELLS IN THE RESULTING MATRIX SET IS 64
- THE USE OF 4 PILOTS WITH 4 FLTS/CELL/PILOT YIELDS A TOTAL OF 1024 FLTS IN THIS MATRIX SET

Figure 9-1. Experimental Plan for Task III Study

Characteristics of the simulation held constant for the duration of the formal experiment were:

- System information update rate (13.3 Hz)
- Display gains and scale factors
- Turbulence level (see Appendix A)

SIMULATION SCHEDULE

A simulation schedule was developed which would counterbalance order effects of the various experimental variables to the maximum extent possible, but would minimize problems associated with transfer between test conditions. In developing this schedule variables were first ranked in order of anticipated sensitivity to transfer due to alternation of variable levels. This ranking, given below, was used as a basis for determining the frequency with which levels of each variable would be alternated in the scheaule defined for data collection with each variable.

- Display formats - least frequently alternated
- Control-augmentation modes
- Approach angles
- Noise/filter combinations - most frequently alternated

For each subject, display format was altered once (for each vehicle), with presentation order of levels of this variable being counterbalanced between subjects. Similarly, for each display format, control modes were varied through the four levels once, with presentation order of levels of this variable being counterbalanced between displays and between subjects. This process was repeated in a comparable manner for the remaining two independent variables listed above. In all cases the required four replications per cell were completed before proceeding to the next scheduled cell.

The data-collection schedule as developed by this process was repeated for each vehicle.

DATA ANALYSIS

Performance data resulting from the formal-simulation phase were analyzed, and are summarized in Section X. Analyses, including the calculation of means, medians, standard deviations and analyses of variance were performed directly from data-output cards with a digital computer.

In the analyses of variance, the subject factor was considered as random, with all other factors considered to be fixed effects.

9-5

SECTION X
STUDY RESULTS - TASK III

Selected results of the analysis of pilot-performance data obtained during the Task III study formal-simulation phase are discussed in this report section. Graphical illustrations of these data are presented in Appendix D. Data judged to be of primary relevance in interpreting effects of the experimental variables under study are presented.

Performance results from each simulated vehicle are discussed separately below, with a further classification of study results into the following general categories:

- Results of analyses of variance performed on dependent variables having values not distributed around zero (e. g. , time and RMS errors)

- Lateral and vertical glide-path errors recorded at 250-foot intervals during the final-approach phase

- Summary results of terminal-data dependent variables having values distributed around zero (e. g. , $\dot{Y}_B$ and ϕ at ground contact)

- Representative samples of pilot control-input and vehicle-response time-history data (samples selected for UH-1 vehicle only)

Reference to independent variables and their associated levels in this report section in figures appearing in Appendix D is simplified by use of the following code:

- Display formats (D)

    D_1: PPI-AR format

    D_2: IEVD format

- Approach angles (A)

    A_1: 6-degree glideslope

    A_2: 15-degree glideslope

10-1

- Measurement noise/filtering combinations (N)

    $N_1 F_1$: no-noise/minimum-filter-lag

    $N_3 F_3$: high-noise/high-filter-lag

- Aircraft control-augmentation mode (C)

    C_1: SAS

    C_2: SAS + OLCS

    C_3: SAS + ψ hold

    C_4: SAS + OLCS + ψ hold

Also since data are referenced or illustrated as a function of mission phase (or data-sampling point), the following additional coding is used:

- Phase (P)

    P_1: initial-approach phase

    P_2: final-approach phase

    P_3: hover phase

    P_4: descent (from hover) phase

    P_5: terminal data recorded at first contact with command hover altitude (Z = 50.0 feet)

    P_6: terminal data recorded at end of hover phase

    P_7: terminal data recorded at ground contact (Z = 0.0 feet)

ANALYSIS-OF-VARIANCE RESULTS FOR UH-1 VEHICLE

Condensations of analysis-of-variance summary tables indicating confidence levels for main effects and interactions are shown in Tables 10-1 through 10-5. Those effects found to be statistically significant at confidence levels between $p < 0.10$ and $p < 0.005$ are indicated.

Table 10-1. Condensation of Analysis-of-Variance Summary Tables; Phase 1; UH-1 Aircraft

Source	Dependent Variable				
	Time	RMS_Z	AI_θ	AI_ϕ	AI_{col}
D			0.100*	0.100	
A		0.025	0.005		0.025
C	0.005			0.005	
N		0.025		0.100	
DA					
DC		0.025			
AC			0.005		
DN				0.005	
AN	0.100		0.025	0.100	
CN					
DAC					
DAN					
DCN					
ACN					0.100
DACN		0.100			0.100

*P < 0.100

Table 10-2. Condensation of Analysis-of-Variance Summary Tables, Phase 2; UH-1 Aircraft

Source	Dependent Variable					
	Time	RMS_Y	RMS_Z	AI_θ	AI_ϕ	AI_{col}
D				0.100*	0.100	
A						
C				0.005	0.005	
N			0.025	0.100	0.025	
DA						
DC						
AC				0.100		
DN		0.100		0.100	0.025	
AN						
CN				0.100	0.025	
DAC						
DAN						
DCN			0.100			
ACN						
DACN						

*P < 0.100

10-3

Table 10-3. Condensation of Analysis-of-Variance Summary
Tables; Phase 3; UH-1 Aircraft

Source	Dependent Variable					
	RMS_X	RMS_Y	RMS_Z	AI_θ	AI_ϕ	AI_{col}
D A C N	0.025* 0.005			0.005 0.025	0.025	
DA DC AC DN AN CN	0.005		0.100	0.100 0.100	0.100 0.025	
DAC DAN DCN ACN	0.025		0.100			0.100
DACN						

*P < 0.025

Table 10-4. Condensation of Analysis-of-Variance Summary
Tables; Phase 4; UH-1 Aircraft

Source	Dependent Variable					
	Time	RMS_X	RMS_Y	AI_θ	AI_ϕ	AI_{col}
D A C N	0.100* 0.100	0.100 0.025	0.100	0.100 0.005 0.100	0.005	
DA DC AC DN AN CN				0.100 0.100	0.100 0.025	0.025
DAC DAN DCN ACN						
DACN						

*P < 0.100

Table 10-5. Condensation of Analysis-of-Variance Summary Tables; Phases 5 and 7; UH-1 Aircraft

Source	Dependent Variable	
	$\dot{Z}$ (Phase 5)	$\dot{Z}$ (Phase 7)
D A C N		0.100[*]
DA DC AC DN AN CN	0.100	0.100
DAC DAN DCN ACN	0.100	
DACN		

[*]$P < 0.100$

10-5

Differences Due to Display Format

Overall differences between the two display formats tested are summarized in Figures D1 through D5 of Appendix D. These data depict trend differences between formats which are consistent with those found in the Task II study. RMS flight-path errors averaged between 15 and 35 feet in all axes, with consistent trends toward slightly lower errors for the IEVD format (D_2). Conversely, pilot control activities were higher for this format (Figures D4 and D5).

Differences Due to Approach Angle

The main effect for approach angles did not yield appreciable differences in performance in this study. The one exception to this finding was for RMS_X errors during hover and descent phases (Figure D6) where, for example, RMS longitudinal errors during hover were approximately seven feet greater with the 6-degree approach angle (A_1). An interpretation of this difference is presented below during discussion of angle-by-control-mode (AC) interaction results.

Differences Due to Noise/Filtering

Effects of the combined measurement-noise/signal-filtering variable are exemplified by data shown in Figures D7 and D8, Appendix D. Altitude RMS errors during final approach (P_2) were approximately 26 feet for the no-noise/minimum-filtering condition ($N_1 F_1$), and increased to 37 feet under the high-noise/maximum-filtering combination ($N_3 F_3$). Longitudinal- and lateral-error measures (RMS_X and RMS_Y) did not yield statistically significant differences for this variable.

Differences Due to Control-Augmentation Mode

Data summarizing the main effect for the four-level control-mode variable are presented in Figures D9 through D13. With one primary exception (RMS_X), these data indicate an improvement in aircraft-control performance for augmentation modes including an OLCS in the pitch and roll axes (C_2 and C_4). Consistent trends (not statistically significant) in RMS_Y and RMS_Z errors during the approach phases (P_1 and P_2) and statistically significant differences in pitch and roll control activity support this finding. Effects of heading-hold implementation were limited to reductions in pitch and roll control activity under the conditions where this hold mode was used in conjunction with pitch- and roll-axis OLCS (see Figures D12 and D13). Trends in RMS_Y data (Figure D10) do, however, suggest further improvement in lateral-axis position control with both modes in which the heading hold was used (C_3 and C_4).

10-6

As noted above, control-augmentation mode differences resulting in terms of RMS_X errors (Figure D9) were not consistent with those yielded by other performance measures. Longitudinal RMS position errors in the hover phase (P_3), for example, averaged between 15 and 20 feet greater with the SAS + OLCS modes (C_2 and C_4) than with the SAS modes (C_1 and C_3). These differences are attributed to a temporarily degrading effect of OLCS in the pitch axis during the terminal portion of the decelerating approach to hover, resulting in a tendency to overshoot the command hover point.

Display-by-Noise (DN) Interaction Results

The significant DN interactions, shown in Figures D14 through D16, are consistent with results obtained in the previous Task II study, and indicate the differential effects which signal degradation had on performance with the two display formats. Relatively greater increases in RMS_y errors resulted with the PPI-AR format (D_1) under the high measurement-noise/filter-lag condition (N_3F_3), while the IEVD format (D_2) yielded larger measures in pilot control activity.

Angle-by-Control-Mode (AC) Interaction Results

Examples of AC-interaction data which are useful for further interpretation of main-effect results discussed above are shown in Figures D17 and D18. It may be observed in Figure D17 that increased RMS_X errors during hover, previously discussed for the approach-angle main effect (Figure D6), are attributable to only test conditions including control modes C_2 and C_4. Similarly from Figure D17, RMS_X error relationship shown for the control-mode main effect (Figure D9) are seen to be a primary result of differences occurring with only the 6-degree glideslope.

Final-approach phase pitch-control-activity data in Figure D18 yield additional qualification to the main-effect data for control modes presented in Figure D12. While OLCS-augmented modes (C_2 and C_4) offered reduced pitch control activity with both approach angles, this reduction was greatest for the steeper 15-degree angle (A_2).

Noise-by-Control-Mode (NC) Interaction Results

Control-activity measures yielded the principal NC-interaction data in this study (Figures D19 through D22). It may be observed in the final-approach (P_2) and hover (P_3) data shown that performance with the OLCS-augmentation modes was least influenced by signal degradation due to measurement noise and filter lags (N_3F_3). Also apparent in these data is the effect of further reduction of control activity with the use of heading hold in conjunction with pitch- and roll-axis augmentation (C_4).

10-7

Flight-Path-Error Interval Data for UH-1 Vehicle

Representative samples of instantaneous vertical and lateral flight-path errors (E_Z and E_Y) recorded at 250-foot intervals during the final-approach phase (P_2) are presented in Figures D23 through D26 of Appendix D. Averages (medians) and variabilities (±34th percentiles from medians) of sampled time-history performance are indicated as previously described in Section VI. Levels of independent variables defining test conditions associated with each figure are indicated by previously defined alphanumeric codes.

Data from test conditions selected for illustration in these figures constitute a comparison of flight-path control for the 6-degree approach (A_1), the IEVD display format (D_2), both noise/filter combinations (N_1F_1 and N_3F_3), and two control-augmentation modes (C_1 = SAS and C_3 = SAS + ψ hold). In a variable code consistent with that used for similar Task II study data, these variable combinations are represented by:

Variables

	Q	N	F	A	C	D	V
Variable Levels	1	1	1	1	1	2	1
	1	1	1	1	3	2	1
	1	3	3	1	1	2	1
	1	3	3	1	3	2	1

This set of treatment combinations was selected to further illustrate trend differences resulting in final-approach-phase RMS_Y and RMS_Z errors (Figures D10 and D11) with control modes C_1 and C_3. By comparing interval data for noise condition N_1F_1 in Figures D23 and D24, it may be noted that the use of heading hold had the effect of reducing altitude errors during the decelerating approach to hover as well as flight-to-flight error variabilities in the lower speed portion of this deceleration (approximately last 1000 feet of range). For the degraded-signal condition N_3F_3 (Figures D25 and D26), heading hold had a similar effect during deceleration, and additionally served to reduce error variabilities during the initial glideslope-acquisition segment of the final approach. These differences are attributed predominantly to cross-coupling effects of collective-lift inputs into the aircraft yaw axis which increase control-task difficulty in the absence of a heading-hold mode.

TERMINAL DATA FOR UH-1 VEHICLE

Terminal position errors, velocities and attitudes recorded at sampling points P_5, P_6 and P_7 as defined earlier in this section are summarized in Figures D27 through D32.

10-8

Data depict performance medians and ±34th-percentile points around each median for the four test conditions discussed above, with results also presented for control-augmentation mode C_2 (SAS + OLCS).

Generally, these measures yielded trends toward decreasing averages and/or variabilities between sampling points P_5 (first contact with 50-foot altitude) and P_7 (ground contact). The heading-hold mode used in conjunction with the three-axis SAS (C_3) did not yield appreciable improvement in terminal-control performance over that resulting with only the three-axis SAS (C_1). Performance differences at touchdown between SAS and SAS + OLCS modes were limited primarily to lateral-axis measures recorded under the degraded-signal condition N_3F_3 (Figures D28 and D32). Maximum 34th-percentile deviations of lateral velocity ($\dot{Y}_B$) and roll attitude (ϕ) at ground contact under this condition were 4.0 ft/sec and 4.5 degree respectively, for the SAS mode, and 1.0 ft/sec and 2.0 degree, respectively, for the SAS + OLCS mode.

CONTINUOUS TIME-HISTORY DATA FOR UH-1 VEHICLE

Typical time histories of control-stick position, vehicle attitudes, and altitude for the following test conditions are presented in Figures D33 through D40, Appendix D:

	Q	N	F	A	C	D	V
	1	1	1	1	1	2	1
	1	3	3	1	1	2	1
	1	1	1	1	2	2	1
Variable Levels	1	3	3	1	2	2	1
	1	1	1	1	3	2	1
	1	3	3	1	3	2	1
	1	1	1	1	4	2	1
	1	3	3	1	4	2	1

(Variables)

Samples shown were selected on a subjective basis, and were judged to be representative of the general form of data resulting for test conditions illustrated. To minimize interactive effects of piloting technique with other experimental variables, all samples were selected from performance records of the same pilot.

By comparing Figures D33 and D34 to Figures D35 and D36 it may be observed that addition of pitch- and roll-axis OLCS to the basic SAS mode had an effect of changing pilot-induced aircraft-response characteristics from relatively high-amplitude and low-frequency to predominantly lower-amplitude. higher-frequency components. This change occurred for both noise/filter conditions simulated.

An example of the contribution of an automatic heading-hold with the three-axis SAS is seen in Figures D34 and D38. During near-hovering flight (hover and descent phases), a higher degree of aircraft-control stability is maintained with the aid of heading hold since the pilot has one less control axis to which his attention must be shared.

CONTROL-LOSS DATA FOR UH-1 VEHICLE

Seven of the 512 (1.3%) simulated approaches and landings flown with the UH-1 during Task III-study formal-date collection resulted in loss of aircraft control. Distributions of these data across variable levels for each independent variable are shown in Table 10-6 (levels numbered 1 and 3 are used for the combined noise/filter variable for consistency with previous codings). Although these data may suggest trend results for variables NF and Λ, only tentative interpretations are advisable since six of the seven control losses occurred with only one of the four pilots.

As in previous study phases, data from flights in which control losses occurred were omitted from other performance analyses.

Table 10-6. Control-Loss Data for UH-1

Variable	Variable Level			
	1	2	3	4
C	0	3	3	1
NF	2*	✕	5	✕
A	1	6	✕	✕
D	4	3	✕	✕

*i.e., two of seven control losses resulted with the combined noise/filter variable level N_1F_1

ANALYSIS-OF-VARIANCE RESULTS FOR XV-5 VEHICLE

Condensations of analysis-of-variance summary tables indicating confidence levels for main effects and interactions are shown in Tables 10-7 through 10-11. Effects found to be statistically significant at confidence levels between $p < 0.10$ and $p < 0.005$ are indicated.

Table 10-7. Condensation of Analysis-of-Variance Summary
Tables; Phase 1; XV-5 Aircraft

Source	Dependent Variable				
	Time	RMS_Z	AI_θ	AI_ϕ	AI_{col}
D		0.025*			
A		0.100		0.025	0.100
C	0.005		0.100	0.005	
N		0.025	0.025	0.025	
DA	0.100				
DC				0.025	
AC	0.005			0.100	
DN					
AN					0.005
CN		0.025	0.025	0.025	
DAC					
DAN					
DCN			0.025		
ACN					
DACN					

*$P < 0.025$

Table 10-8. Condensation of Analysis-of-Variance Summary
Tables; Phase 2; XV-5 Aircraft

Source	Dependent Variable					
	Time	RMS_Y	RMS_Z	AI_θ	AI_ϕ	AI_{col}
D						
A						
C			0.100*	0.100	0.005	
N		0.025	0.025	0.100	0.025	
DA		0.100				
DC			0.100			
AC						0.025
DN						
AN					0.005	
CN				0.025	0.005	
DAC				0.005		
DAN						
DCN				0.100		
ACN						
DACN						

*$P < 0.100$

10-11

Table 10-9. Condensation of Analysis-of-Variance Summary
Tables; Phase 3; XV-5 Aircraft

Source	Dependent Variable					
	RMS_X	RMS_Y	RMS_Z	AI_θ	AI_ϕ	AI_{col}
D A C N			0.100*	0.100 0.100	0.005	
DA DC AC DN AN CN	0.100 0.100	0.100				0.100
DAC DAN DCN ACN	0.100	0.100				0.100
DACN						

*P < 0.100

Table 10-10. Condensation of Analysis-of-Variance Summary
Tables; Phase 4; XV-5 Aircraft

Source	Dependent Variable					
	Time	RMS_X	RMS_Y	AI_θ	AI_ϕ	AI_{col}
D A C N	0.025 0.100	0.100* 0.025 0.100		0.100	0.005	
DA DC AC DN AN CN	0.100	0.100	0.25			0.100 0.100
DAC DAN DCN ACN			0.100		0.100	0.100
DACN						

*P < 0.100

Table 10-11.   Condensation of Analysis-of-Variance
Summary Tables; Phases 5 and 7;
XV-5 Aircraft

| Source | Dependent Variables | |
	$\dot{Z}$ (Phase 5)	$\dot{Z}$ (Phase 7)
D λ C N	0. 100*	
DA DC AC DN AN CN		
DAC DAN DCN ACN	0. 100	
DACN		

*P < 0. 100

Differences Due to Display Format

Data depicting the effect of display-format differences on position-control performance and control-activity level are summarized in Figures D41 through D45. Consistent but statistically non-significant trend differences with the XV-5 vehicle were similar to those resulting with the UH-1, and suggest a tendency for higher RMS position errors but lower-pitch- and roll-axis control activity with the PPI-AR format (D_1). RMS errors for all position-control axes averaged less than 35 feet.

Differences Due to Approach Angle

The approach-angle variable again yielded few statistically significant results from the analyses of variance performed. Results of altitude-control (Z-axis) performance are shown by example in Figures D46 and D47 of Appendix D. Differences in RMS_Z (Figure D46) were significant for the initial-approach and hover phases P_1 and P_3) but were relatively small in an absolute sense, averaging between 2 and 5 feet. Vertical velocities sampled at first contact with the command 50-foot hover altitude (P_5) averaged approximately 5 ft/sec, as shown in Figure D47 and were reduced to 4.5 ft/sec at ground contact (P_7).

Differences Due to Noise/Filtering

Contributions of the combined measurement-noise and signal-filtering variable to performance change with the XV-5 vehicle are exemplified by data shown in Figures D48 through D51. Lateral and vertical RMS errors during final approach were increased by approximately 6 feet under the degraded-signal condition N_3F_3 (Figures D48 and D49). It may be noted that final-approach RMS_Y errors recorded under conditions N_1F_3 and N_2F_3 are consistent with performance under the same conditions in the Task II study (see Figure C75, Appendix C). Control-activity data, summarized in Figures D50 and D51, also reflect anticipated increases during all approach and landing phases under condition N_3F_3.

Differences Due to Control-Augmentation Mode

Examples of significant main-effect data for the control-augmentation-mode variable depict effects similar to those discussed previously for the UH-1 aircraft. Typical performance results obtained with the XV-5 vehicle presented in Figures D52 through D55, summarize these effects. RMS_X errors recorded during hover and descent phases (Figure D52) were greatest for modes which included pitch- and roll-axis OLCS augmentation. As with the UH-1, this result is attributed to a temporary degrading effect of OLCS in the pitch axis

during deceleration to hover which increased the likelihood of hover-point overshoot. Conversely, position errors in this axes, as exemplified by RMS_Z data in Figure D53, indicate small (less than 5 feet) but statistically significant reductions in approach-path errors for the two modes which included an OLCS (C_2 and C_4). Pitch and roll control-activity measures yielded reduced control activity for OLCS-equipped modes in most instances (Figures D54 and D55), with trends toward further reductions under conditions which also included a heading-hold mode (C_3 and C_4).

Noise-By-Control-Mode (NC) Interaction Results

Relatively few significant interactions resulted from the analyses of XV-5 flight-performande data which were considered useful for further interpretation or qualification of main-effect data discussed above. Exceptions to this finding were data representing NC interactions for pitch and roll control activity recorded during initial- and final-approach phases (Figures D56 through D59). These interactions have the same general form as NC interactions resulting with the UH-1 vehicle, and indicate relatively less increase in pilot control activity under the degraded-signal condition (N_3F_3) with OLCS-augmented control modes (C_2 and C_4).

FLIGHT-PATH-ERROR INTERVAL DATA FOR XV-5 VEHICLE

Vertical and lateral flight-path-error samples (E_x and E_Y) recorded during the final-approach phase are presented in Figures D60 through D63). Error averages (medians) and variabilities are shown for test conditions identical to those described above for UH-1 flight data to allow a direct comparison of piloting performance resulting with the two aircraft simulated.

Under noise/filter condition N_1F_1 (Figures D60 and D61), error envelopes were nominally the same as those resulting from the UH-1 vehicle (see Figures D23 and D24), with ±34th-percentile ranges exceeding flight-path errors of 50 feet for only brief periods during deceleration to hover. However, trends in data variability resulting under the degraded-signal conditions N_3F_3 were less similar for the two aircraft. Unlike performance data shown for the UH-1 (Figures D25 and D26), comparable interval data for the XV-5 (Figures D62 and D63) indicate no appreciable change in performance attributable to addition of a heading-hold mode. Also, XV-5 data under condition N_3F_3 reflect more of a "rectangular" distribution of performance variability as a function of range, while UH-1 performance variabilities were greatest during the initial portion of the approach and generally decreased throughout the remainder of the approach to hover. This difference is attributed to the more predominant collective-input and rotational-axis cross-coupling effects associated with the UH-1 during the initial glideslope-acquisition portion of the approach.

TERMINAL DATA FOR XV-5 VEHICLE

Figures D64 through D69 of Appendix D are examples of terminal position-error, velocity and attitude data recorded at sampling points P_5, P_6 and P_7 during flights with the XV-5 aircraft. Examples are for the same test conditions for which UH-1 data were previously presented (Figures D27 through D32). For a majority of performance-measure and test-condition combinations shown, trends toward decreasing averages and/or variabilities are apparent across consecutive sampling points beginning at P_5 (first contact with 50-foot altitude). Terminal-performance measures do not, in most instances, reflect appreciable differences due to degraded-signal effects or due to levels of the control-augmentation-mode variable illustrated. Performance characteristics at sample points P_5, P_6 and P_7 with control mode C_4 (not illustrated) were not distinguishably different from those shown in Figures D64 through D69.

CONTROL-LOSS DATA FOR XV-5 VEHICLE

Of the 512 simulated approaches and landings flown with the XV-5 in this formal-data-collection phase, five flights (less than 1 percent) resulted in aircraft control loss. These data are distributed across each Task III experimental variable as indicated in Table 10-12. Again, because of the small number of control-loss events relative to the total number of flights attempted, relationships between experimental variables evaluated and control-loss likelihood cannot be clearly specified. Of importance in these data are the small number of control-loss events, and the fact that approximately the same proportion of losses resulted with both aircraft simulated in Task III (seven and five losses for the UH-1 and XV-5 respectively).

As in previous study phases, data from flights in which control losses occurred were omitted from other performance analyses.

Table 10-12. Control-Loss Data for XV-5

Variable	Variable Level			
	1	2	3	4
C	2	1	2	✕
NF	4*	✕	1	✕
A	3	2	✕	✕
D	1	4	✕	✕

*i.e., four of five control losses resulted with the combined noise/filter variable level N_1F_1

10-16

SECTION XI
SUMMARY AND CONCLUSIONS

The primary objective of the two study tasks described in this report was to investigate, by means of real-time man-in-the-loop simulation techniques, the effects of piloting performance of approach-signal degradation and aircraft control-augmentation variables. These tasks were performed to support the overall objectives of the JANAIR-sponsored SAA program being performed at Honeywell -- the investigations of display requirements for manually-controlled IFR steep approaches and landings with vertical-lift aircraft. Each of the above variables is related directly to the problem of display requirements for IFR steep approach since each implies a category of conditions or constraints within which a selected display configuration may be operated. By also simultaneously investigating the effects of this relevant task variables (aircraft types, approach angles, display formats and quickening gains), an increased degree of generality of study results could be obtained.

The following paragraphs summarize results and present conclusions from the Task II and Task III SAA study phases.

SUMMARY OF RESULTS - TASK II

UH-1 Vehicle

Although not consistently supported by statistical significance, consistent trends in results obtained suggest a difference between display formats simulated in the form of a tradeoff between position-control accuracy and pilot control activity. Flight-path deviations tended to be lower with the IEVD format while control activities were lower for the PPI-AR display. However, interactions of display formats with measurement-noise and filtering variables indicated that these differences occurred predominantly under high measurement-noise conditions. Control-losses also resulted more frequently with the PPI-AR format (eight of ten losses were with this display), but because of the relatively low incidence of these events and the fact that a majority occurred with only one pilot, only limited generalization from this result is advisable.

Effects of display quickening-gain variation yielded results similar to those found in the display comparison. Generally, "high-gain" quickening produced lower longitudinal and lateral position errors but higher levels of control activity, although increments in both position-error and control-activity levels due to increased measurement noise were relatively greater with the high-gain alternative. Under intermediate and high measurement-noise conditions, altitude errors during final approach were greater with high-gain quickening, indicating that some sacrifice of attention to the altitude-control task was caused by increased attention demands placed upon the pilot by this quickening-gain level.

11-1

Performance differences due to approach (glideslope) angle indicated larger lateral and vertical flight path errors as well as flight-to-flight error variabilities for the steeper 15-degree approach. Generally, flight-to-flight variabilities in command-path deviation decreased near termination of the approach to hover for both approach angles simulated.

The main effect for measurement noise yielded the antiticpated result of both increased position errors and control activities with increasing noise. Degrading effects of noise were greatest at increased ranges from the signal source, as would be expected, because of the transformations of angular signals to an inertial-position reference frame with X_I, Y_I, Z_I coordinates. Contributions of signal filtering varied as a function of range and aircraft velocity. At increased ranges, where transformed measurement (input) noise levels were greatest, increased signal filtering had a net beneficial effect upon performance. During hover and descent phases, where noise levels were relatively lower, increased filtering yielded trends toward degraded pilot-control performance. This latter result is attributed in part to the greater sensitivity of aircraft control to signal lags in hovering flight where effects of aerodynamic damping are absent. Noise and filtering variable interaction results thus support a requirement for varying the extent of signal filtering as a function of the level of measurement noise and flight condition

XV-5 Vehicle

Display-format differences resulting with the XV-5 were similar to those summarized above for the UH-1. In most instances, RMS position errors under high measurement-noise conditions were greater for the PPI-AR format, while control activities were higher for the IEVD format.

The indirect effect of high-gain quickening on altitude control during final approach under high-noise conditions, previously noted for the UH-1, was not found with the XV-5. Also, the approach-angle variable did not yield significant differences in flight-path-control accuracy (RMS_Y and RMS_Z) during the final approach. These results are attributed to the lower level of control difficulty associated with glideslope acquisition and maintenance with the XV-5 because of the relatively lower degree of "collective" (lift input) cross coupling into other control axes in this vehicle. As with the UH-1, position errors were generally lower with high-gain quickening, but measures of pitch and roll control activity did not yield statistically significant differences due to quickening-gain.

Relationships between measurement noise and XV-5 piloting performance, in terms of position errors and control activity, were consistent with results given above for the UH-1. Additionally, interactive effects of measurement-noise and filtering variables exhibited similar trends, indicating differential effects of signal filtering as a function of noise level and flight conditions.

Terminal-data samples of translational velocities and position errors indicated that performance envelopes described by either of these parameters are larger at approach termination (50-foot hover altitude, as simulated) than at ground contact. This finding, characteristic of performance with both vehicles tested, suggests the desirability of terminating the approach at hover rather than ground contact if visibility conditions are such that an earlier transition to VFR flight is not possible.

SUMMARY OF RESULTS - TASK III

UH-1 Vehicle

Display format differences yielded by the Task III study were consistent with those found in Task II, and were again attributable to a major extent to effects of degraded measurement-signal characteristics. Flight-path errors tended to be lower, and pilot-control activities higher, with the IEVD format.

The approach-angle variable did not yield significant differences in approach path control accuracy, although differences due to this variable were found for RMS_X (longitudinal error) in hover and descent phases. Larger longitudinal errors in these phases were attributed to a temporary degrading effect of pitch-axis OLCS during the terminal portion of the decelerating approach to hover, which resulted in a tendency to overshoot the hover point. More difficulty was experienced with the deceleration task on the 6-degree approach since the longitudinal component of deceleration was greater on this angle than on the steeper 15-degree gradient.

With the above exception, results indicated a general improvement in aircraft-control performance for augmentation modes including an OLCS in the pitch and roll axes. Also, pilot control activities with the OLCS-augmentation modes simulated were least influenced by signal degradation due to measurement noise and filtering lags. Effects of adding a heading-hold mode were limited primarily to reductions in pilot control activity under conditions where this hold mode was used in conjunction with pitch- and roll-axis OLCS. Consistent trends in RMS_Y data did, however, suggest further improvement in lateral-axis position control for both modes with which the heading hold was included.

XV-5 Vehicle

Effects of experimental variables on performance with the XV-5 vehicle were consistent, in most instances, with those summarized above for the UH-1.

In both study tasks (II and III), aircraft control losses experienced by the subject/pilots while attempting to complete the simulated IFR approach and

landing task tended to occur less frequently with the XV-5 aircraft. For Tasks II and III respectively, percentages of flights resulting in control loss with the XV-5 were 0.69 percent and 0.98 percent, compared to 0.87 percent and 1.3 percent for the UH-1. Although these differences averaged across study tasks represent approximately a 28 percent increase in probability of control loss with the UH-1 aircraft, generalization of conclusions from this finding are not warranted since the subject samples used in all study-task/vehicle data-collection phases (e.g., Task II/UH-1) were not identical.

CONCLUSIONS

Based on the results of simulator evaluations performed in the SAA Task II and Task III studies, the following general conclusions can be drawn. A number of conclusions previously established in the Task I study (Ref. 1) were supported in the present studies and are therefore included in this list:

- Within the constraints specified for this study, and for the approach-profile characteristics commanded, the performance of IFR steep-angle approaches and landings is possible under all conditions.

- Of the various approach and landing task segments simulated, the final approach, including a deceleration to hover, is considered to be the most difficult phase to fly. During this phase, the pilot is required to respond to varying forward and vertical velocity commands while maintaining a prescribed flight path.

- Based on terminal data recorded at an altitude of 50 feet (termination of command approach path), and at ground contact, a termination at hover is considered preferable to termination of the command-approach profile at ground contact. This alternative is preferable especially for shallow approach angles or in landing zones where the size of the terminal-error envelope is critical.

- The effects of approach angle vary as a function of the vehicle flown and the axis of error measurement. For example, altitude errors during the approach increase with approach angle for the UH-1 vehicle, reflecting the greater difficulty of controlling simultaneous low forward velocities and high vertical velocities with this aircraft. This conclusion is consistent with handling qualities characteristic of rotary-wing aircraft under these flight conditions. Increased approach angle has relatively less effect on task difficulty with the XV-5 because of the lower degree of axis cross coupling associated with this vehicle.

- Data trends indicate higher control activities but lower flight-path errors with the IEVD format under degraded measurement-signal conditions, while performance differences due to display format are less with decreased signal degradation. Thus in the selection of basic display-format characteristics for a specific approach-aid system and system application, consideration to the available level of measurement-signal integrity is recommended.

- Generally, the higher-gain quickening alternatives tested offer improved flight-path control but are also more sensitive to increases in measurement noise, indicating a possible requirement for gain scheduling as a function of measurement noise level and/or the level of flight-path control precision required.

- A higher degree of measurement noise filtering is desirable during approach than during hovering flight near the signal source. Increased signal lags caused by filtering have relatively less influence if some degree of aircraft aerodynamic stabilization is maintained. Additionally, angular noise levels transformed to inertial position estimates have a more degrading effect upon piloting performance at increased ranges from the signal source. For these reasons it is considered preferable to vary the degree of signal filtering as a function of measurement-noise level, range from the signal source, aircraft velocity, or some combination of these variables.

- Data trends generally indicate beneficial effects from the use of outer-loop control augmentation modes simulated. The predominant effect is found under high measurement noise/filter lag conditions where outer-loop augmentation contributes to reduction of the level of pilot-control activity. An exception to this general conclusion is that the use of pitch-axis attitude-feedback augmentation has a degrading effect on control of longitudinal velocity during the deceleration-to-hover maneuver. For this reason, pitch-axis attitude-response characteristics are not considered desirable during this terminal deceleration or transition to hover.

SECTION XII
REFERENCES

1. Wolf, J.D. and Hoppe, R.B. Aircraft Displays for Steep Angle Approaches. J ANAIR Report No. 681215, July 1970.

2. Anon. 1969 Encyclypedia of Vertical Lift Craft. Vertical World, November 1968.

3. NASA Langley Research Center, VTOL and STOL Technology in Review. Astronautics and Aeronautics, September 1968.

4. Campbell, J.P. Vertical Takeoff and Landing Aircraft. The MacMillan Co., New York, 1962.

5. Dept. of the Army. Principles of Rotary Wing Flight. TM 1-260, September, 1957.

6. Seckel, E., and Traybar, J.J. Piloting and VTOL Instrumentation. Astronautics and Aeronautics, September 1965.

7. Alelyumas, P. V/STOL: Many Designs, Few Planes. Space/Aeronautics, May 1965.

8. Stambler, I. V/STOL: The Quest for Stability. Space/Aeronautics, May 1965.

9. Powe, W. E., et al. Study of Requirements for VTOL Research Simulator for the Study of Control and Display Problems. Rept. No. 2120-920002, Bell Aerosystems Co., April 1963.

10. Seckel, E., et al, A Note on the Effect of Helicopter Dynamics on Steep Instrument Approaches. Report No. 600. Dept of Aeronautical Engineering, Princeton University, February 1962.

11. Youens, F. P., Approach and Landing Problems in Jet VTOL Aircraft. AGARD Report 489, October 1964.

12. Reeder, J.P., The Impact of V/STOL Aircraft on Instrument Weather Operations, NASA TN D-2702, February 1965.

13. Illingworth, J.K.B., and Shazler, J.E., Blind Flying of V/STOL Aircraft, with Particular Reference to Takeoff and Landing. AGARD Report, June 1960.

14. Adams, G.D. V/STOL Approach System Flight Tests: Final Report. FAA Report No. RD-66-95, December 1966.

15. Trant, J.P., and Algranti, J.S., Investigation of VTOL Approach Methods by Use of Ground-Controlled-Approach Procedures. NASA TN D-1489, October 1962.

16. Gilbertson, D.K. Study of Tactical Army Aircraft Landing Systems (TAALS). Tech. Report ECOM-03367-4, January 1966.

17. American Helicopter Society. 24th Annual National Forum Proceedings. Steep Angle Descent Systems for VTOL Aircraft. (No. 204). 1968.

18. Mitchell, H.W. Helicopter Approach Aids. Journal of the Royal Aeronautical Society, Vol. 66, February 1962.

19. Sullivan, N., and Taylor, J.K., Tactical Instrument Landing (TACLAND) System Study. Tech. Report AFFDL-TR-68-22, May 1968.

20. U.S. Army Electronics Lab. Approach and Landing Systems, January 1964.

21. Litchford, G.B. Synthesis of a Multifunctional Tactical Landing System. Tech. Report AFFDL-TR-67-188, January 1968.

22. Dax, P.R., et al. Tactical Instrument Landing Systems Study. Tech. Report AFFDL-TR-68-12, March 1968.

23. Klass, P.J. New ILS Sought for Civil, Military Roles. Av. Week and Space Technology, February 10, 1969.

24. Ryan Aeronautical Co. Detailed Aircraft Specification: XV-5A Flight Research Aircraft. Report No. 62B125A, December 1964.

25. Reschak, R.J., Category II Performance and Limited Handling Characteristic Tests of the YUH-1D and a 44 foot Rotor. Air Force FTC TDR-63-43, November 1964.

26. Williams, P.R. and Kronholm, M.B. Technical Report on Simulation Studies of an Integrated Electronic Vertical Display. Norden Div., United Aircraft Co. Report No. 1161 R 0021, December 1965.

27. Wooding, H.C. and Simpson, J.A. Interim Technical Report on Integrated Electronic Vertical Display Research. Norden Div., United Aircraft Co. Report No. 1161 R 0028, February 1967.

28. Radio Technical Commission for Aeronautics. Request for Landing Aid System Concept Descriptions. Paper 24-69/SC117-48, January 1969.

29. Radio Technical Commission for Aeronautics. Request for Landing and System Concept Descriptions: Attachment 2; Tentative Technical Requirements. Paper 23-69/SC117-47, January 1969.

30. P   t, T. R., and Bordner, G. W.   Synthesis of an Optimal Set of
       ar Track-While-Scan Smoothing Equations.   IRE Transactions on
    utomatic Control, July 1962.

31. Bjorklund, H. A.   Spectral Analysis Handbook.   Honeywell Inc., 1969.

32. Skelton, G. B.   Investigation of Effects ofGusts on V/STOL Craft in Tran-
    sition and Hover.   Honeywell Report No. 12060-FR1, June 1968.

33. Sonneborn, W.   UH-1C Data for Hybrid Computer Simulation.   Bell Heli-
    copter Co., Report No. 204-099-892.

34. Anon.   Handbook of Geophysics, Revised Edition.   The MacMillan Company,
    New York, 1961.

35. Chilton, R. G.   Some Measurements of Atmospheric Turbulence Obtained
    with Flow Direction Vanes Mounted on an Airplane.   National Advisory
    Committee for Aeronautics, TN 3313, 1954.

36. Mueller, L. J.   Problems Unique to VTOL Automatic Flight Control.
    Paper presented at Military Aircraft Systems and Technology Meeting,
    Washington, D. C., September 1964.   Honeywell Inc., 1964.

37. Buffum, R. S. and Robertson, W. T.   A Hover Augmentation System for
    Helicopters.   Journal of Aircraft, Vol. 4, July-August 1967.

38. Sideris, G.   Mastering the Control Variables.   Space/Aeronautics, Vol.
    53, May 1970.

39. Army Advanced Automatic Flight Control System Study.   Technical Report
    ECOM-1216-5, July 1966.

40. General Electric Co.   XV-5 Lift Fan Flight Research Aircraft Program:
    Final Systems Analysis and Flight Simulation Report, Vol. II.   Report No.
    157, March 1965.

APPENDIX A
SIMULATOR DESCRIPTION

APPENDIX A
SIMULATOR DESCRIPTION

SIMULATION FACILITY

All simulations were performed on the Honeywell hybrid-simulation facility. This facility, consisting of both digital and analog computers, was specifically designed for simulation programs where real-time performance measures are desired under varied experimental conditions.

In general, the analog portion of the hybrid computer was used to provide calculations of relatively low accuracy. The digital portion of the computer was used to provide the high-speed and accuracy calculations and, in this particular study, to control the simulation. This is common practice because of the extensive logic and decision-making capabilities of the digital machine.

Figure A1 shows a model of the SAA system and the organization of the hybrid-computer facility in the mechanization of this system. Variable-velocity simulations of both aircraft were programmed on this facility. Nonlinear force and moment equations and aerodynamic lags were computed digitally, while inertial dynamics were synthesized on the analog portion of the hybrid simulator. Examples of the flight characteristics gained by this variable-velocity-simulation technique include: (1) complete aerodynamic cross coupling in all control axes in the presence of gusts, control inputs and vehicle drift rates, and (2) continuous change in vehicle trim conditions as a function of airspeed and aerodynamic loading.

A brief description of equipment included in the Honeywell hybrid-computer facility follows.

Digital Computer (XDS Sigma-5)

The digital computer was a high-speed, medium-word-length machine specifically designed for hybrid simulations, real-time control, and rapid computation. The main characteristics of this machine are:

- 32-bit word
- 40K memory, rapid-access disc (3 million, 9-bit bytes)
- 0.85-μsec cycle time
- Floating-point hardware
- Real-time FORTRAN IV language

A1

⑨
MEASUREMENT
ERRORS AND NOISE   FLIGHT - SYSTEM MODEL

② ───────── ③ ───────── ④ ───────── ⑤
AIRCRAFT   AIRBORNE
POSITION   →   COMPUTER   →   DISPLAYS   →   PILOT
SENSORS

①   ⑧   ⑦   ⑥
GROUND   ATTITUDE   CONTROL
STATION   AND RATE ← AIRCRAFT ←   SYSTEM
                  SENSORS

                                  ⑩
                              TURBULENCE

COMPUTER SIMULATION OF FLIGHT SYSTEM

① ② ③ ④ ⑦ ⑨ ⑩   ⑥ ⑦ ⑧
DIGITAL COMPUTER AND   ANALOG COMPUTER
PERIPHERAL I/O EQUIPMENT

INPUT/OUTPUT AND GENERAL
CONTROL

CALCULATION AND GENERATION   INERTIAL DYNAMICS
OF DISPLAY
                                        FEEDBACK OF
NONLINEAR FORCE AND MOMENT   CONTROL INPUTS
EQUATIONS
                                        ATTITUDE AND RATE
MODELS OF: SENSORS

  GROUND STATION   STABILITY-AUGMEN-
                                        TATION SYSTEM
  POSITION SENSORS
                                        AUTOPILOT
  AIRBORNE COMPUTER

  TURBULENCE AND NOISE
  FILTER

                        D/A
                        A/D

            ④   ⑤   ⑥
           CRT   →   PILOT   →   CONTROL
                                     STATION

* CIRCLED NUMBERS SHOW WHERE SPECIFIC SUBSYSTEM MODELS WERE
  SIMULATED

Figure A1. SAA Simulation Organization

A2

Peripheral Equipment

The peripheral equipment available in this computer system included:

- 1000-line-per-minute printer
- Card reader
- Two magnetic tape units
- Console input/output typewriter
- Character display

Display Equipment

Display equipment included a 19-inch digitally addressed CRT.

Analog Computers and Hybrid Link

The analog portion of the hybrid problem was programmed on a 100-amplifier analog computer. Information flowing into and out of the analog portion of the system emanated from and entered the digital portion via a linkage system of digital-to-analog (D/A) and analog-to-digital (A/D) converters.

The link system included a small-capacity analog computer, and provided the means of coupling the larger analog computer with the digital computer.

The link included:

- 24 channels of A/D with simultaneous sample and hold
- 24 channels of A/D without sample and hold
- 20 channels of D/A
- 6 discrete-input channels
- 6 discrete-output channels
- 10 kHz real-time-interrupt clock

Pilot's Control Station

A pilot's control station was positioned directly in front of the computer-addressed display scope, and consisted of a mobile platform on which the following controls were mounted:

A3

- Pitch and roll center stick with trim
- Collective stick
- Rudder pedals

Displacements and forces of the various controls on the pilot's control station used with both vehicle simulations were:

Control	Displacement/Force
Pitch-stick travel (fore-aft)	±6. 5 in.
Pitch-stick breakout	1. 5 lb
Pitch-stick force gradient	1. 3 lb/in.
Roll-stick travel (lateral)	6. 5 in.
Roll-stick breakout	1. 2 lb
Roll-stick force gradient	0. 8 lb/in.
Rudder-pedal travel	3. 0 in.
Rudder-pedal breakout	1. 0 lb
Rudder-pedal force gradient	1. 0 lb/in.
Collective-stick travel	8. 0 in.
Collective-stick torque	5. 0 ft-lb

Additional controls used by the pilot were the standard thumb-actuated trim button, used for pitch- and roll-axis trim inputs, and a two-position "trigger" switch. The latter switch was used only with the XV-5 aircraft simulation as a "vector-angle" control device.

COMPUTER PROGRAM ORGANIZATION

The total computer program for each vehicle simulated consisted of one main program which provided overall control, and several subroutines which performed distinct program functions. The program was modular in design, allowing the programming for each primary function to be developed and checked out independently. This modular design also promoted ease of interpretation, usage, and program modification, and the capability to store independent subprograms on magnetic tape.

A brief description of the functions of the main program and each of the subroutines follows:

A4

Program Name	Function
MAIN	Provided overall control of simulation.
	Controlled communications between analog and digital.
	Generated system disturbances in the form of turbulence and measurement noise.
	Permitted experimenter to change experimental conditions through input of a 7-digit ID number on console typewriter.
	Permitted changes through typewriter of other parameters not normally varied during formal experimentation.
	Calculated experimental performance measures and output them to printer and magnetic tape.
DISPLAY	Calculated appropriate variables and called appropriate display software routines for generation of moving portions of display.
FORCE (and associated functions)	Generated vehicle body-axis forces and moments given vehicle velocities, angular rates and attitudes, and control inputs.
RAND	Generated random-number sequence used for simulation of turbulence and measurement noise. This sequence had a Gaussian distribution with specified mean and standard deviation.
ACCU	Provided smoothing of simulated measurements of position in space through filtering with the α-β filter model.
DISTAB	Read in data for all display-background information (i. e., all nonmoving portions of display).

VEHICLE SIMULATIONS

XV-5 Aircraft

The fan, or vertical-lift mode, of the XV-5 was simulated. This variable-velocity simulation was developed for an earlier control system study at Honeywell (Ref. 32), with a detailed discussion of equations and programming being presented in this reference. For the Task II study, the XV-5 was simulated with a three-axis rate-stability-augmentation system as described in Section VII of this report. Other control-augmentation modes evaluated as part of the Task III study phase are also described in this section.

UH-1 Aircraft

The UH-1 simulation employed the simulated-rotor method of modeling a variable-velocity helicopter. As in the XV-5, the digital program generated forces and moments as a function of flight condition and control inputs. The UH-1 vehicle was also simulated with a three-axis rate-stability-augmentation system in the Task II study and additional control-augmentation modes in the Task III study.

The main-rotor equations (Ref. 33) show that the computation of lift from the blades is exerted essentially by four blades at azimuth angles of 0 degrees (forward), 90 degrees (to right), 180 degrees and 270 degrees. The lift and drag from each blade is then halved since the vehicle has actually only two blades. Because the rotor equations contained higher frequencies than the aerodynamic equations, it was necessary to compute these twice during each single time step of the computer program.

Time lags between digital and analog computations resulted in reducing the phase margin of the yaw axis to the point of instability. This effect was removed by predicting the next set of values which the digital program would see. The prediction was accomplished by multiplying the current acceleration by the time step of the program and adding it to the current value of rate obtained from the analog. This method accrued only short-term error since the analog was still relied upon for steady-state values.

DISPLAY SIMULATIONS

The two display formats evaluated (PPI-AR and IEVD) were programmed for presentation on a computer-addressed CRT display. The refresh rate of this display was approximately 50 Hz and was independent of the information-update rate. The display information-update rate of 13.3 updates/sec was limited by the program time step (i.e., the time required for the digital computer to complete one cycle of calculations).

Background portions of the display were set up through the subroutine DISTAB while moving sections of the display were initialized during the non-real-time portion of the program. All moving portions of the display were double buffered (i. e., while the picture for one time step was being computed the picture for the last time step was being displayed).

TURBULENCE SIMULATION

A simplified gust-perturbation model was developed for use in the data-collection phase of the study. Based on data cited in Refs. 34 and 35, a gust profile was programmed which randomly varied both gust duration and magnitude. Durations were from 1 to 10 seconds, relative to a stationary object, with duration decreasing as a function of aircraft forward velocity. Single-axis component magnitudes randomly varying from zero to plus and minus 5 knots were selected to yield a nominal increase in pilot control difficulty during the approach and landing task. The three-axis gust components were identical in their range of magnitude variation (Ref. 35), and when combined, generated a maximum gust vector of approximately ±8.5 knots with a mean of zero knots. Gust conditions did not change as a function of altitude (Ref. 34).

SIMULATION USAGE

Primary control of the simulation was maintained by the digital computer through a console typewriter, while secondary control was maintained through switches on the analog computer and on the control station itself. Switch options on the analog included:

- Starting and stopping a mission (e. g., passing from non-real-time operation to a real-time mode)

- Inhibiting printout of performance data (used during checkout and debug)

- Transferring control from the analog back to the typewriter console

- Transferring start control of the mission to a button on the pitch and roll stick of the control station

Console typewriter options included:

- Complete control of experimental conditions through a 7-digit ID number

- Specification of starting run number which was thereafter automatically incremented at the start of each run

- Outputs of performance and run-summary data on magnetic tape

- Output of magnetic tape data on printer

- Variation of experimental conditions not controlled by ID number

SIMULATOR LIMITATIONS AND CONSTRAINTS

A fundamental assumption associated with a laboratory simulation of a complex task and environment is that not all elements and variations in the task and environment are duplicated. A tradeoff between the inclusion of additional elements in the simulation, and their associated cost, must be made so as to maximize the amount and validity of problem-oriented information within specified cost constraints. Limitations of the simulations for this study are listed below. If the interpretation of performance data described in this report is tempered with a knowledge of these limitations, a meaningful assessment of pilot performance on the IFR steep-angle approach task is possible.

- A fixed-base control station was used. The lack of kinesthetic and auditory cues results in the simulator pilot not being able to attend to motion and sound cues normally experienced in aircraft flight. The fixed-base simulator does, however, require the pilot to gain all control information from his visual displays, thus avoiding the confounding of experimental variables (e. g., displays) with other sensory inputs.

- Only two aircraft, of the large variety of vertical-lift vehicles under study, were simulated. The results of this study are limited in their generality to the extent that the handling qualities and aerodynamic characteristics of the simulated UH-1 and XV-5 differ from other vertical-lift aircraft.

- The UH-1 and XV-5 were simulated with their normal gross weights of 8500 and 9200 pounds, respectively, with no consideration given to approach and landing constraints associated with an overload or high density-altitude conditions.

- Ground effects and mean-wind conditions were not simulated. Effects of these variables interact with each other and with terrain features, and therefore would more appropriately be investigated in a study where these effects are treated as experimental variables.

A8

APPENDIX B
SPECTRAL AND DISTRIBUTION CHARACTERISTICS
OF NOISE SIMULATED

APPENDIX B

SPECTRAL AND DISTRIBUTION CHARACTERISTICS
OF NOISE SIMULATED

To describe the effects of the α-β filter and the rate-limiting technique on reduction of simulated measurement-system noise, the following functions were computed using a collection of special-purpose programs on the XDS Sigma-5 computer:

- Normalized Autocorrelation $(\bar{R}_X)$

$$\bar{R}_X(\tau) = \frac{R_X(\tau)}{R_X(o)} = \frac{\langle X(t)\, X(t+\tau)\rangle}{\sigma_X^2} = \lim_{T\to\infty}\ \frac{1}{2\sigma_X^2\, T} \int_{-T}^{T} X(t)\, X(t+\tau)\, dt$$

(B1)

where

$R_X(\tau)$ = autocorrelation function (ACF) of $X(t)$

$R_X(0)$ = value of ACF at $\tau = 0$ sec

$X(t)$ = value of function X at time t sec

$X(t+\tau)$ = value of function X at time $t+\tau$ sec

σ_X^2 = variance of function X

τ = parameter representing the amount of shifting of $X(t)$

$\langle\ \rangle$ = denotes time average of function enclosed

- Power Spectral Density (S_X)

$$S_X(f) = \mathcal{F}\{R_X(\tau)\} = \int_{-\infty}^{\infty} R_X(\tau)\, e^{-j2\pi f}\, d\tau$$

(B2)

where

$S_X(f)$ = power spectral density (PSD) of $X(t)$

f = frequency (Hz)

B1

τ = parameter representing the amount of shiftir $\cdot$ of $X(t)$

$\mathscr{F}\{R_X(\tau)\}$ = Fourier transform of $R_X(\tau)$

* Cumulative Probability Density (P)

$$P(x_i) = P_r(X \le x_i) = \sum p(x_i) \qquad -\infty < x_i < \infty \qquad (B3)$$

where

$p(x_i)$ = discrete probability density at $X = x_i$

$P(x_i)$ = discrete cumulative probability density for $X \le x_i$

In general, a digital computer cannot solve integral equations, and therefore all integrals must be replaced by summations. In practice, however, this method leads to equations which are very time consuming even for a digital computer.

The method employed here assumes that the function being analyzed is periodic and that it is known at 2^N points in time. The latter requirement implies that the period of the function can be partitioned into 2^N parts and the function evaluated at each division as well as at time zero. The equations obtained for $R_X(\tau)$ and $S_X(f)$ are based upon the above assumptions and make us of the Cooley-Tukey Algorithm. Because of their complexity, they are omitted from the text, but a derivation of them appears in Reference 31.

The value of N chosen was 10 and corresponds to 1024 subdivisions. This value provided sufficient data to describe the effects of filtering and rate limiting. Sample results of this analysis appear in Figures B1 through B14. The notation used for subscripts of R and S was the following:

X: random noise input to filter/limiter system

$\hat{X}$: position-output estimate from α-β filter

$\hat{\dot{X}}$: rate-output estimate from α-β filter

$\hat{\dot{X}}_{lim}$: rate-output estimate from rate limiter
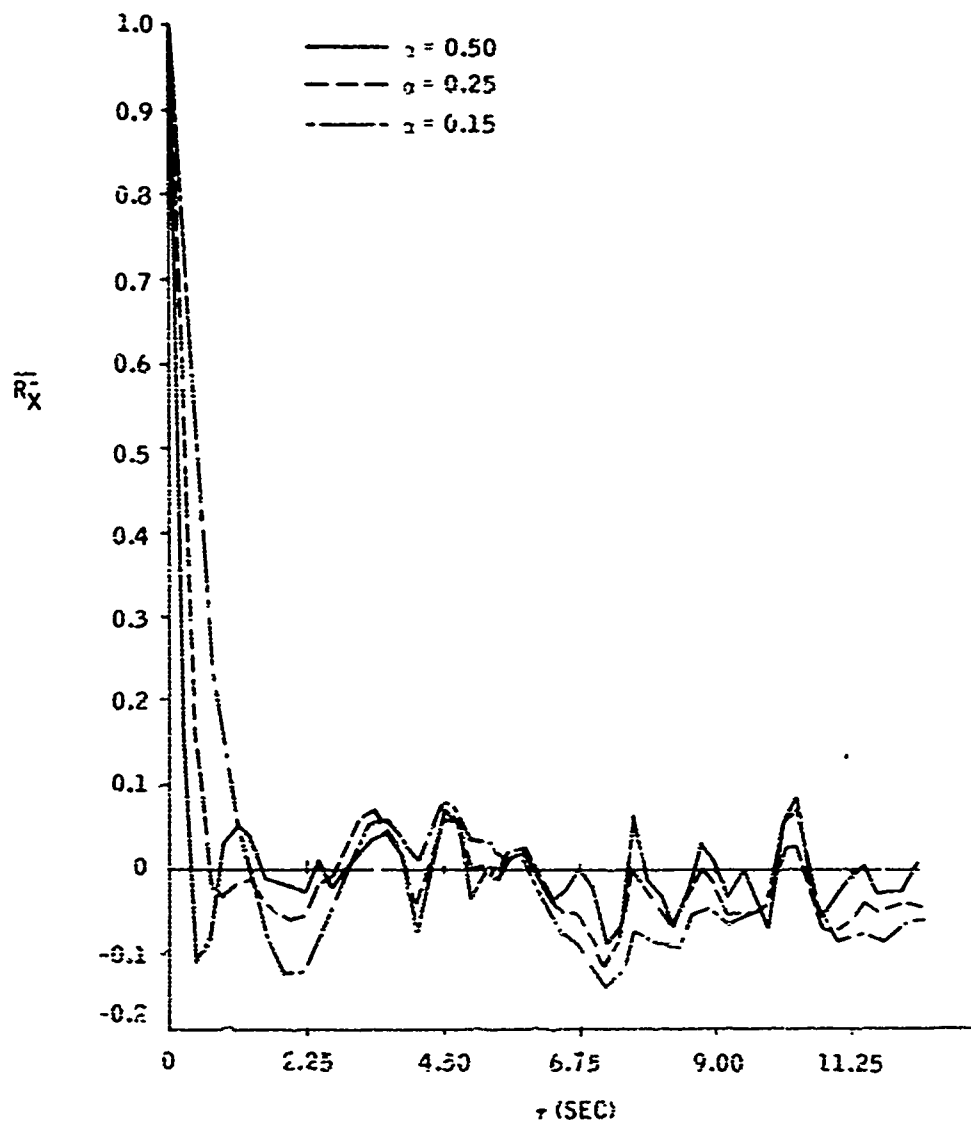
Figure B1. Normalized Autocorrelation of Position Output of $\alpha-\beta$ Filter; $\sigma_{\dot{X}} = 15$ ft

B3
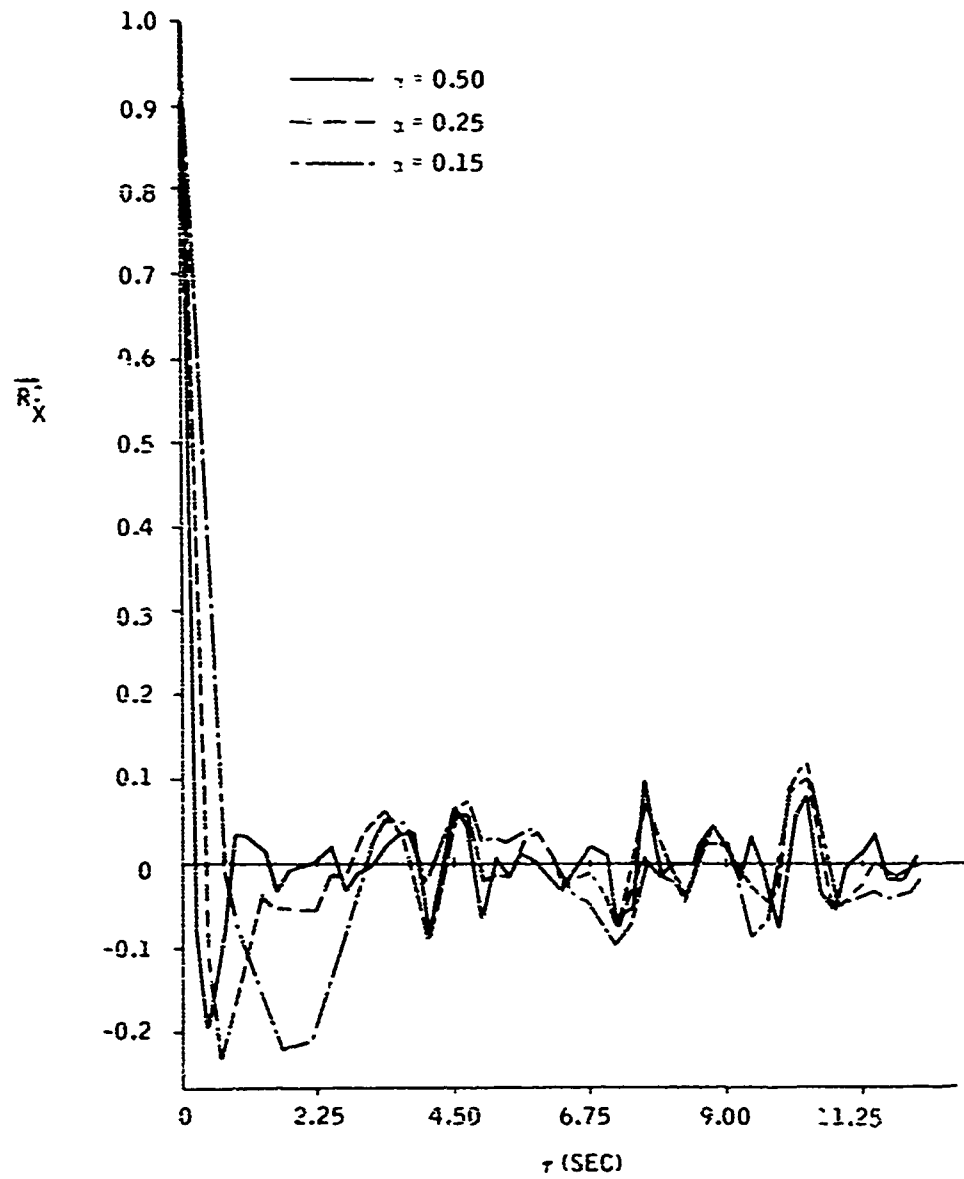
Figure B2. Normalized Autocorrelation of Rate Output of α-β Filter; $\sigma_X = 15$ ft

B4
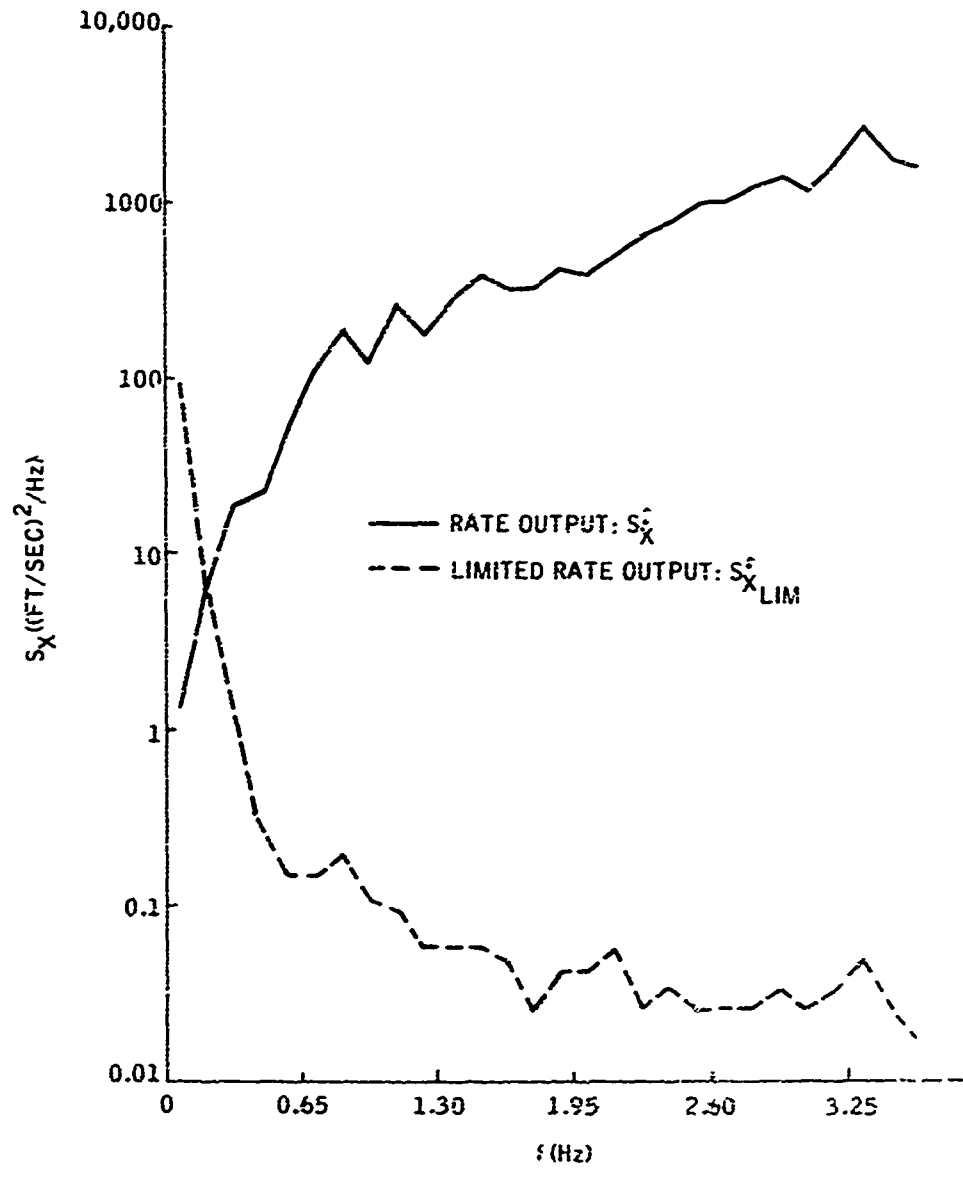
Figure B3. Power Spectral Density of Rate Output and Limited Rate Output of α-β Filter; $\alpha = 1.00$; $\sigma_X = 15$ ft

B5
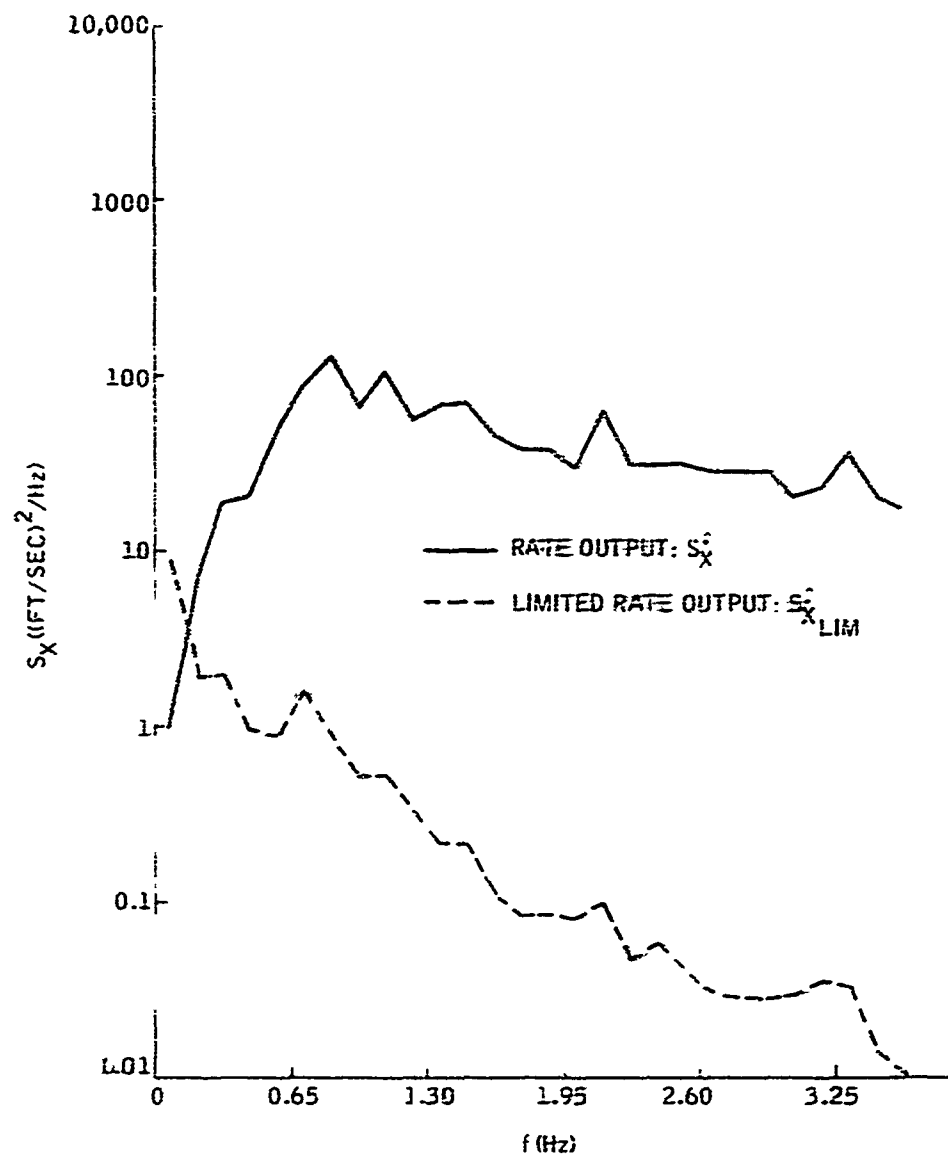
Figure 34. Power Spectral Density of Rate Output and Limited Rate Output of $\alpha-\beta$ Filter; $\alpha = 0.50$; $\sigma_X = 15$ ft

B6
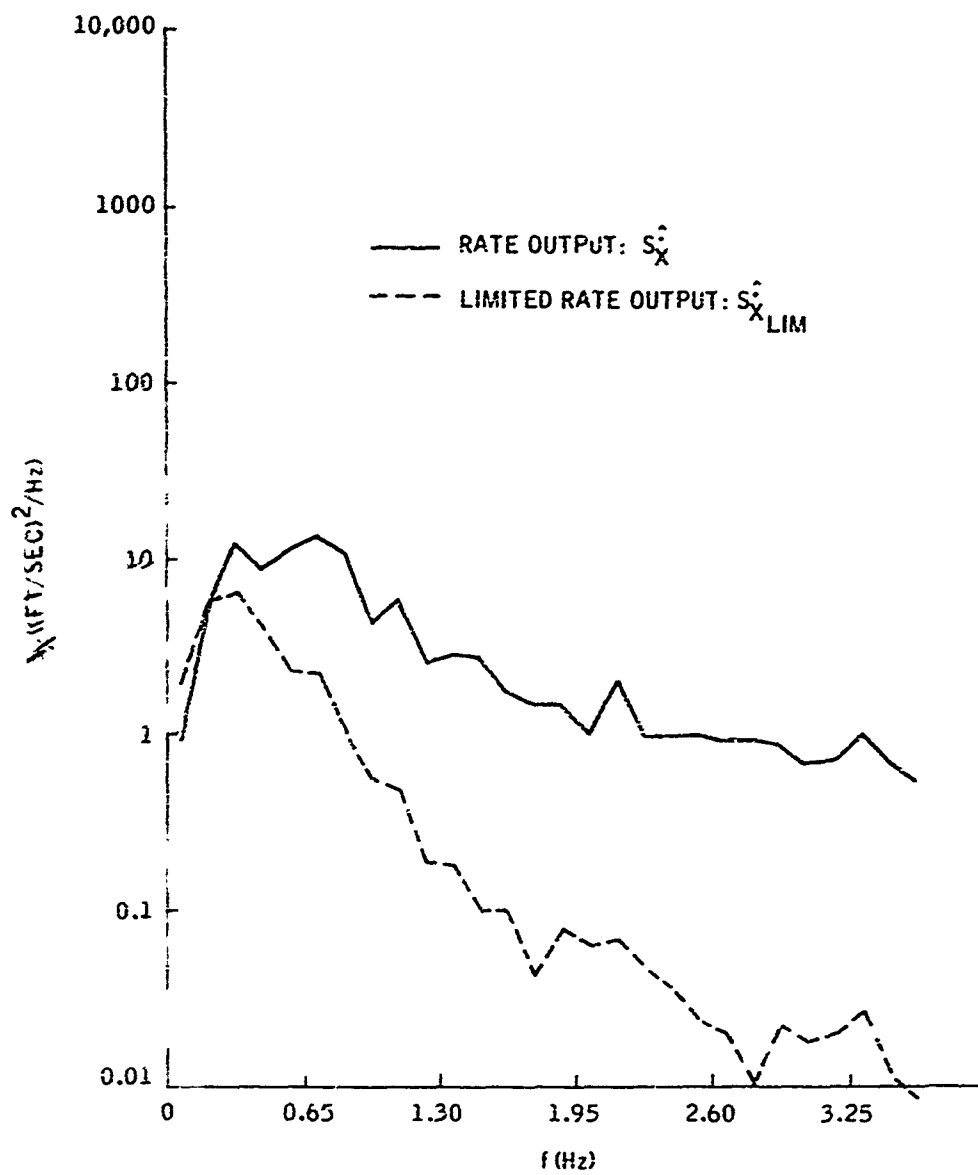
Figure B5. Power Spectral Density of Rate Output and Limited Rate Output of α-β Filter; $\alpha = 0.25$; $\sigma_X = 15$ ft

B 7
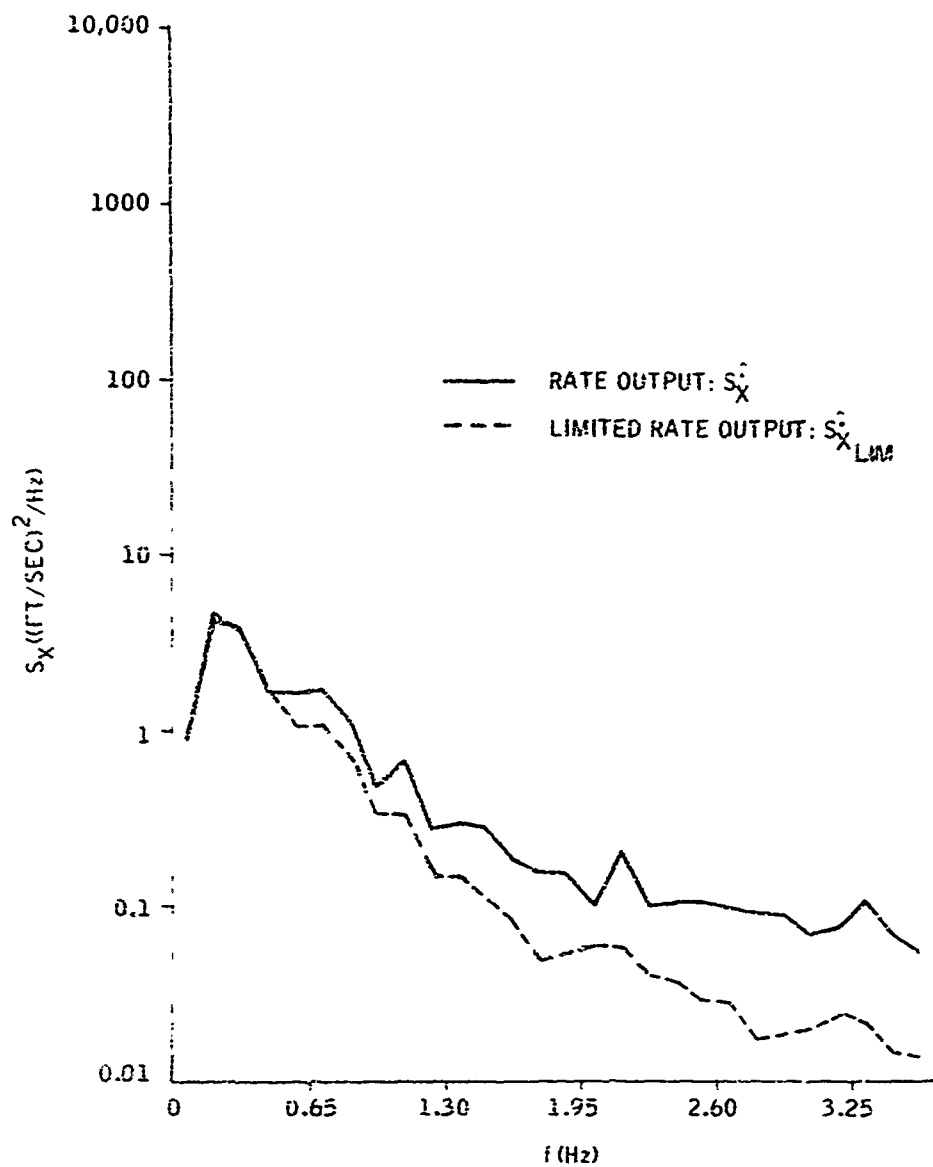
Figure B6. Power Spectral Density of Rate Output and Limited Rate Output of α-β Filter; $\alpha = 0.15$; $\sigma_X = 15$ ft

B8
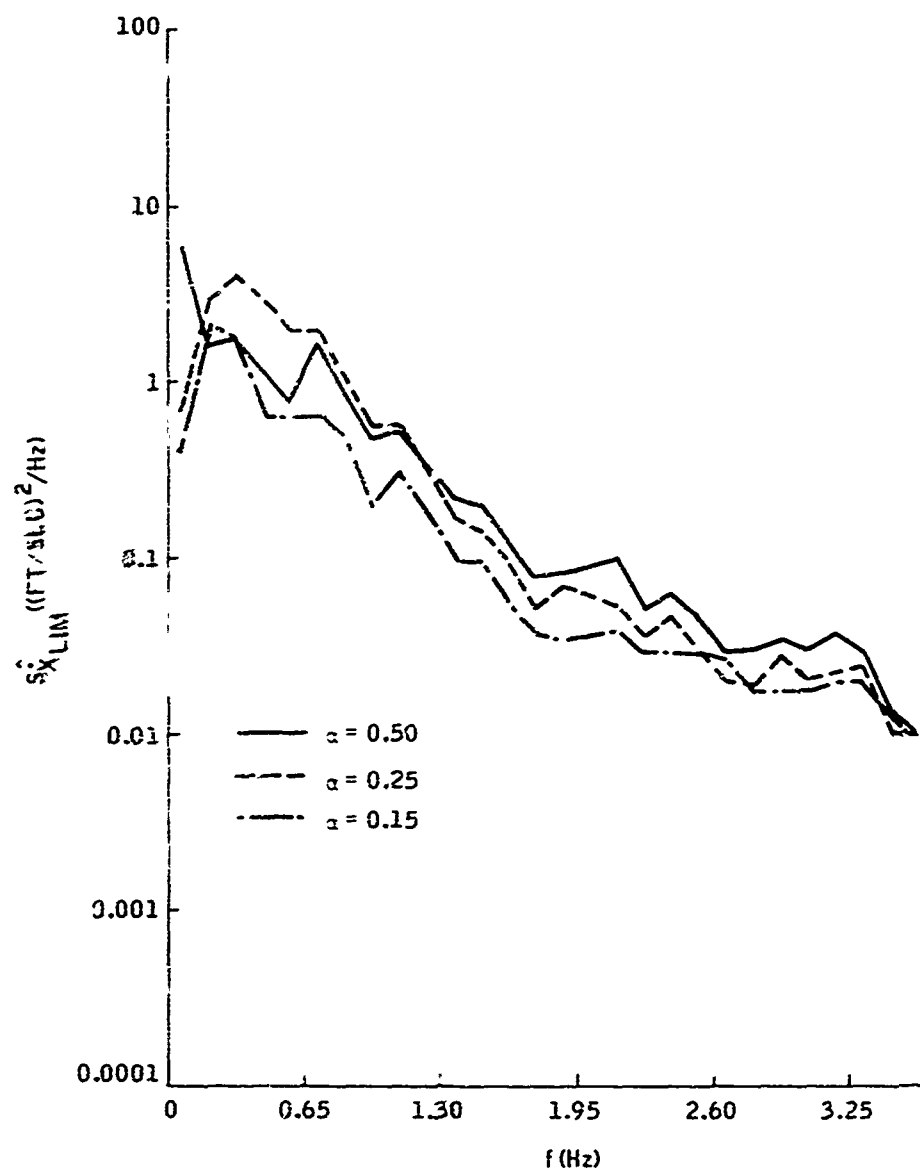
Figure B7. Power Spectral Density of Limited Rate Output of α-β Filter; $\sigma_X = 10$ ft

B9
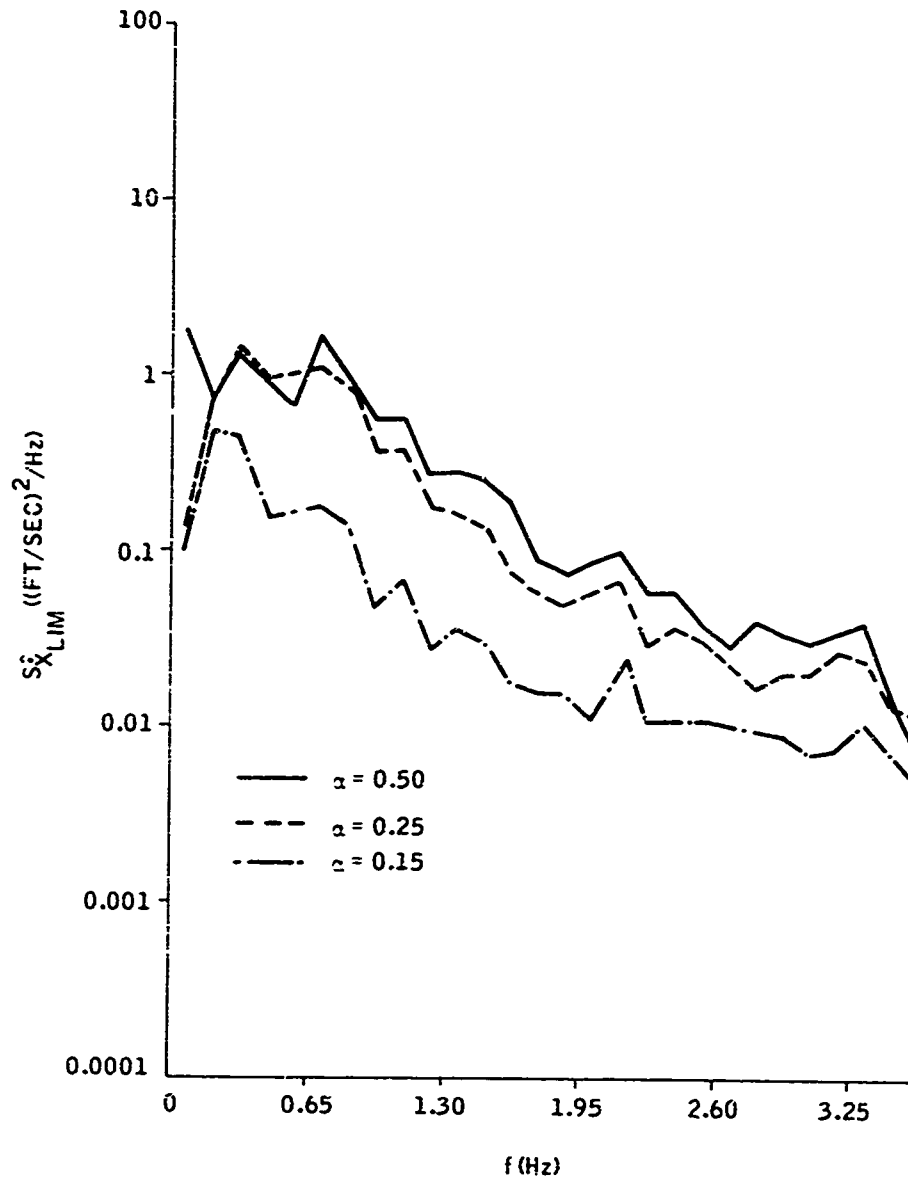
Figure B8. Power Spectral Density of Limited Rate Output of α-β Filter; σ_X = 5 ft
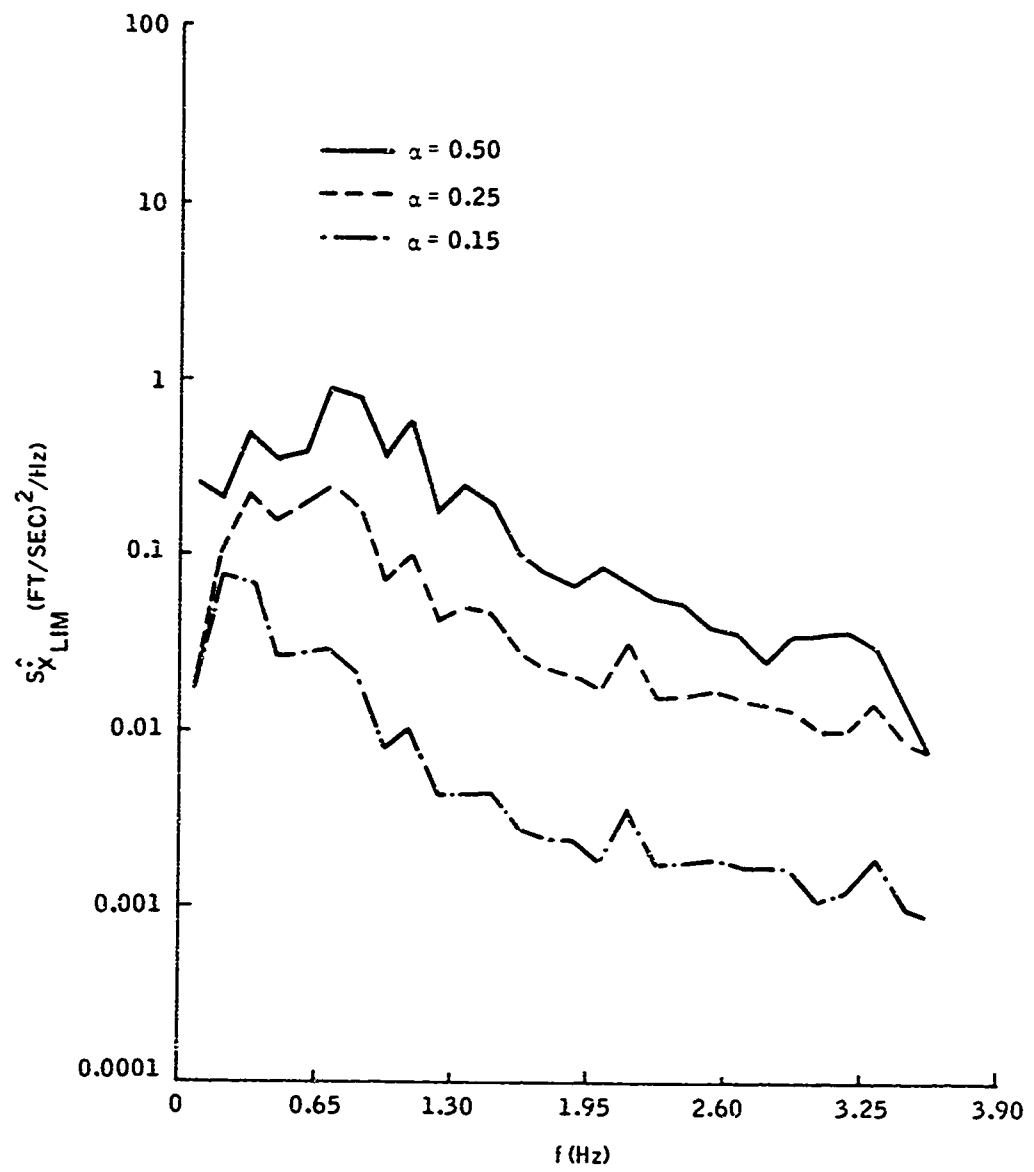
Figure B9. Power Spectral Density of Limited Rate Output of α-β Filter; $\sigma_X = 2$ ft

B11
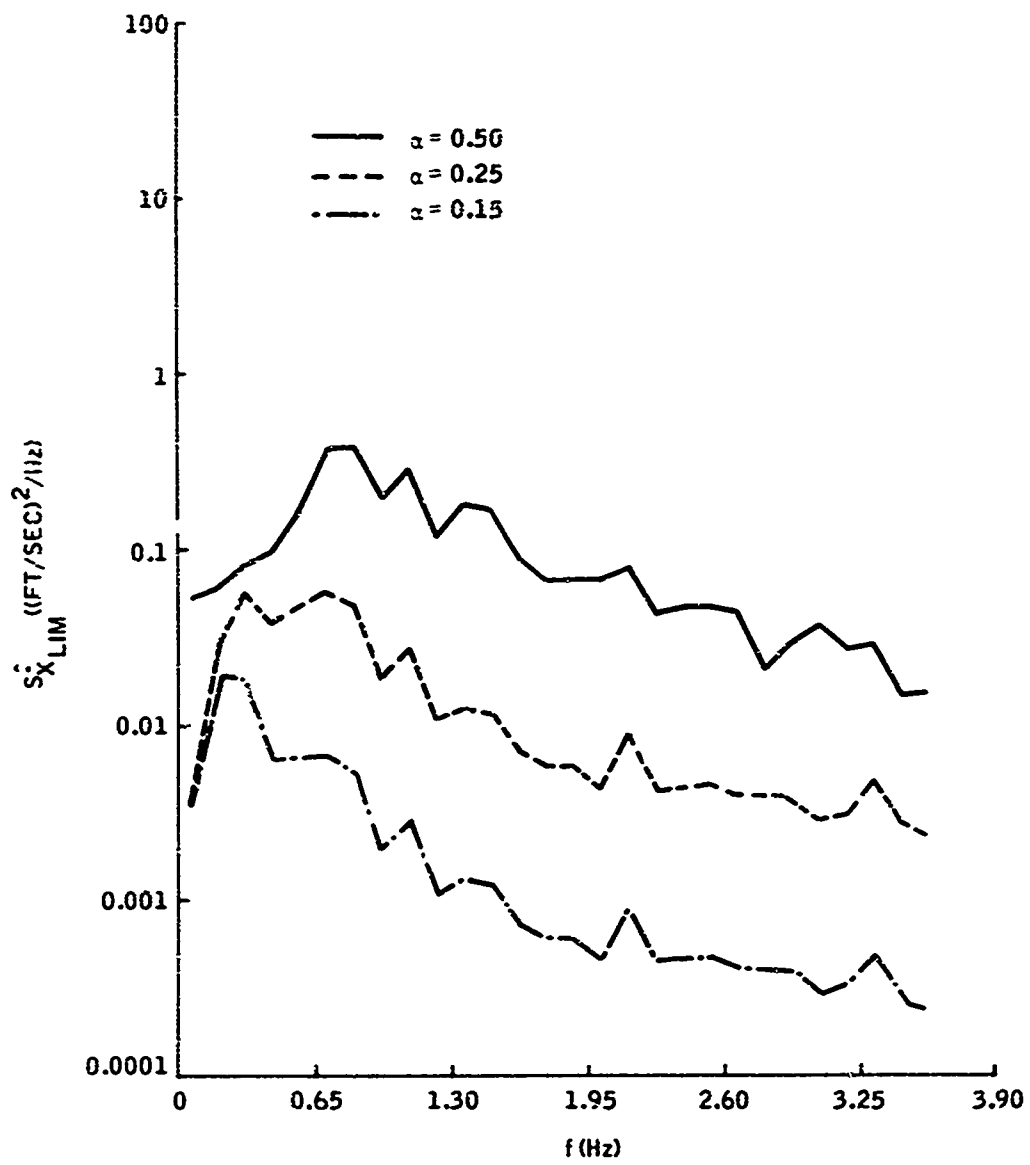
Figure B10. Power Spectral Density of Limited Rate Output of α-β Filter; $\sigma_X = 1$ ft
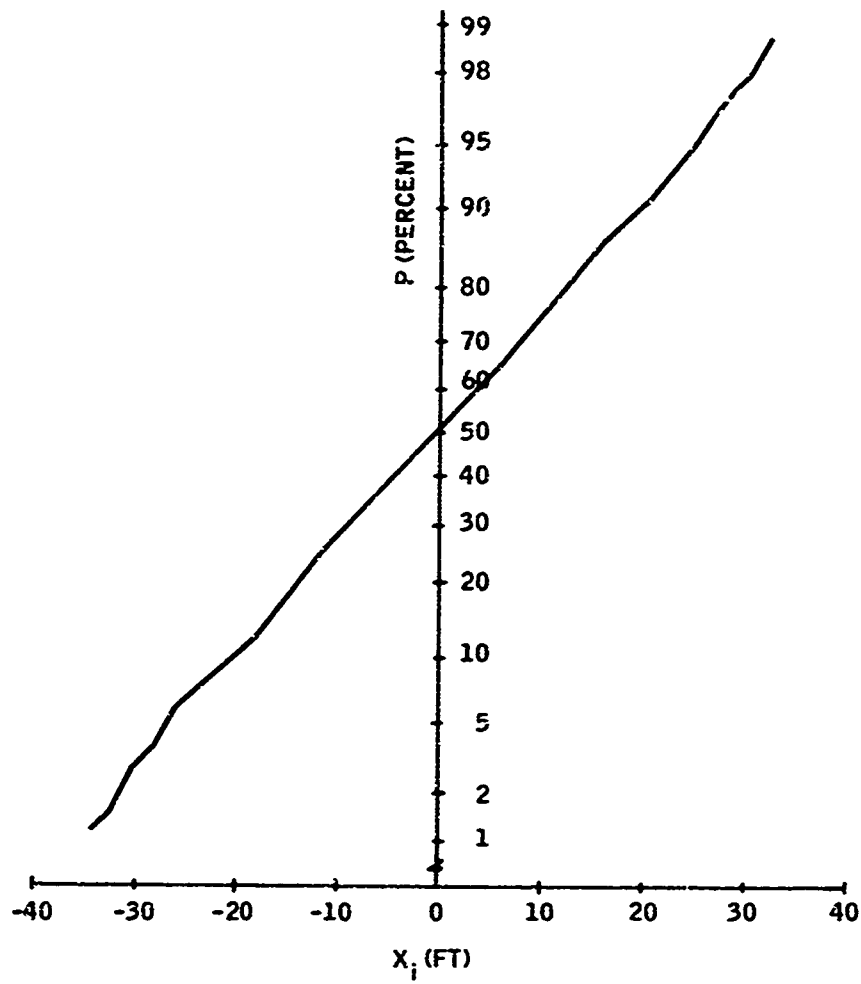
Figure B11. Cumulative Probability Density of Random Noise; $\sigma_X = 15$ ft

B13
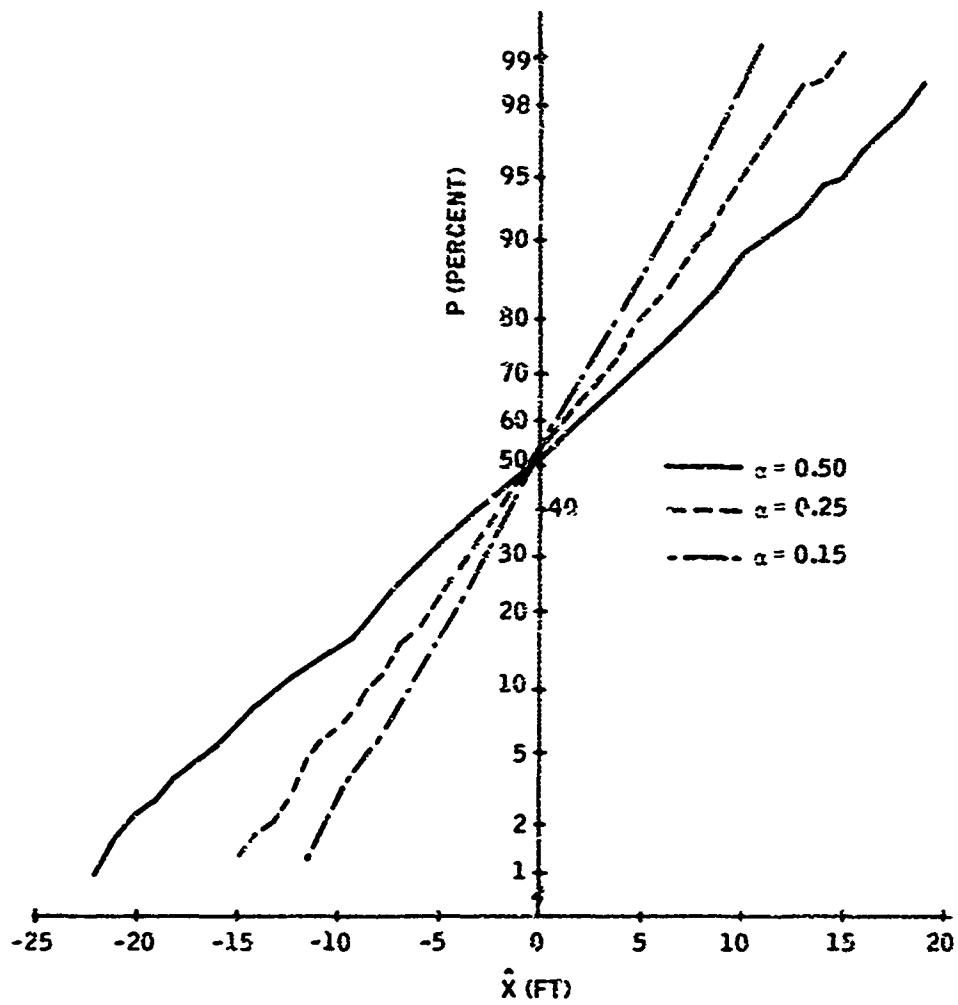
Figure B12. Cumulative Probability Density of Position
Output of α-β Filter; $\sigma_X = 15$ ft

B14
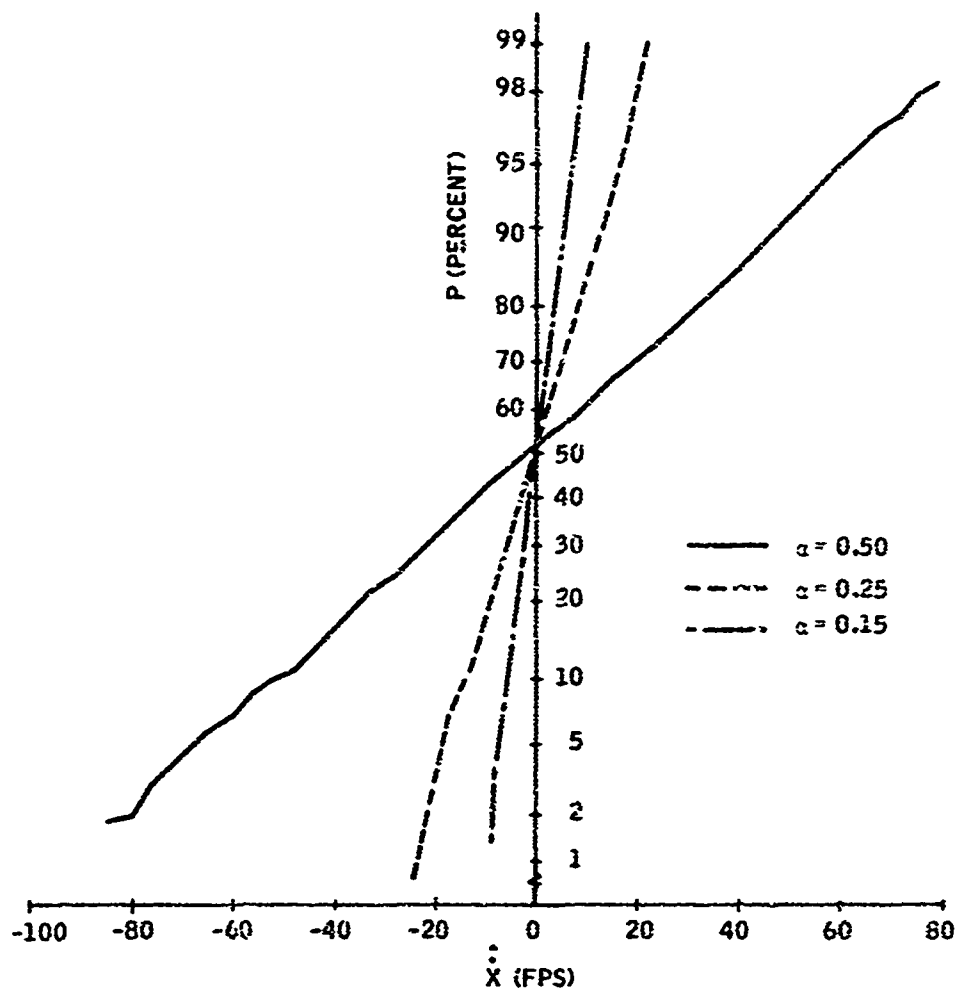
Figure B13. Cumulative Probability Density of Rate Output of α-β Filter; $\sigma_X = 15$ ft

B15
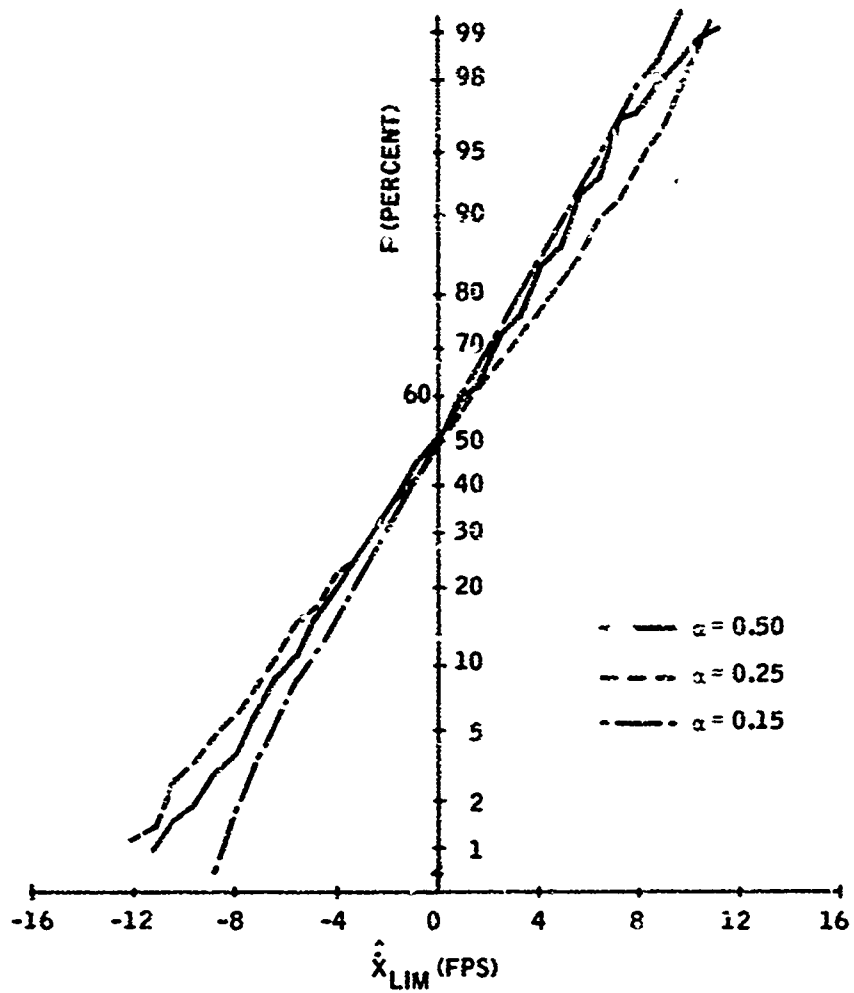
Figure B14. Cumulative Probability Density of Limited Rate Output of $\alpha-\beta$ Filter; σ_X = 15 ft

B16

APPENDIX C

FORMAL SIMULATION DATA
FOR TASK II STUDY
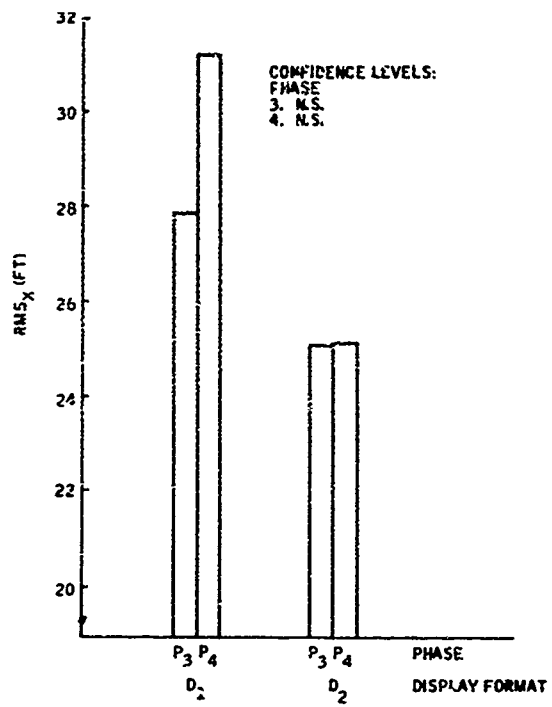
Figure C1. Mean RMS$_X$ Error for Each Display Format and Phase: UH-1 Aircraft

Figure C2. Mean RMS$_Y$ Error for Each Display Format and Phase: UH-1 Aircraft

C1
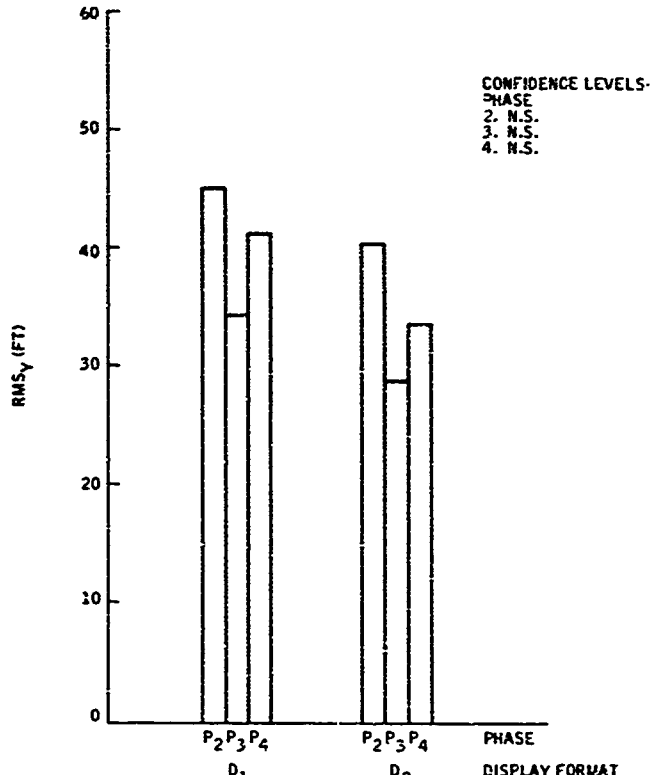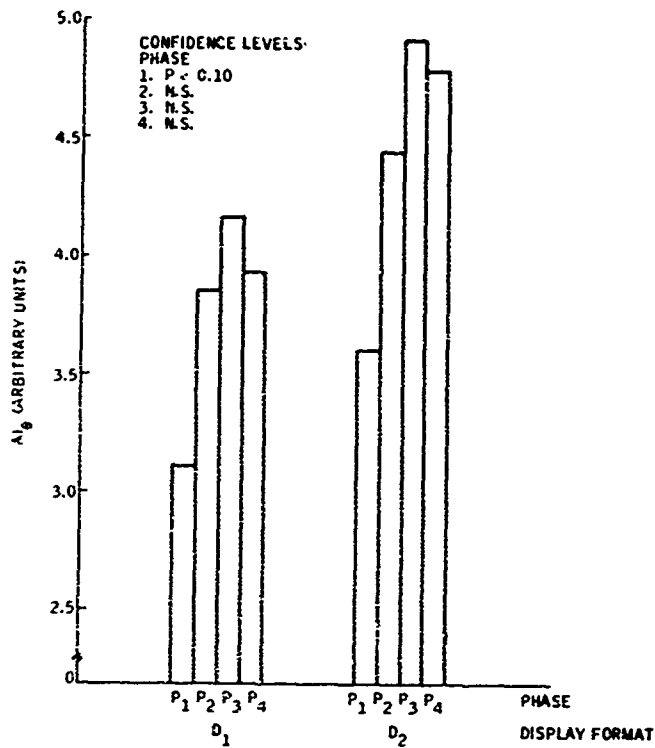
Figure C3. Mean AI_θ for Each Display Format and Phase: UH-1 Display

CONFIDENCE LEVELS:
PHASE
1. P < 0.10
2. N.S.
3. N.S.
4. N.S.

AI_θ (ARBITRARY UNITS)

5.0
4.5
4.0
3.5
3.0
2.5
0

P_1 P_2 P_3 P_4 P_1 P_2 P_3 P_4 PHASE
D_1 D_2 DISPLAY FORMAT

Figure C4. Mean AI_ϕ for Each Display Format and Phase: UH-1 Aircraft

CONFIDENCE LEVELS:
PHASE
1. P < 0.10
2. P < 0.10
3. N.S.
4. N.S.

AI_ϕ (ARBITRARY UNITS)

16
15
14
13
12
11
0

P_1 P_2 P_3 P_4 P_1 P_2 P_3 P_4 PHASE
D_1 D_2 DISPLAY FORMAT

CONFIDENCE LEVELS:
PHASE
2. P < 0.10
3. N.S.
4. N.S.

RMS$_Y$ (FT)

60
50
40
30
20
10
0

P$_2$ P$_3$ P$_4$ P$_2$ P$_3$ P$_4$ PHASE

A$_1$ A$_2$ APPROACH ANGLE
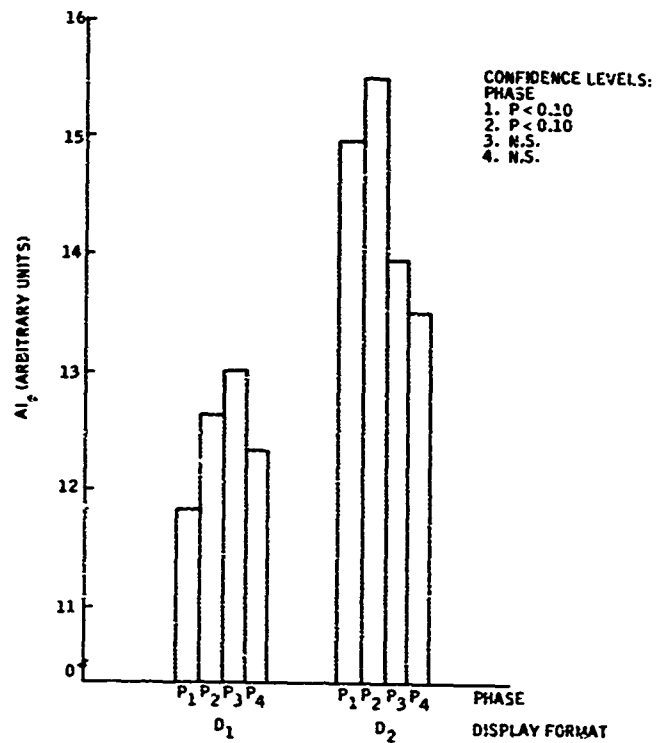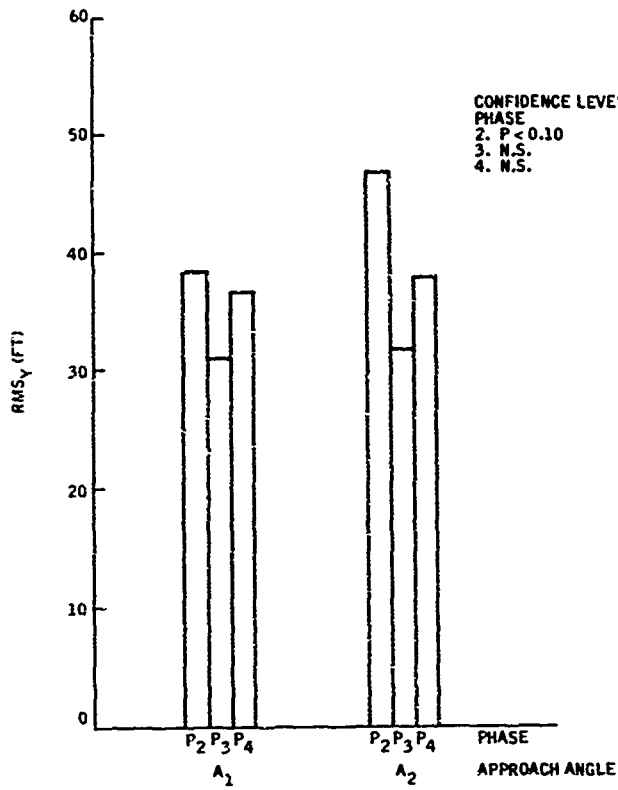
Figure C5. Mean RMS$_Y$ Error for
Each Approach Angle and
Phase: UH-1 Aircraft

Figure C6. Mean RMS$_Z$ Error for
Each Approach Angle
and Phase: UH-1 Air-
craft

CONFIDENCE LEVELS:
PHASE
1. P < 0.10
2. P < 0.10
3. N.S.

RMS$_Z$ (FT)

50
40
30
20
10
0

P$_1$ P$_2$ P$_3$ P$_1$ P$_2$ P$_3$ PHASE

A$_1$ A$_2$ APPROACH ANGLE

C3
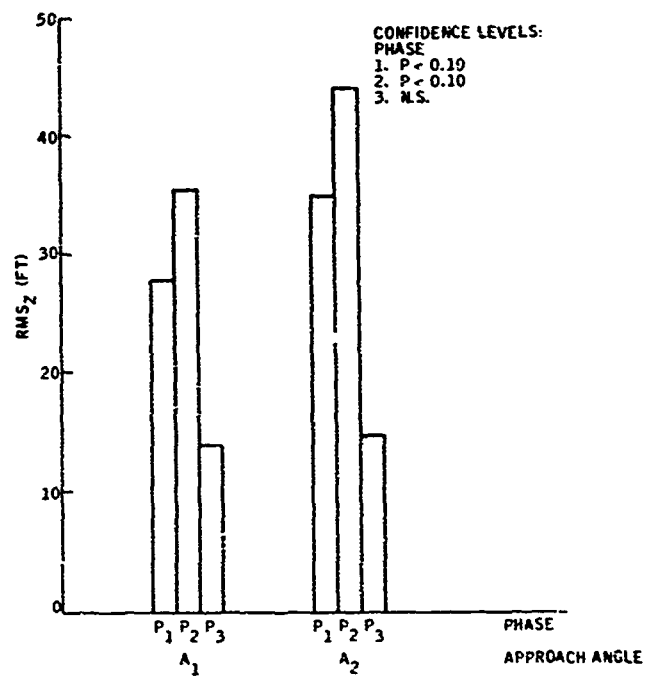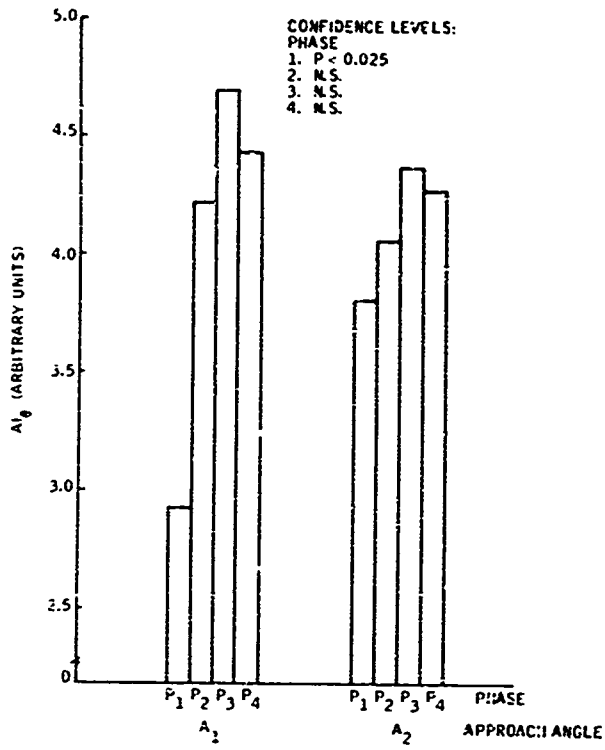
Figure C7.   Mean AI_θ for Each Approach
Angle and Phase: UH-1 Air-
craft

Figure C8.   Mean AI_{COL} for Each
Approach Angle and
Phase: UH-1 Aircraft

C4
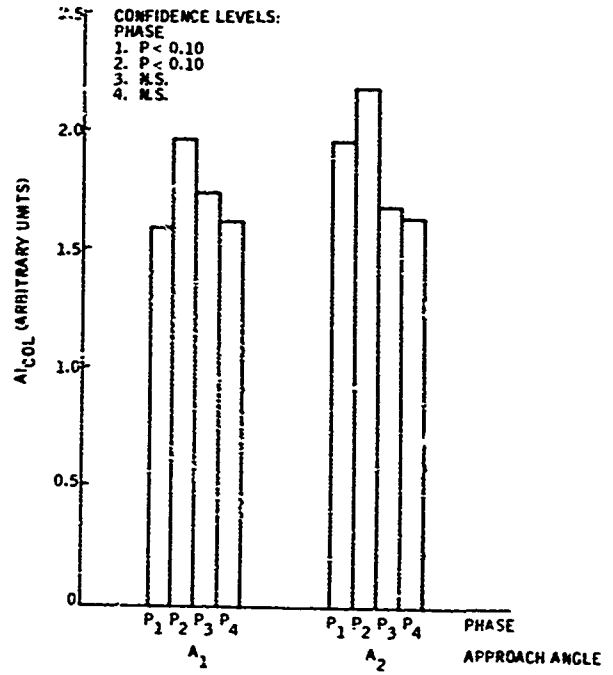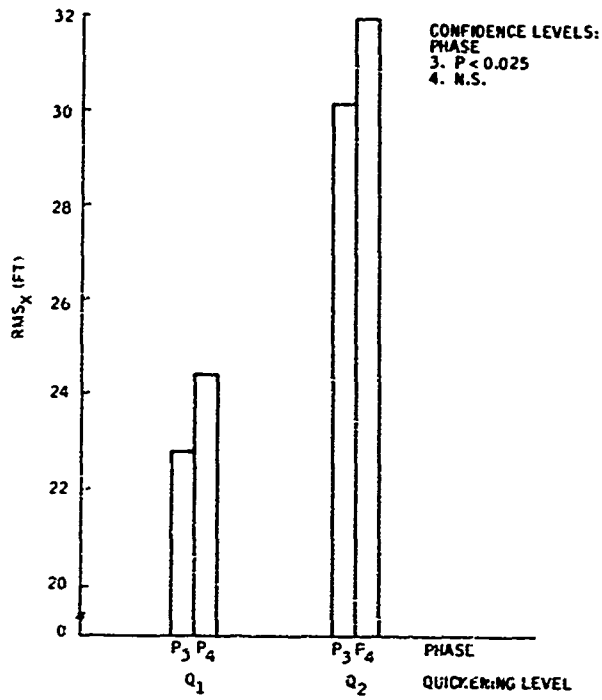
Figure C9. Mean RMS$_X$ Error for Each Quickening Level and Phase: UH-1 Aircraft

CONFIDENCE LEVELS:
PHASE
3. P < 0.025
4. N.S.

Figure C10. Mean RMS$_Y$ Error for Each Quickening Level and Phase: UH-1 Aircraft

CONFIDENCE LEVELS:
PHASE
2. N.S.
3. P < 0.10
4. N.S.

C5
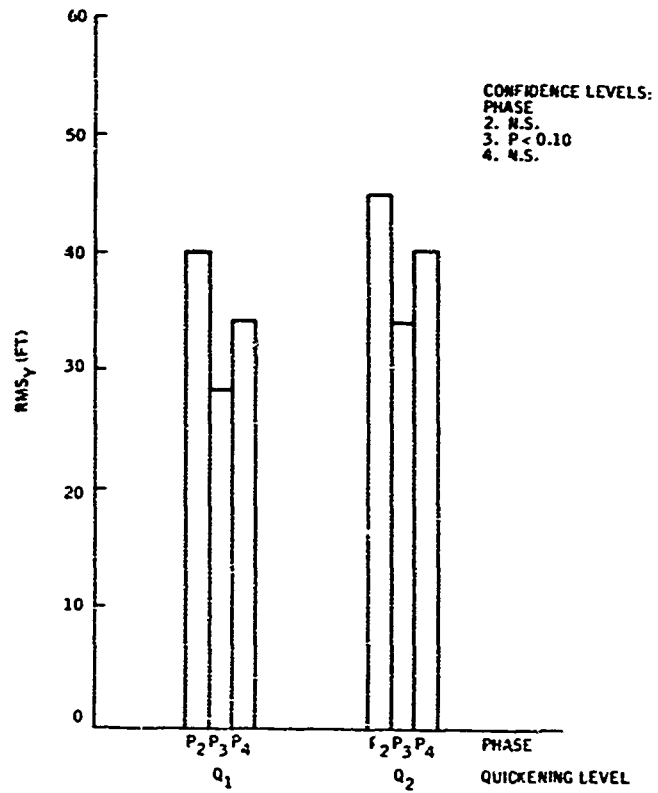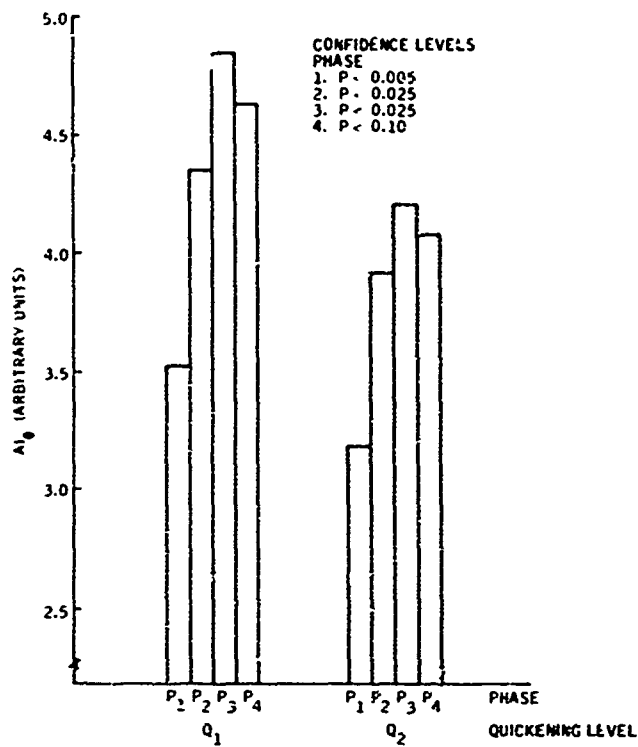
Figure C11. Mean AI_θ for Each Quickening Level and Phase: UH-1 Aircraft

Figure C12. Mean AI_ϕ for Each Quickening Level and Phase: UH-1 Aircraft

C6
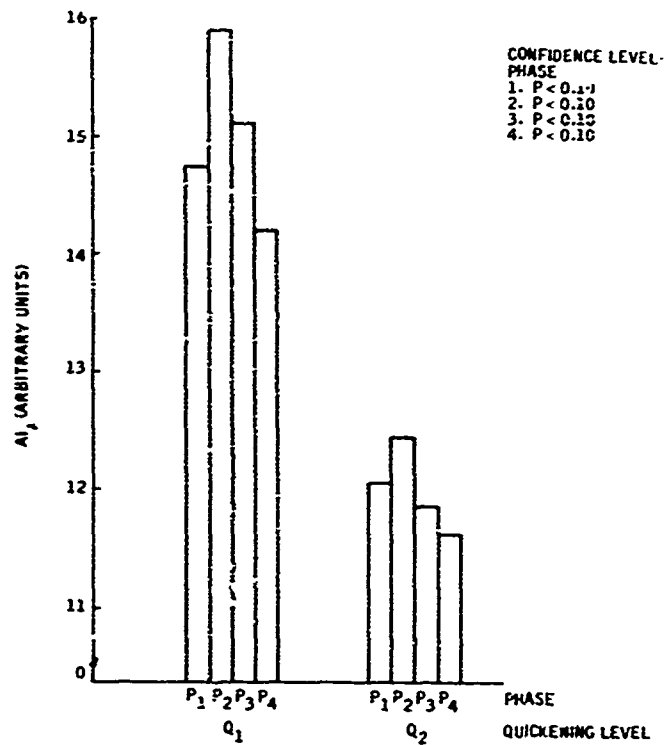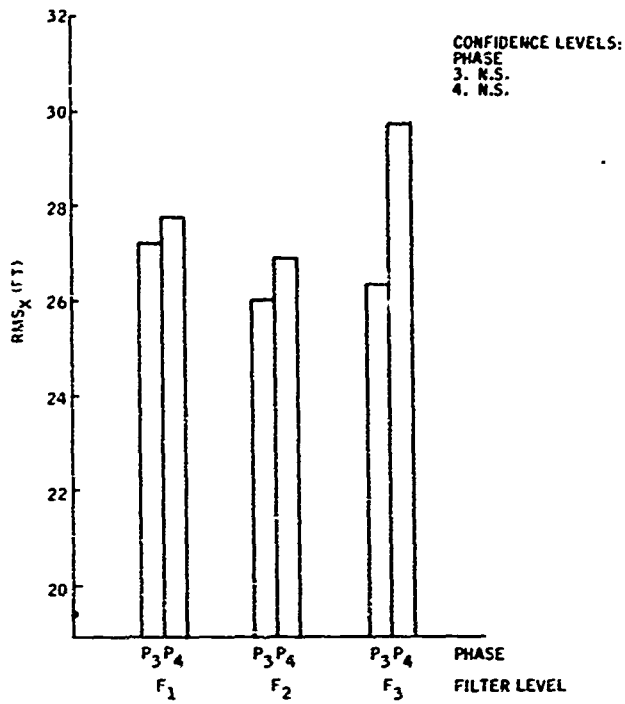
Figure C13. Mean RMS_X Error for Each Filter Level and Phase: UH-1 Aircraft

Figure C14. Mean RMS_Y Error for Each Filter Level and Phase: UH-1 Aircraft

C7
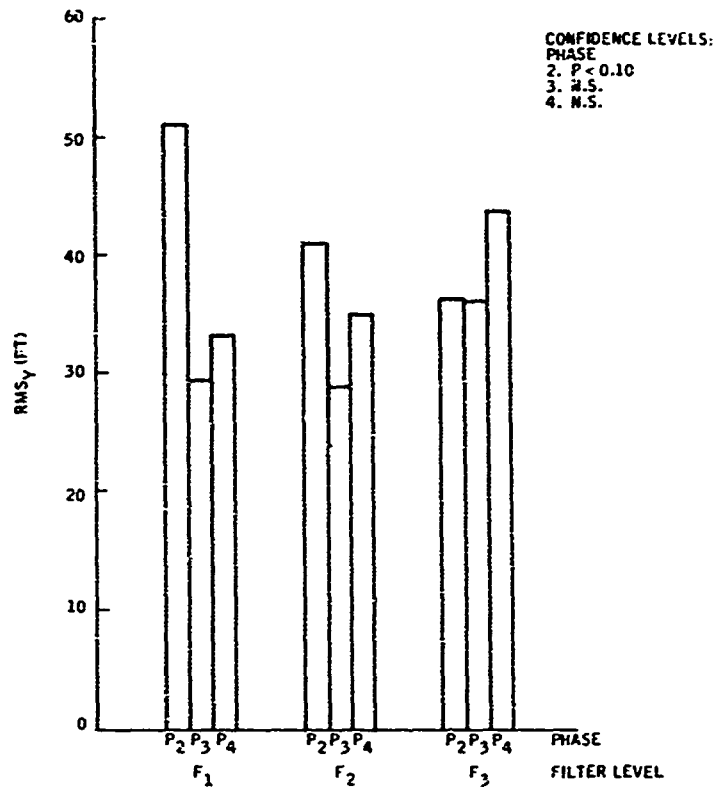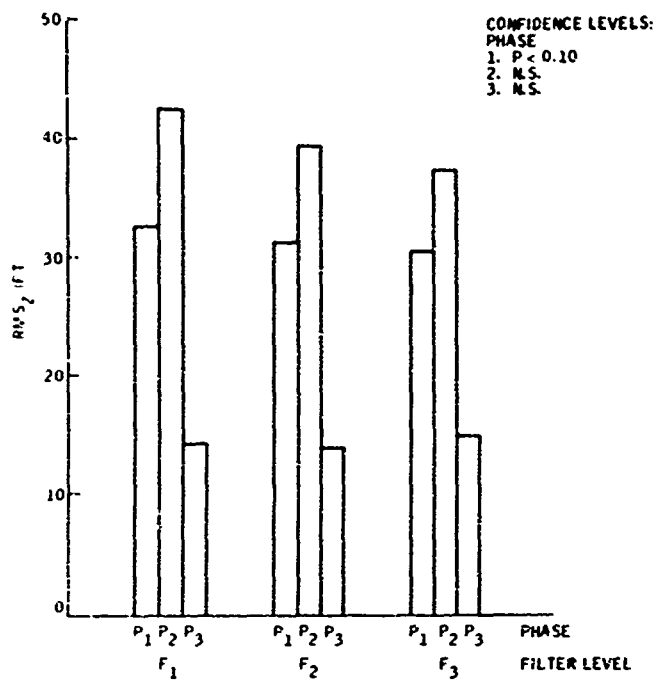
Figure C15. Mean RMS_Z Error for Each Filter Level and Phase: UH-1 Aircraft

Figure C16. Mean RMS_Y Error for Each Noise Level and Phase: UH-1 Aircraft

C8
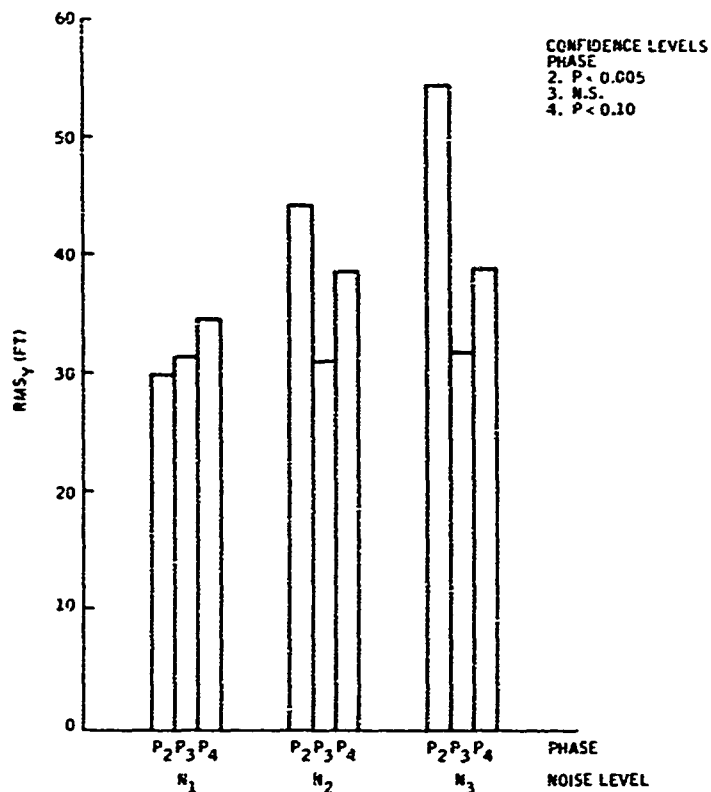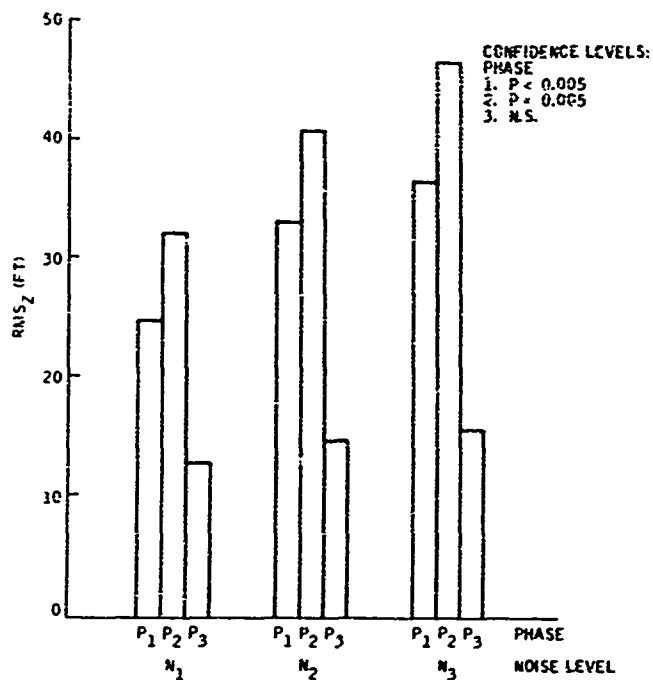
Figure C17. Mean RMS_Z Error for Each Noise Level and Phase: UH-1 Aircraft

Figure C18. Mean AI_θ for Each Noise Level and Phase: UH-1 Aircraft

C9
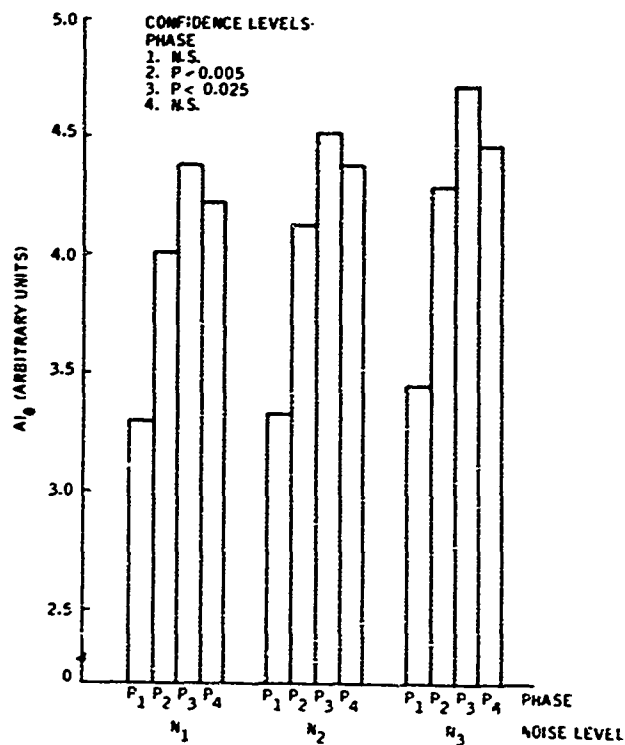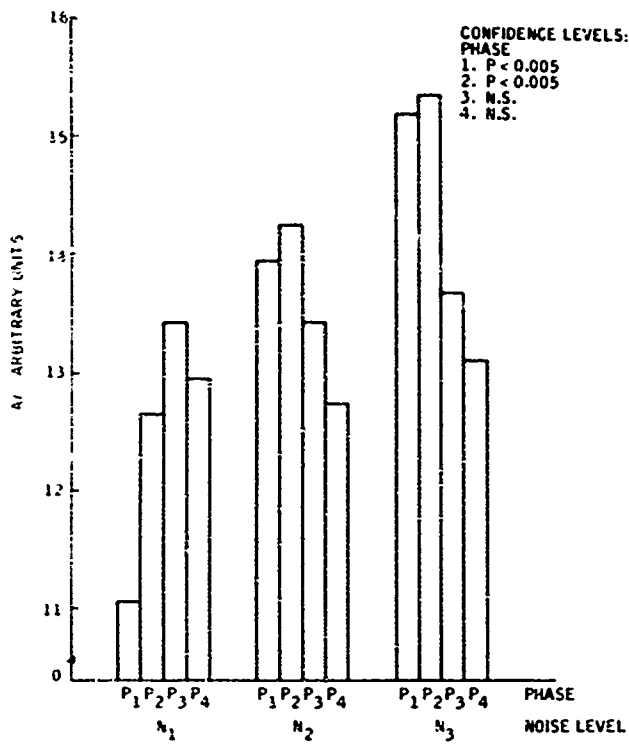
Figure C19. Mean AI_ϕ for Each Noise Level and Phase: UH-1 Aircraft

Figure C20. Mean RMS_Z Error for Each Display Format and Approach Angle; Phase P_2; UH-1 Aircraft

C10
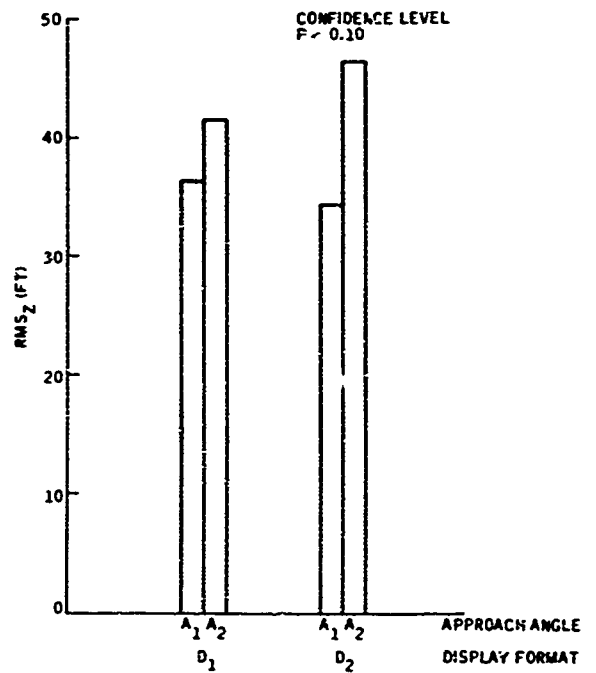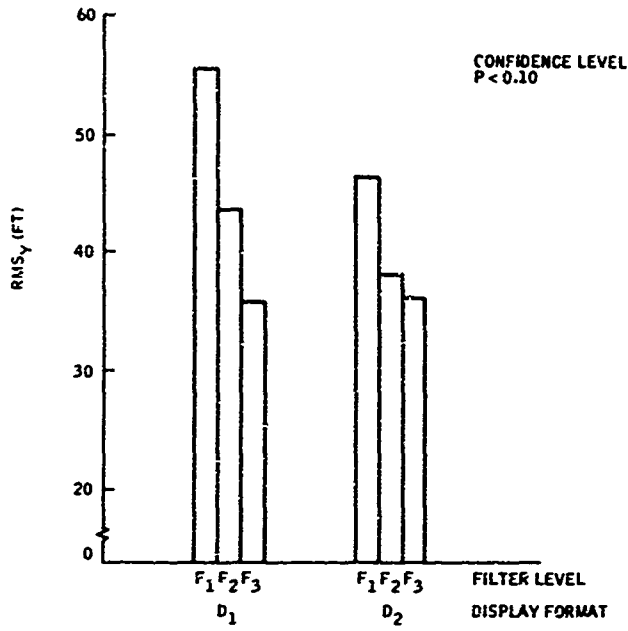
Figure C21. Mean RMS$_Y$ Error for Each Display Format and Filter Level: Phase P$_2$; UH-1 Aircraft

Figure C22. Mean AI$_\phi$ for Each Display Format and Noise Level: Phase P$_1$; UH-1 Aircraft

C11
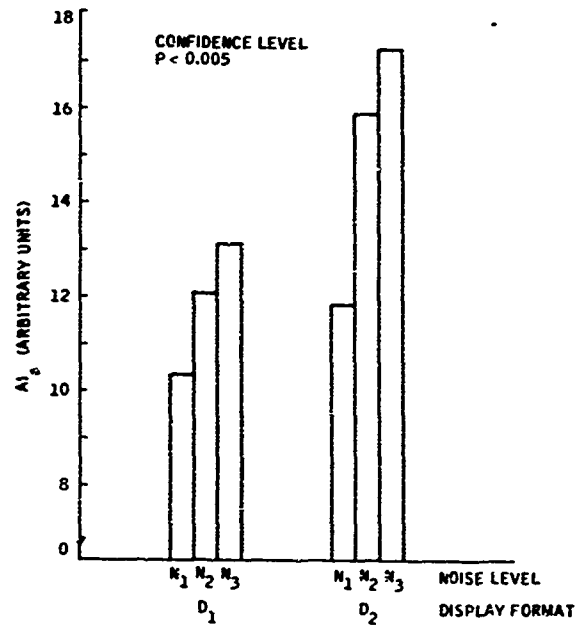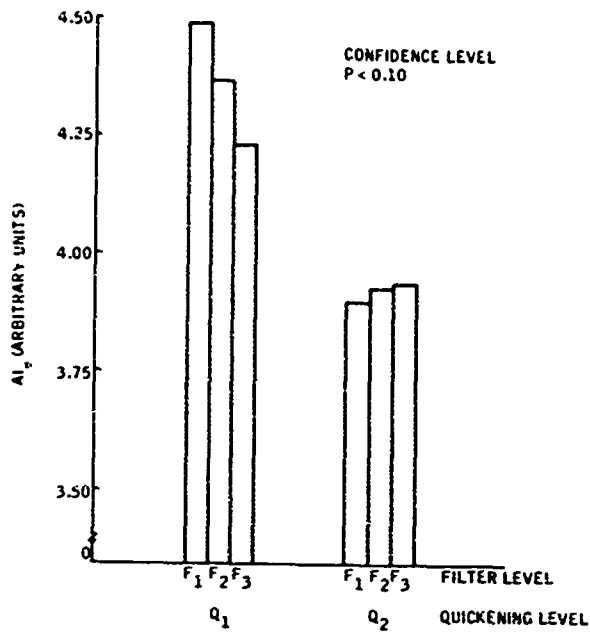
Figure C23. Mean AI_θ for Each
Quickening Level and
Filter Level: Phase P_2;
UH-1 Aircraft

Figure C24. Mean RMS_X Error for
Each Quickening Level
and Noise Level: Phase
P_4; UH-1 Aircraft

C12

CONFIDENCE LEVEL
P < 0.10
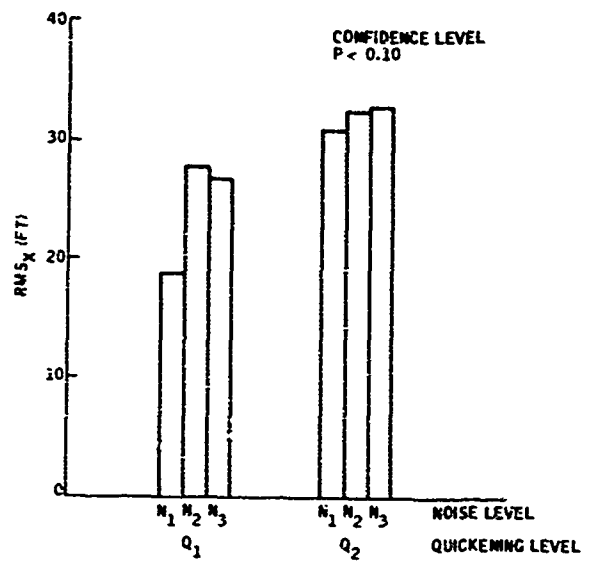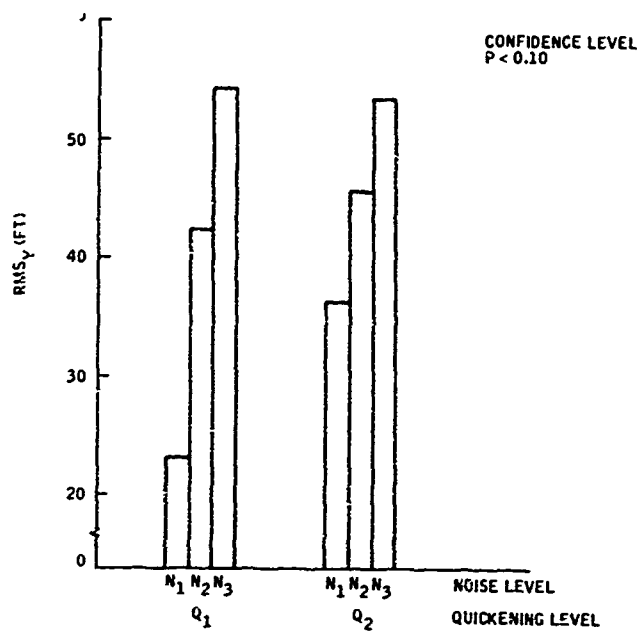
Figure C25.   Mean RMS_Y Error for
Each Quickening Level
and Noise Level: Phase
P_2; UH-1 Aircraft

Figure C26.   Mean RMS_Z Error for
Each Quickening Level
and Noise Level: Phase
P_2; UH-1 Aircraft
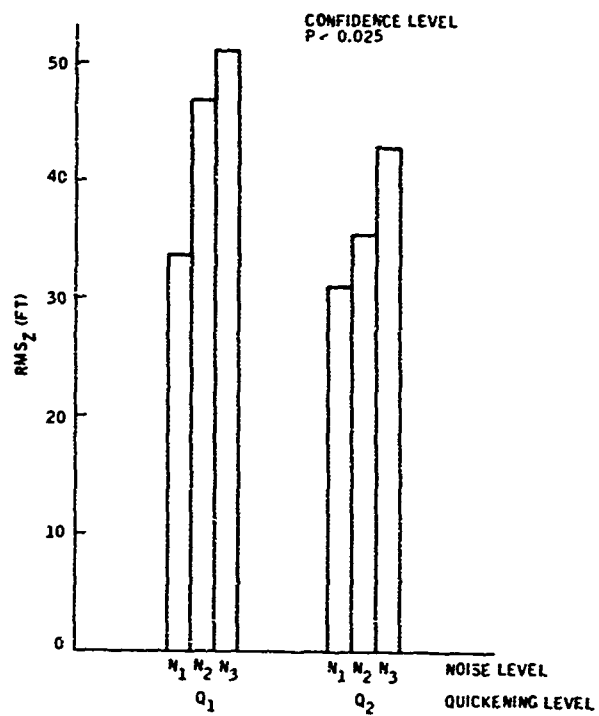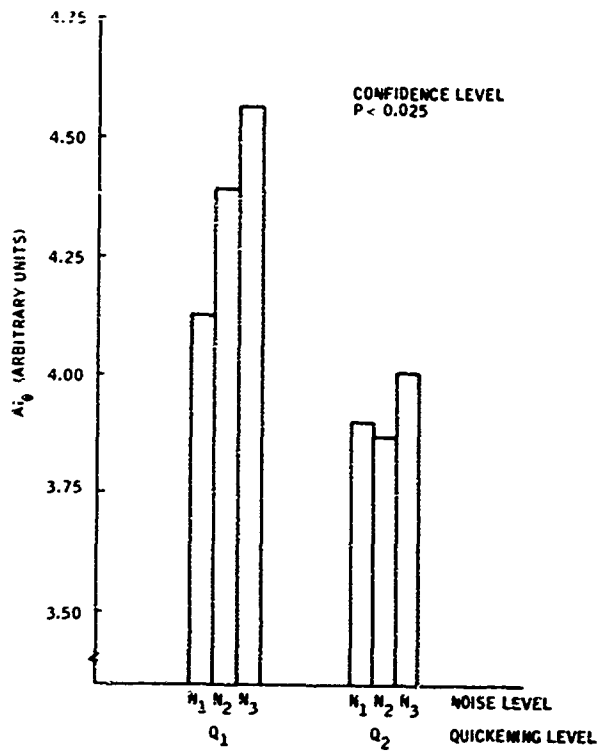
CONFIDENCE LEVEL
P < 0.025

C13

CONFIDENCE LEVEL
P < 0.025

Figure C27. Mean AI_θ for Each Quickening Level and Noise Level: Phase P_2; UH-1 Aircraft

CONFIDENCE LEVEL
P < 0.005

Figure C28. Mean AI_ϕ for Each Quickening Level and Noise Level: Phase P_2; UH-1 Aircraft

C14
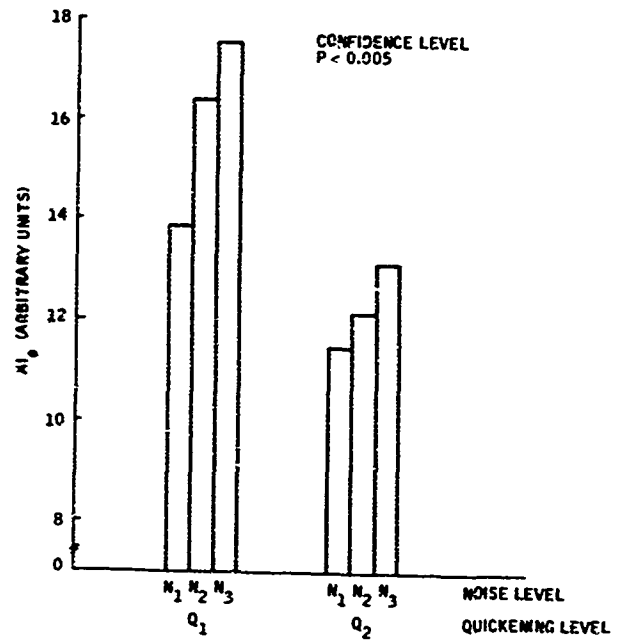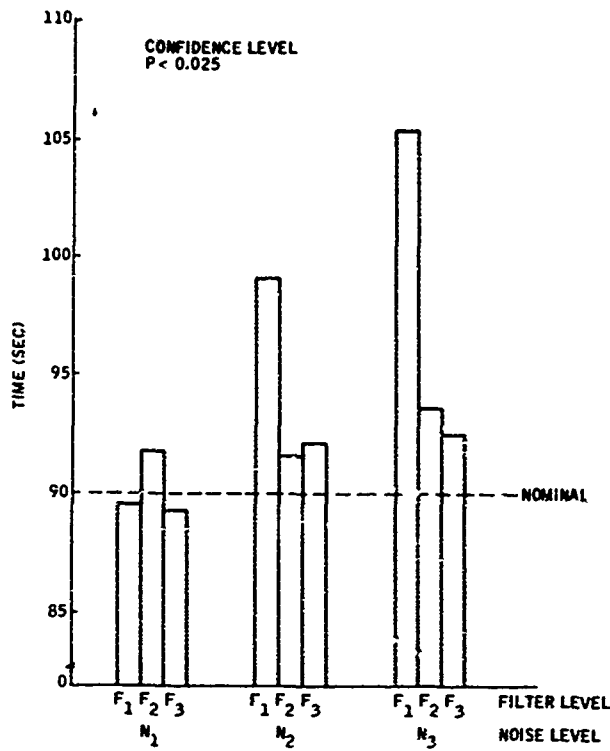
Figure C29.   Mean Time for Each Noise
              Level and Filter Level:
              Phase P_2; UH-1 Aircraft

Figure C30.   Mean RMS_X Error for
              Each Noise Level and
              Filter Level: Phase P_4;
              UH-1 Aircraft

C15
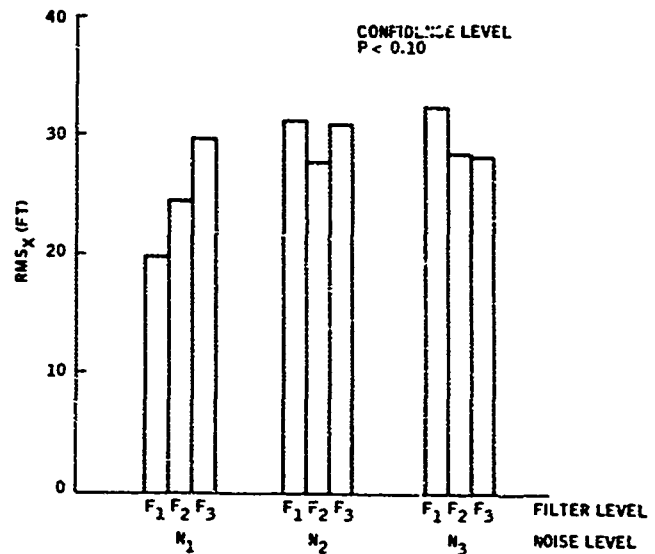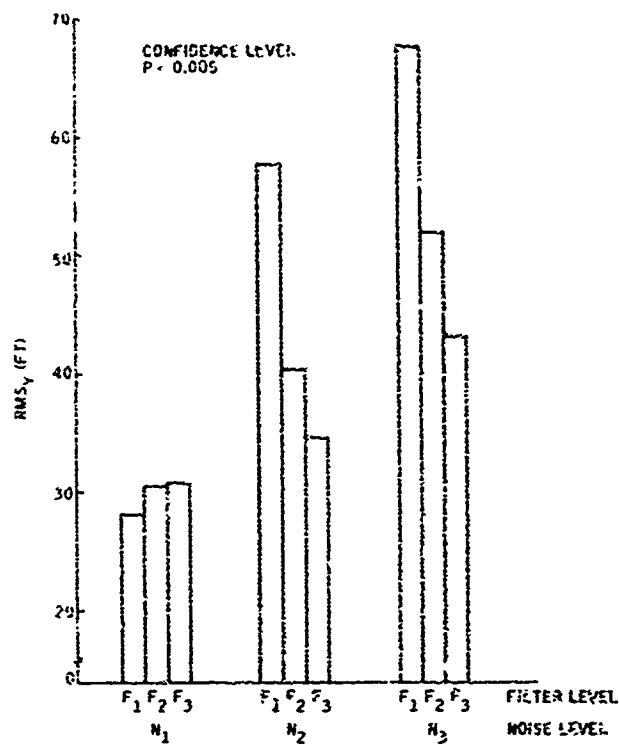
Figure C31. Mean RMS_Y Error for Each Noise Level and Filter Level; Phase P_2; UH-1 Aircraft

Figure C32. Mean RMS_Z Error for Each Noise Level and Filter Level; Phase P_2; UH-1 Aircraft

C16
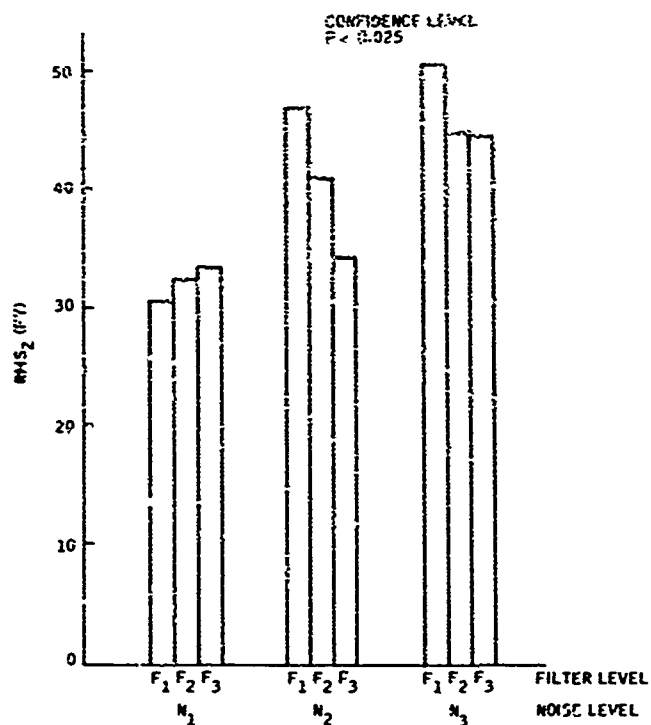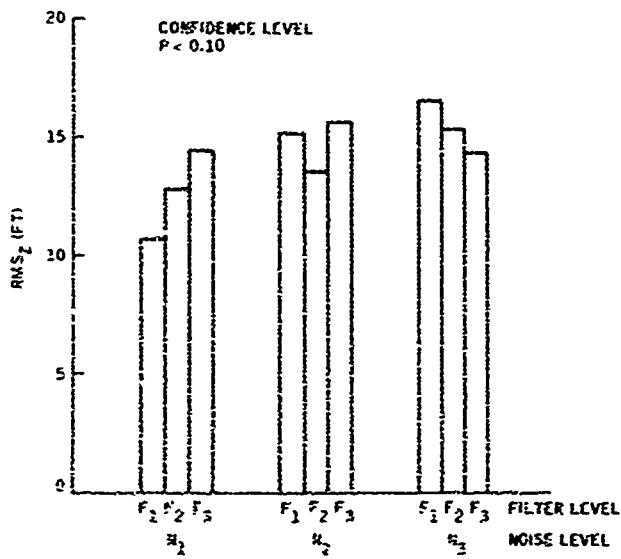
Figure C33. Mean RMS$_Z$ Error for Each Noise Level and Filter Level: Phase P$_3$; UH-1 Aircraft

C17
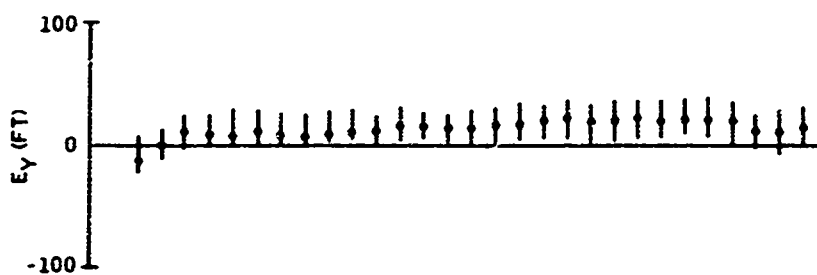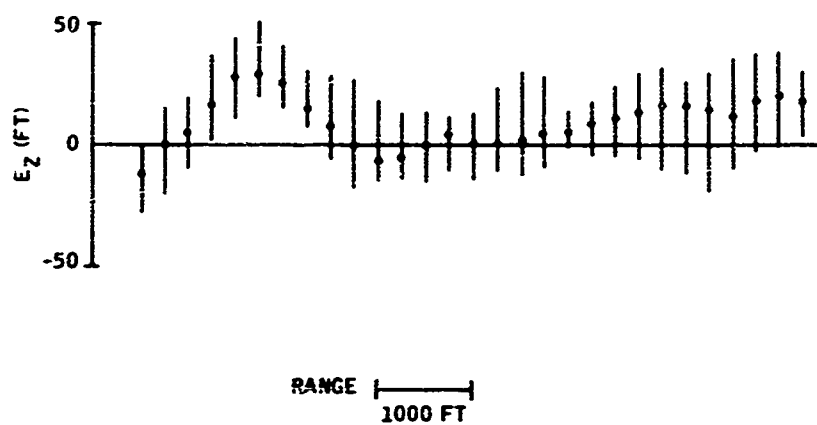
Figure C34. Final Approach Median and ±34th-Percentile
Data at 250-ft Intervals: UH-1 Aircraft
(1 of 6)

C18
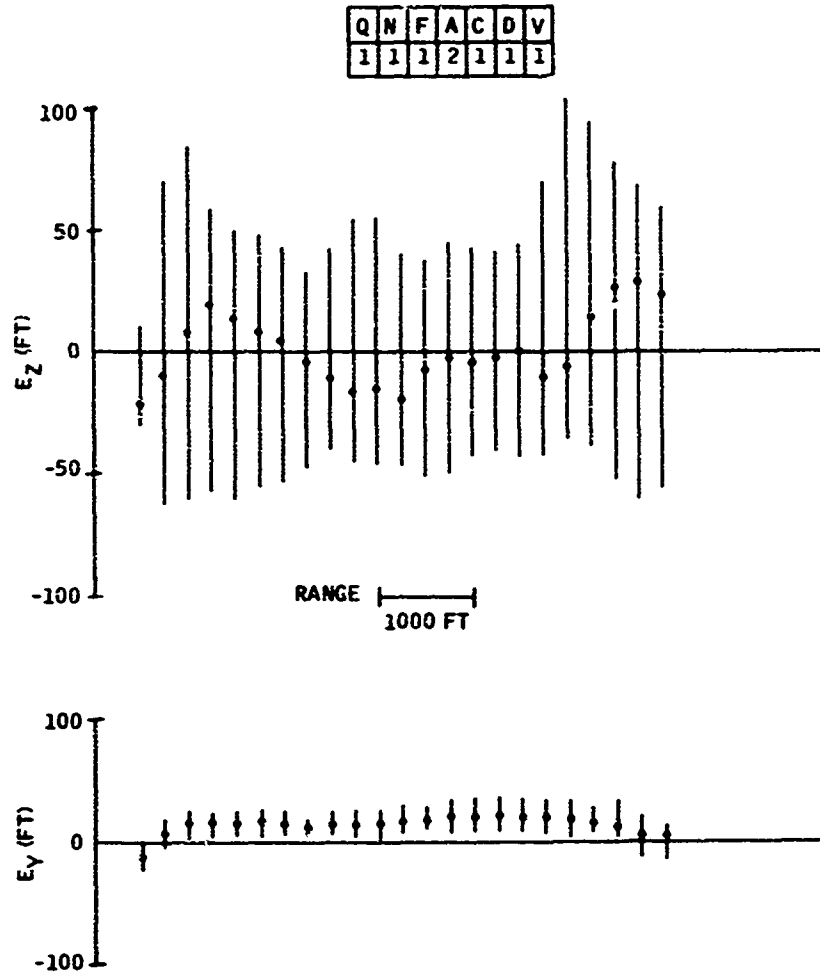
Figure C35. Final Approach Median and ±34th-Percentile
Data at 250-ft Intervals: UH-1 Aircraft
(2 of 6)

C19
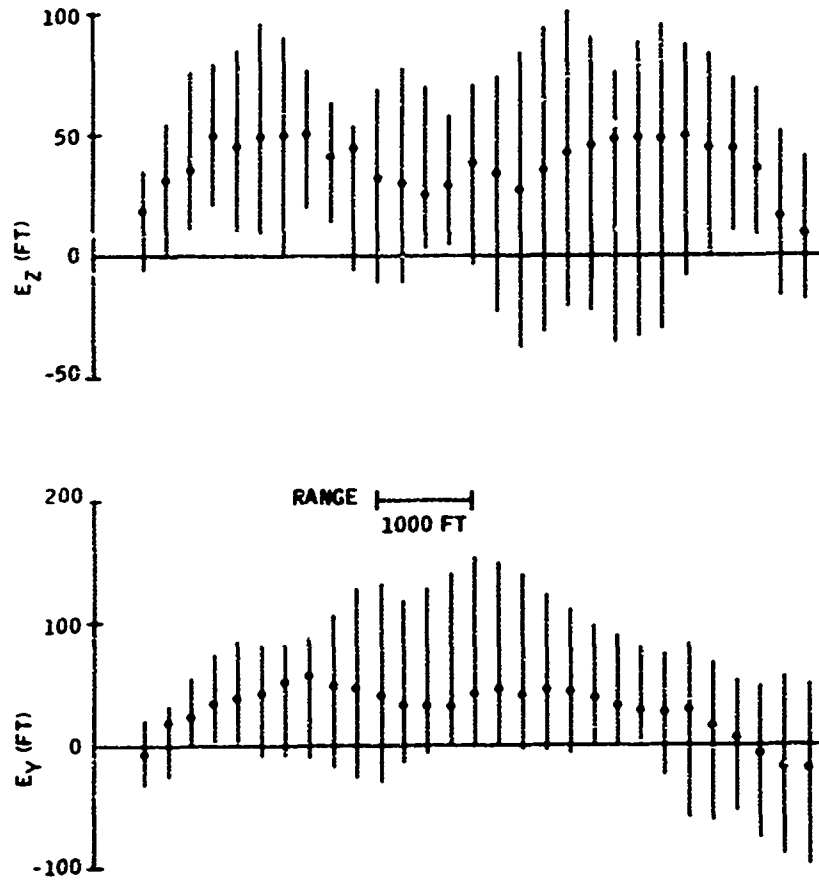
Figure C36.   Final Approach Median and ±34th-Percentile
Data at 250-ft Intervals: UH-1 Aircraft
(3 of 6)

C20
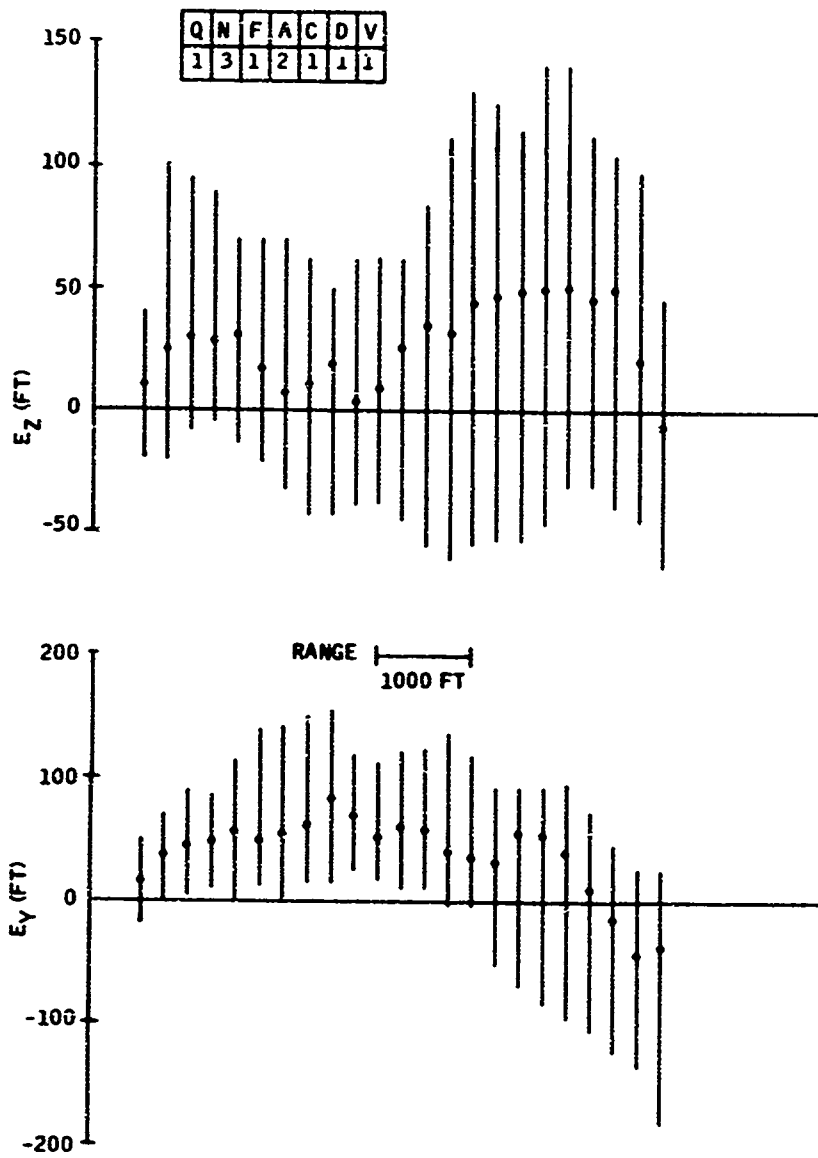
Figure C37.   Final Approach Median and ±34-Percentile
Data at 250-ft Intervals: UH-1 Aircraft
(4 of 6)
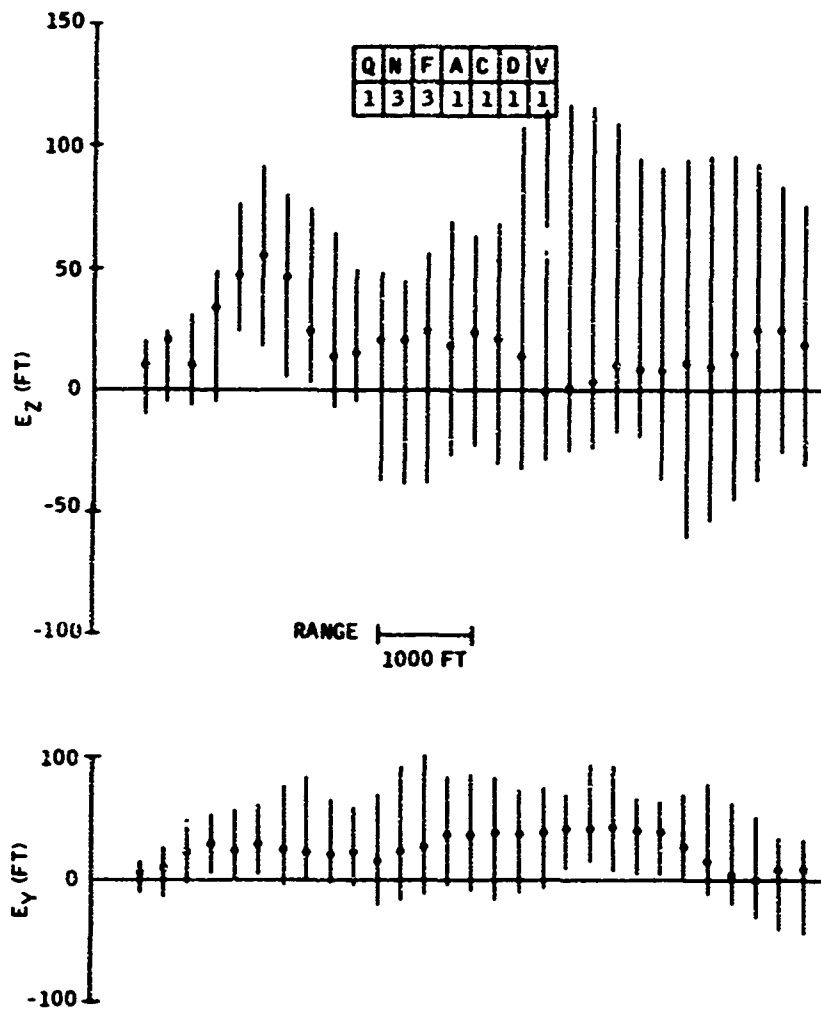
Figure C38. Final Approach Median and ±34th-Percentile
Data at 250-ft Intervals: UH-1 Aircraft
(5 of 6)
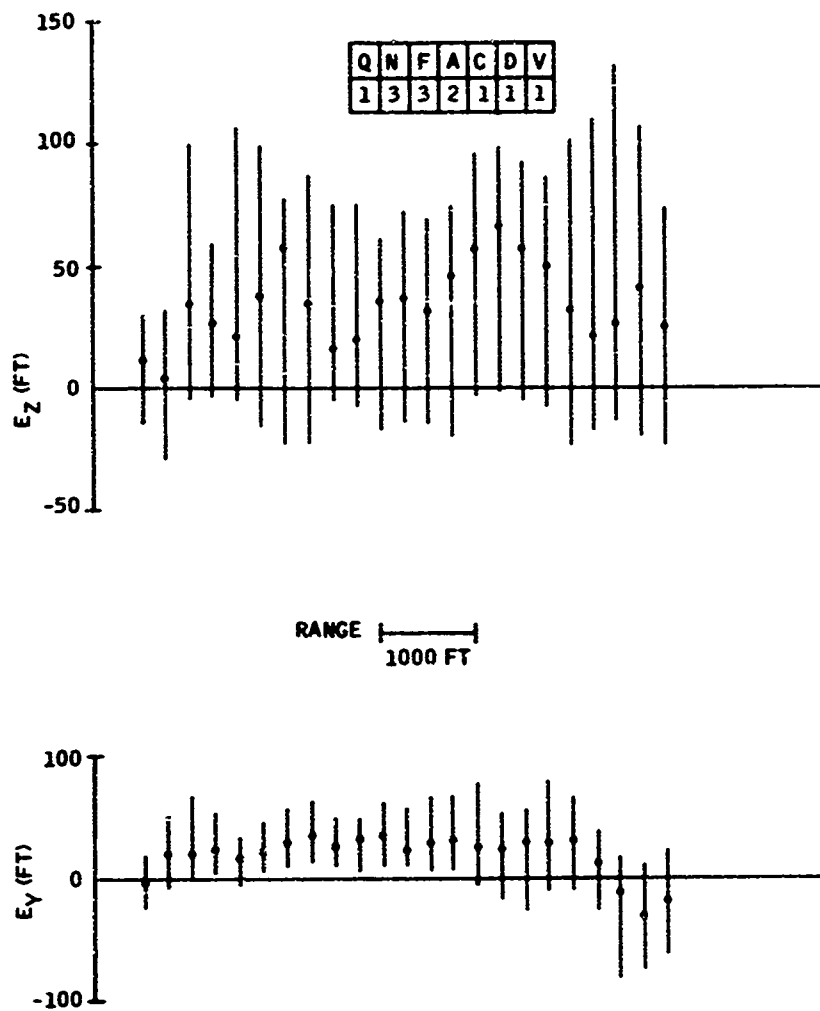
Figure C39. Final Approach Median and ±34th-Percentile
Data at 250-ft Intervals: UH-1 Aircraft
(6 of 6)

C23
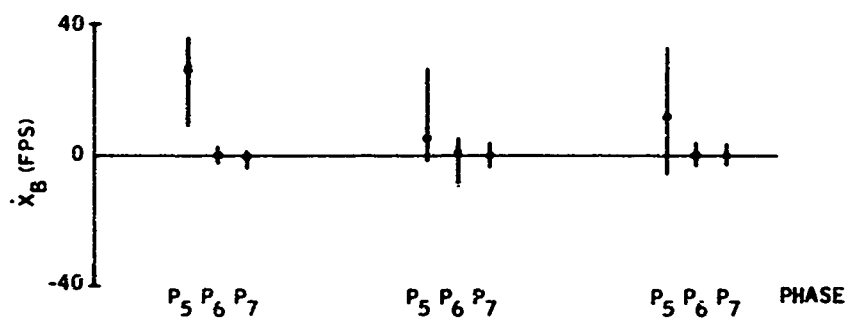
Figure C40. Terminal Median and ±34th-Percentile Data for $\ddot{X}_B$: UH-1 Aircraft

C24

Figure C41.   Terminal Median and ±34th-Percentile Data
for $\dot{Y}_B$: UH-1 Aircraft

C25

Q	N	F	A	C	D	V
1	1	1	1	1	1	1

Q	N	F	A	C	D	V
1	3	1	1	1	1	1

Q	N	F	A	C	D	V
1	3	3	1	1	1	1

P_5 P_6 P_7 P_5 P_6 P_7 P_5 P_6 P_7 PHASE

Q	N	F	A	C	D	V
1	1	1	2	1	1	1

Q	N	F	A	C	D	V
1	3	1	2	1	1	1

Q	N	F	A	C	D	V
1	3	3	2	1	1	1

P_5 P_6 P_7 P_5 P_6 P_7 P_5 P_6 P_7 PHASE
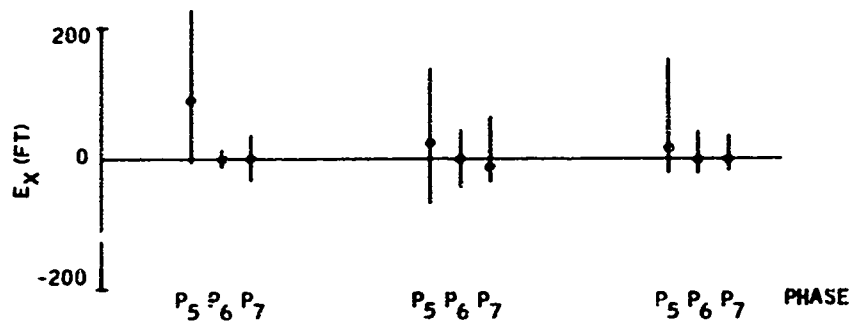
Figure C42.   Terminal Median and ±34th-Percentile Data
for E_X: UH-1 Aircraft

Q	N	F	A	C	D	V
1	1	1	1	1	1	1

Q	N	F	A	C	D	V
1	3	1	1	1	1	1
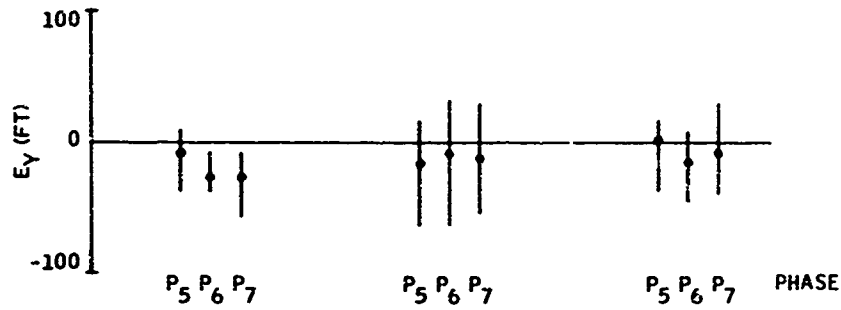
Q	N	F	A	C	D	V
1	3	3	1	1	1	1

Q	N	F	A	C	D	V
1	1	1	2	1	1	1

Q	N	F	A	C	D	V
1	3	1	2	1	1	1

Q	N	F	A	C	D	V
1	3	3	2	1	1	1

Figure C43. Terminal Median and ±34th-Percentile Data for E_Y: UH-1 Aircraft

C27
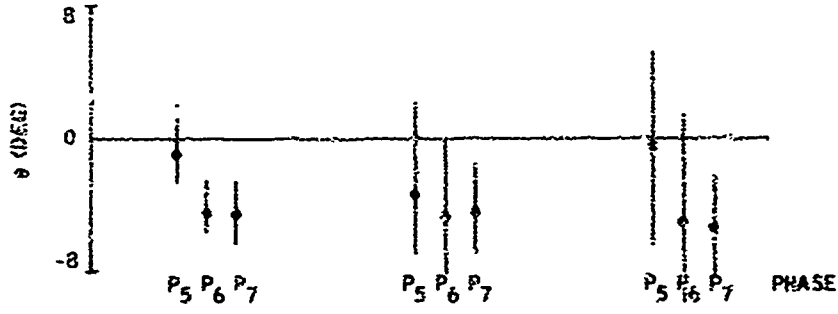
Figure C44. Terminal Median and ±34th-Percentile Data
for θ: UH-1 Aircraft

C28
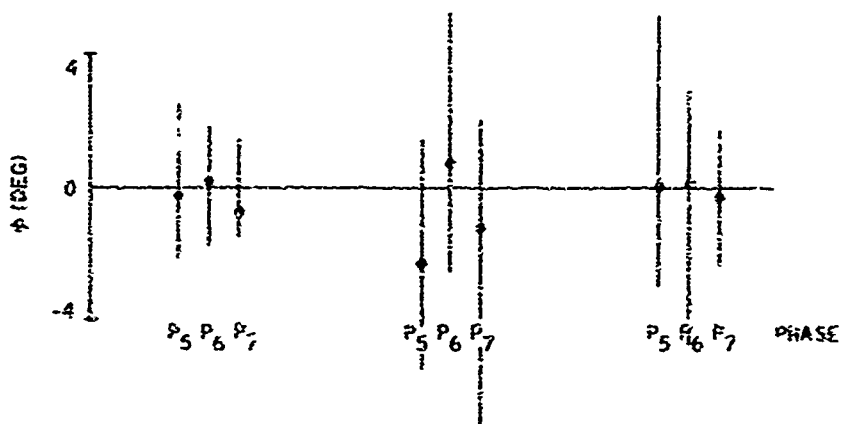
Figure C45. Terminal Median and ±34th-Percentile Data for ϕ: UH-1 Aircraft
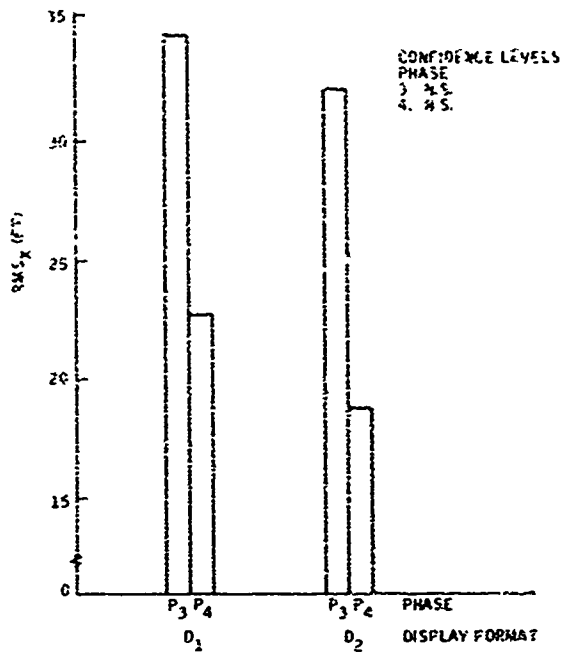
Figure C46. Mean RMS$_X$ Error for Each Display Format and Phase: XV-5 Aircraft

Figure C47. Mean RMS$_Y$ Error for Each Display Format and Phase: XV-5 Aircraft

C30
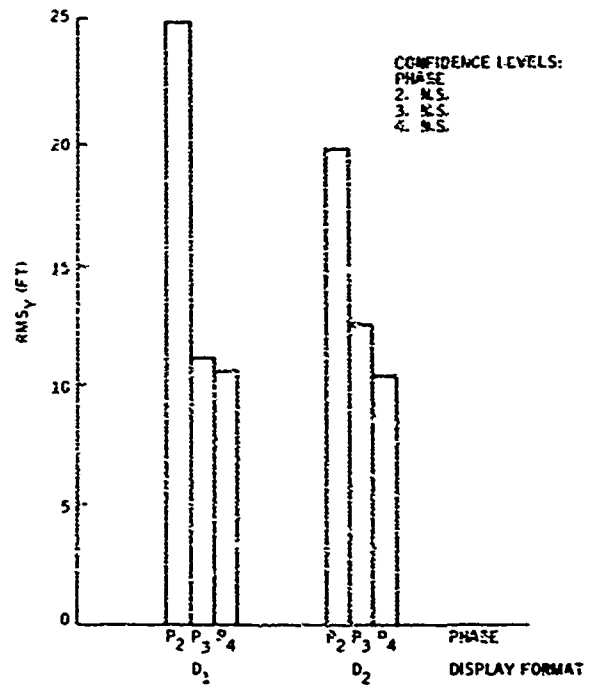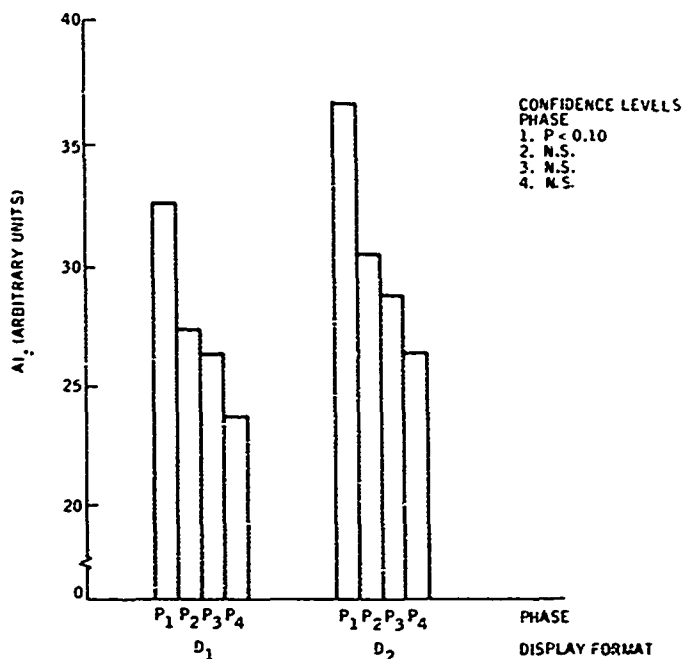
Figure C48. Mean AI_ϕ for Each Display Format and Phase: XV-5 Aircraft

Figure C49. Mean AI_θ for Each Display Format and Phase: XV-5 Aircraft

C31

CONFIDENCE LEVELS
PHASE
1. P < 0.10
2. N.S.
3. N.S.
4. N.S.
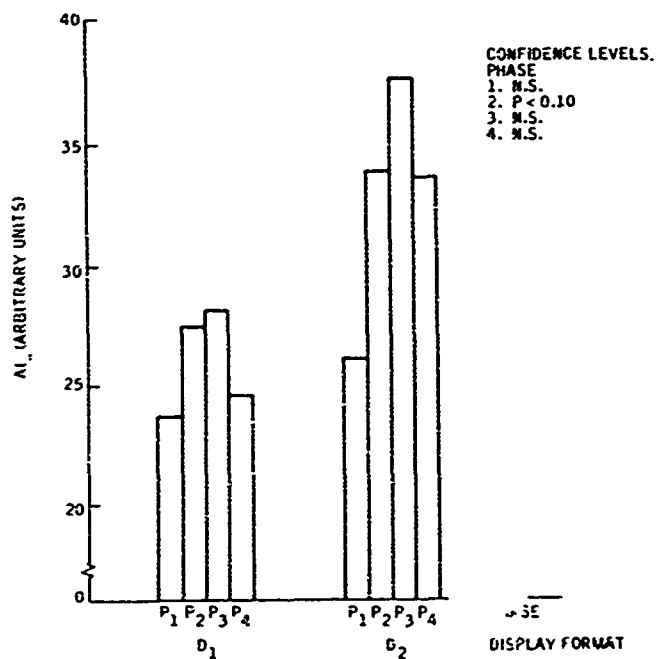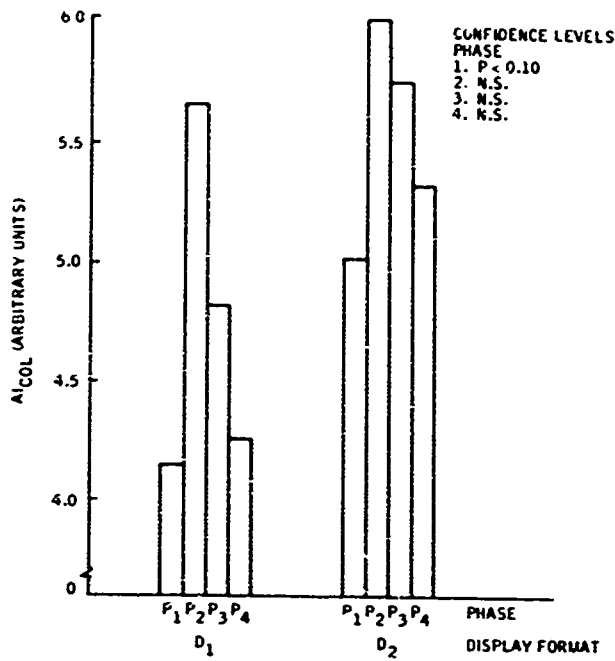
Figure C50. Mean AI_{COL} for Each Display Format and Phase: XV-5 Aircraft

CONFIDENCE LEVELS:
PHASE
1. N.S.
2. P < 0.025
3. N.S.
4. P < 0.10

Figure C51. Mean AI_θ for Each Approach Angle and Phase: XV-5 Aircraft

C32
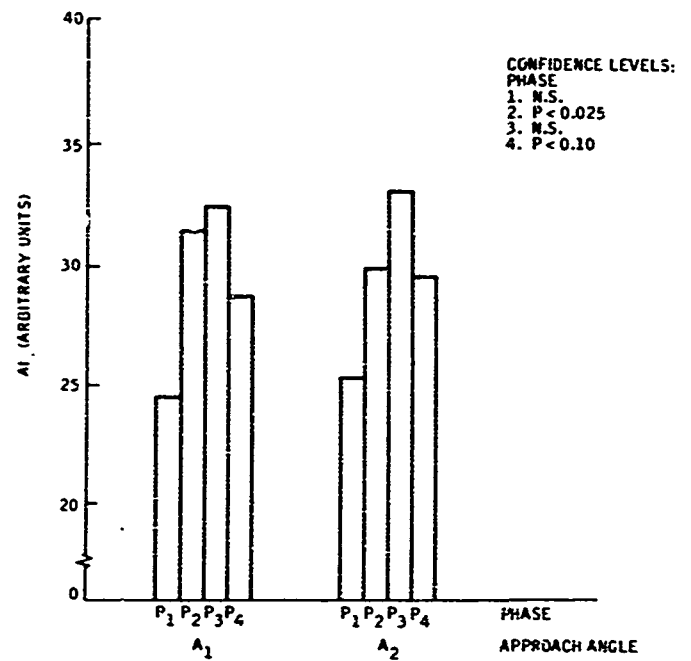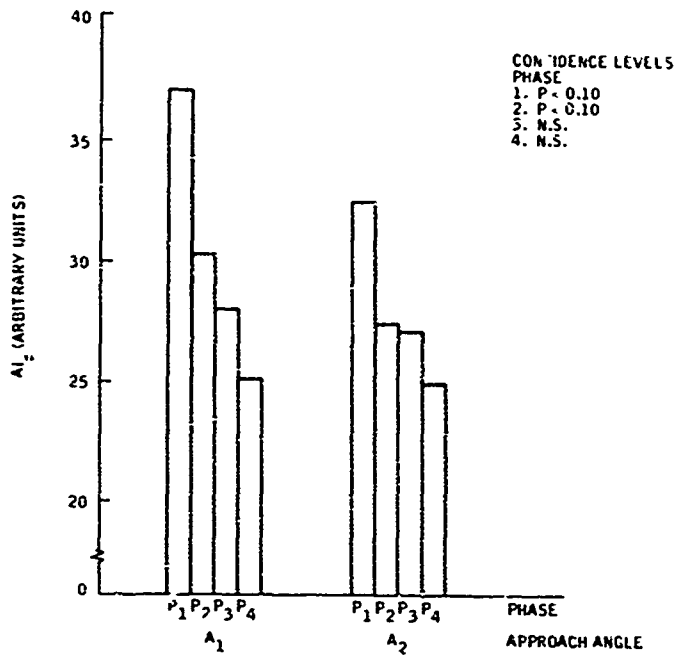
Figure C52. Mean AI_{ϕ} for Each Approach Angle and Phase: XV-5 Aircraft

Figure C53. Mean RMS_X Error for Each Quickening Level and Phase: XV-5 Aircraft

C33
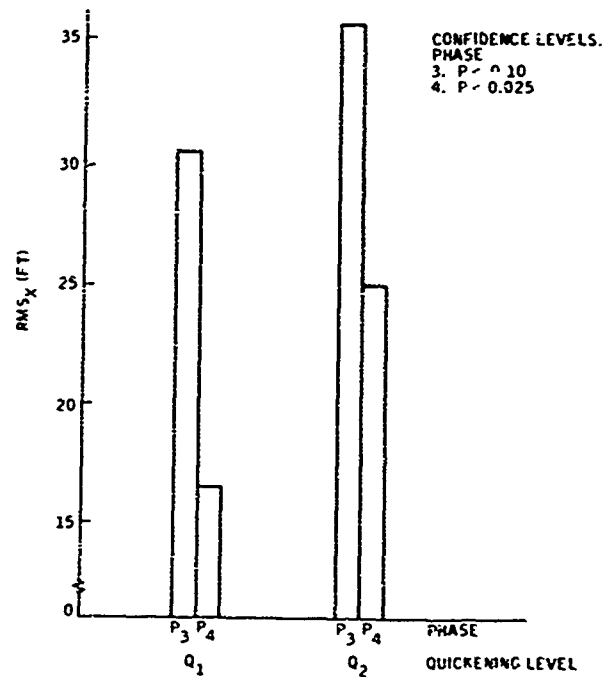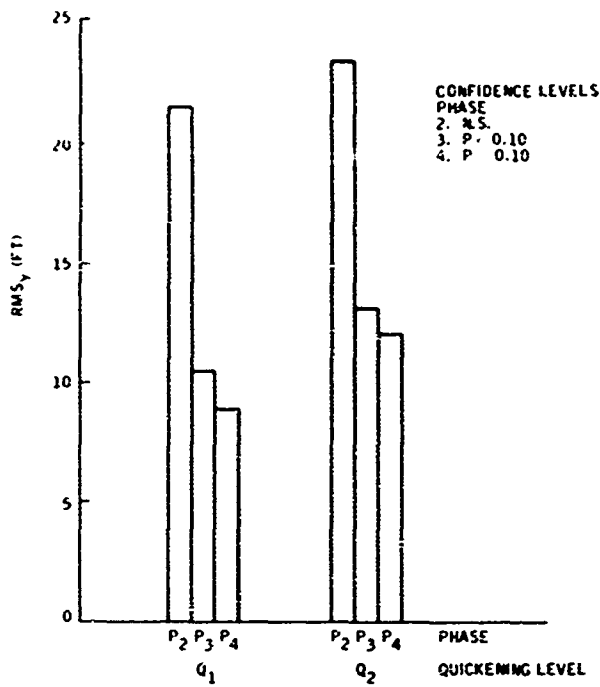
Figure C54. Mean RMS$_Y$ Error for Each Quickening Level and Phase: XV-5 Aircraft

Figure C55. Mean RMS$_X$ Error for Each Filter Level and Phase: XV-5 Aircraft

C34
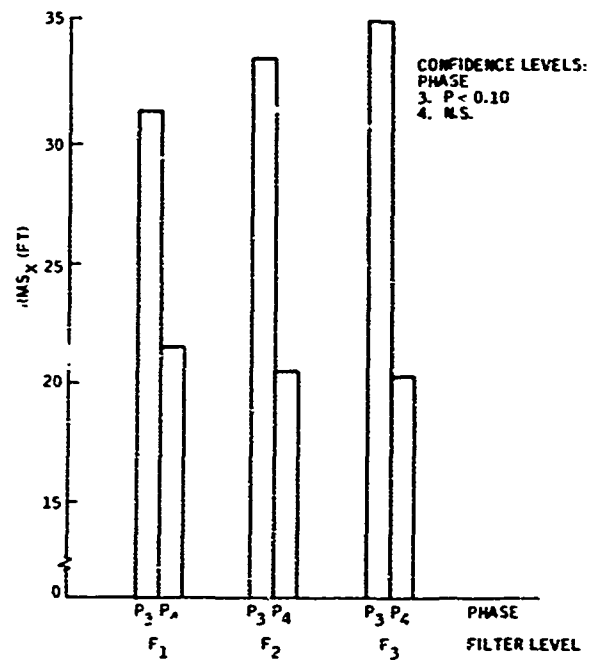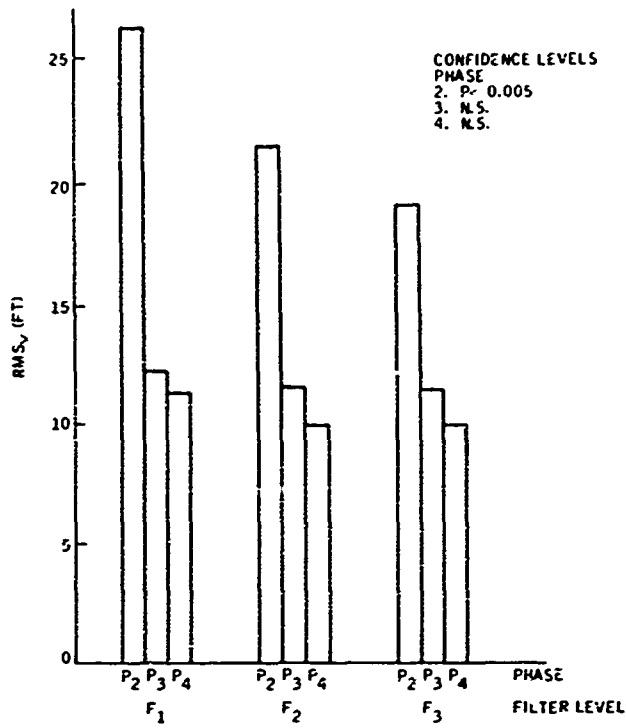
Figure C56. Mean RMS_Y Error for
Each Filter Level and
Phase: XV-5 Aircraft

Figure C57. Mean RMS_Z Error for
Each Filter Level and
Phase: XV-5 Aircraft
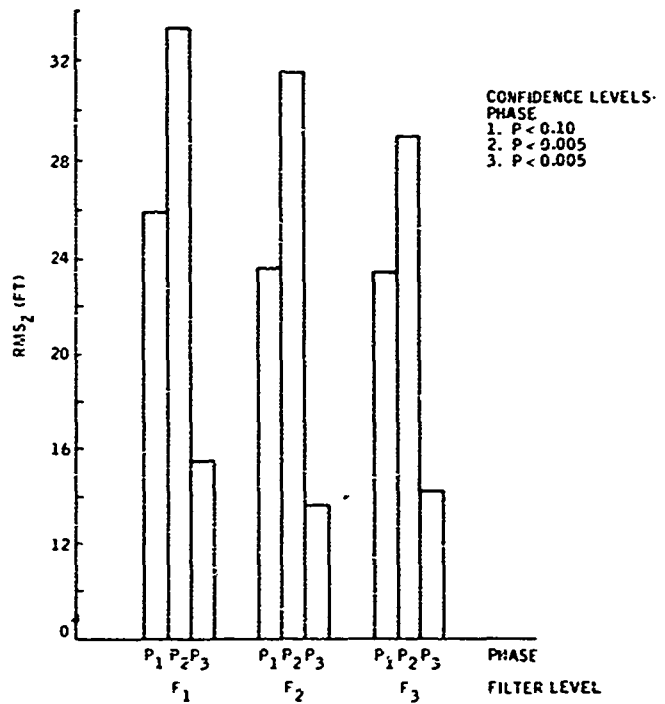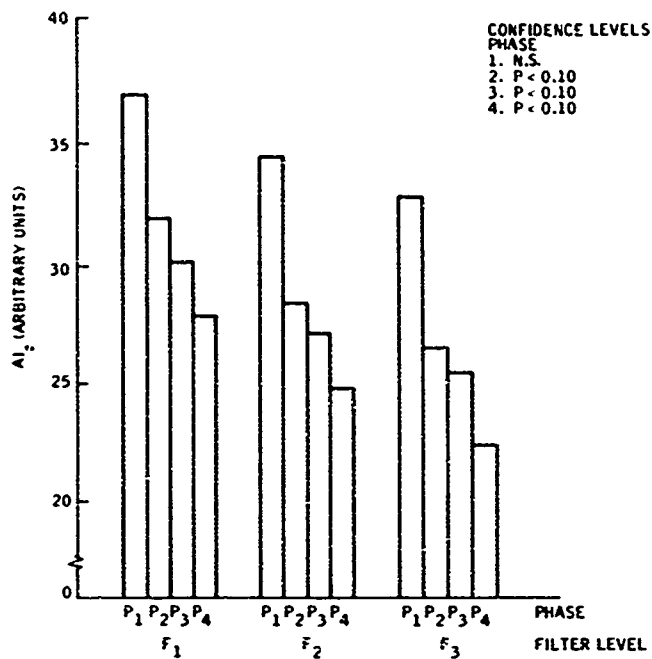
C35

Figure C58. Mean AI_ϕ for Each Filter Level and Phase: XV-5 Aircraft

Figure C59. Mean RMS_X Error for Each Noise Level and Phase: XV-5 Aircraft

C36
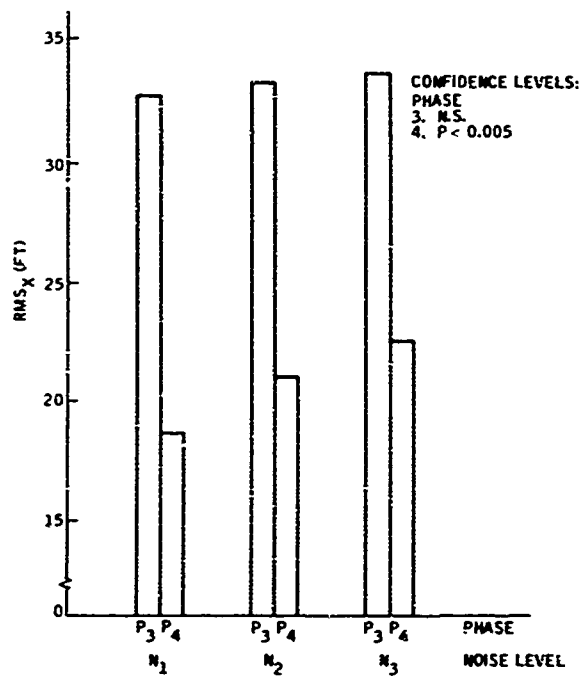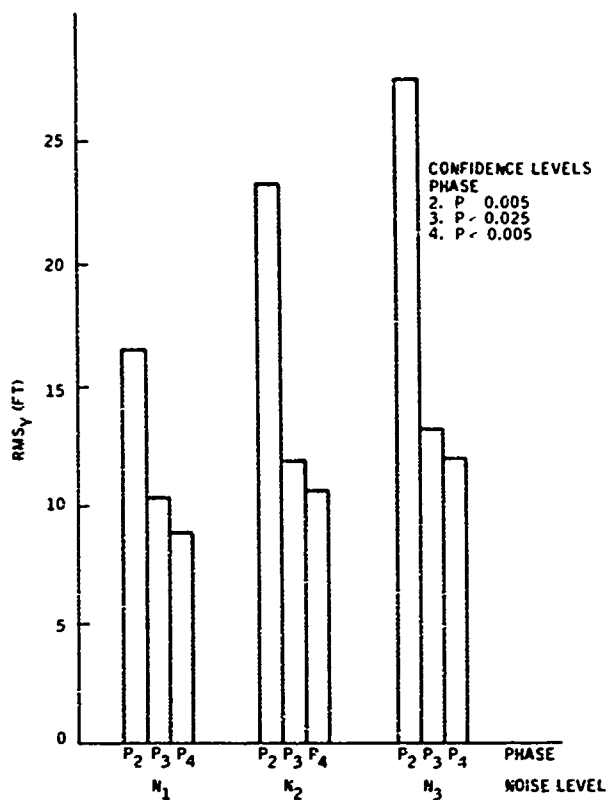
Figure C60. Mean RMS_Y Error for Each Noise Level and Phase: XV-5 Aircraft

Figure C61. Mean RMS_Z Error for Each Noise Level and Phase: XV-5 Aircraft

C37
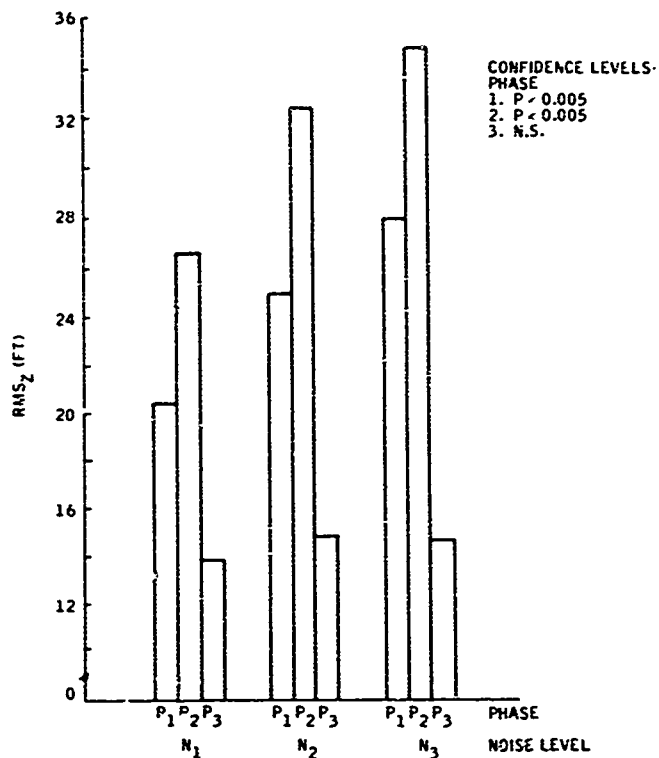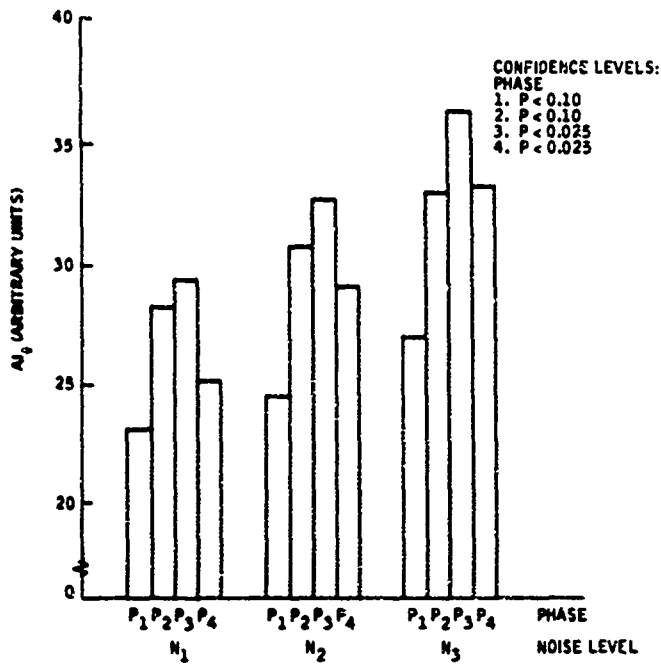
Figure C62. Mean AI_θ for Each Noise Level and Phase: XV-5 Aircraft

Figure C63. Mean AI_ϕ for Each Noise Level and Phase: XV-5 Aircraft

C38
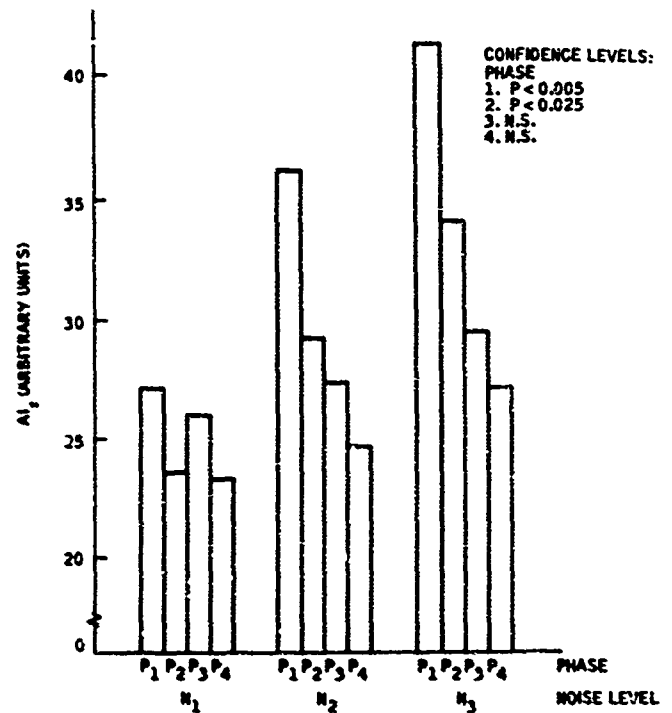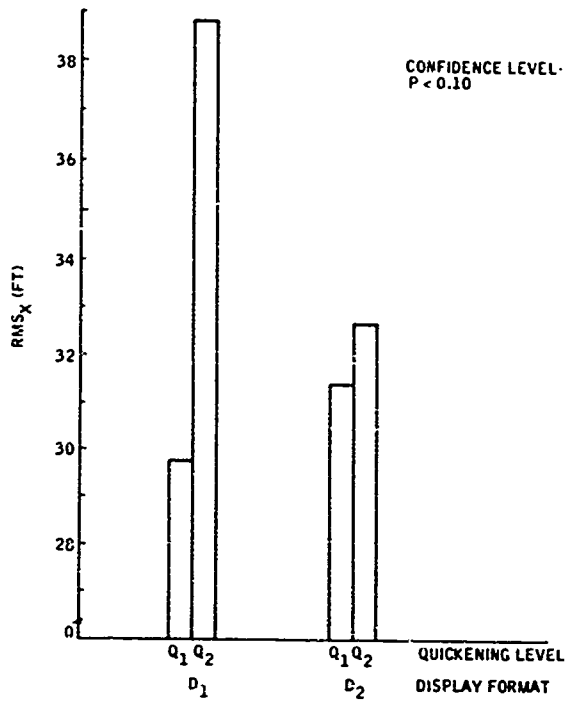
Figure C64. Mean RMS_X Error for Each Display Format and Quickening Level: Phase P_3; XV-5 Aircraft

Figure C65. Mean RMS_Y Error for Each Display Format and Noise Level: Phase P_2; XV-5 Aircraft

C39
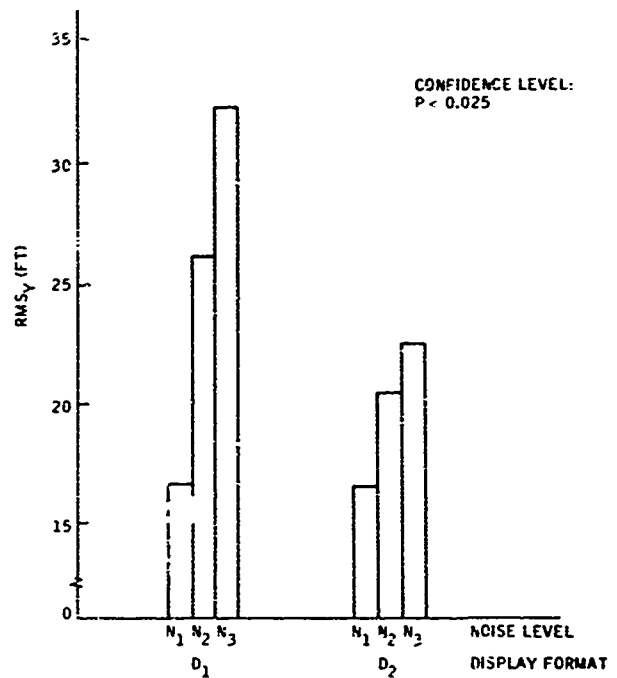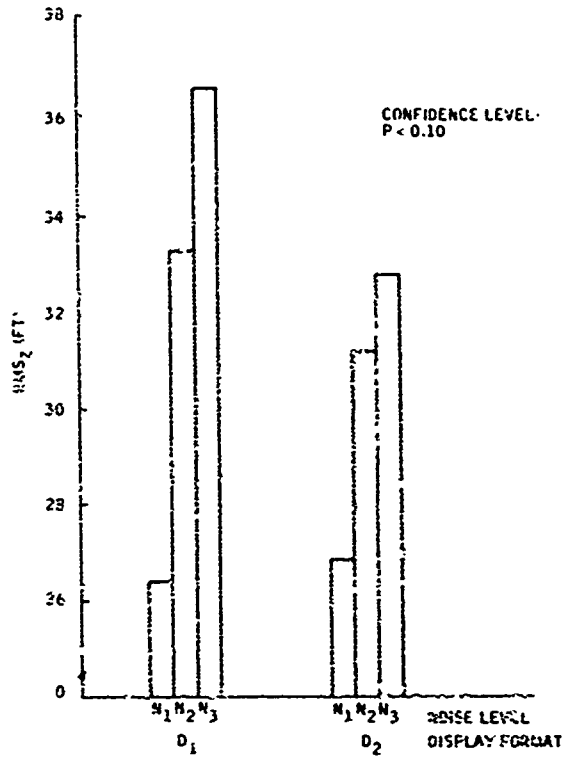
Figure C66. Mean RMS_Z Error for Each Display Format and Noise Level: Phase P_2; XV-5 Aircraft

Figure C67. Mean AI_θ for Each Display Format and Noise Level: Phase P_3; XV-5 Aircraft
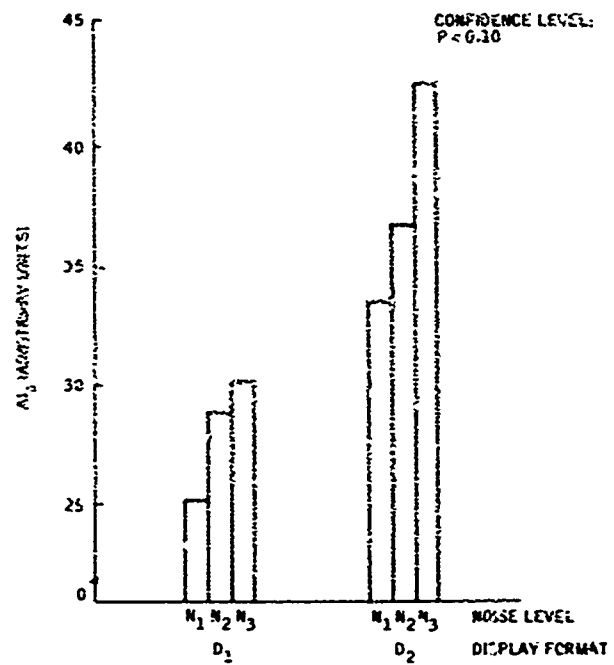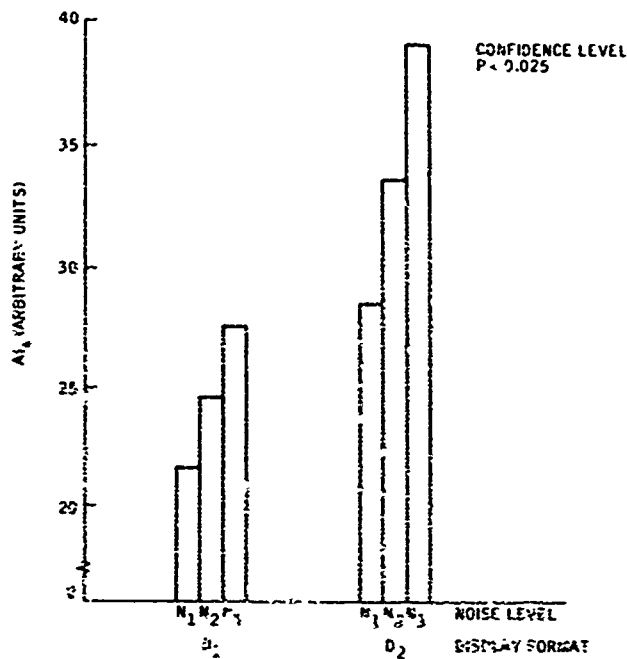
Figure C68. Mean AI$_6$ for Each Display Format and Noise Level: Phase P$_4$; XV-5 Aircraft

Figure C59. Mean RMS$_X$ Error for Each Quickening Level and Noise Level: Phase P$_4$; XV-5 Aircraft
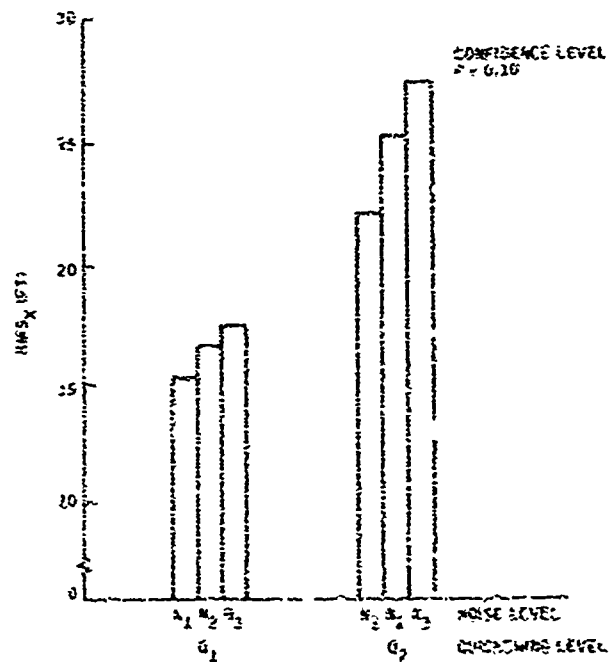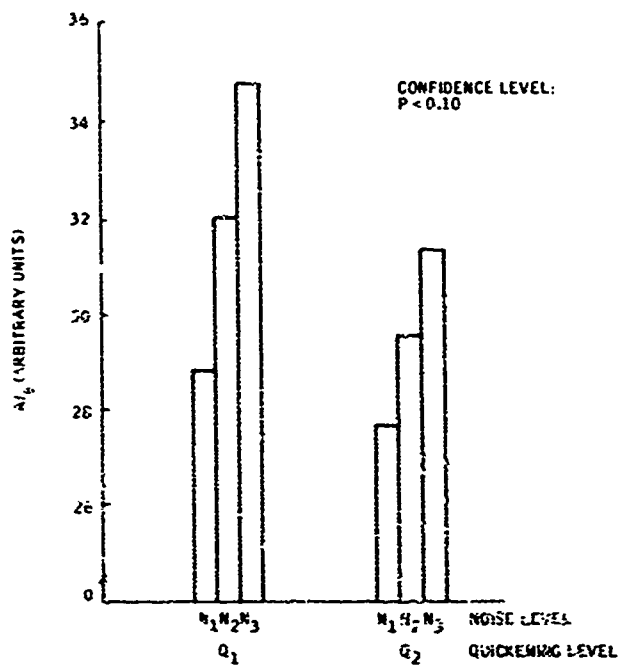
Figure C70. Mean AI_θ for Each Quickening Level and Noise Level: Phase P_2; XV-5 Aircraft

Figure C71. Mean AI_ϕ for Each Quickening Level and Noise Level: Phase P_2; XV-5 Aircraft
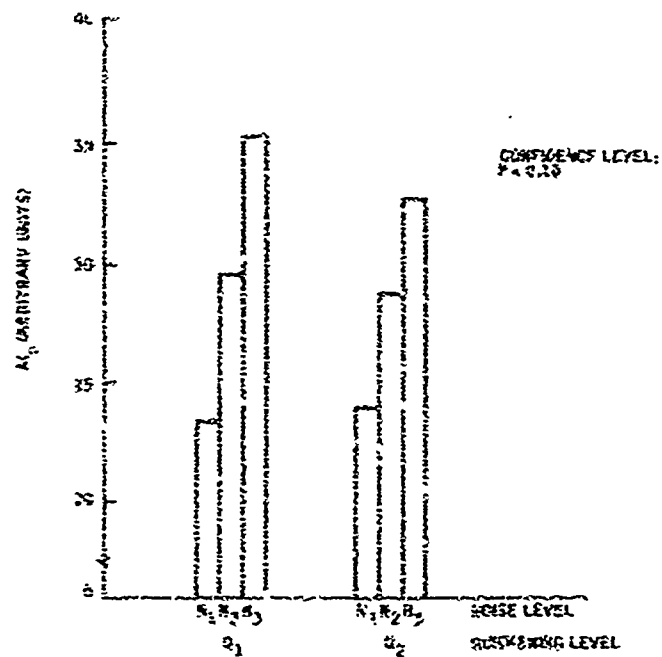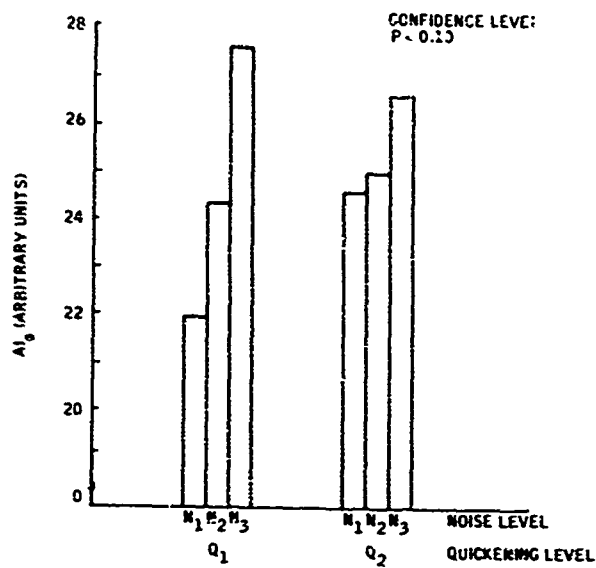
Figure C72. Mean AI_ϕ for Each Quickening Level and Noise Level: Phase P_4; XV-5 Aircraft

Figure C73. Mean Time for Each Noise Level and Filter Level: Phase P_2; XV-5 Aircraft

C43
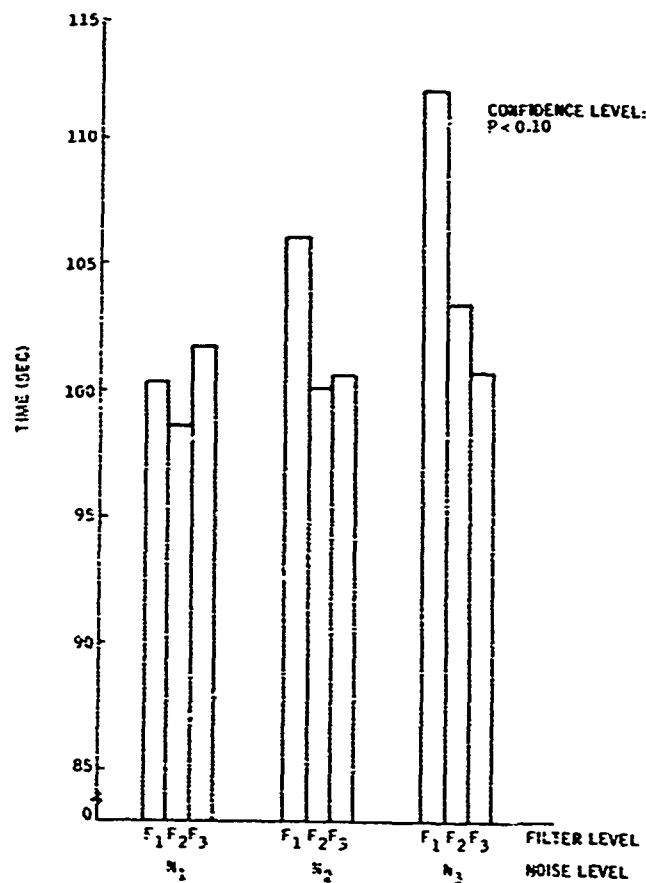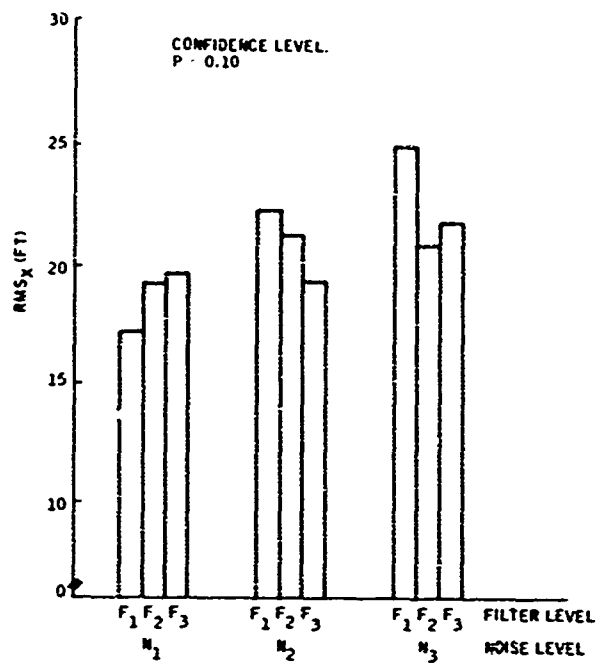
Figure C74. Mean RMS_x Error for Each Noise Level and Filter Level: Phase P_4; XV-5 Aircraft

Figure C75. Mean RMS_y Error for Each Noise Level and Filter Level: Phase P_2; XV-5 Aircraft

C44
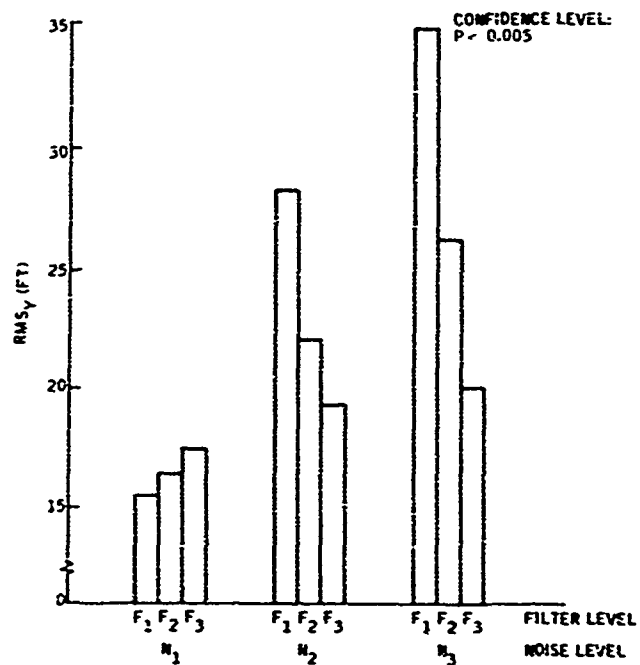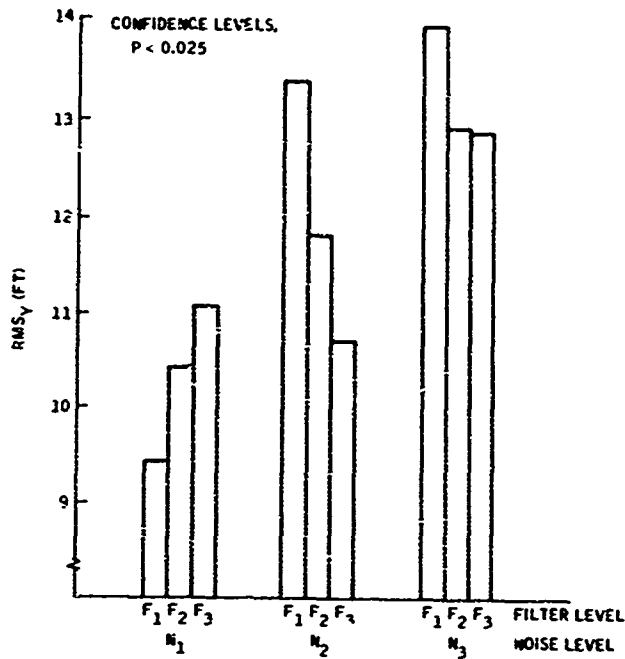
Figure C76. Mean RMS$_y$ Error for Each
Noise Level and Filter
Level: Phase P$_3$; XV-5
Aircraft

Figure C77. Mean RMS$_y$ Error for
Each Noise Level and
Filter Level: Phase P$_4$;
XV-5 Aircraft

C45
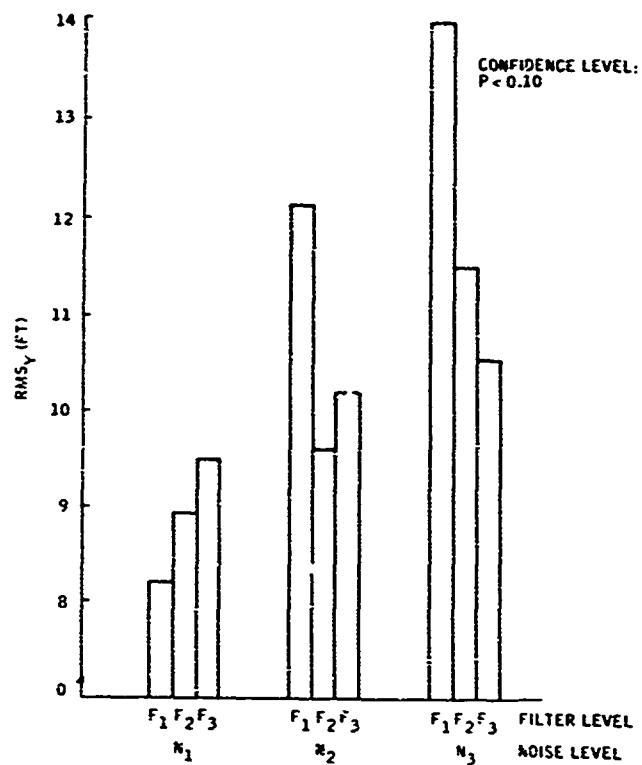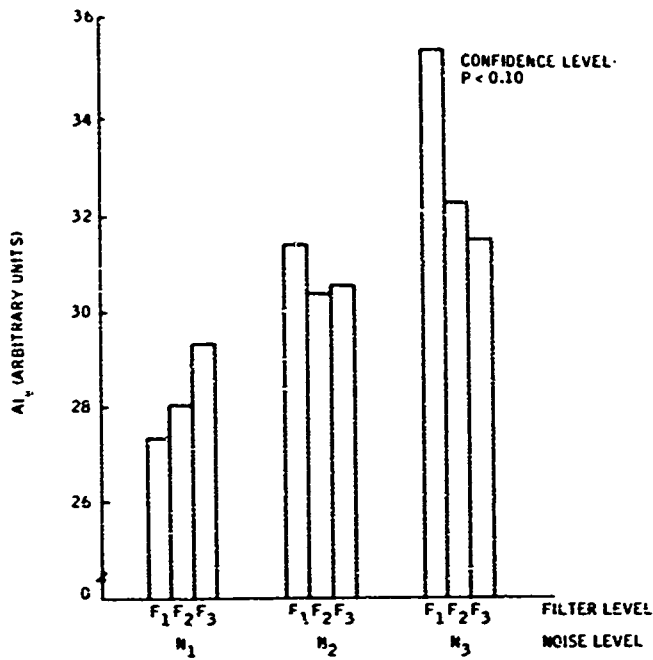
Figure C78. Mean AI_θ for Each Noise Level and Filter Level: Phase P_2; XV-5 Aircraft

Figure C79. Mean AI_ϕ for Each Noise Level and Filter Level: Phase P_2; XV-5 Aircraft
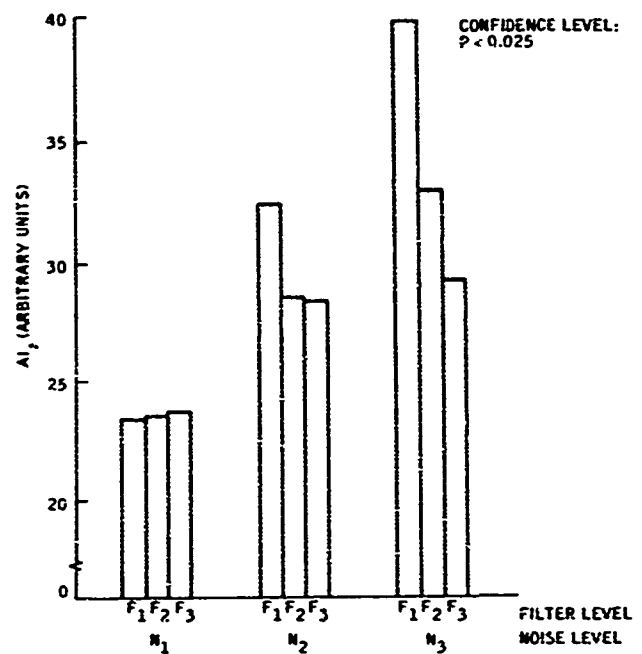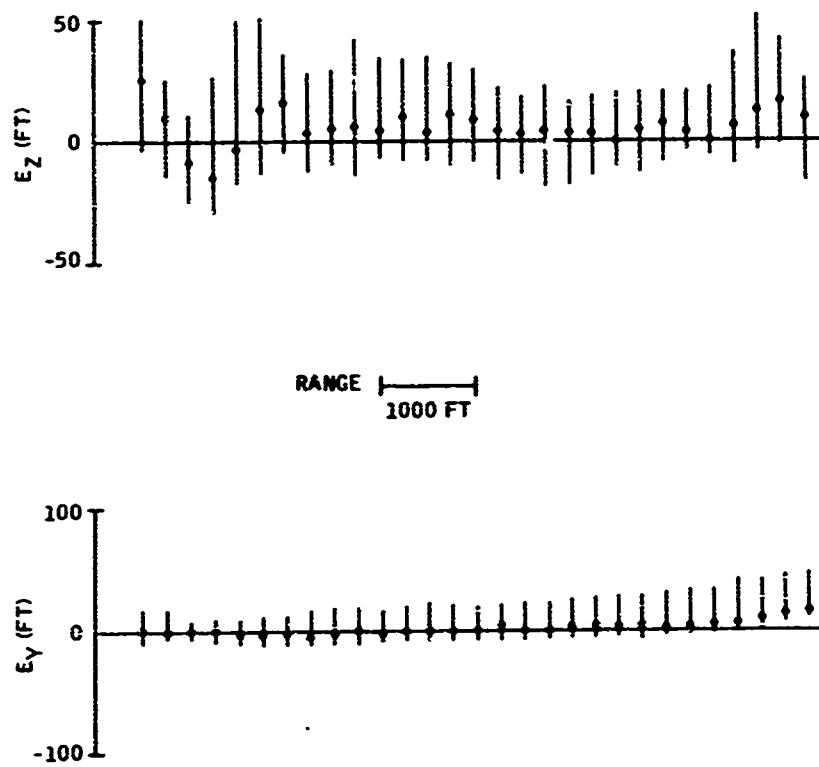
Figure C80.   Final Approach Median and ±34th-Percentile
Data at 250-ft Intervals: XV-5 Aircraft
(1 of 6)

C47
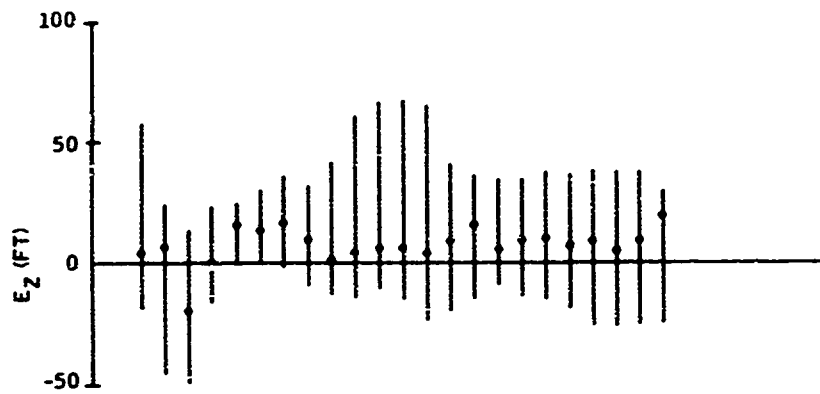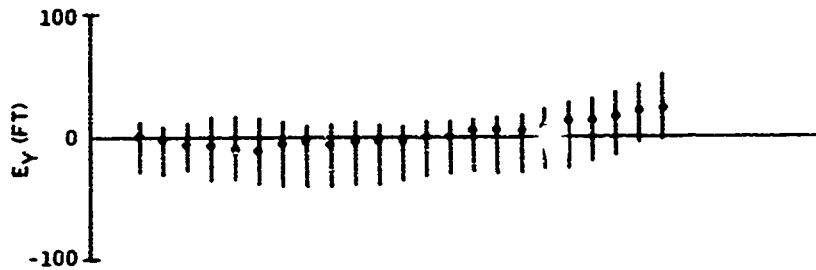
Figure C81. Final Approach Median and ±34th-Percentile
Data at 250-ft Intervals: XV-5 Aircraft
(2 of 6)
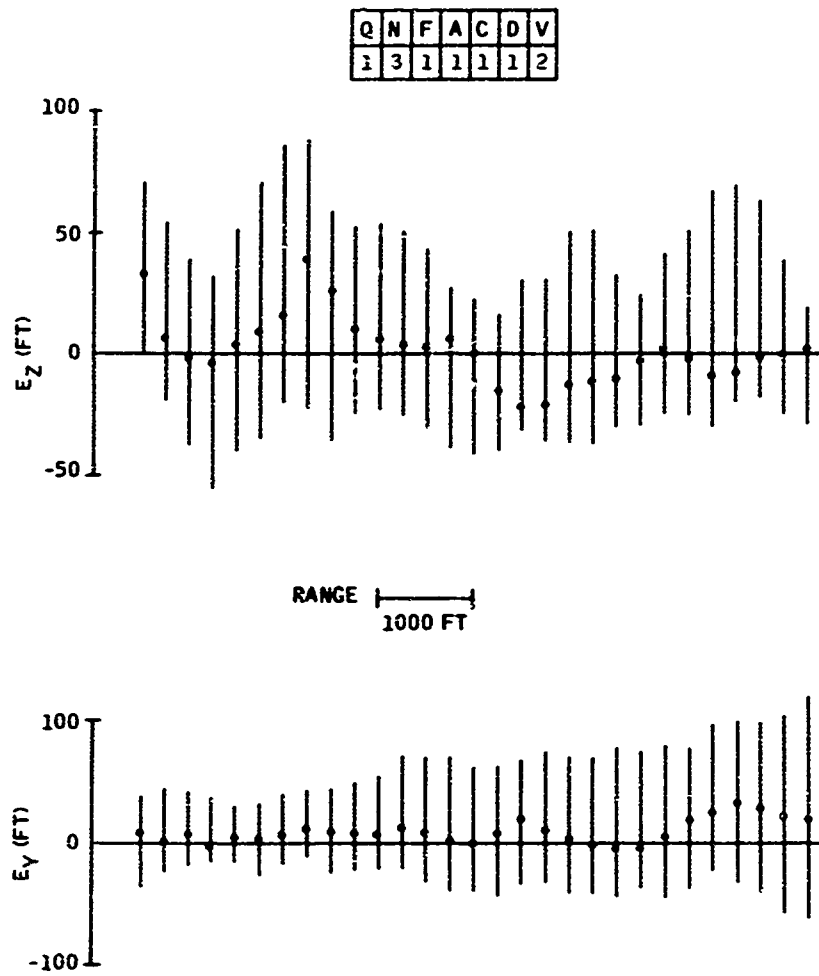
Q	N	F	A	C	D	V
1	3	1	1	1	1	2

Figure C82. Final Approach Median and ±34th-Percentile
Data at 250-ft Intervals: XV-5 Aircraft
(3 of 6)

C49
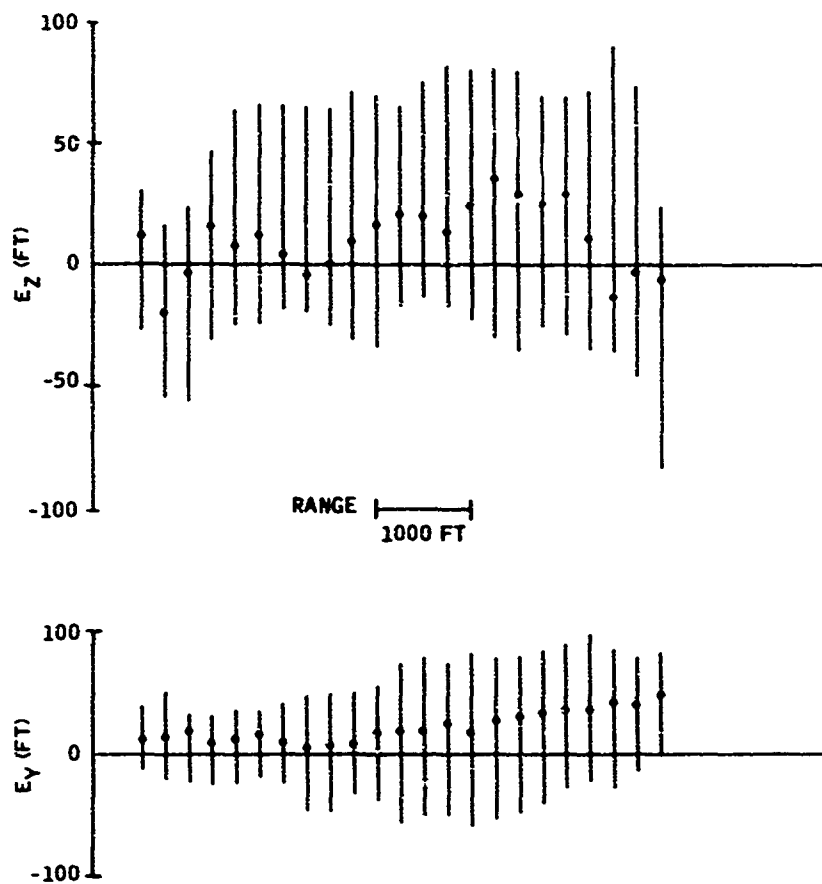
Figure C83. Final Approach Median and ±34th-Percentile
Data at 250-ft Intervals: XV-5 Aircraft
(4 of 6)
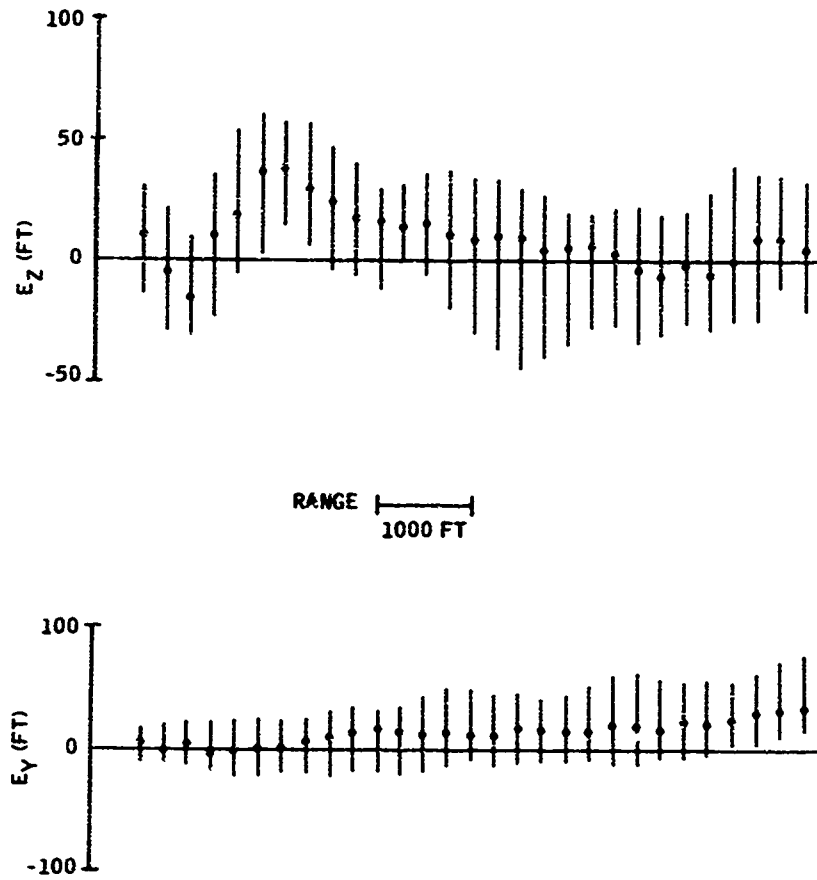
Figure C84. Final Approach Median and ±34th-Percentile Data at 250-ft Intervals: XV-5 Aircraft (5 of 6)
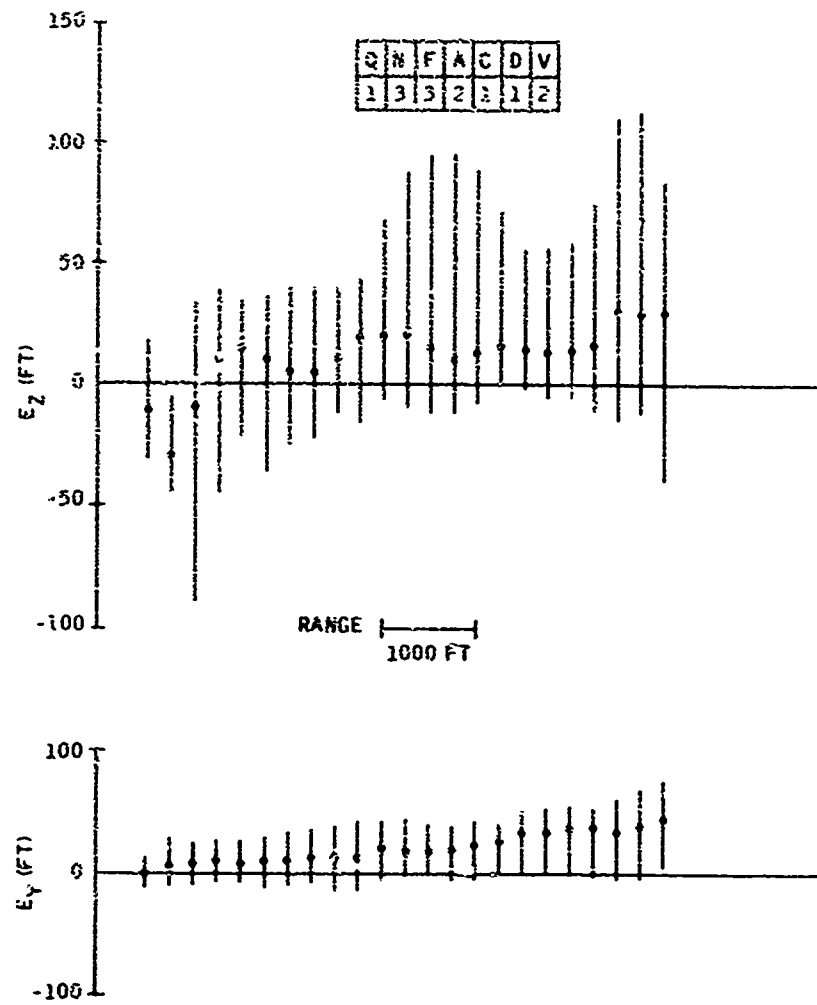
Figure C85. Final Approach Median and ±34th-Percentile
Data at 250-ft Intervals: XV-5 Aircraft
(6 of 6)

Q	N	F	A	C	D	V		Q	N	F	A	C	D	V		Q	N	F	A	C	D	V
1	1	1	1	1	1	2		1	3	1	1	1	1	2		1	3	3	1	1	1	2

$\dot{X}_B$ (FPS)

40

0

-40

P_5 P_6 P_7 P_5 P_6 P_7 P_5 P_6 P_7 PHASE
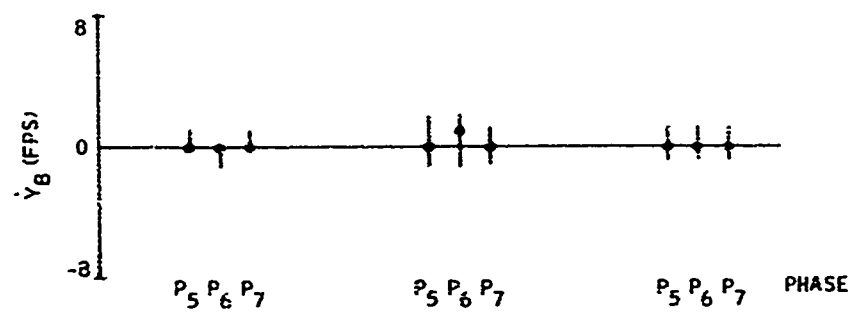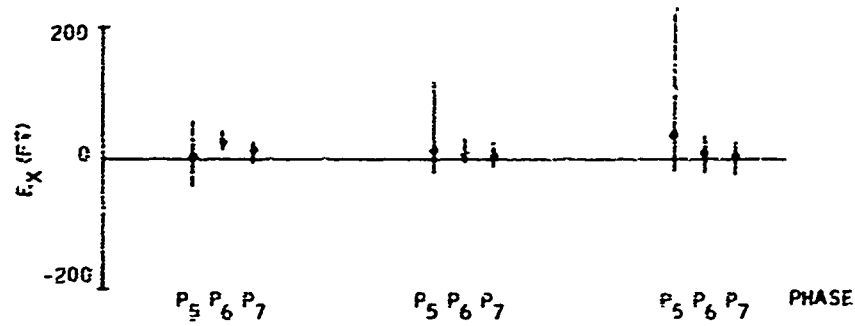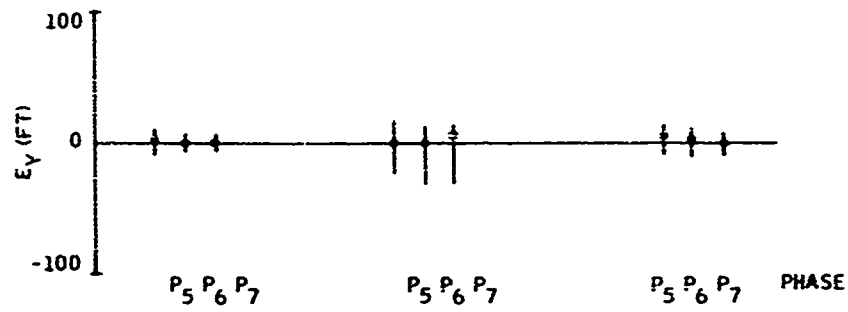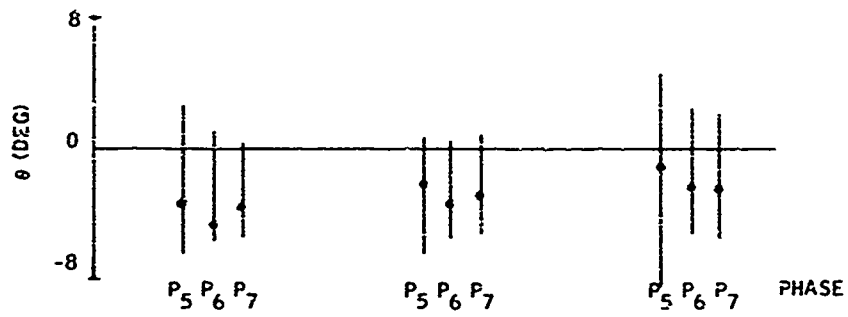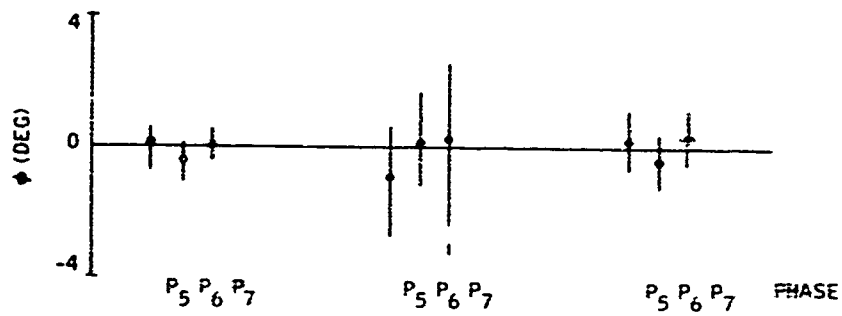
Q	N	F	A	C	D	V		Q	N	F	A	C	D	V		Q	N	F	A	C	D	V
1	1	1	2	1	1	2		1	3	1	2	1	1	2		1	3	3	2	1	1	2

$\dot{X}_B$ (FPS)

40

0

-40

P_5 P_6 P_7 P_5 P_6 P_7 P_5 P_6 P_7 PHASE

Figure C36.   Terminal Median and ±34th-Percentile Data
for $\dot{X}_B$: XV-5 Aircraft

C53

Figure C87.   Terminal Median and ±34th-Percentile Data
for $\dot{Y}_B$:   XV-5 Aircraft

Figure C88. Terminal Median and ±34th-Percentile Data for E_X: XV-5 Aircraft

C55

Figure C89. Terminal Median and ±34th-Percentile Data for E_Y: XV-5 Aircraft

Figure C90.   Terminal Median and ±34th-Percentile Data
for θ: XV-5 Aircraft

Figure C91. Terminal Median and ±34th-Percentile Data for 2: XV-5 Aircraft

APPENDIX D

FORMAL SIMULATION DATA
FOR TASK III STUDY
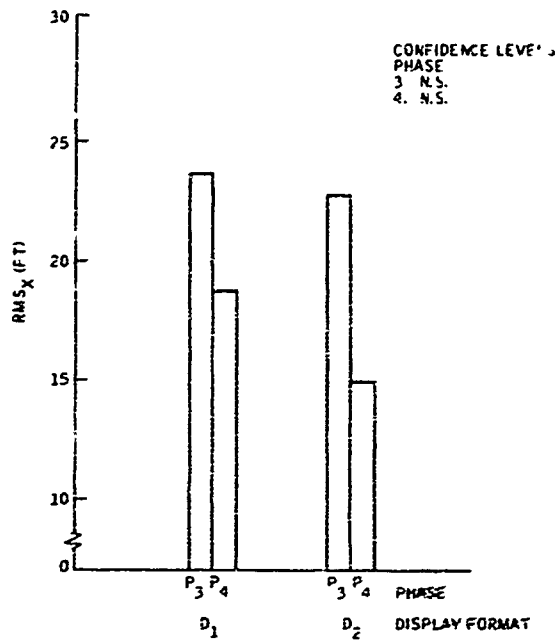
Figure D1. Mean RMS$_X$ Error for Each Display Format and Phase: UH-1 Aircraft

Figure D2. Mean RMS$_Y$ Error for Each Display Format and Phase: UH-1 Aircraft

D1
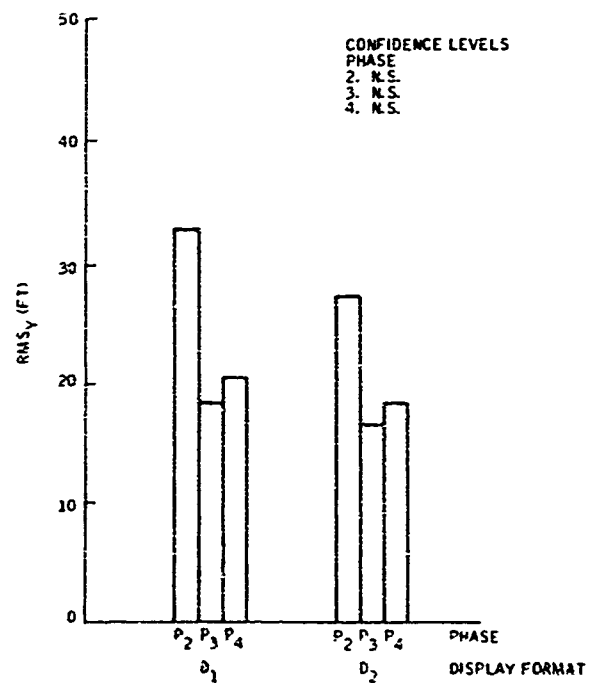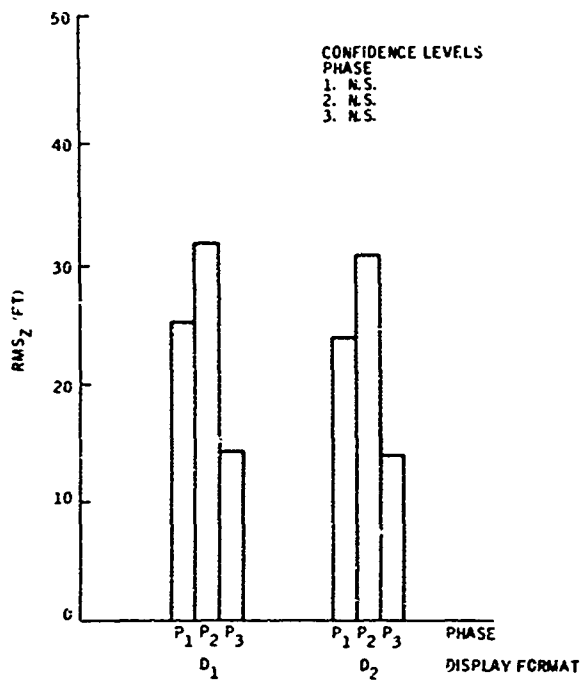
Figure D3. Mean RMS_Z Error for Each Display Format and Phase: UH-1 Aircraft

Figure D4. Mean AI_θ for Each Display Format and Phase: UH-1 Aircraft

D2
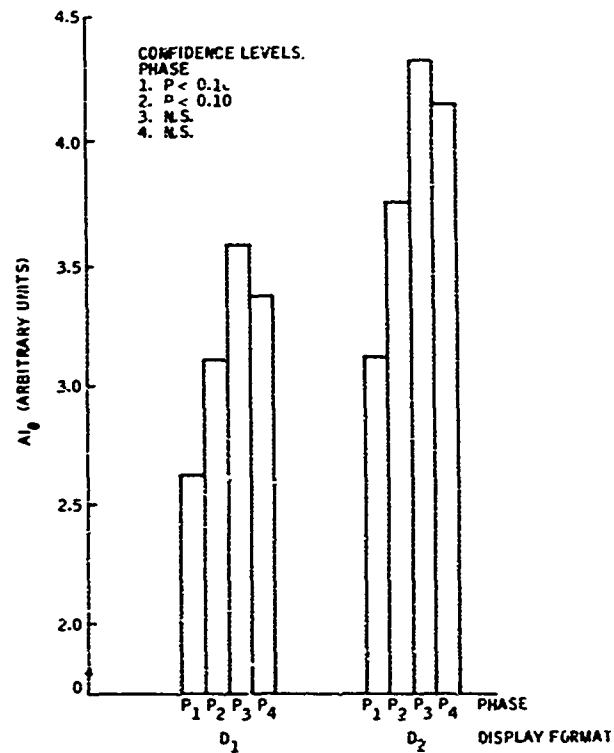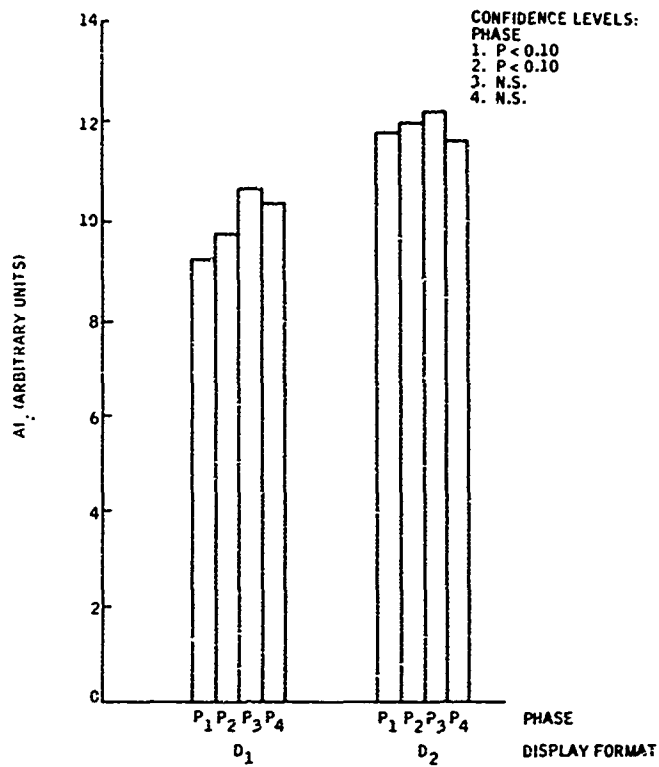
Figure D5. Mean AI_ϕ for Each Display Format and Phase: UH-1 Aircraft

Figure D6. Mean RMS_X Error for Each Approach Angle and Phase: UH-1 Aircraft
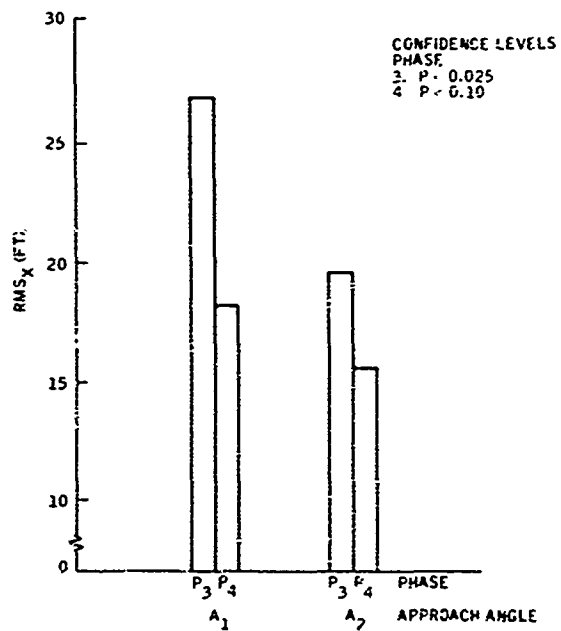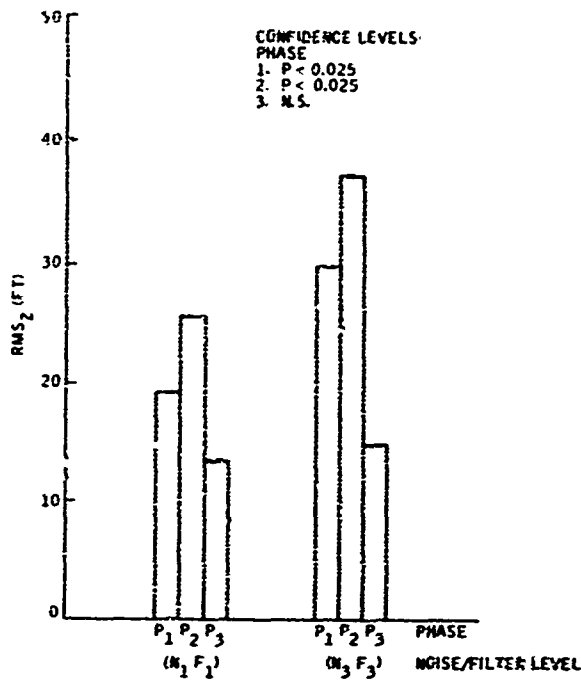
Figure D7. Mean RMS_Z Error for Each
Noise/Filter Level and
Phase: UH-1 Aircraft

Figure D8. Mean AI_θ for Each
Noise/Filter Level and
Phase: UH-1 Aircraft

D4
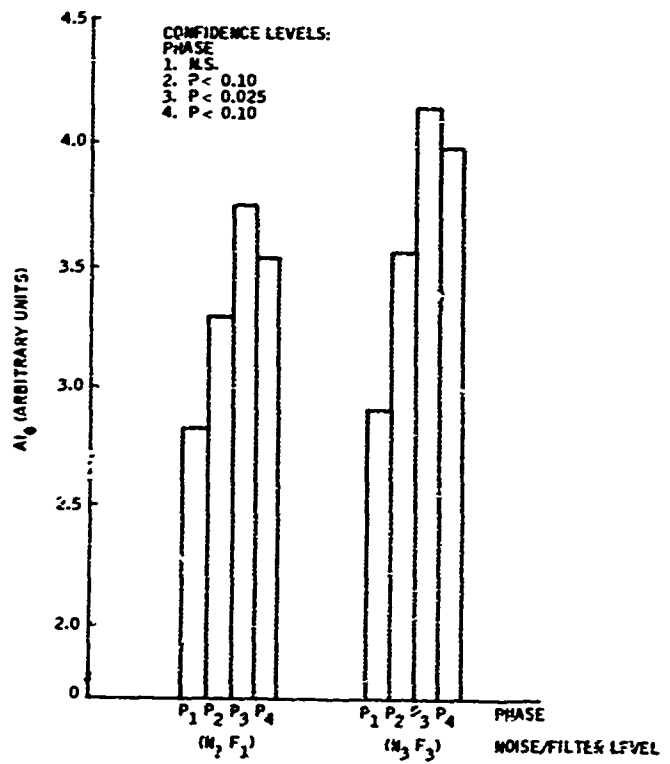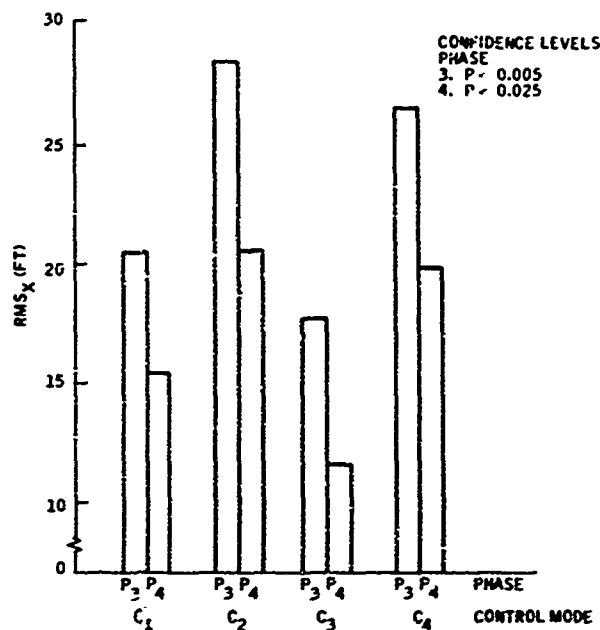
Figure D9. Mean RMS_X Error for Each Control Mode and Phase: UH-1 Aircraft

Figure D10. Mean RMS_Y Error for Each Control Mode and Phase: UH-1 Aircraft

D5
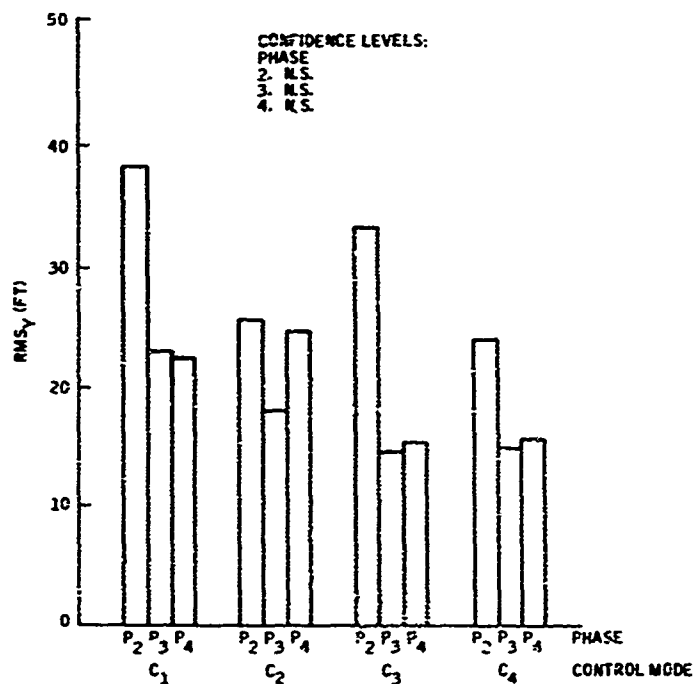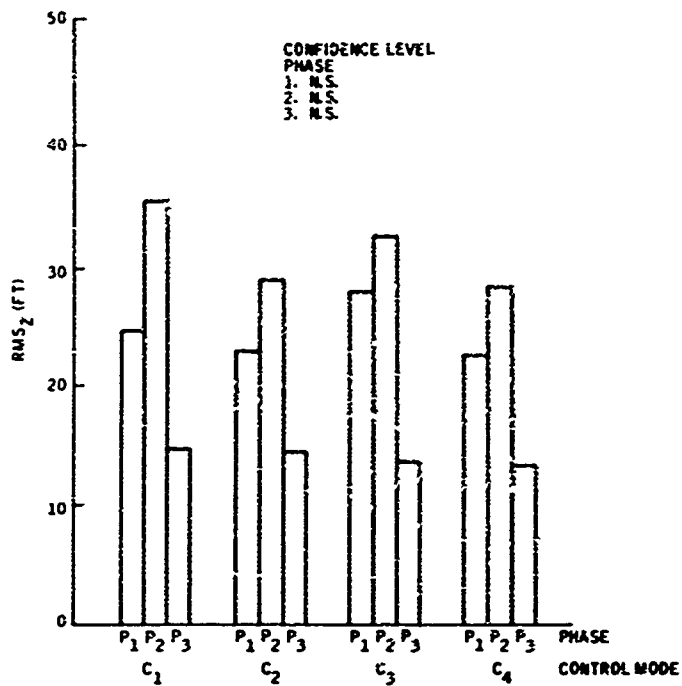
Figure D11. Mean RMS_Z Error for
Each Control Mode and
Phase: UH-1 Aircraft

Figure D12. Mean AI_θ for Each
Control Mode and
Phase: UH-1 Aircraft

D6
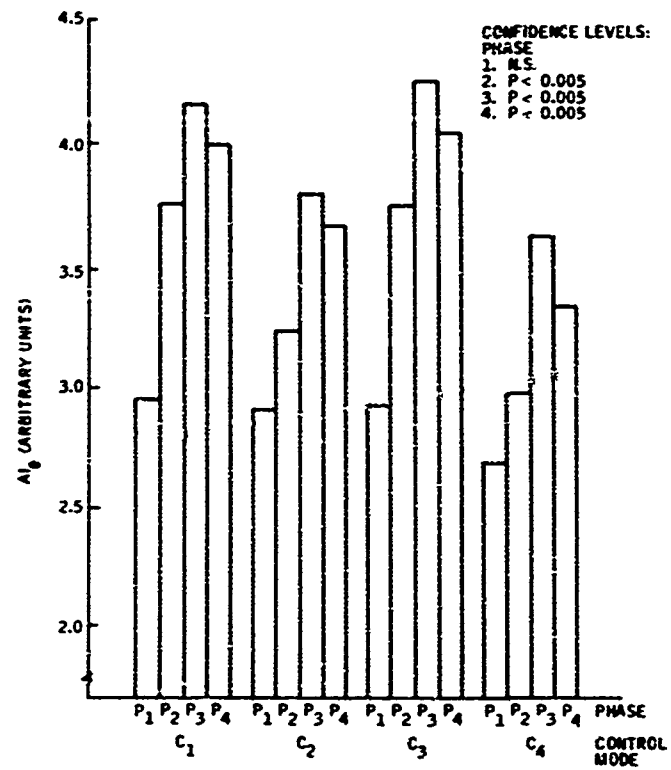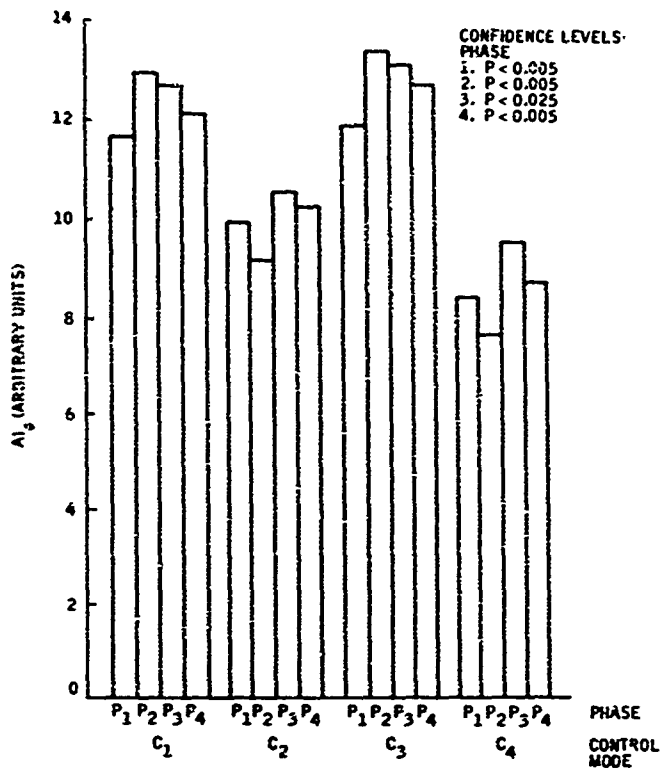
Figure D13. Mean AI_ϕ for Each Control Mode and Phase: UH-1 Aircraft

Figure D14. Mean RMS_y Error for Each Display Format and Noise/ Filter Level: Phase P_2; UH-1 Aircraft
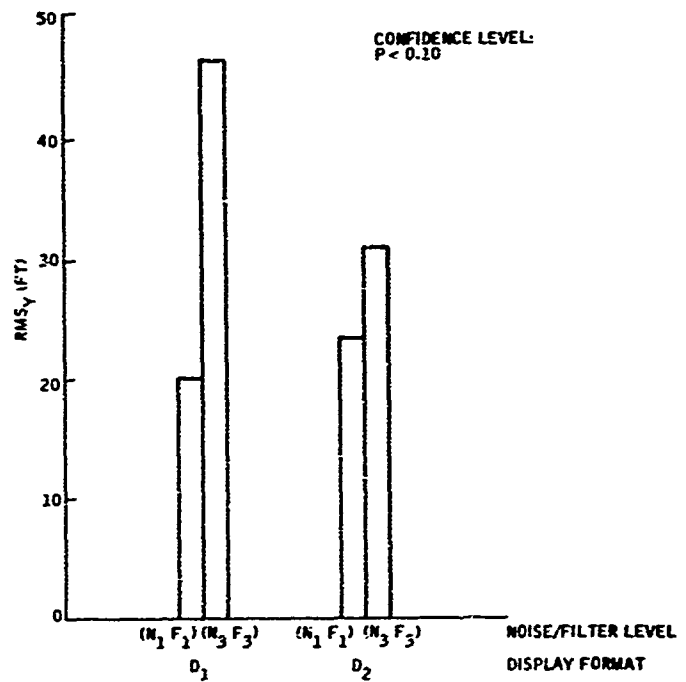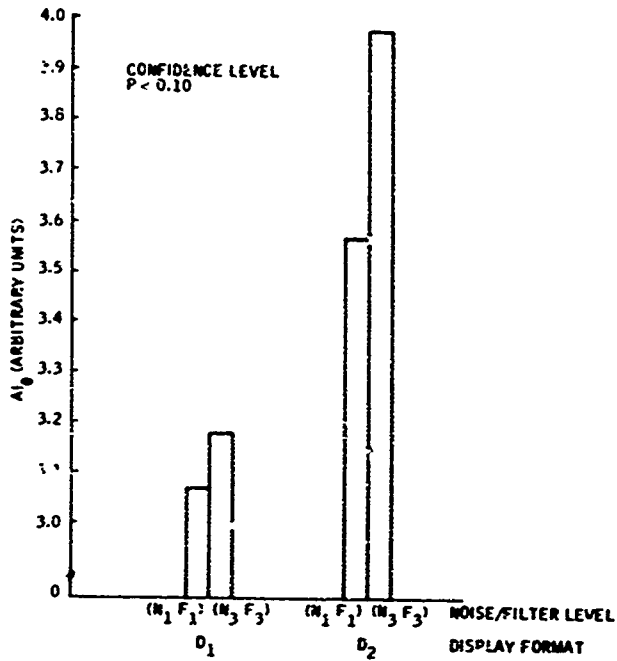
D7

Figure D15. Mean AI_θ for Each Display Format and Noise/Filter Level: Phase P_2; UH-1 Aircraft

Figure D16. Mean AI_ϕ for Each Display Format and Noise/Filter Level: Phase P_2; UH-1 Aircraft

D8

CONFIDENCE LEVEL:
P < 0.005

RMS_X (FT)

35

30

25

20

15

0

c_1 c_2 c_3 c_4 c_1 c_2 c_3 c_4 CONTROL MODE

A_1 A_2 APPROACH ANGLE
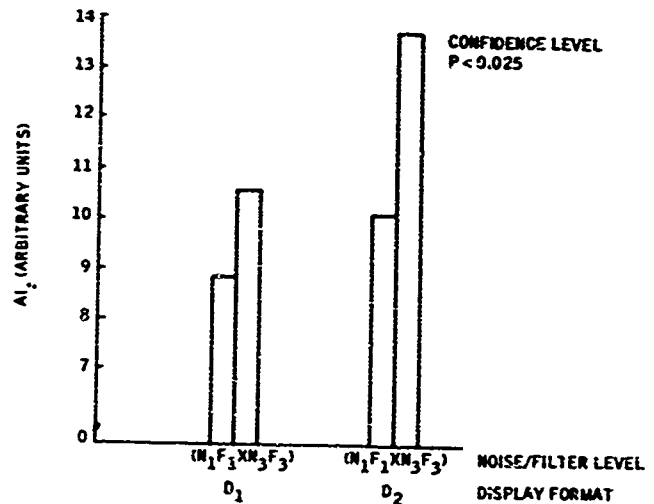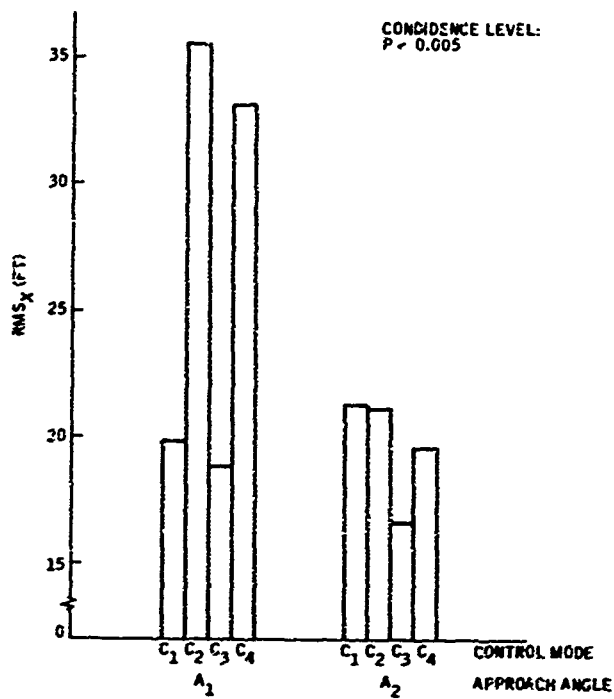
Figure D17. Mean RMS_X Error for Each Approach Angle and Control Mode: Phase P_3; UH-1 Aircraft

Figure D18. Mean AI_θ for Each Approach Angle and Control Mode: Phase P_2; UH-1 Aircraft
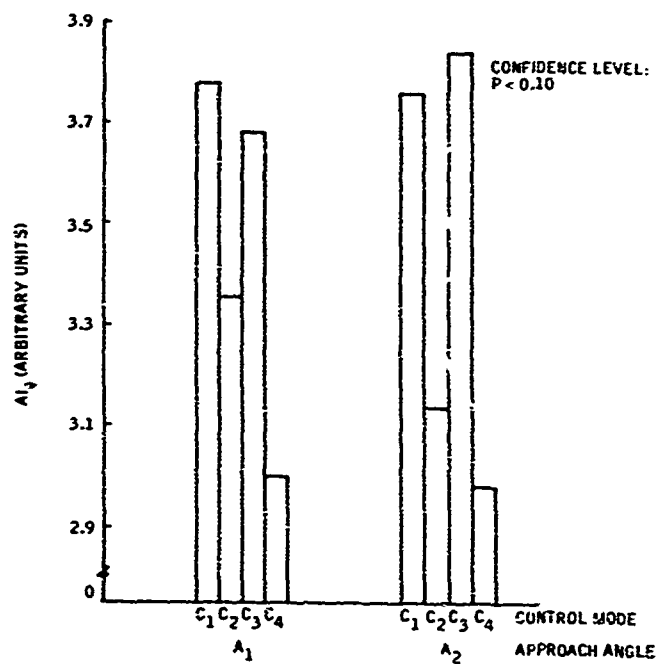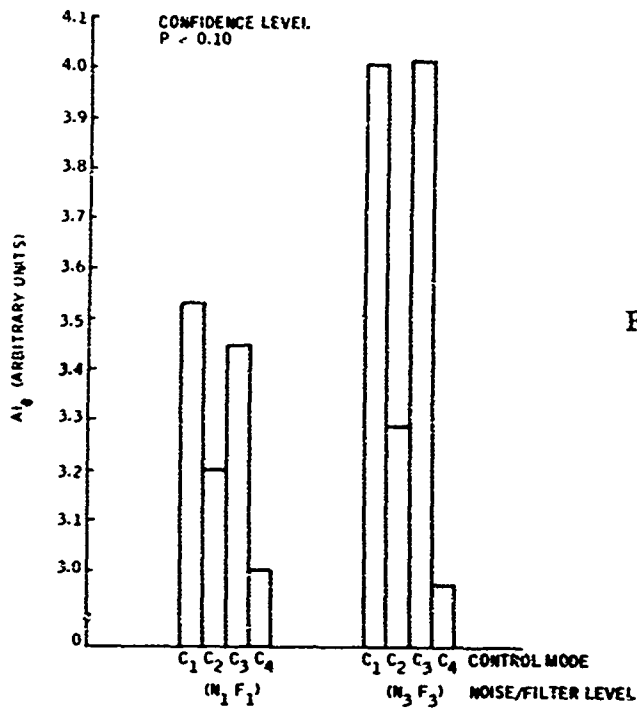
3.9

3.7

3.5

3.3

3.1

2.9

0

AI_θ (ARBITRARY UNITS)

CONFIDENCE LEVEL:
P < 0.10

c_1 c_2 c_3 c_4 c_1 c_2 c_3 c_4 CONTROL MODE

A_1 A_2 APPROACH ANGLE

D9

Figure D19. Mean AI_θ for Each Noise/ Filter Level and Control Mode: Phase P_2; UH-1 Aircraft

Figure D20. Mean AI_θ for Each Noise Level and Control Mode: Phase P_3; UH-1 Aircraft

Figure D21. Mean AI_ϕ for Each Noise/Filter Level and Control Mode: Phase P_2; UH-1 Aircraft

Figure D22. Mean AI_ϕ for Each Noise/Filter Level and Control Mode: Phase P_3; UH-1 Aircraft

D11
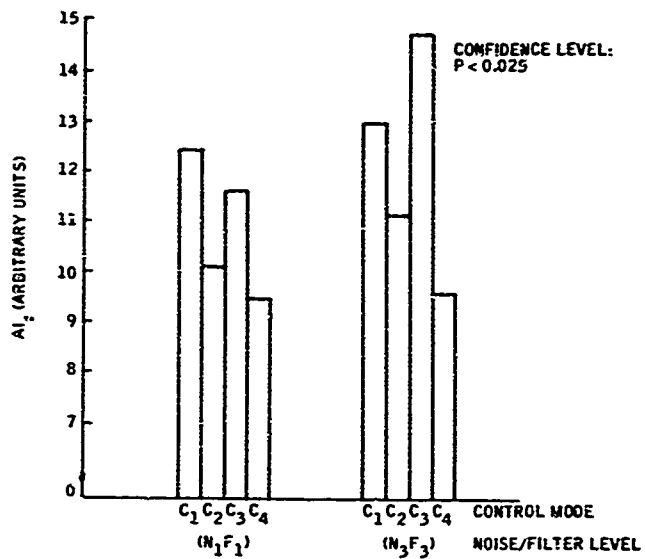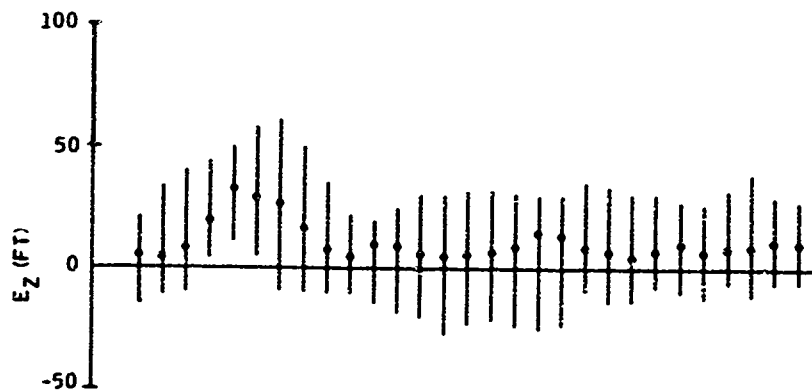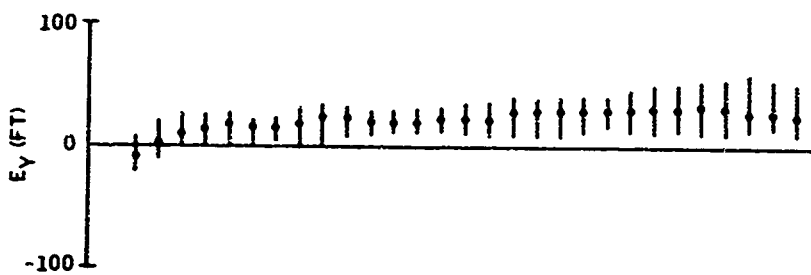
Figure D23.   Final-Approach Median and ±34th-Percentile
Data at 250-ft Intervals: UH-1 Aircraft
(1 of 4)
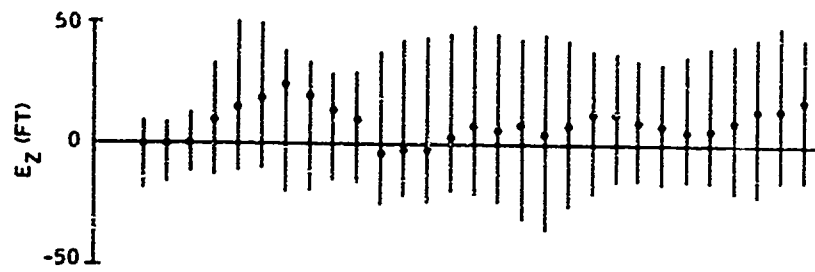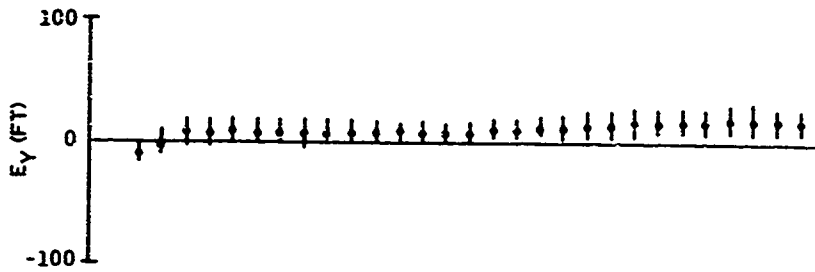
Figure D24. Final-Approach Median and ±34th-Percentile
Data at 250-ft Intervals: UH-1 Aircraft
(2 of 4)

D13

Figure D25. Final-Approach Median and ±34th-Percentile
Data at 250-ft Intervals: UH-1 Aircraft
(3 of 4)

D14
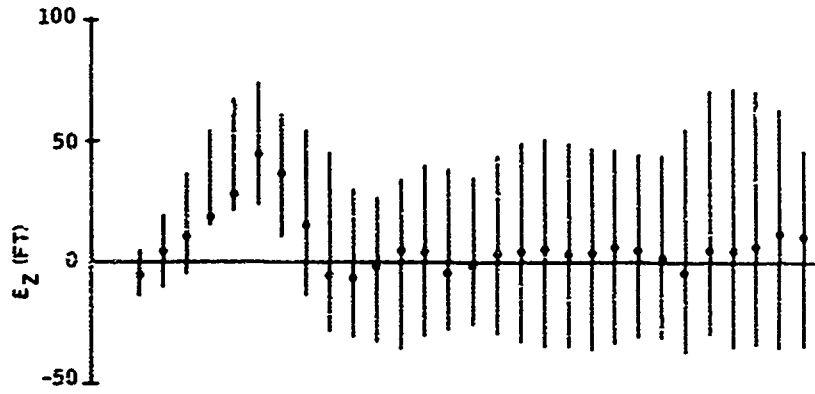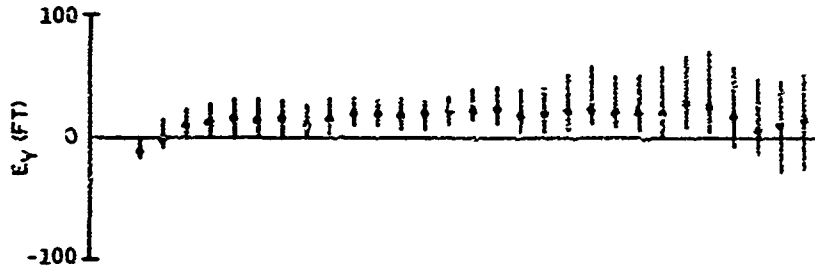
Figure D26. Final-Approach Median and ±34th-Percentile
Data at 250-ft Intervals: UH-1 Aircraft
(4 of 4)

D15

Figure D27.   Terminal Median and ±34th-Percentile Data for $\dot{X}_B$: UH-1 Aircraft
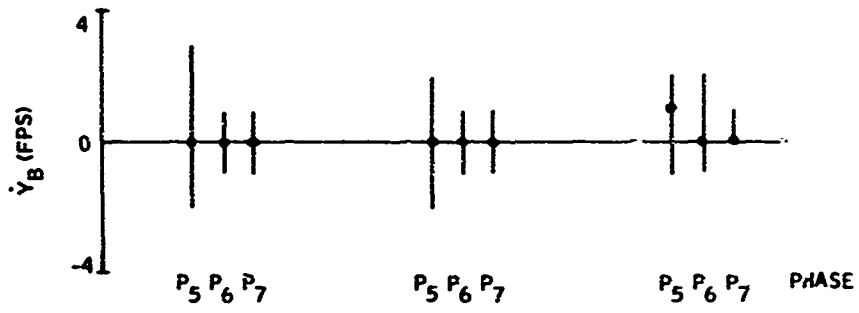
Figure D28. Terminal Median and ±34th-Percentile Data for $\dot{Y}_B$: UH-1 Aircraft

Q	N	F	A	C	D	V
1	1	1	1	1	2	1

Q	N	F	A	C	D	V
1	1	1	1	2	2	1

Q	N	F	A	C	D	V
1	1	1	1	3	2	1

E_X (FT) — values plotted from -200 to 200 across phases P_5 P_6 P_7 (PHASE)

Q	N	F	A	C	D	V
1	3	3	1	1	2	1

Q	N	F	A	C	D	V
1	3	3	1	2	2	1

Q	N	F	A	C	D	V
1	3	3	1	3	2	1

E_X (FT) — values plotted from -200 to 200 across phases P_5 P_6 P_7 (PHASE)

Figure D29.   Terminal Median and ±34th-Percentile Data
for E_X: UH-1 Aircraft

D18

Q	N	F	A	C	D	V
1	1	1	1	1	2	1

Q	N	F	A	C	D	V
1	1	1	1	2	2	1

Q	N	F	A	C	D	V
1	1	1	:,;	?	1	

E_Y (FT)

40

0

-40

P_5 P_6 P_7 P_5 P_6 P_7 P_5 P_6 P_7 PHASE

Q	N	F	A	C	D	V
1	3	3	1	1	2	1

Q	N	F	A	C	D	V
1	3	3	1	2	2	1

Q	N	F	A	C	D	V
1	3	3	1	3	2	1

E_Y (FT)

40

0

-40

P_5 P_6 P_7 P_5 F_6 P_7 P_5 P_6 P_7 PHASE

Figure D30.   Terminal Median and ±34th-Percentile Data
for E_Y: UH-1 Aircraft

Figure D31. Terminal Median and ±34th-Percentile Data
for θ: UH-1 Aircraft

Q	N	F	A	C	D	V
1	1	1	1	1	2	1

Q	N	F	A	C	D	V
1	1	1	1	2	2	1

Q	N	F	A	C	D	V
1	1	1	1	3	2	1

Q	N	F	A	C	D	V
1	3	3	1	1	2	1

Q	N	F	A	C	D	V
1	3	3	1	2	2	1

Q	N	F	A	C	D	V
1	3	3	1	3	2	1

Figure D32. Terminal Median and ±34th-Percentile Data
for ϕ: UH-1 Aircraft

D21
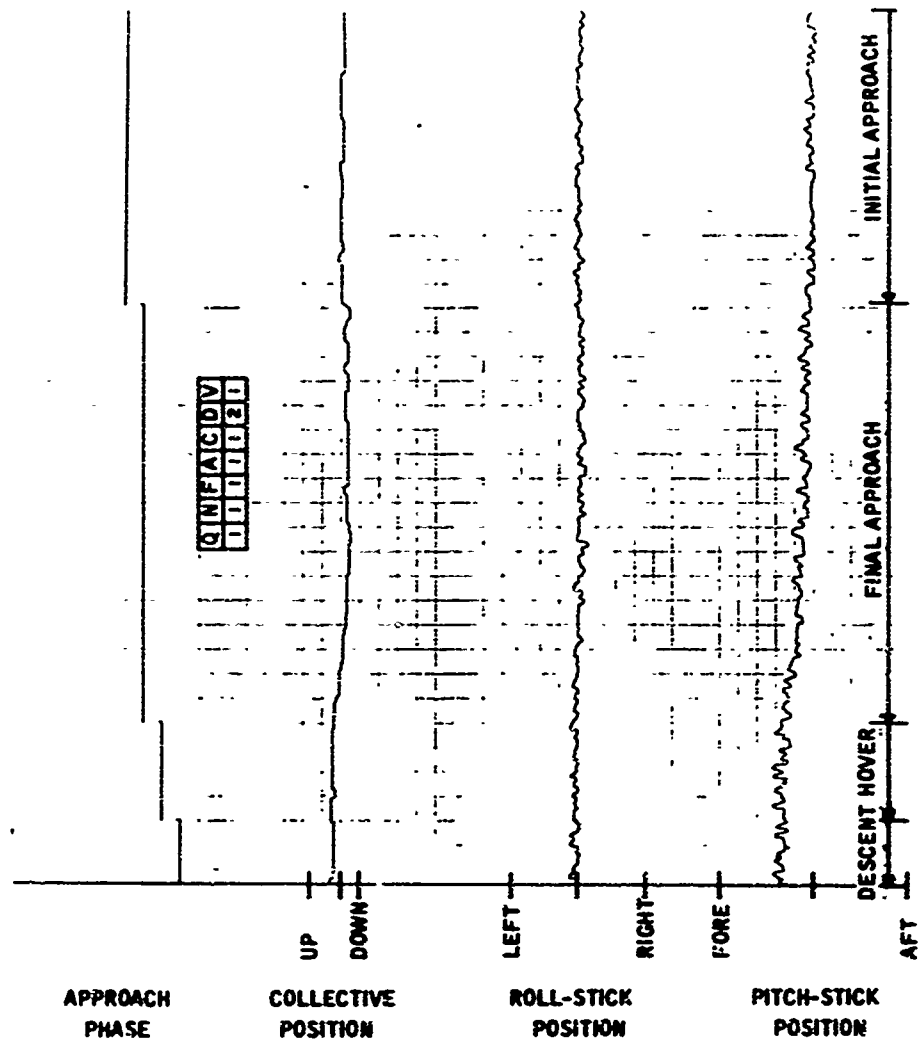
Figure D33.   Continuous Time-History Recordings;
UH-1 Aircraft (part 1 of 2)

D22

Figure D33.   Continuous Time-History Recordings:
UH-1 Aircraft (part 2 of 2)

D23
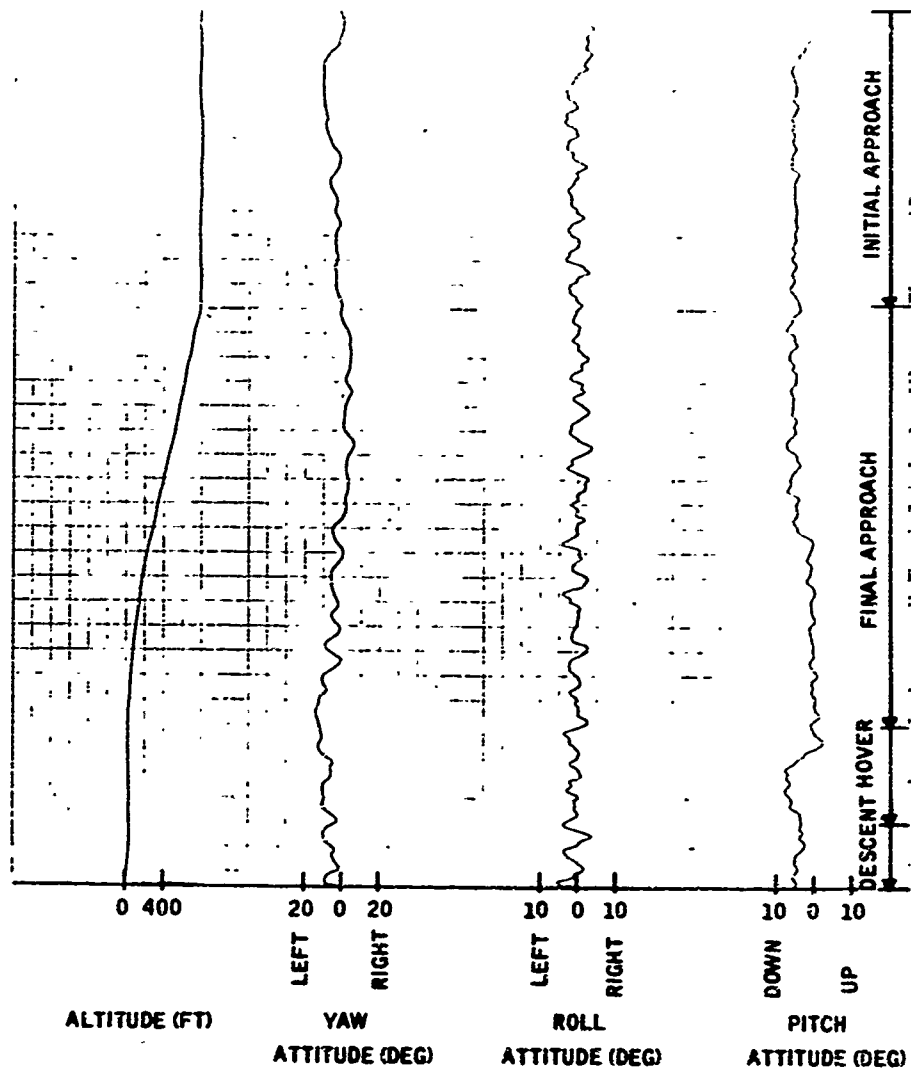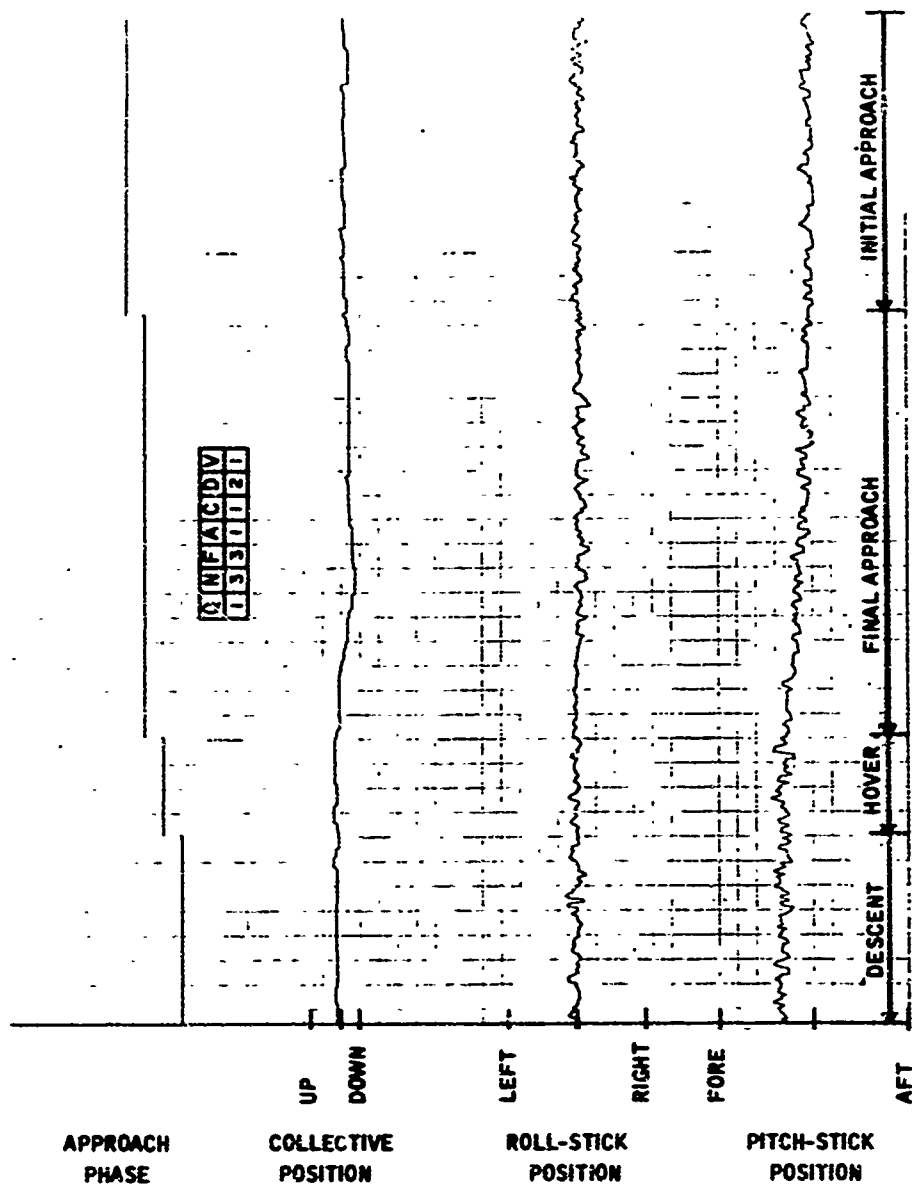
Figure D34. Continuous Time-History Recordings:
UH-1 Aircraft (part 1 of 2)

Figure D34. Continuous Time-History Recordings:
UH-1 Aircraft (part 2 of 2)
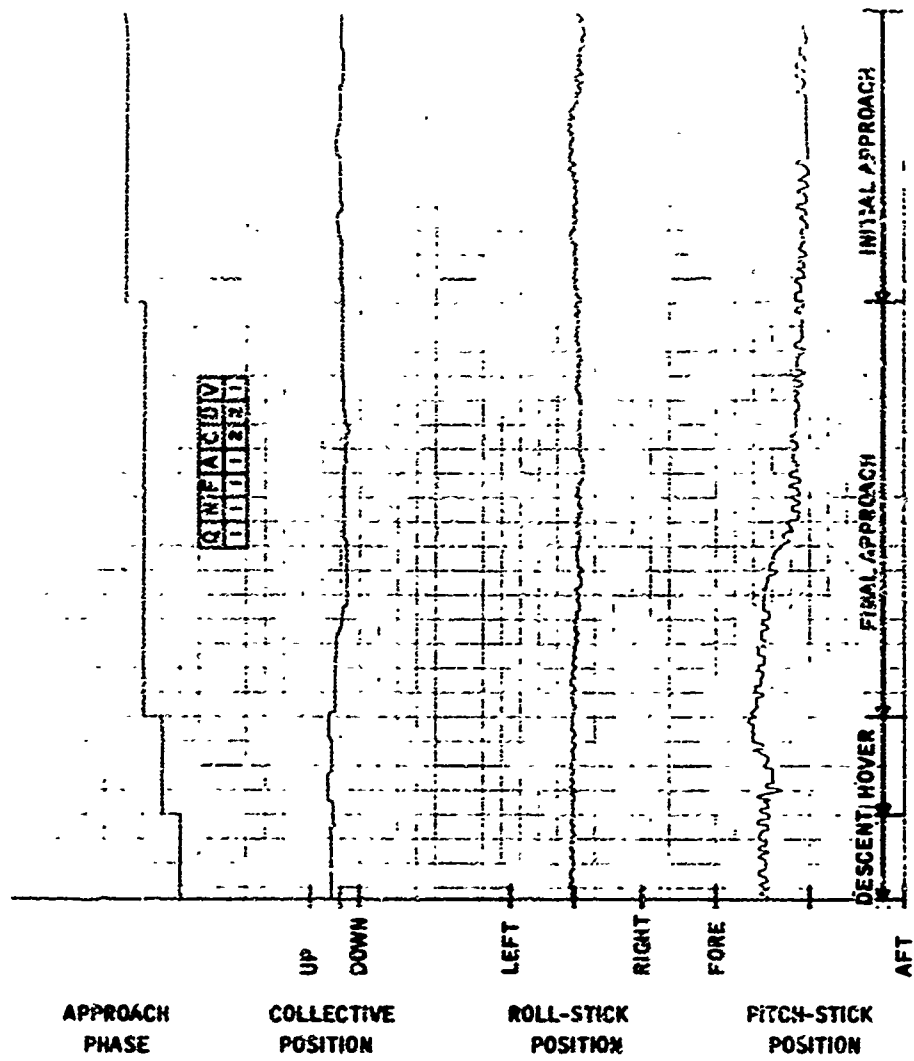
D25

Figure D35. Continuous Time-History Recordings:
UH-1 Aircraft (part 1 of 2)

D26

Figure D35. Continuous Time-History Recordings:
UH-1 Aircraft (part 2 of 2)

D27
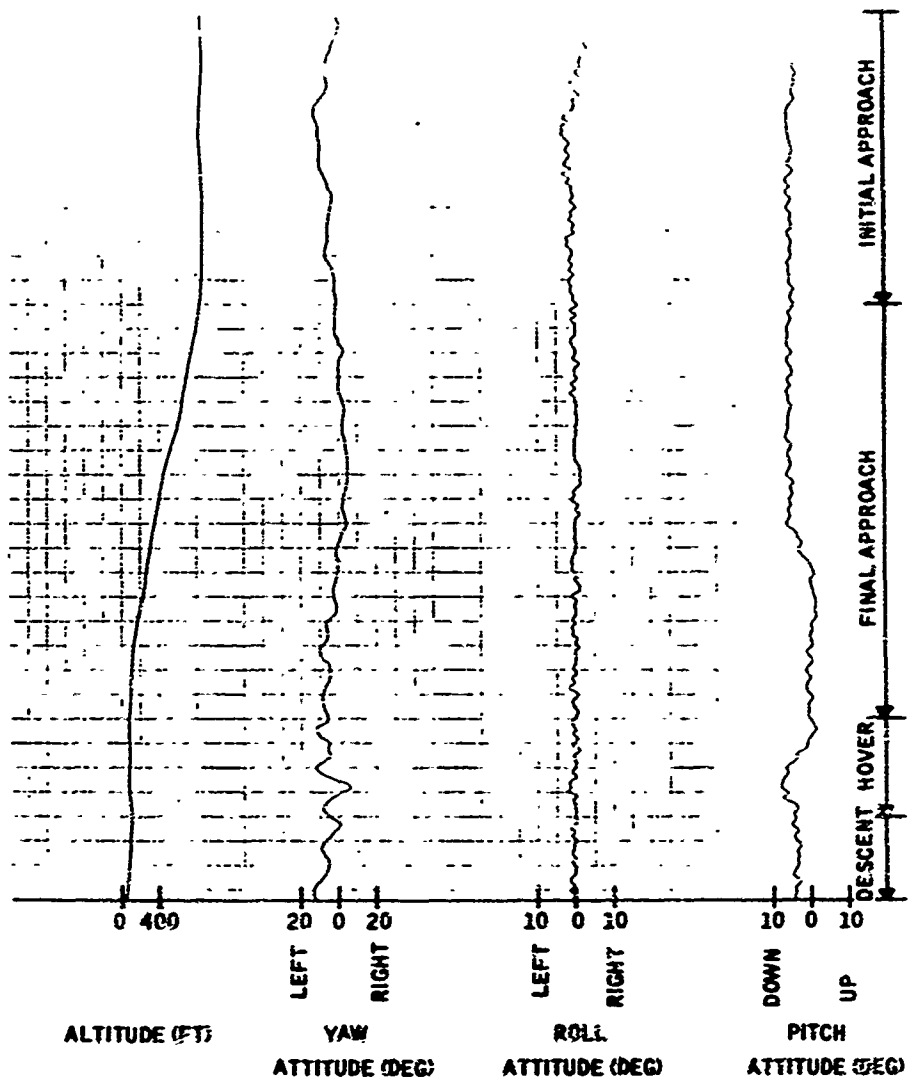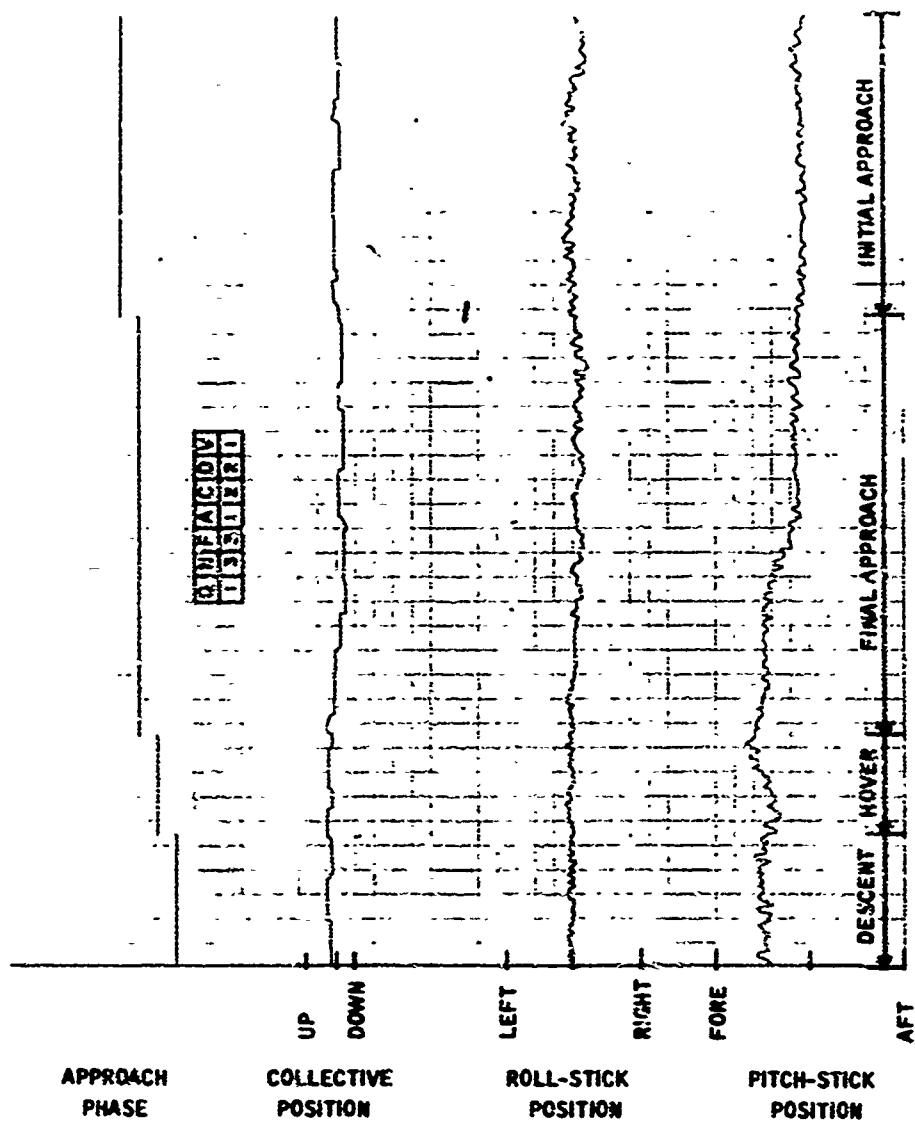
Figure D36. Continuous Time-History Recordings:
UH-1 Aircraft (part 1 of 2)
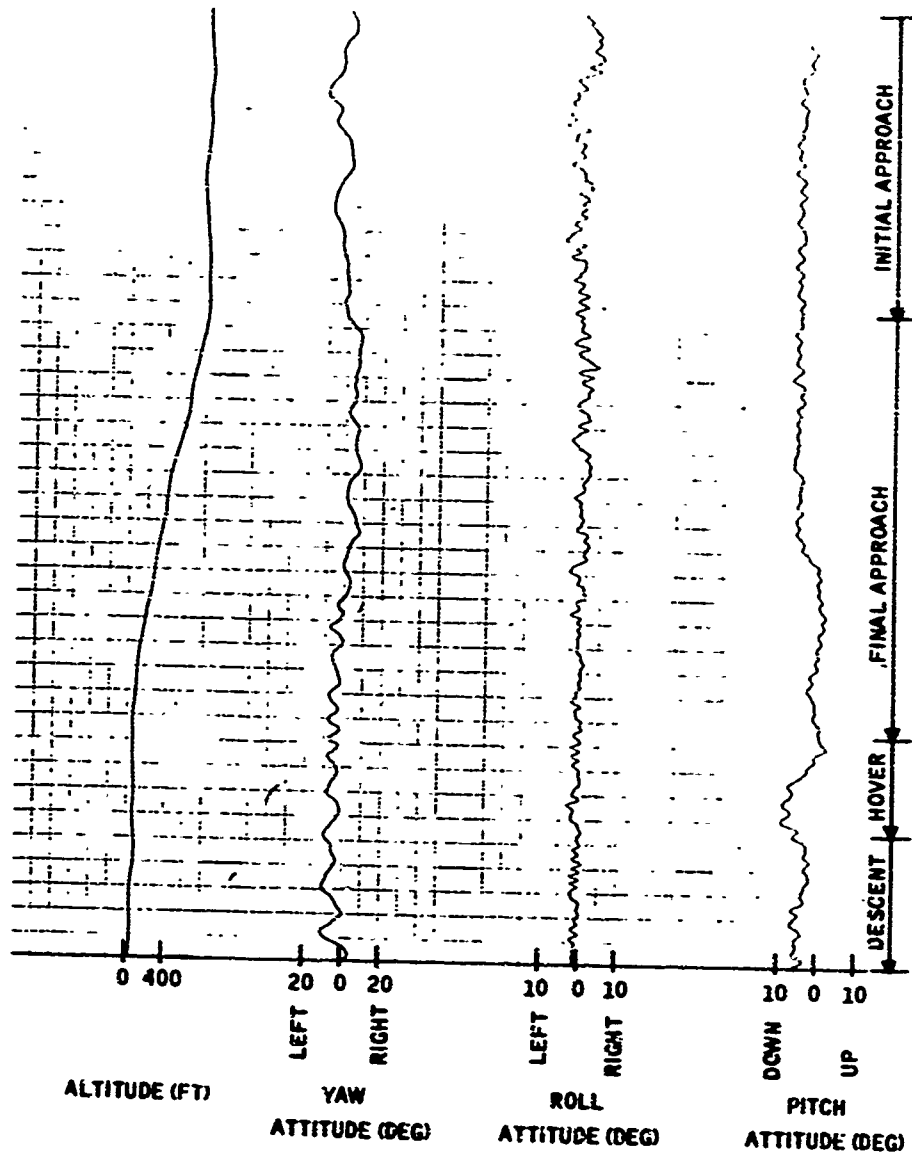
Figure D36. Continuous Time-History Recordings:
UH-1 Aircraft (part 2 of 2)
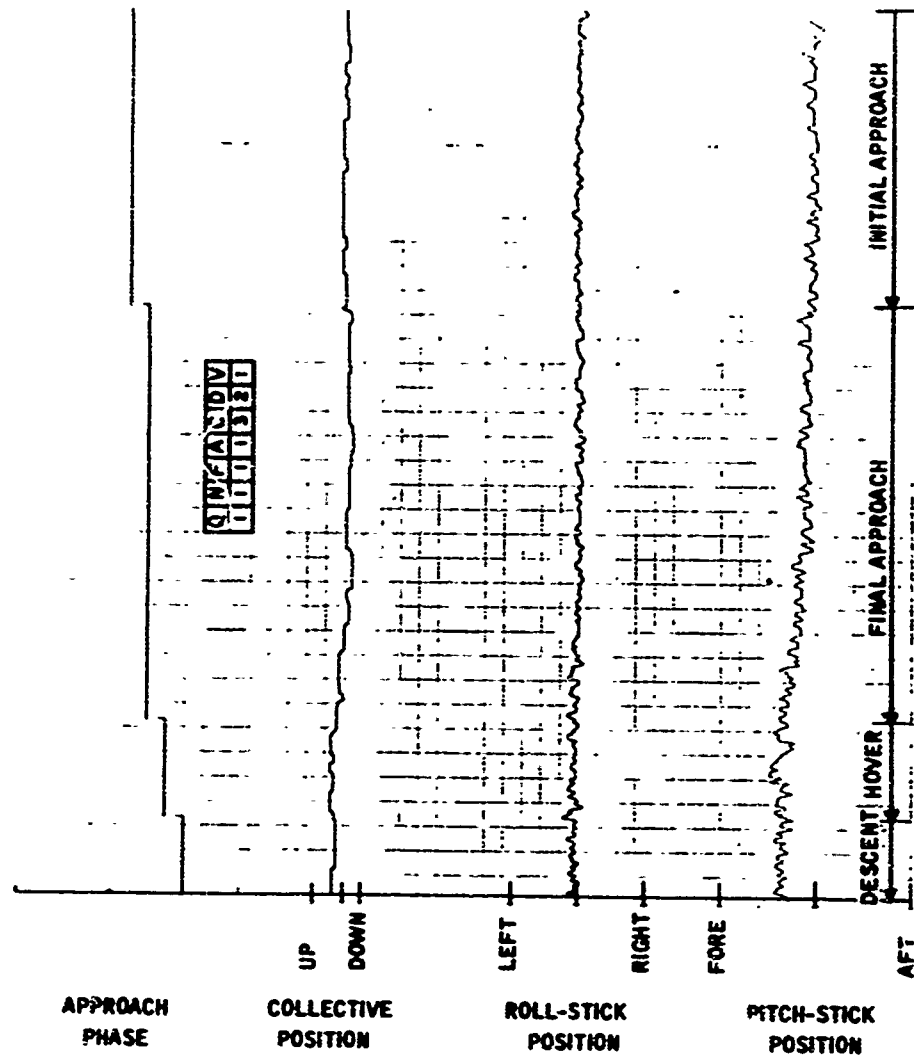
Figure D37. Continuous Time-History Recordings:
UH-1 Aircraft (part 1 of 2)
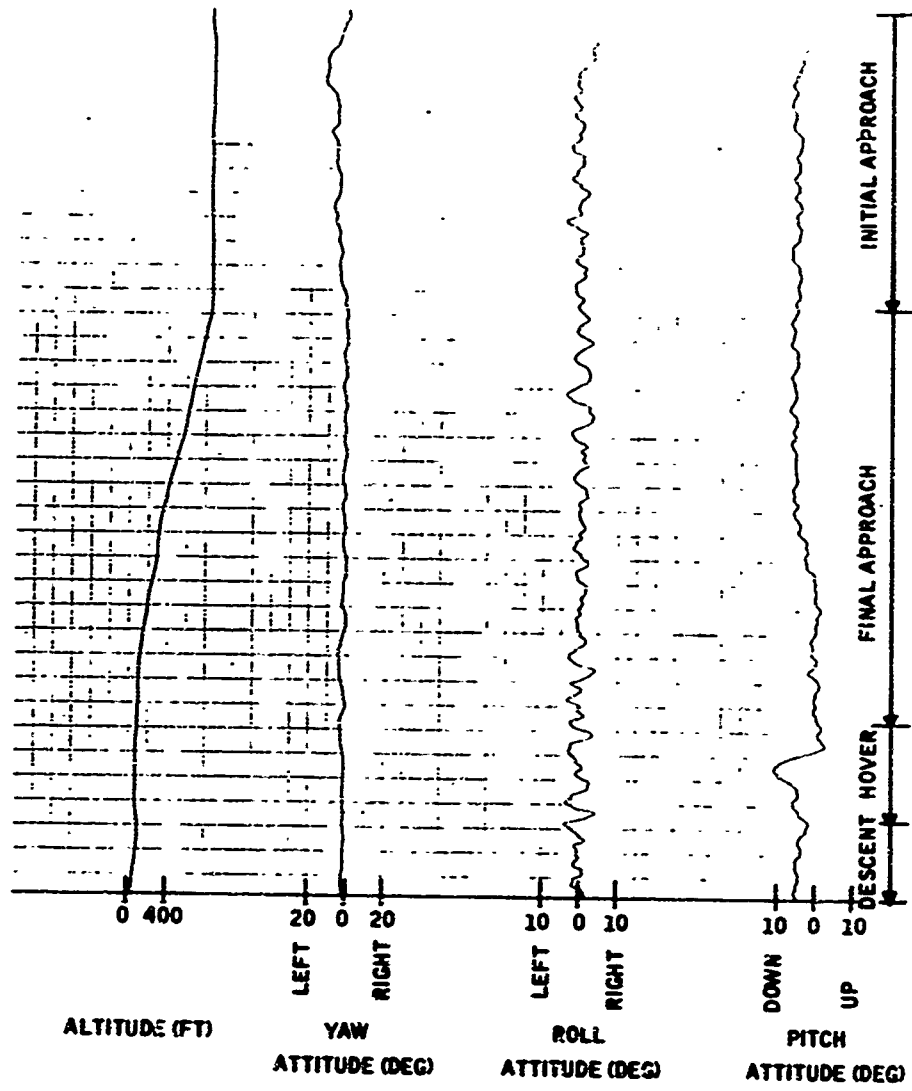
Figure D37. Continuous Time-History Recordings:
UH-1 Aircraft (part 2 of 2)
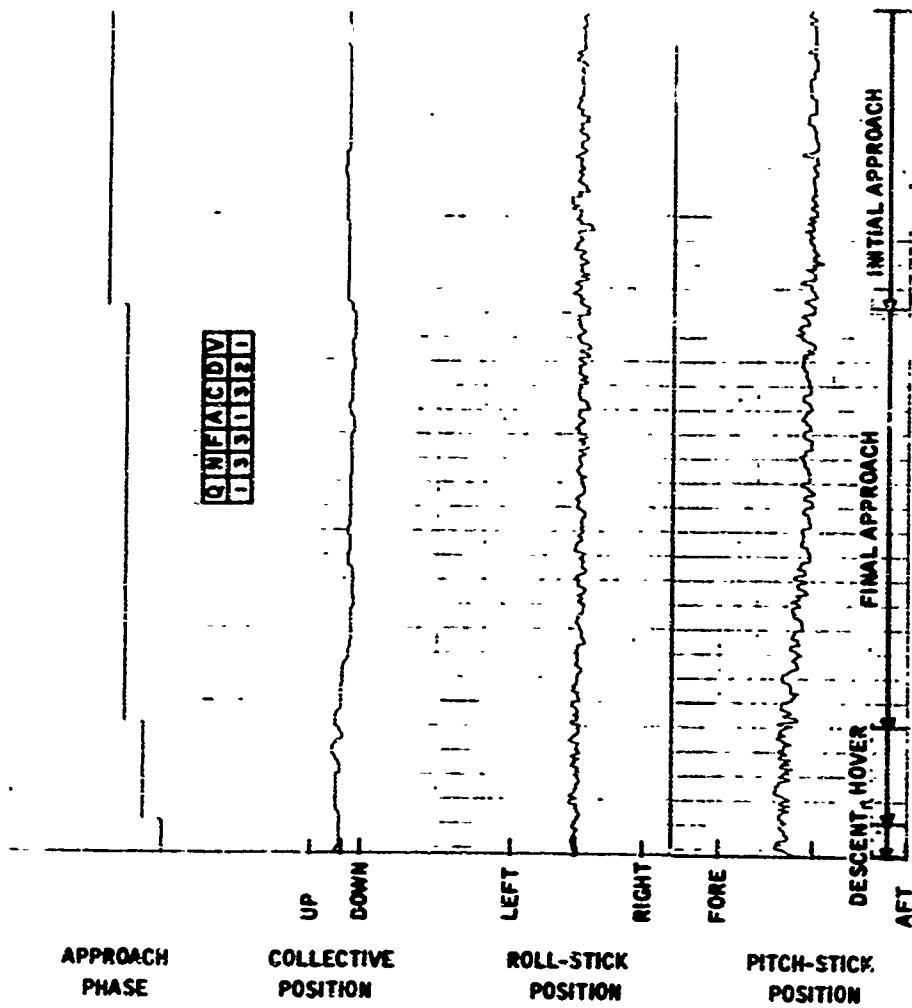
Figure D38. Continuous Time-History Recordings:
UH-1 Aircraft (part 1 of 2)
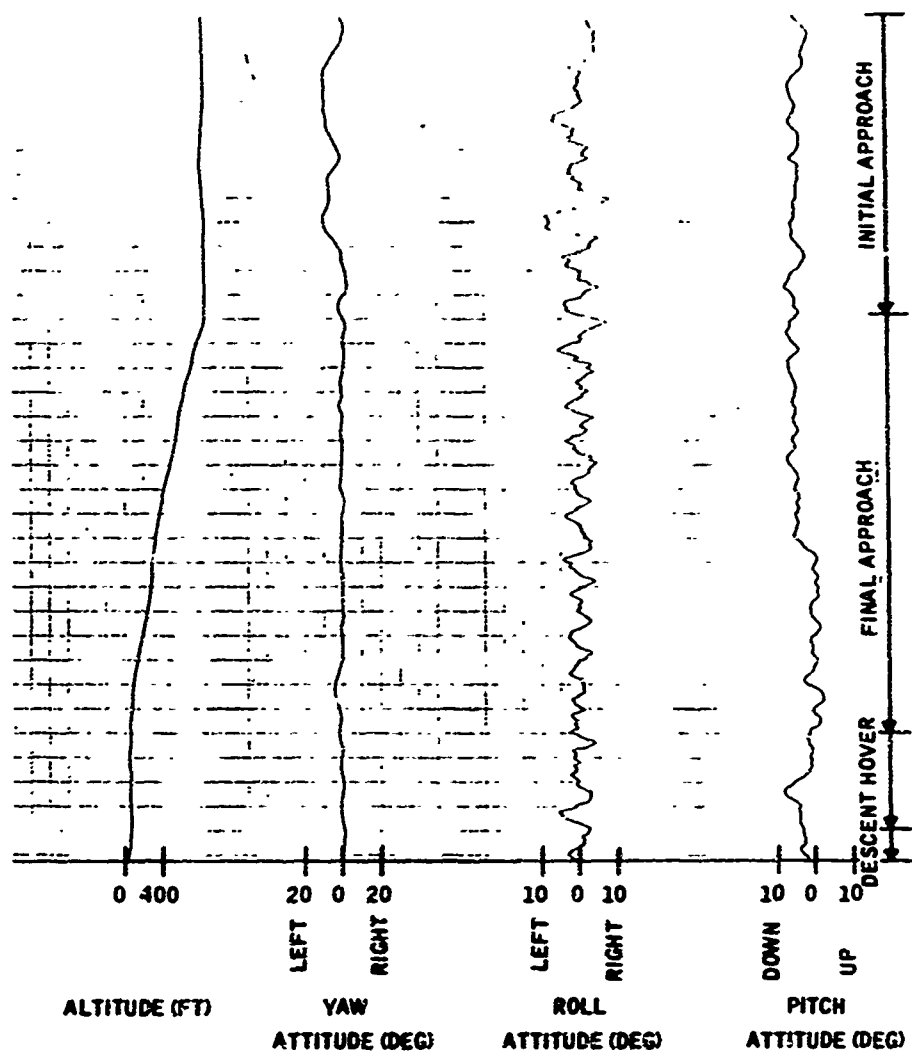
Figure D38. Continuous Time-History Recordings:
UH-1 Aircraft (part 2 of 2)
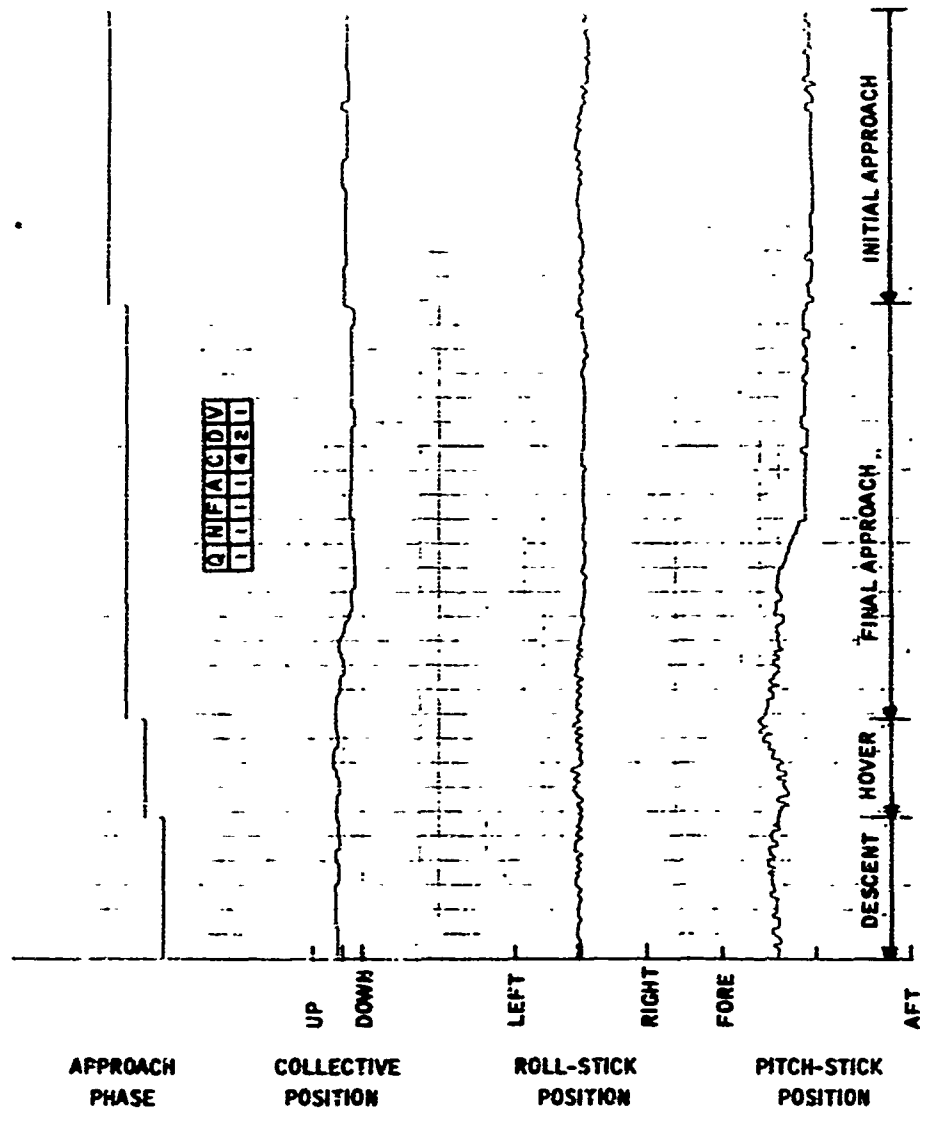
Figure D39. Continuous Time-History Recordings:
UH-1 Aircraft (part 1 of 2)
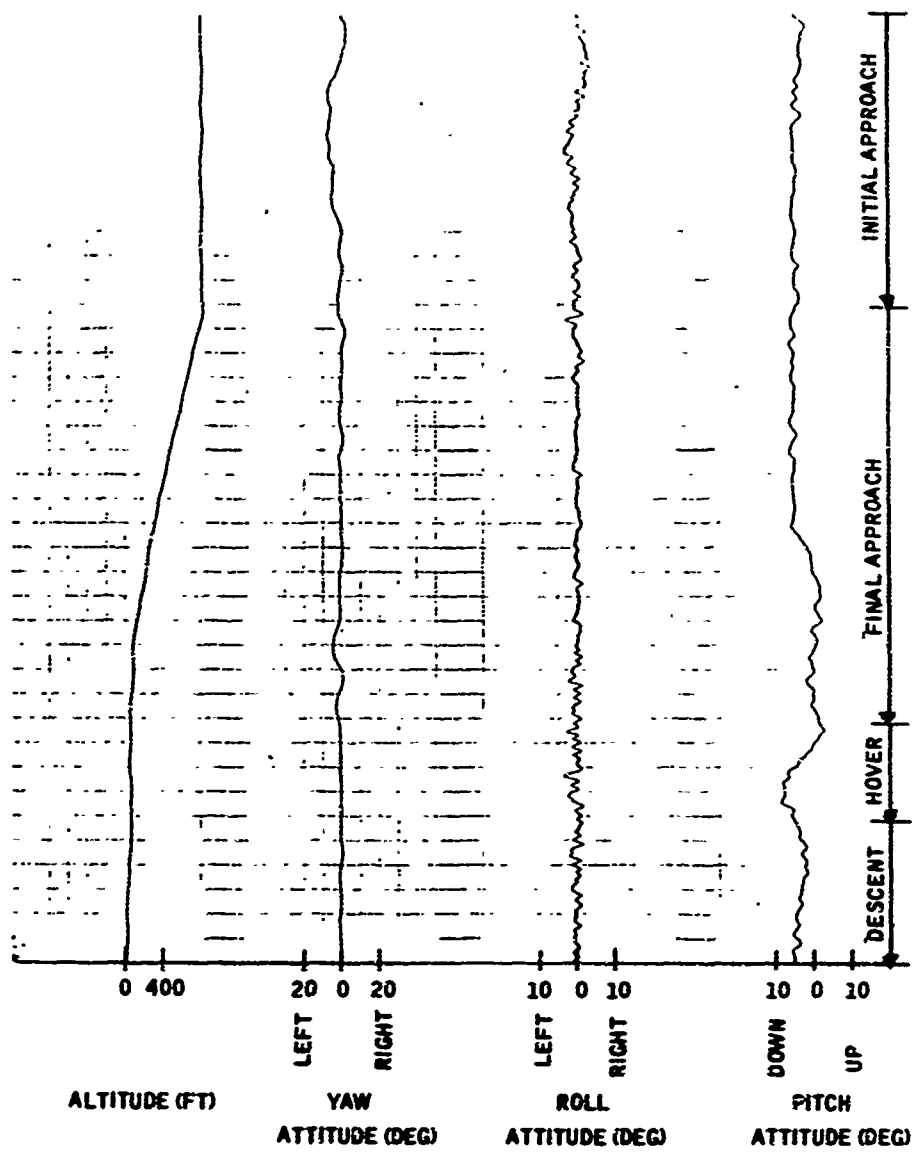
Figure D39. Continuous Time-History Recordings:
UH-1 Aircraft (part 2 of 2)

Figure D40.   Continuous Time-History Recordings:
UH-1 Aircraft (part 1 of 2)

D36

Figure D40. Continuous Time-History Recordings:
UH-1 Aircraft (part 2 of 2)

D37
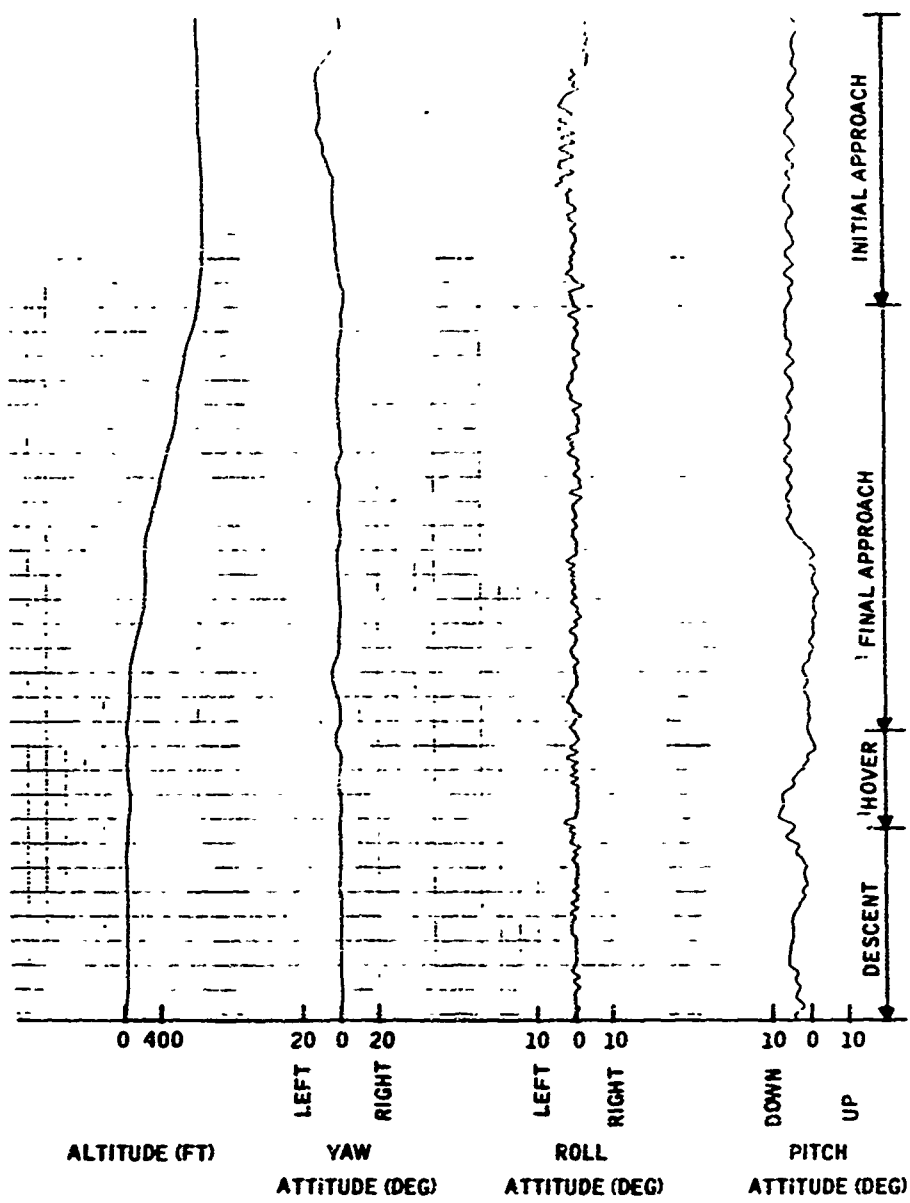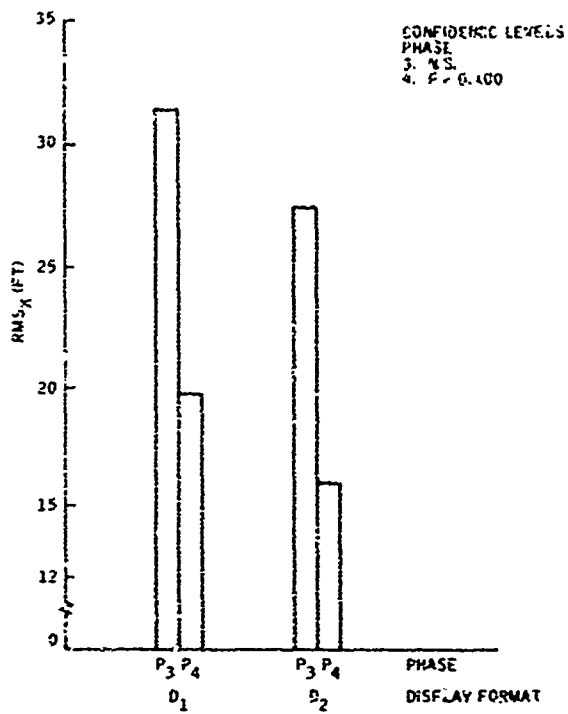
Figure D41. Mean RMS$_X$ Error for
Each Display Format and
Phase: XV-5 Aircraft

Figure D42. Mean RMS$_Y$ Error for Each
Display Format and Phase:
XV-5 Aircraft

D38
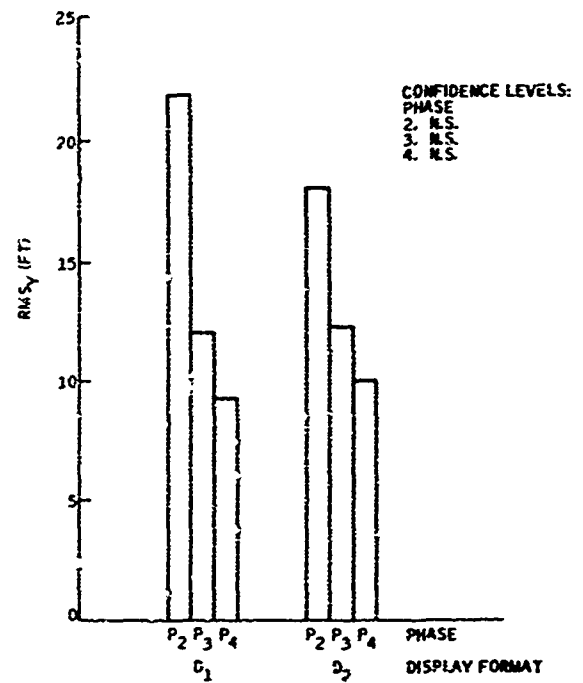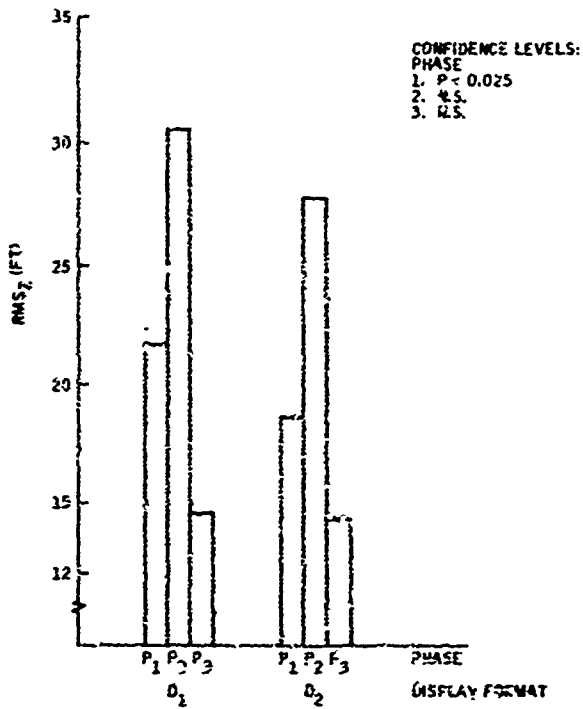
Figure D43. Mean RMS$_Z$ Error for Each Display Format and Phase: XV-5 Aircraft

Figure D44. Mean AI$_\theta$ for Each Display Format and Phase: XV-5 Aircraft

D39

30

CONFIDENCE LEVELS
PHASE
1 N.S.
2. N.S.
3. N.S.
4. N.S.

25

AI_z (ARBITRARY UNITS)

20

15

10

0

P_1 P_2 P_3 P_4 P_1 P_2 P_3 P_4 PHASE
D_1 D_2 DISPLAY FORMAT
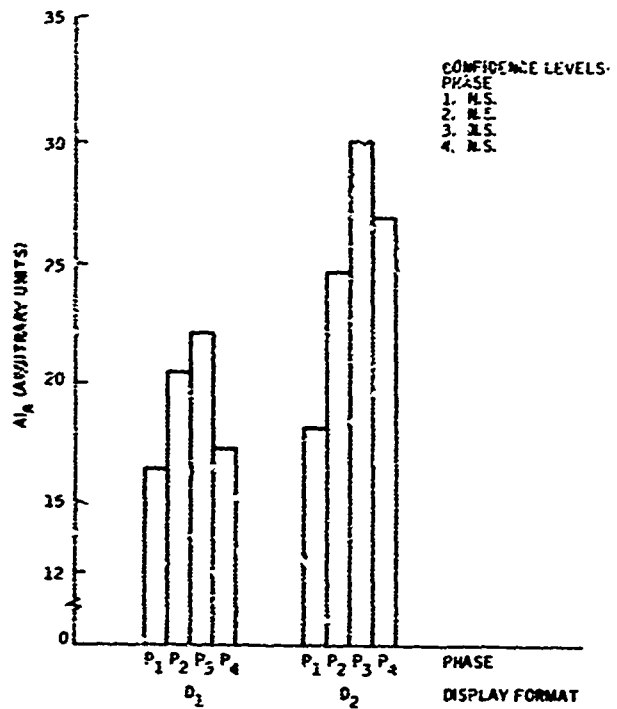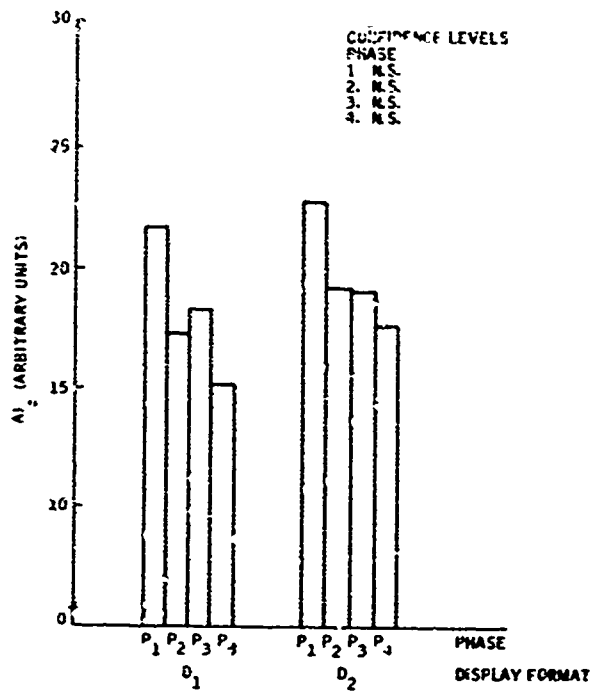
Figure D45. Mean AI_c for Each Display
Format and Phase: XV-5
Aircraft

Figure D46. Mean RMS_Z Error for
Each Approach Angle and
Phase: XV-5 Aircraft

35

CONFIDENCE LEVELS·
PHASE
1. $P < 0.100$
2. N.S.
3. $P < 0.100$

30

RMS_Z (FT)

25

20

15

12

0

P_1 P_2 P_3 P_1 P_2 P_3 PHASE
A_1 A_2 APPROACH ANGLE

D40
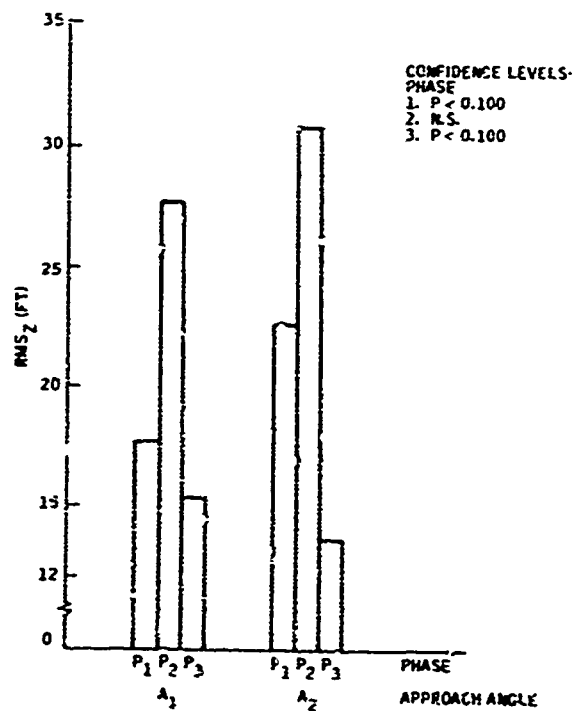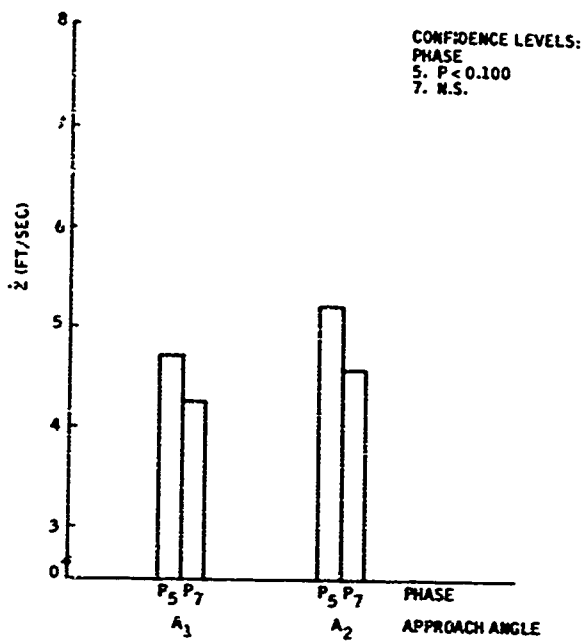
Figure D47. Mean $\dot{Z}$ for Each Approach Angle and Phase: XV-5 Aircraft

Figure D48. Mean RMS_y Error for Each Noise/Filter Level and Phase: XV-5 Aircraft
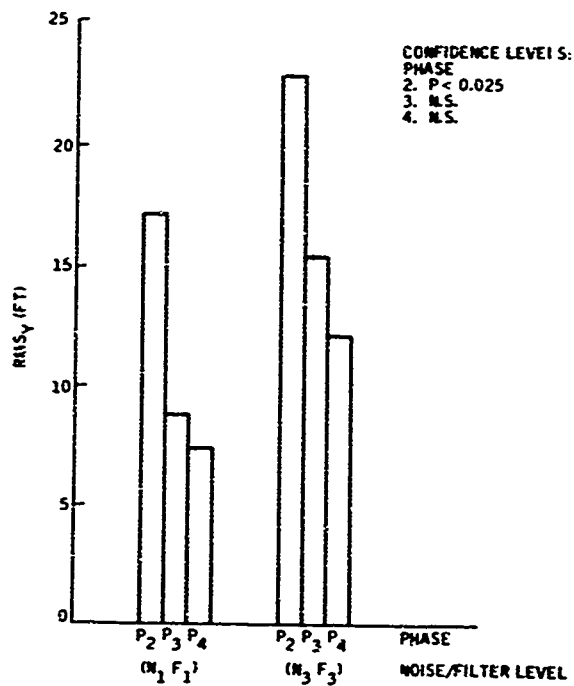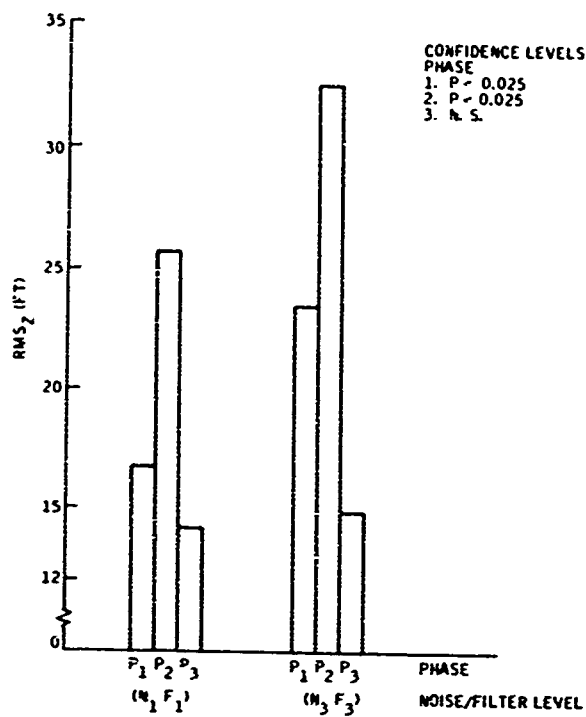
Figure D49. Mean RMS_Z Error for Each Noise/Filter Level and Phase: XV-5 Aircraft

Figure D50. Mean AI_θ for Each Noise/Filter Level and Phase: XV-5 Aircraft
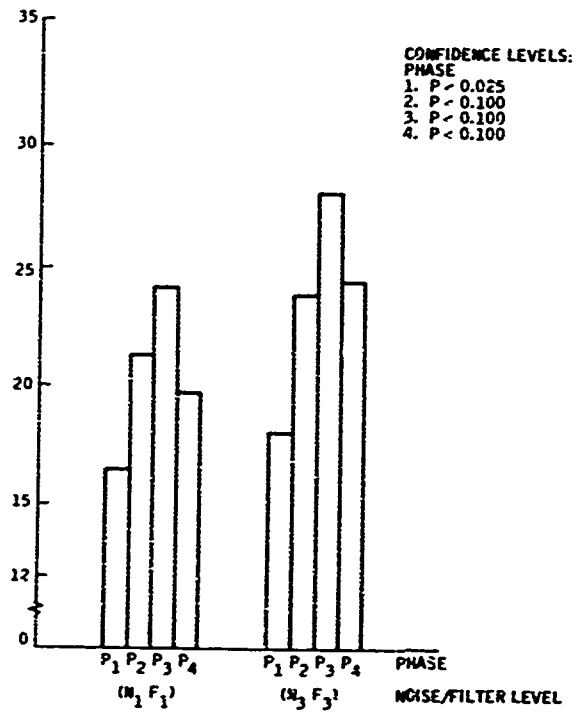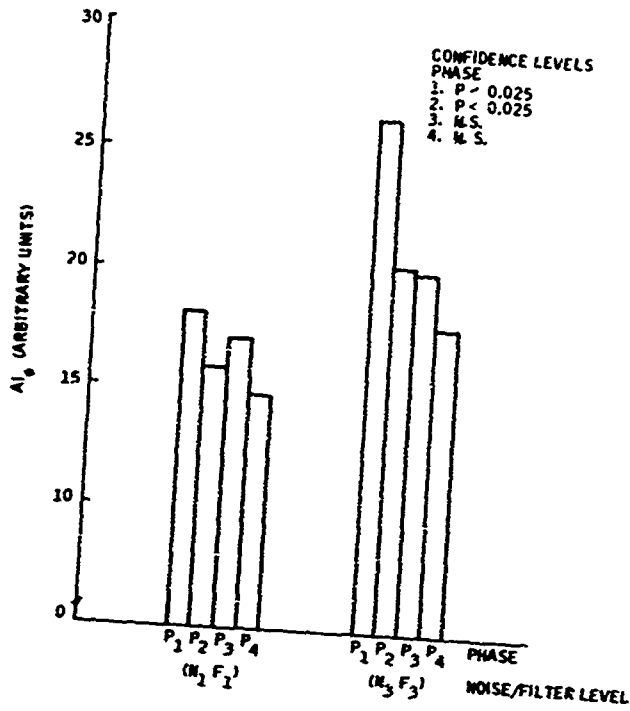
Figure D51. Mean AI_ϕ for Each Noise/Filter Level and Phase: XV-5 Aircraft

Figure D52. Mean RMS_X Error for Each Control Mode and Phase: XV-5 Aircraft

D43
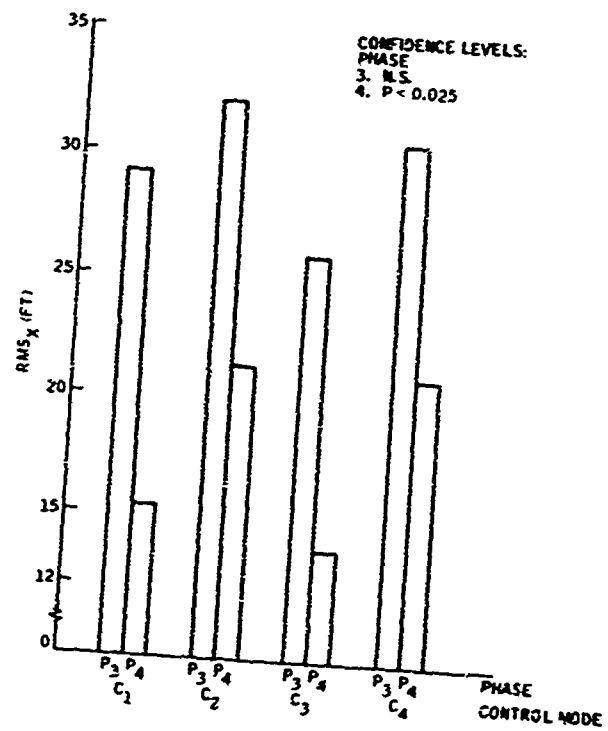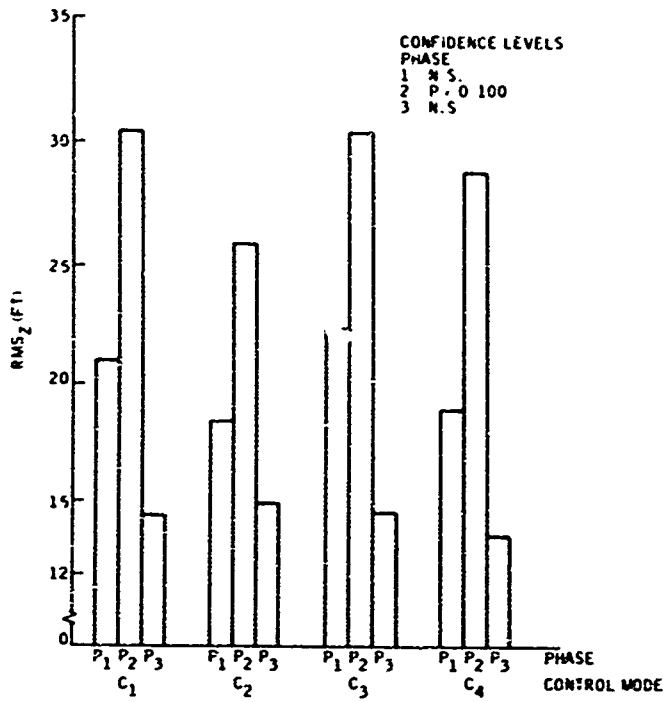
Figure D53. Mean RMS_Z Error for Each Control Mode and Phase: XV-5 Aircraft

Figure D54. Mean AI_θ for Each Control Mode and Phase: XV-5 Aircraft

D44
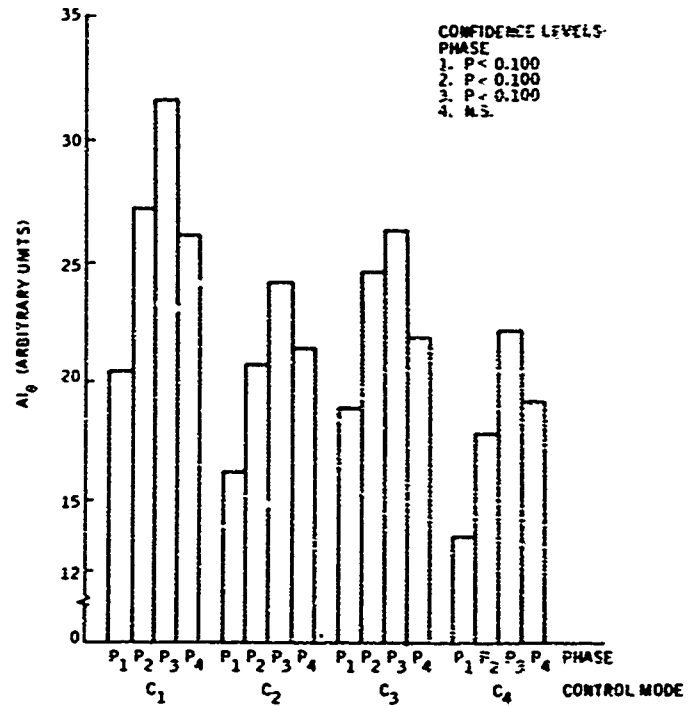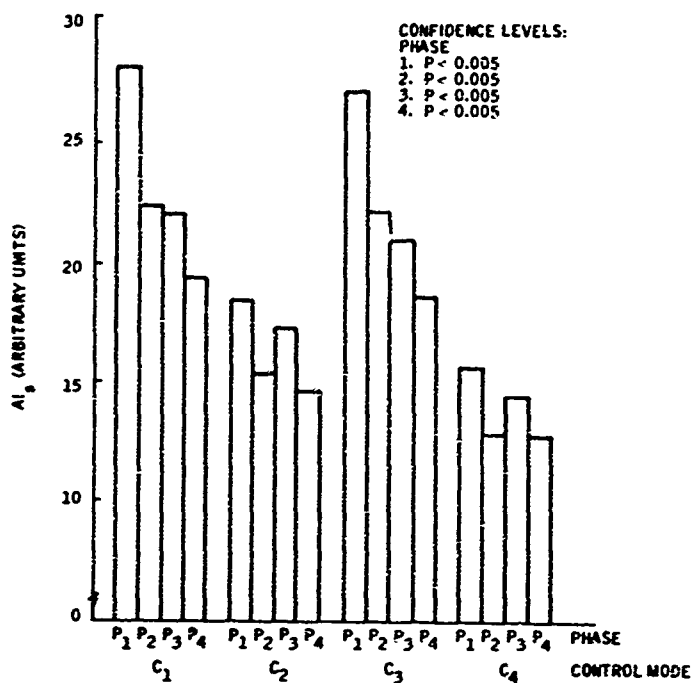
Figure D55.   Mean AI_ϕ for Each Control Mode and Phase: XV-5 Aircraft

Figure D56.   Mean AI_θ for Each Noise/Filter Level and Control Mode: Phase P_1; XV-5 Aircraft
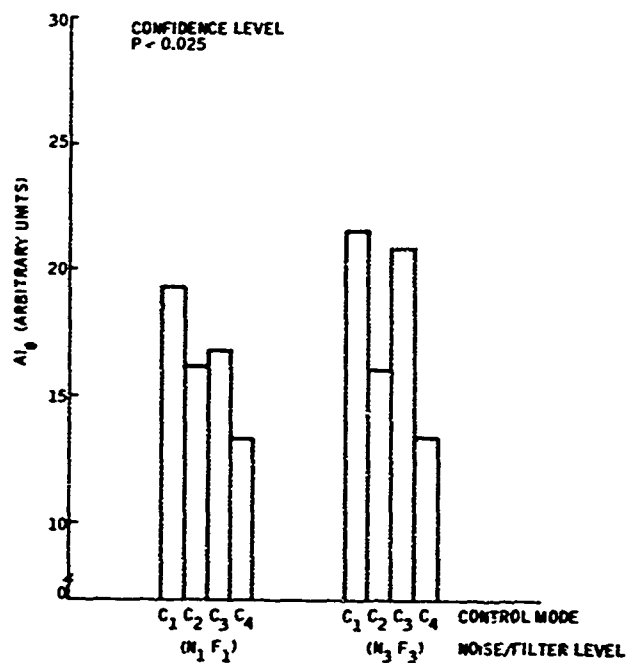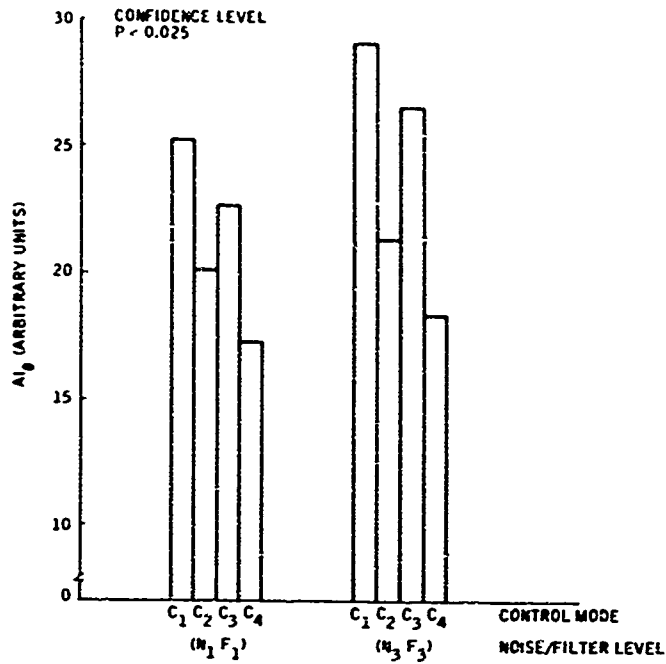
Figure D57. Mean AI_θ for Each Noise/ Filter Level and Control Mode: Phase P_2; XV-5 Aircraft

Figure D58. Mean AI_ϕ for Each Noise/ Filter Level and Control Mode: Phase P_1; XV-5 Aircraft
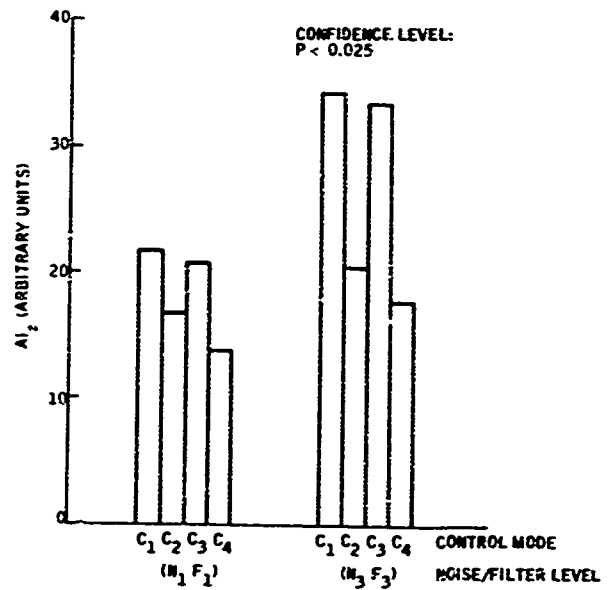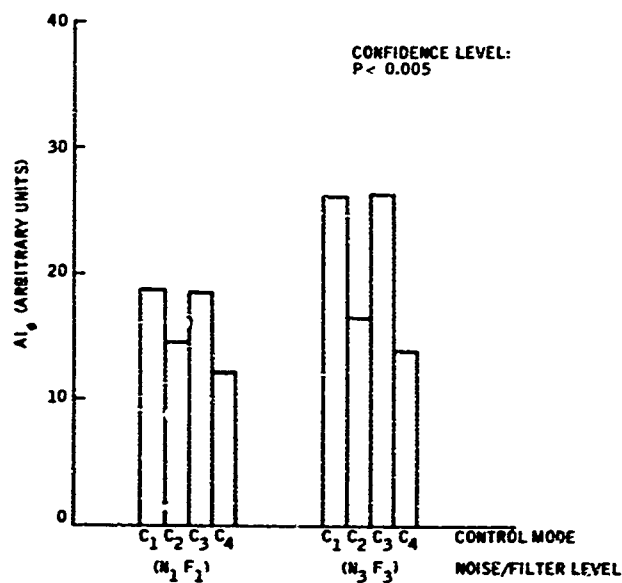
Figure D59.   Mean AI_ϕ for Each Noise/Filter Level and
Control Mode: Phase P_2; XV-5 Aircraft

D47
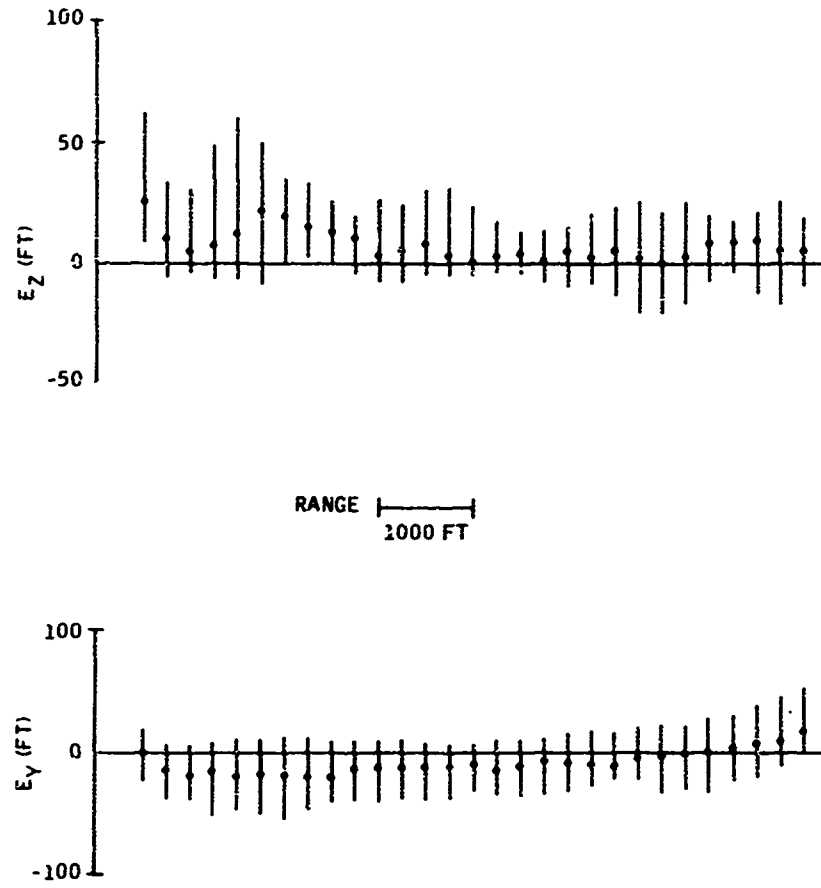
Figure D60. Final-Approach Median and ±34th-Percentile
Data at 250-ft Intervals: XV-5 Aircraft
(1 of 4)

Q	N	F	A	C	D	V
1	1	1	1	3	2	2
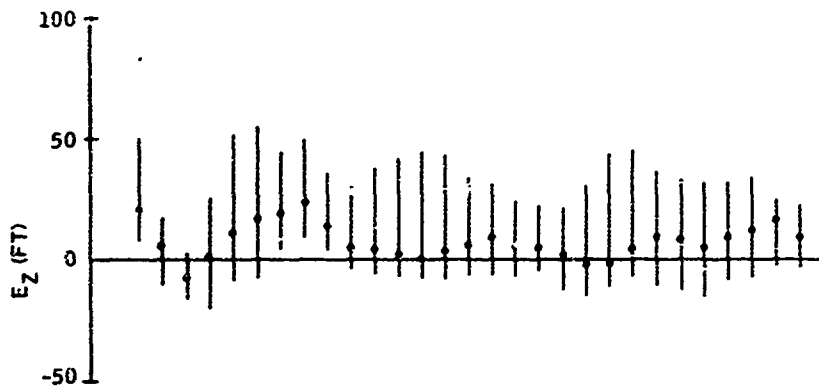
RANGE |——————|
1000 FT
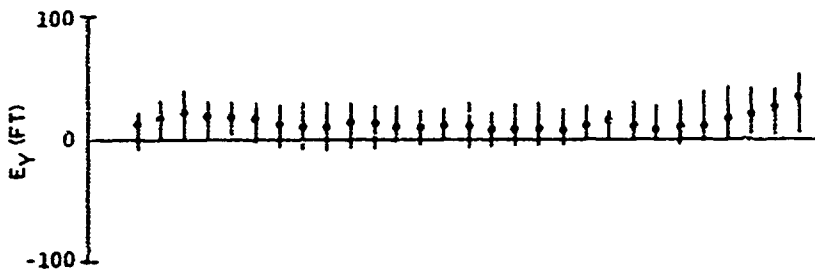
Figure D61. Final-Approach Median and ±34th-Percentile Data at 250-ft Intervals: XV-5 Aircraft (2 of 4)

D49

Q	h	F	A	C	D	V
1	3	3	1	1	2	2
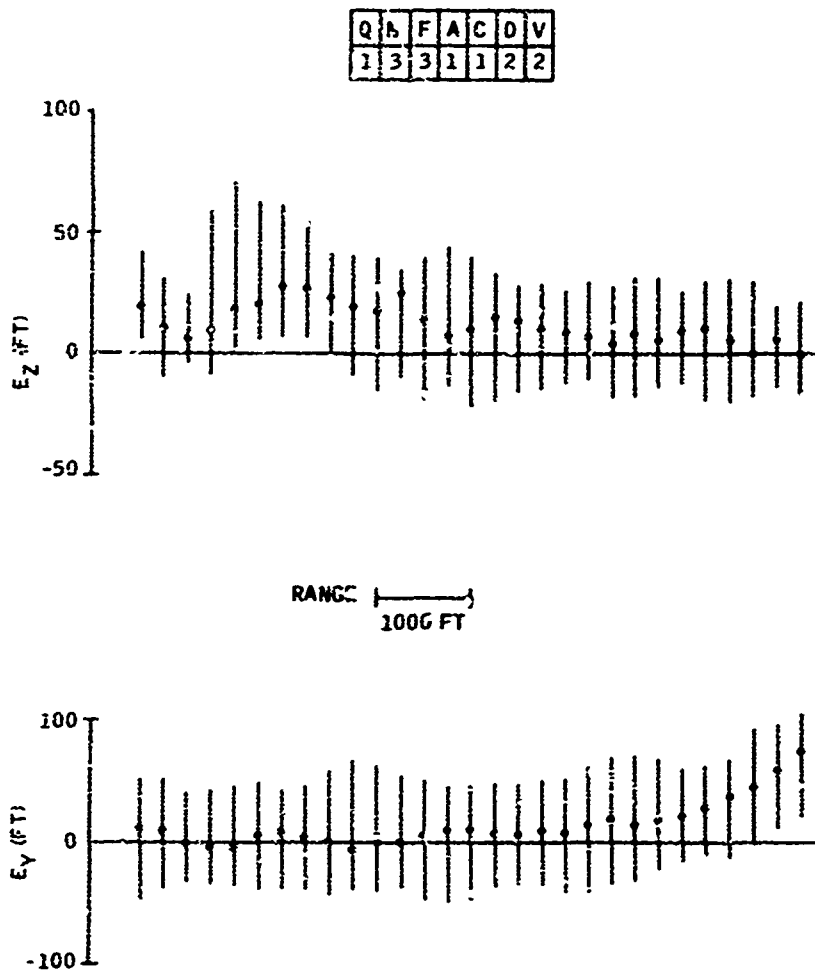
Figure D62.   Final-Approach Median and ±34th-Percentile
Data at 250-ft Intervals: XV-5 Aircraft
(3 of 4)
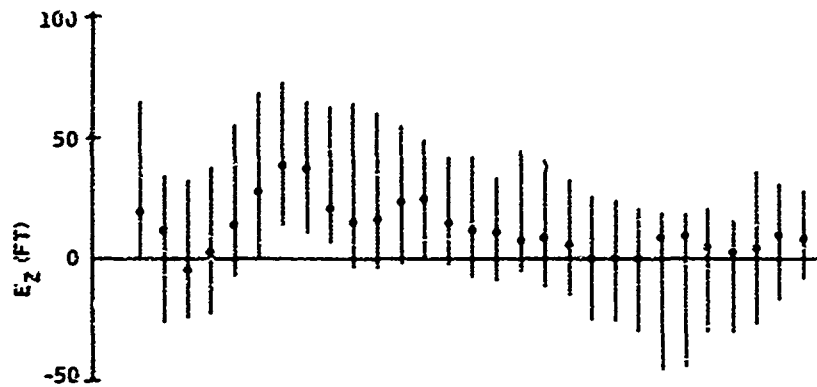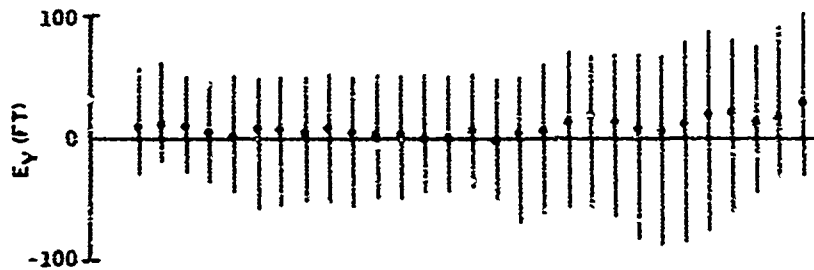
Figure D63. Final-Approach Median and ±34th-Percentile Data at 250-ft Intervals: XV-5 Aircraft (4 of 4)

D51

Q	N	F	A	C	D	V
1	1	1	1	1	2	2

Q	N	F	A	C	D	V
1	1	1	1	2	2	2

Q	N	F	A	C	D	V
1	1	1	1	3	2	2
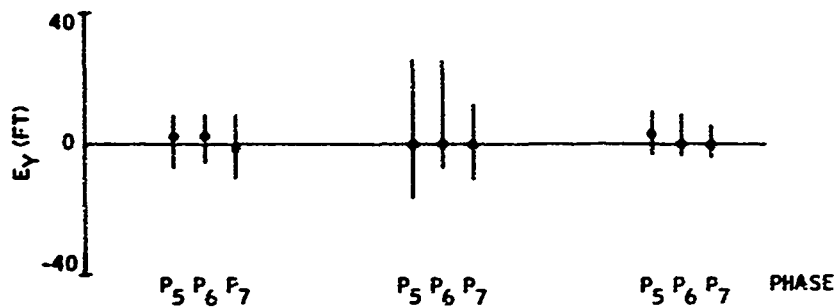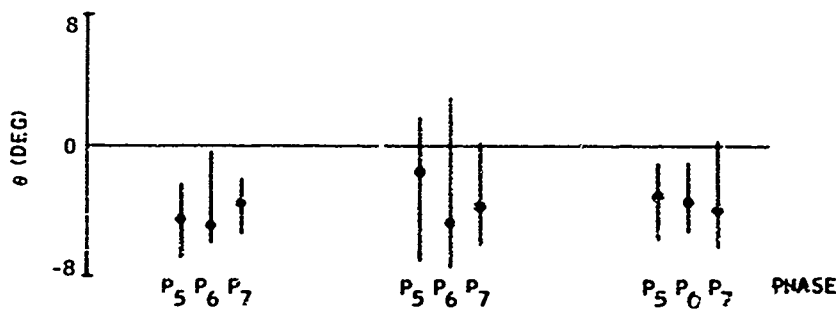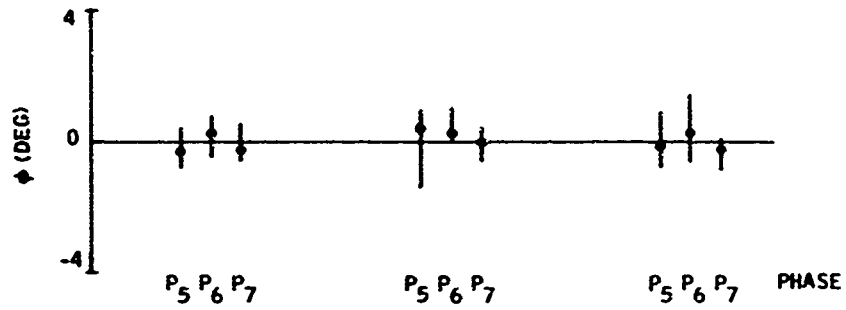
Q	N	F	A	C	D	V
1	3	3	1	1	2	2

Q	N	F	A	C	D	V
1	3	3	1	2	2	2

Q	N	F	A	C	D	V
1	3	3	1	3	2	2

Figure D64.   Terminal Median and $\pm$34th-Percentile Data
for $\dot{X}_B$:   XV-5 Aircraft

D 52

Figure D65.   Terminal Median and ±34th-Percentile Data
for $\dot{Y}_B$:   XV-5 Aircraft

D53

Figure D66. Terminal Median and ±34th-Percentile Data for E_X: XV-5 Aircraft

D54

Figure D67.   Terminal Median and ±34th-Percentile Data
for E_Y: XV-5 Aircraft

Figure D68. Terminal Median and ±34th-Percentile Data
for θ: XV-5 Aircraft

Q	N	F	A	C	D	V		Q	N	F	A	C	D	V		Q	N	F	A	C	D	V
1	1	1	1	1	2	2		1	1	1	1	2	2	2		1	1	1	1	3	2	2

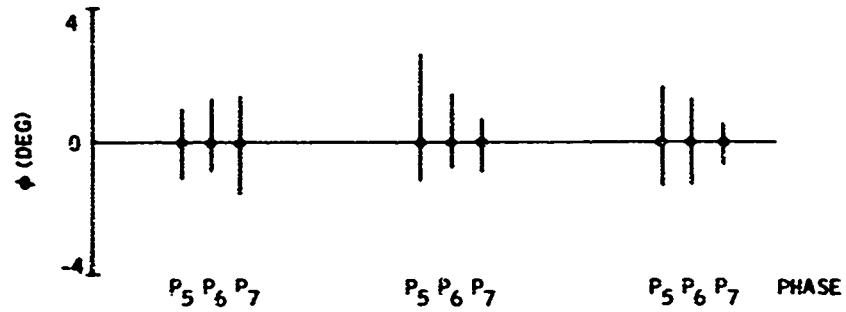| Q	N	F	A	C	D	V		Q	N	F	A	C	D	V		Q	N	F	A	C	D	V
1	3	3	1	1	2	2		1	3	3	1	2	2	2		1	3	3	1	3	2	2

Figure D69.   Terminal Median and ±34th-Percentile Data
for ϕ: XV-5 Aircraft